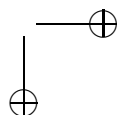
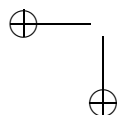
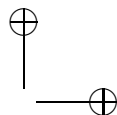
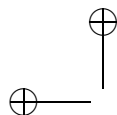


Ornicopter Multidisciplinary Analyses and Conceptual Design

Jia Wan



Ornicopter Multidisciplinary Analyses and Conceptual Design

Proefschrift

ter verkrijging van de graad van doctor
aan de Technische Universiteit Delft,
op gezag van de Rector Magnificus prof.dr.ir. K.C.A.M. Luyben,
voorzitter van het College van Promoties,
in het openbaar te verdedigen op woensdag 18 juni 2014 om 10:00 uur
door

Jia WAN

Master of Science, Beihang University
geboren te Leshan, China.

Dit proefschrift is goedgekeurd door de promotor:
Prof.dr.ir. M. van Tooren

Copromotor Dr. M. Pavel

Samenstelling promotiecommissie:

Rector Magnificus,	voorzitter
Prof.dr.ir. M. van Tooren,	Technische Universiteit Delft, promotor
Dr. M. Pavel,	Technische Universiteit Delft, copromotor
Prof.dr.ir. T. van Holten,	Technische Universiteit Delft
Prof.dr.ir. L. Veldhuis,	Technische Universiteit Delft
Prof. D. Schrage,	Georgia Institute of Technology
Prof. M. Gennaretti	Roma Tre University
Prof. Dr.-Ing. M. Hajek	Technische Universität München

ISBN XX-XXX-XXXX-X

Summary

The tail rotor of conventional helicopters has always been considered a necessary ‘evil’. It is necessary to counteract the reaction torque of the engine and to control the helicopter in yaw but it consumes substantial power, has only marginal control authority under unfavourable wind conditions, and it is noisy, vulnerable and dangerous. A solution to all these problems would be a helicopter concept that eliminates the need for a tail rotor. The so-called ‘Ornicopter’, a helicopter with flapping blades, is such a concept.

The mechanism of the Ornicopter is inspired by bird flight. When birds flap their wings they are able to generate both a lifting force and a propelling force from this single movement. Instead of propelling a helicopter blade by spinning it around and deriving lift from this rotating movement, as is done in conventional helicopter configurations, the Ornicopter flaps its blades like a bird and derives both lift and a propulsive force from this movement. In this case the blades propel themselves and there is no longer a need for a direct torque supplied by the engine to rotate the blades. The Ornicopter’s rotor, therefore, will not cause a reaction torque on the fuselage, which makes the tail rotor’s anti-torque function redundant.

The goal of the present thesis is to develop a thorough understanding of the Ornicopter concept and its feasibility throughout a realistic flight envelope. The first part presents the analysis of the Ornicopter’s main characteristics regarding performance, stability, controllability, handling qualities, as well as an exploratory vibratory analysis. In the second part a preliminary design and sizing thereof are presented based on the conclusions obtained in the first part.

The basis for the Ornicopter’s study is an analytically-derived flight mechanics model. The model is based on the blade element theory (BET) and considers 6 rigid body degrees of freedom (DoF), 3 DoF blade flapping dynamics and 3 DoF Pitt-Peters inflow dynamics. Previous mathematical models developed as a proof of the Ornicopter concept have concentrated mainly on hovering flight. The model developed in this thesis is capable of representing the Ornicopter’s dynamics well within its entire operational flight envelope. As a benchmark for the Ornicopter’s specifications, the Bölkow Bo-105 helicopter is used. The Bo-105 helicopter is a light twin-engine, multi-purpose helicopter developed in Germany in the 1970s. For the initial values of the design parameters of the Ornicopter (such as rotor radius, blade loading, rotor tip velocity, vertical fin size) the Bo-105 helicopter design is used. A 2×2 anti-symmetric rotor flapping configuration (with two opposite blades flapping in the same direction) is used for the Ornicopter

in order to eliminate the necessity for a tail rotor. Using these design parameters it is demonstrated that the Ornicopter rotor can generate enough propulsive torque to rotate the blades with modest flapping amplitudes (maximum less than 9 deg). The present thesis demonstrates that, compared to the Bo-105 helicopter, the Ornicopter concept suffers from higher required power, a smaller flight envelope (mainly due to the larger rotor stall area) and lower yaw stability. All these drawbacks are attributed to the large rotor blade angle of attack variation introduced by the forced flapping mechanism and the absence of a tail rotor.

In the second part of this thesis, the Ornicopter concept is optimized for performance. Keeping the performance specifications of the Bo-105 as the objectives, the design values (blade radius, blade loading etc) are turned to fit the Ornicopter concept and no longer use the Bo-105 design values. The design optimization is formulated through minimization of the required power, while satisfying the stall area requirement. The thesis proves that the optimal design for the Ornicopter as compared to the Bo-105 benchmark is characterized by a lower blade loading, increased rotor tip velocity and larger vertical fin size. This optimal design results in an enlarged flight envelope due to the reduced rotor stall area and improved yaw stability in forward flight. Nevertheless, despite these improvements in the Ornicopter’s flight envelope, there is a slight increase in required power when compared with the Bo-105 specification (approximately 5% at 150 knots). To compensate for the higher profile power needed for the Ornicopter’s optimal design, a larger rotor radius is required in order to reduce the induced power and keep the increase in the total required power to a minimum.

This thesis may be considered as a first step in rationalizing the expectations regarding the Ornicopter’s tailless helicopter design. The thesis proved that this new concept shows a slightly poorer performance than that of conventional helicopters regarding power consumption in forward flight and service ceiling. This is disappointing since one of the assumptions was that the elimination of the tail rotor would also eliminate the power consumption associated with a tail rotor. Further analyses of the Ornicopter’s performance (such as endurance, payloads, climbing performance, and environmental performance related to safety and noise), costs or maintenance should be performed for a comprehensive understanding of the advantages and disadvantages of this helicopter concept.

Contents

Summary	v
List of Figures	xiv
List of Tables	xv
Nomenclature	xvii
1 Introduction	1
1.1 General Background	1
1.2 Aim of the Thesis	3
1.3 Thesis Outline	5
2 The Ornicopter Concept	7
2.1 Introduction	7
2.1.1 The Flapping Blade Concepts	7
2.1.2 The Ornicopter Concept	9
2.2 The Benchmark Helicopter	9
2.3 The Basic Ornicopter Principle	12
2.3.1 The Vanished Reaction Torque	12
2.3.2 Controlling the Ornicopter	14
2.3.3 Basic Flapping Configurations	17
2.4 Preliminary Theoretical Analyses	19
2.4.1 Power Requirement in Hover	20
2.4.2 Forced Flapping Moment and Angle	23
2.4.3 Flapping Configuration	26
2.4.4 Controlling the Ornicopter	27
2.4.5 Vibratory Loads	30
2.4.6 The Effect of Blade Flexibility	30
2.5 Practical Implementation and Test	32
2.5.1 Forced Flapping Mechanisms	32
2.5.2 Insight of the Shaft Torque	37
2.5.3 Windtunnel Test	40
2.5.4 The Demonstrator Model	45

2.6	Conclusion	46
3	The Ornicopter Model	47
3.1	The Level of Modelling	47
3.2	The Generic Helicopter Flight Mechanics Model - Delcopter	49
3.2.1	Assumptions	49
3.2.2	Reference Frame	50
3.2.3	The Component Models	53
3.2.4	The System of Equations of Motion	53
3.2.5	Model Linearisation	55
3.2.6	The Control System	59
3.3	Validation for the Generic Helicopter Model	61
3.3.1	The Trim	61
3.3.2	The Main Rotor Torque	63
3.3.3	The Dynamic Response	63
3.4	Adaptations of the Delcopter to the Ornicopter Model	64
3.4.1	The Forced Flapping Mechanism	65
3.4.2	The Flapping Equation of Motion	65
3.4.3	The Forces and Moments Generated by One Blade	66
3.4.4	The Total Hub Forces and Moments	66
3.4.5	The Tail Rotor and Yaw Control	67
3.5	Validation of the Ornicopter Model	67
3.6	Conclusion	68
4	Concept Analyses and Comparisons	71
4.1	Introduction	71
4.2	The Trim Analysis	71
4.3	Efficiency and Required Power	75
4.3.1	Power Calculation	75
4.3.2	The Figure of Merit	77
4.3.3	Required Power	77
4.4	The Flight Envelope	79
4.4.1	The Calculation Criteria	80
4.4.2	Flight Envelopes of the Ornicopter and Bo-105	81
4.5	Autorotation	84
4.6	Stability and Controllability	85
4.6.1	Stability Derivatives	86
4.6.2	The Natural Modes	90
4.6.3	Control Derivatives	93
4.7	Handling Qualities	97
4.7.1	Yaw Control Power	97
4.7.2	Bandwidth and Phase Delay	98
4.7.3	Attitude Quickness	105
4.7.4	Lateral-directional Oscillatory Requirement	110
4.7.5	Yaw Control in Sideslip	111

4.8	Vibratory Loads and Preliminary Solutions	112
4.8.1	The Cause of Vibratory Loads	113
4.8.2	New Configurations	114
4.9	Conclusion	117
5	The Ornicopter Design	119
5.1	Design Requirements and Method	119
5.2	The Design Parameters	121
5.2.1	Rotor Sizing	121
5.2.2	Vertical Fin	121
5.2.3	Pitch Flap Coupling	122
5.3	Sensitivity Analyses	123
5.3.1	The Rotor Radius	123
5.3.2	The Blade Area	126
5.3.3	The Tip Velocity	126
5.3.4	The Fin Size	127
5.3.5	The Pitch Flap Coupling	129
5.3.6	Conclusion	132
5.4	The Design Database	132
5.5	The Design Process	134
5.5.1	Design Space	134
5.5.2	Design Optimization	142
5.6	Comparisons with the Bo-105	149
5.6.1	The Flight Envelope	149
5.6.2	Autorotation	151
5.6.3	Natural Modes of Motion	151
5.6.4	Handling Qualities	153
5.7	Discussion	157
5.7.1	Weight Prediction	157
5.7.2	Influence of the Helicopter Size	157
5.7.3	Different Design Requirements	159
5.8	Conclusion	159
6	Conclusions and Recommendations	161
6.1	Conclusions	161
6.1.1	Impacts of the Ornicopter Concept	161
6.1.2	Ornicopter Design	162
6.2	Recommendations	164
6.2.1	Improving the Model	164
6.2.2	Analyses for More Disciplines	165
6.2.3	Hybrid Concept	165
A	The Ornicopter Rotor Model in Hovering	167
A.1	Hub Force and Moment for One Blade	167
A.2	Forced Flapping Motion	171

A.3 The Total Hub Forces and Moments	173
B Bo-105 Data	177
B.1 Bo-105 Design Data	177
B.2 Flight Test Data	179
C An Ordering Scheme for Model Simplification	183
C.1 Simplification Method	183
C.2 Demonstration	186
D Development of the Generic Flight Mechanics Model	189
D.1 Generic Model Components	189
D.1.1 The Main Rotor Model	189
D.1.2 The Tail Rotor Model	197
D.1.3 Velocity Transformation	198
D.1.4 Other Components	199
D.2 Expressions of the Generic Flight Mechanics Model	200
D.2.1 Rotor Hub Forces and Moments	201
D.2.2 Flapping Equation	211
Bibliography	219
Samenvatting	221
Acknowledgements	223
Curriculum Vitae	225

List of Figures

1.1	Propulsion from a flapping wing [25]	2
1.2	Example of helicopter evaluation aspects	3
1.3	Thesis flow chart	5
2.1	Sketch of blade movement [12]	8
2.2	The windtunnel model developed by Küssner [11]	8
2.3	Sketch of the freewheeling flapping wing [2]	9
2.4	Sketch of a possible Ornicopter design	10
2.5	Principle of a forced flap mechanism using a push-pull rod and swashplate [33]	10
2.6	Three-view drawing of the Bo-105	11
2.7	Lift and drag forces acting on an Ornicopter blade during one revolution when a constant pitch angle is applied	13
2.8	The forces and moments acting on a conventional helicopter and the Ornicopter [30]	14
2.9	Schematic representation of yaw control by introducing a reaction torque	15
2.10	Cyclic control of Ornicopter [37]	16
2.11	Principle of the four bladed double teeter rotor [34]	18
2.12	Principle of the 2×2 AS configuration [34]	18
2.13	Principle of the three-bladed 1-plane rotor [34]	19
2.14	Blade configuration for the rotor model	20
2.15	Aerodynamic environment at a typical blade element	21
2.16	Bending of a flexible blade and a rigid blade for a given flapping power [35]	31
2.17	The windtunnel test model with swashplate mechanisms [36]	33
2.18	Sketch of the gearwheel mechanism	34
2.19	Detailed design of the gearwheel mechanism [16]	34
2.20	Principle of the eccentric mechanism [16]	35
2.21	The eccentric mechanism for the double teeter configuration [16]	36
2.22	Principle of the multiple disc mechanism [16]	36
2.23	Multiple disc mechanism for 2×2 AS configuration [16]	37
2.24	Forces on the forced-flapping swash plate	38
2.25	Sketch of the Ornicopter rotor components	39

2.26	Side-view of the test section of Küssner’s windtunnel test [11]	40
2.27	Variation of the rotor torque M_a and engine torque M_i with respect to the forced flapping angle [11]	41
2.28	The Ornicopter windtunnel model [32]	42
2.29	Rotor torque (M_z) and rotor thrust (T) as a function of collective pitch for a double teeter Ornicopter with twelve degrees of flapping [32]	42
2.30	Rotor thrust as a function of the collective pitch for the Ornicopter with and without twelve degrees of flapping [32]	43
2.31	Rotor torque as a function of the collective pitch for various flapping values [32]	44
2.32	Power curves for a conventional helicopter and Ornicopter [32]	44
2.33	The Ornicopter demonstrator model [15]	45
3.1	Forces and moments on helicopters	51
3.2	The rotor hub reference	52
3.3	Trim values for the Bo-105	62
3.4	Main rotor torque of the Bo-105	63
3.5	Flight test No. 9: positive longitudinal 3-2-1-1 input	64
3.6	The blade hinge configuration of the Ornicopter	65
3.7	Propulsive torque as a function of the amplitude of flapping motion . . .	68
4.1	Trim values of the Ornicopter and Bo-105 in forward flight	72
4.2	Hub horizontal force (H) of the Ornicopter in forward flight	74
4.3	Average flapping amplitude of the Ornicopter blades as a function of forward velocity	74
4.4	Higher average C_d with a larger AoA variation	75
4.5	Figure of Merit predictions for the Bo-105 and Ornicopter rotor	78
4.6	Power required of the Ornicopter and Bo-105	79
4.7	Flight envelope of the Ornicopter and Bo-105 defined by different criteria	81
4.8	The rotor stall area of the Ornicopter and Bo-105 versus velocity	82
4.9	The angle of attack distribution on the Bo-105 rotor at 150 knots	82
4.10	The angle of attack distribution on the Ornicopter rotor at 150 knots . .	83
4.11	Direct and coupling force derivatives as a function of flight velocity . . .	86
4.12	Variation of M_u and M_w with forward speed	87
4.13	Variation of Z_w with forward speed	88
4.14	Variation of L_v and N_v with forward speed	88
4.15	X_q and Y_p as a function of flight speed	89
4.16	Variations of the direct and coupled damping derivatives	90
4.17	N_r , L_r and N_p as a function of flight speed	91
4.18	Loci of the Ornicopter and Bo-105 eigenvalues as a function of forward speed	92
4.19	$t_{1/2}$ and T for Dutch roll	93
4.20	First set of control derivatives a function of flight speed	94
4.21	Variation of direct and coupling moment derivatives	95
4.22	Yaw control derivatives as a function of flight speed	96

4.23	Maximum yaw rate for different yaw control inputs (40 knots)	98
4.24	Bandwidth and phase delay definition	99
4.25	Bandwidth and phase delay in pitch and roll directions (5 knots)	100
4.26	Bandwidth and phase delay in the yaw direction (hover and low speed)	101
4.27	Bandwidth and phase delay in the yaw direction (forward flight)	101
4.28	Magnitude and phase responses of different ORNIcopter models in the yaw direction (80 knots)	102
4.29	Magnitude and phase responses of the Bo-105 and Ornicopter in the yaw direction (80 knots)	104
4.30	Bandwidth and phase delay in the yaw direction with different SCAS gains (80 knots)	104
4.31	Attitude quickness definition	105
4.32	Pitch attitude quickness of the Bo-105 and Ornicopter (30 knots)	106
4.33	Yaw attitude quickness of Bo-105 and Ornicopter (30 knots)	107
4.34	Yaw responses of the Bo-105 and Ornicopter for rectangular step control input	108
4.35	Yaw attitude quickness of the Bo-105 and Ornicopter with the SCAS (30 knots)	109
4.36	Lateral-directional oscillation grading	110
4.37	Yaw control deflection as a function of sideslip velocity ($u=0$ knot)	111
4.38	Yaw control deflection as a function of the sideslip angle ($u=80$ knots)	113
4.39	Amplitudes of harmonic components of the Ornicopter rotor thrust	115
4.40	Amplitudes of harmonic components of the Ornicopter rotor torque	115
4.41	Vibratory level of the Ornicopter as a function of velocity and configurations	117
5.1	Sketch for blade pitch flap coupling	123
5.2	Impact of the rotor radius on the stall area and required power	124
5.3	Flapping amplitude and collective pitch as a function of the rotor radius	125
5.4	Impact of the blade area on the stall area and required power	126
5.5	Impact of the blade area on the flapping amplitude and collective pitch	127
5.6	Impact of the tip velocity on the stall area and required power	127
5.7	Impact of the fin size on the stall area and required power	128
5.8	Impact of the fin size on the flapping amplitude and collective pitch	128
5.9	Impact of the pitch flap angle coupling on the stall area and required power	129
5.10	Impact of the pitch flap angle coupling on the flapping amplitude and collective pitch	130
5.11	Impact of the pitch flap rate coupling on the stall area and required power	131
5.12	Impact of the pitch flap rate coupling on the flapping amplitude and collective pitch	131
5.13	Flow chart for the design database	134
5.14	Design space with different tip velocities for hovering ($\bar{S}_{vs} = 5$)	136
5.15	Design space with different tip velocities for the hovering ceiling condition ($\bar{S}_{vs} = 5$)	137
5.16	Design space with different tip velocities for forward flight ($\bar{S}_{vs} = 5$)	138
5.17	Design space with different vertical fin sizes for forward flight ($\bar{V}_t = 1.1$)	140

5.18	Feasible design space (10% higher power, $\bar{V}_t = 1.1$, $\bar{S}_{vs} = 5.0$)	141
5.19	Feasible design space (20% larger stall area, $\bar{V}_t = 1.1$, $\bar{S}_{vs} = 5$)	142
5.20	Design parameter history for $w_f = 0.5$	145
5.21	Design constraints for $w_f = 0.5$	145
5.22	Normalised required power of the optimal Ornicopter design as a function of w_f	146
5.23	Optimal designs for different w_f	147
5.24	Design requirements at different w_f	147
5.25	The flight envelope of the optimal Ornicopter and Bo-105	150
5.26	Comparisons of natural modes for the Ornicopter and the Bo-105	152
5.27	Dutch roll mode with the handling qualities rating	154
5.28	The pitch bandwidth and phase delay	154
5.29	The pitch attitude quickness	155
5.30	The yaw bandwidth (hovering and low speed)	156
5.31	The yaw bandwidth (forward flight)	156
5.32	The yaw altitude quickness	157
5.33	Trends of blade loading coefficient versus MGTOW [22]	158
A.1	Blade configuration for the rotor model	167
A.2	Aerodynamic environment at a typical blade element	168
B.1	Flight test No. 11: positive lateral 3-2-1-1 input	180
B.2	Flight test No. 13: positive collective 3-2-1-1 input	181
B.3	Flight test No. 15: positive pedal 3-2-1-1 input	182
C.1	RMSE as a function of calculation time	187
D.1	Blade hinge configuration	189

List of Tables

2.1	Main design parameters of the Bo-105	11
2.2	Bo-105 performance predicted by Delcopter	12
2.3	Flapping sets for different configurations	27
2.4	Harmonic components on the rotor hub	30
3.1	Levels of rotor modelling [10]	48
3.2	Time constants of the actuator	60
4.1	Eigenvector for Dutch roll mode (partial)	93
4.2	Flapping sets for different configurations	116
5.1	Impacts of the design parameters on the Ornicopter stall area and re- quired power	133
5.2	Variation of the design parameters	133
5.3	Design requirements	135
5.4	Boundaries of the design parameters	143
5.5	Optimized Ornicopter rotor design	149
6.1	Characteristics of the Ornicopter concept	164
B.1	Bo-105 data	177
C.1	Ordering scheme	184
C.2	Results of simplifications with different highest orders	187

Nomenclature

Latin Symbols

c	Blade chord	$[m]$
dD	Drag force generated on the blade element	$[N/m]$
dL	Lift force generated on the blade element	$[N/m]$
e_f	Nondimensional flapping hinge offset	
$k_{\theta 1}$	Pitch flap angle coupling	
$k_{\theta 2}$	Pitch flap rate coupling	
k_l	Tip loss factor	
k_p	Power margin factor	
k_r	Blade root cut factor	
m_{aero}	Non-dimensional aerodynamic flapping moment on the rotor blade	
m_{ff}	Non-dimensional flapping moment on the blade generated by the forced flapping mechanism	
\hat{m}_{ff}	Amplitude of the non-dimensional forced flapping moment	
p, q, r	Rotational velocity components of the helicopter along the fuselage x -, y - and z -axes. Positive when roll to right, pitch up and yaw to right	$[rad/s]$
$\bar{p}, \bar{q}, \bar{r}$	Rotational velocity components of the helicopter along the fuselage x -, y - and z -axes, normalized by Ω	
r_e	Radius position of the blade element	$[m]$
u, v, w	Translational velocity components of the helicopter along the fuselage x -, y - and z -axes. Positive for flight forward, right-hand side and downward	$[m/s]$
v_i	Induced velocity	$[m/s]$
v_{i0}, v_{is1}, v_{ic1}	Rotor uniform and first harmonic inflow velocity	$[m/s]$
v_p	Perpendicular velocity component on the blade element	$[m/s]$

v_t	Tangent velocity component on the blade element	$[m/s]$
w_f	Weight factor for the required power in forward flight	
x, y, z	Component position in the body reference	$[m]$
A, B	The state and control matrices of a linear system	
A, B, C	Sine, cosine and constant coefficients of the m_{ff}	
C_1, C_2	Non-denominational lateral and longitudinal aerodynamic moments on the rotor	
C_d	Drag coefficient of aerofoil= $C_{d0} + C_{d2}\alpha^2$	
C_H	Rotor horizontal force coefficient	
C_l	Lift coefficient of the aerofoil	
C_{l_α}	Aerofoil lift curve slope	$[rad^{-1}]$
C_Q	Rotor shaft torque coefficient	
C_S	Rotor side force coefficient	
C_T	Rotor thrust coefficient	
C_{T_b}	Thrust coefficient calculated using blade element theory	
C_{T_λ}	Thrust coefficient calculated from momentum theory	
I_β	Flap moment of inertia	$[kg \cdot m^2]$
I_x, I_y, I_z	Moments of inertia of the helicopter about the x -, y - and z -axes	$[kg \cdot m^2]$
I_{xz}	Product of inertia of the helicopter about the x - and z -axes	$[kg \cdot m^2]$
K	SCAS gain matrix	
K_β	Flapping stiffness	$[N \cdot m/rad]$
$\hat{\mathbf{L}}^{-1}$	Inflow gain matrix for Pitt-Peters inflow model	
L	Lift force on aerofoil	$[N]$
L, M, N	Moment components on the helicopter along the fuselage x -, y - and z -axes. Positive for roll right, pitch up and yaw right	$[N \cdot m]$
M	Apparent mass matrix for Pitt-Peters inflow model	
M_1, M_2	Lateral and longitudinal aerodynamic moments on rotor disc	$[N \cdot m]$
M_a	Mass of a helicopter	$[kg]$
M_{aero}	Aerodynamic flapping moment on the rotor blade	$[N \cdot m]$
M_b	Mass of rotor blade	$[kg]$
M_β	First moment of mass of the rotor blade	$[kg \cdot m]$
M_{ff}	Flapping moment on the blade generated by the forced flapping mechanism	$[N \cdot m]$
M_Q	Rotor aerodynamic torque	$[N \cdot m]$
M_x, M_y	Lateral and longitudinal rotor hub moments	$[N \cdot m]$
M_z	Rotor shaft torque	$[N \cdot m]$
N_b	Number of blades	

Nomenclature

xix

\bar{P}	Non-dimensional required power, normalized by the required power of the Bo-105	
P_{dyn}	Dynamic pressure	$[kg/(m \cdot s^2)]$
P_e	Available engine power	$[W]$
P_{e0}	Available engine power at sea level	$[W]$
P_{ff}	Power consumed by the forced flapping mechanism	$[W]$
P_i	Rotor induced power	$[W]$
P_{ideal}	Ideal rotor power	$[W]$
P_p	Rotor profile power	$[W]$
P_{sh}	Rotor shaft power	$[W]$
Q_i	Generalized force	
R	Rotor radius	$[m]$
R_{ef}	Blade hinge offset	$[m]$
\bar{S}	Non-dimensional stall area on the main rotor	
\bar{S}_{max}	Maximum allowable non-dimensional stall area on the main rotor	
S_β	Blade flapping stiffness number $\frac{\lambda_\beta^2 - 1}{\gamma/8}$	
S_e	Equivalent vertical fin area	$[m^3 \cdot rad]$
\bar{S}_f	Stall design constraint in forward flight	
\bar{S}_{hs}	Stall design constraint at the hovering ceiling	
S_{stall}	Total stall area on the main rotor	$[m^2]$
\bar{S}_{vs}	Non-dimensional vertical fin size, normalized by the fin size of the Bo-105	
\mathbf{T}_{A2B}	Transformation matrix between reference frame A and B	
T, H, S	Rotor thrust, horizontal (forward positive) and sideways (right side positive) hub forces	$[N]$
T_k	Total kinetic energy	$[W]$
\mathbf{U}	Control input vector	
U_{eff}	Effective air flow velocity	$[m/s]$
U_∞	Incoming air flow velocity	$[m/s]$
\mathbf{V}	Velocity vector	$[m/s]$
V_t	Blade tip velocity	$[m/s]$
\bar{V}_t	Non-dimensional rotor tip velocity, normalized by the tip velocity of the Bo-105	
\mathbf{X}	Model state vector	
X, Y, Z	Force components on the helicopter along the fuselage x -, y - and z -axes	$[N]$

Greek Symbols

α	Angle of attack	$[rad]$
α_{eff}	Aerofoil effective angle of attack	$[rad]$
α_{sh}	Rotor shaft tilt angle	$[rad]$
β	Flapping angle of the blades	$[rad]$
$\dot{\beta}$	Flapping rate of the blades	$[rad/s]$
$\hat{\beta}$	Amplitude of the blade flapping motion	$[rad]$
$\beta_0, \beta_{s1}, \beta_{c1}$	Rotor blade coning, lateral and longitudinal flapping angles. Positive when coning upward, tilting left or forward	$[rad]$
$\bar{\beta}, \beta_{ave}$	Average flapping motion of all blades	$[rad]$
$\vec{\beta}$	Flapping state vector	$[rad]$
γ	Lock number = $\frac{\rho c C_{l\alpha} R^4}{I_\beta}$	
η	Flapping angle of the forced flapping mechanism	$[rad]$
$\dot{\eta}$	Flapping rate of the forced flapping mechanism	$[rad/s]$
$\hat{\eta}$	Amplitude of the forced flapping mechanism motion	$[rad]$
η_{s1}, η_{c1}	Lateral and longitudinal flapping angles of the forced flapping mechanism	$[rad]$
$\bar{\eta}_{s1}, \bar{\eta}_{c1}$	Average lateral and longitudinal flapping angles of the forced flapping mechanism for all blades	$[rad]$
θ	Blade pitch angle	$[rad]$
$\theta_0, \theta_{s1}, \theta_{c1}$	Collective, longitudinal (positive for pitch up) and lateral (positive for roll left) cyclic control	$[rad]$
θ_{tw}	Blade twist angle	$[rad]$
$\lambda_0, \lambda_{s1}, \lambda_{c1}$	Rotor uniform and first harmonic inflow velocities (normalized by ΩR)	
λ_β	Flap frequency ratio $\lambda_\beta^2 = 1 + \frac{K_\beta}{I_\beta \Omega^2}$	
λ_i	Inflow ratio = $\frac{v_i}{V_t}$	
μ	Advance ratio $V/\Omega R$	
μ_x, μ_y, μ_z	Translational velocity components of the helicopter along the fuselage x -, y - and z -axes, normalized by ΩR	
ρ	Air density	$[kg/m^3]$
σ	Rotor solidity = $\frac{N_b c}{\pi R}$	
σ_s	Blade solidity = $\frac{c}{\pi R}$	
τ	Time constant of the actuator	$[s]$
τ_p	System phase delay	$[deg]$
φ	Induced angle	$[rad]$
ψ	Blade azimuth angle	$[rad]$

Nomenclature

xxi

ω_{BW}	System bandwidth	$[rad/s]$
Ψ, Θ, Φ	Helicopter heading, pitch and roll angles	$[rad]$
Ω	Rotational velocity of the rotor	$[rad/s]$

Subscripts

$f_{us,vs,hs}$	Fuselage, vertical stabilizer, horizontal stabilizer
h, hc, f	Hovering, hovering ceiling and forward flight conditions
hub	Main rotor hub
mr, tr	Main rotor, tail rotor
$s1, c1$	The first order sine and cosine harmonic component
s	For a single blade

Superscripts

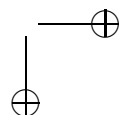
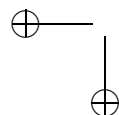
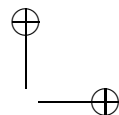
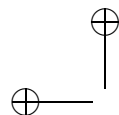
(k)	For the k^{th} blade
-------	------------------------

Abbreviations

DoF	Degree of freedom
EoM	Equation of motion
HHC	High harmonic control
HQR	Handling qualities rating
HQs	Handling qualities
IBC	Individual blade control
RPM	Revolution per minute
TPP	Tip-path plane

Other Symbols

$\dot{u} = \frac{du}{dt}$	Differentiation with respect to time t
$\beta' = \frac{d\beta}{d\psi}$	Differentiation with respect to the azimuth angle ψ



1

Introduction

1.1 General Background

Human interest in vertical flight can be traced back to more than 2000 years ago. The Chinese toy top, also known as the bamboo-copter, first invented around 400 BC [21], is still popular today. Despite the long history of this small toy, manned, powered vertical flight, mainly the helicopter, dates back only to the last century, i.e. the 1930s. Development since then, however, has been fast and today's helicopters are relatively safe, reliable and versatile. They play an indispensable role in modern civilian and military life.

Among the large number of helicopters, the single main rotor/tail rotor (conventional) configuration is the main configuration in use today. The configuration of a helicopter is, to a large extent, determined by the manner in which the reaction torque of the main rotor is counteracted. For conventional helicopters, the tail rotor is used for this purpose, as well as for generating yaw control.

Although the tail rotor gives the helicopter extreme manoeuvrability, it also has many unfavourable characteristics: it consumes power, and has only marginal control authority under unfavourable wind conditions; it is noisy, vulnerable and dangerous. Research has shown that about 50% of U.S. civil helicopter accidents related to airframe failure or malfunction between 1963 and 1997 are connected to the tail rotor system (including the drive train, control system, tailboom and tail rotor) [14].

Different solutions have been proposed in an attempt to solve the shortcomings of the classical tail rotor system. Some configurations have been successfully developed and implemented, such as: the Fenestron system, the NOTAR system (NO TAIL Rotor), the tandem helicopter, the coaxial helicopter and the synchropter (intermeshing rotors) configuration.

The Fenestron system (sometimes called the fantail or fan-in-fin) is one of the most

well-known solutions. It is a ducted fan with a shrouded design in the tail skin [23]. Another successful solution was developed by McDonnell Douglas and is the NOTAR system which uses a variable pitch fan located internally in the tail boom to blow the air out [21]. Although both the above solutions have been successfully applied in modern helicopters to replace the tail rotor, they have considerable disadvantages, such as the loss of control effectiveness in forward flight [21, p. 324]. Besides the two conventional tail rotor alternatives mentioned above, the other three tailless helicopter configurations mentioned (the tandem, the coaxial and the synchropter configuration) share the same basic principle and use a second main rotor in order to counteract the reaction torque of the main rotor.

In 2002, Delft University of Technology proposed the ‘Ornicopter’ configuration as an alternative manner to eliminate the tail rotor. The main idea behind the Ornicopter is that, instead of counteracting the rotor torque, it is better to use a rotor concept that does not generate a torque.

The name ‘Ornicopter’ came from the combination of ‘Orni-thopter’ and ‘Helicopter’. As its name suggests, the Ornicopter can be considered as a helicopter version of the Ornithopter, the aircraft that flies like a bird by flapping its wings [8].

Figure 1.1 [25] presents the general principle of deriving propulsion from flapping wings. When birds flap their wings, they are able to derive both a lifting force and a propelling force. This effect was discussed in 1909 by Knoller [19] and three years later independently by Betz [5], and was demonstrated in 1922 in a wind tunnel experiment by Katzmayer [18]. It is also known as the Knoller-Betz or Katzmayer effect. It represents the ability of a sinusoidally plunging airfoil to produce thrust, as illustrated in Fig. 1.1.

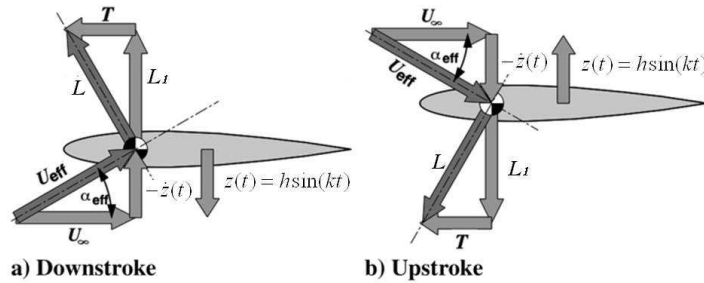


Figure 1.1: Propulsion from a flapping wing [25]

The figure represents the forces on the airfoil during the up and down movement of a flapping wing (the so-called up and down stroke). During the down stroke, the blade plunges with a distance $z(t)$, i.e. $z(t) = h \sin(kt)$, defined as a function of the nondimensional plunge amplitude h and flapping frequency k . This creates a vertical air flow relative to the airfoil ($-\dot{z}(t) = \partial z / \partial t$). Combining it with the horizontal incoming air flow (U_∞) results in an effective airfoil angle of attack (α_{eff}). In this way, a net aerodynamic force (L) is generated on the airfoil which can be decomposed into a vertical lift force component (L_1) and a positive horizontal thrust force component (T) in the direction of flying. During the up stroke, the rising of the wing results once

more in a positive thrust component T (see Fig. 1.1.b). This yields to a time-averaged positive thrust force on the flapping wing for one complete up and down motion.

In conventional helicopters, the rotor blades are driven by the shaft torque to rotate, and they generate lift from this rotating motion. This will cause a reaction torque on the fuselage that needs to be compensated for by an anti-torque device. In the case of the Ornicopter, the blades flap in the same manner as a bird and derive both lift and propulsive force from this movement. Thus, the Ornicopter combines the flapping wing principle with the helicopter principle. As the blades propel (i.e. rotate) themselves, there is no longer a need for a direct torque supplied by the engine to rotate the blades. Therefore, the Ornicopter rotor will not generate a reaction torque on its fuselage. This makes the anti-torque device redundant.

1

1.2 Aim of the Thesis

A helicopter is a complex system and the concept evaluation involves multidisciplinary analyses. Figure 1.2 shows an example of different aspects, such as flight characteristics (e.g. performance), financial respective (e.g. the life cycle cost) and environmental effects (noise and emission). Different helicopter configurations will affect the helicopter from different respects, and each configuration has its own advantages and disadvantages. In this sense, the Ornicopter concept should be compared with conventional helicopters in order to pinpoint its pros and cons.

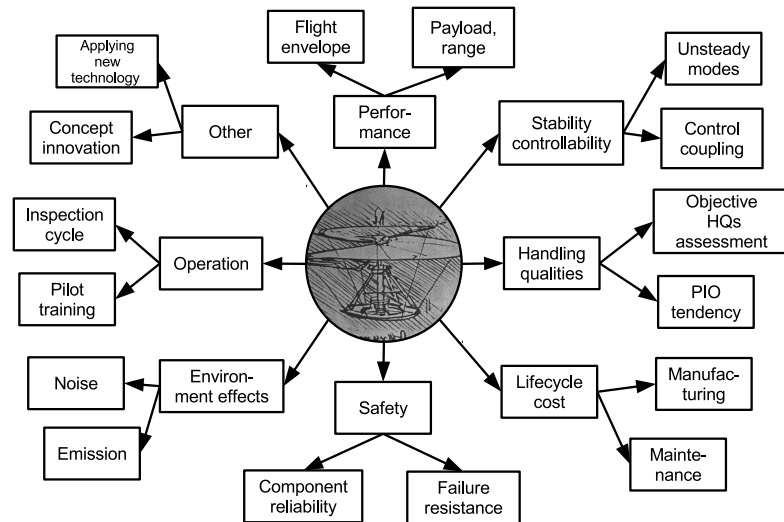


Figure 1.2: Example of helicopter evaluation aspects

Meanwhile, it is also important to understand the physical reasons that cause these

advantages or disadvantages. With this fundamental understanding, the Ornicopter concept can be improved.

The goal of the present thesis is to develop a thorough understanding of the Ornicopter concept and its feasibility throughout its operational flight envelope. Specifically, the following questions will be answered:

1

As compared to a conventional helicopter,

- 1. what are the characteristics of the Ornicopter regarding performance, stability, controllability, and handling qualities,**
- 2. and how can an Ornicopter with comparable or improved flight performance be designed?**

To give a better view of the thesis scope, the following terms are defined:

Performance

The helicopter performance considered in this thesis relates to three aspects: the required power, the main rotor stall area and the flight envelope (altitude vs speed) as defined by the power and stall criteria. The performance analysis investigates whether the Ornicopter requires more power than conventional helicopters, and if its flight envelope is comparable to that of a conventional helicopter.

Stability and Controllability

The stability and controllability refer to the stability derivatives, control derivatives and the natural modes of the helicopter body motion DoF. Comparisons present values of the derivatives and mode characteristics of Ornicopter and a benchmark helicopter. The physical reasons causing the differences between them are discussed.

Handling Qualities

The handling qualities analyses in this thesis are based on ADS-33 criteria [4]. The analyses are concerned with quantifiable handling qualities matrices, such as bandwidth and phase delay, attitude quickness, lateral-directional oscillation and the yaw control in sideslip.

Design

The design of the Ornicopter refers to the design parameter values as shown in Appendix B. The initial Ornicopter design is the same as the benchmark helicopter Bo-105. Afterwards, based on performance analyses, the Ornicopter design is unfrozen and some Ornicopter design parameters are optimized.

The Benchmark Helicopter

The Bölkow Bo-105 is selected as the benchmark helicopter in this thesis. It is used for the model validation and comparisons with the Ornicopter for the above mentioned aspects. Its performance data will be considered as design requirements for the Ornicopter design.

The following limitations apply to this thesis:

1. The Ornicopter research mainly relates to the fields of performance, stability, controllability, and handling qualities. Other disciplines, such as safety and cost, should be considered in future research.

2. The flight mechanics model developed in this thesis has the assumptions and simplifications presented in Section 3.2.1.
3. Only one benchmark helicopter is used in this thesis. Possible size (different weight categories) effects on the Ornicopter are not studied.
4. The practical implementation of the Ornicopter concept is not studied, such as the detailed design of the forced flapping mechanism and the mechanism implementation of pitch flapping rate coupling.
5. The Ornicopter’s weight breakdown is not considered in this thesis. It is assumed that the Ornicopter’s forced flapping mechanism has the same weight as the tail rotor system, i.e. the Ornicopter has the same gross weight as the Bo-105.

1.3 Thesis Outline

The outline for this thesis is defined as follows, and Figure 1.3 presents the structure of this thesis.

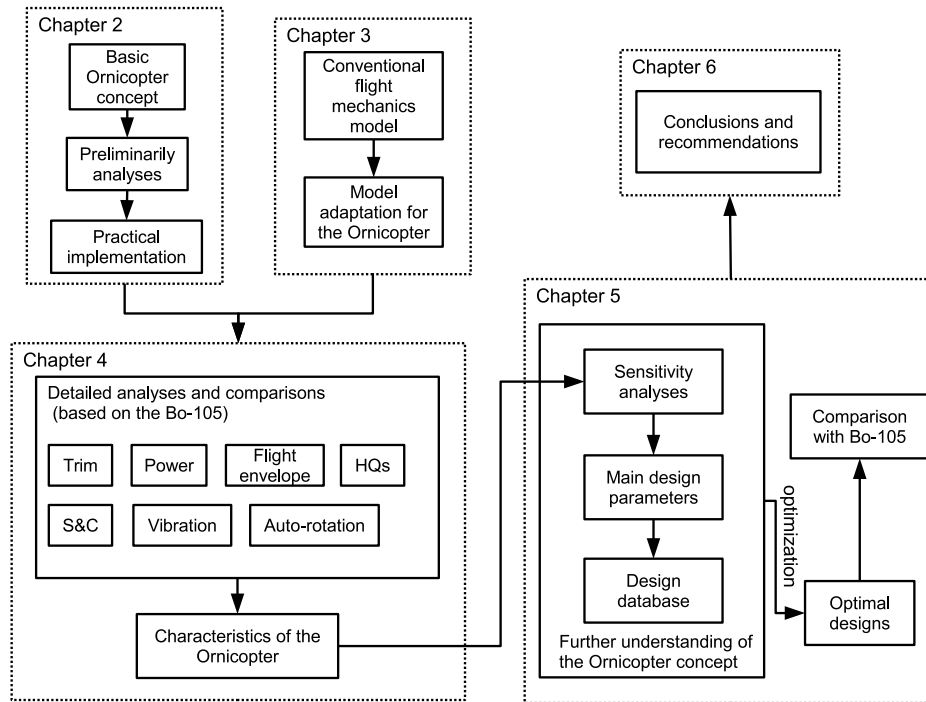


Figure 1.3: Thesis flow chart

Chapter 2 presents the Ornicopter concept. Preliminary analyses are performed for

basic concept understanding, such as generating the propulsive torque and controlling the yawing moment.

Chapter 3 develops first a flight mechanics model for conventional helicopters. This model is based on the blade element theory (BET) and considers 6 degrees of freedom (DoF) rigid body dynamics, 3 DoF blade flapping dynamics, 3 DoF main rotor inflow dynamics and 1 DoF tail rotor inflow dynamics. After validation, the model is adapted to the Ornicopter concept.

Chapter 4 conducts the analyses of the performance, stability, controllability, and handling qualities for the Ornicopter concept. The Ornicopter is compared with the conventional Bo-105 helicopter. Comparisons in this chapter show the Ornicopter’s advantages and disadvantages.

Chapter 5 unfreezes the Ornicopter design. First, sensitivity analyses are performed to find the most influential design parameters for the Ornicopter performance. Afterwards, a design database is derived for the Ornicopter. Based on this, the Ornicopter design is optimized. The ‘optimal’ Ornicopter is compared again with the Bo-105 helicopter.

Chapter 6 gives conclusions and recommendations.

2

The Ornicopter Concept

In 2002, Delft University of Technology proposed the Ornicopter concept [32]. By actively flapping its blades, a single rotor/tailless Ornicopter configuration can be developed. In this chapter, the basic concept of this configuration will be explained. Afterwards, some preliminary theoretical analyses for the Ornicopter concept will be presented. At the end, some practical implementation issues will be briefly discussed.

2.1 Introduction

2.1.1 The Flapping Blade Concepts

Inspired by birds, efforts have been made to invent a flapping wing aircraft (also known as an ornithopter). The flapping wing concept can also be applied to the rotary-wing aircraft. A flapping blade concept was first proposed by Passat in 1921. It was called the ‘Helithopter’ and had a rotor with four blades forced to flap simultaneously [20].

In the 1930s, two devices were patented by Hans Georg Küssner, a German aerodynamicist, at the ‘Gottingen Aerodynamic Test Establishment’ [11, 12]. His invention, the so-called ‘Flapping Propulsion Rotor’, was based on the flapping blades concept. In his patent, the flapping actuation device was based on an oil-hydraulic pump system to simultaneously flap up and down a pair of centrally hinged rotor blades [11]. Figure 2.1 shows a sketch of the blade motion in Küssner’s design. The blade is forced to flap, and hence the tip-path plane (TPP) tilts into a certain direction.

In order to demonstrate his concept, Küssner also developed a wind tunnel model, see Fig. 2.2 [11], and showed experimentally that the reaction torque could be completely compensated for by the rotating flapping blades in such a concept.

At the end of the 1990s, Dr. Vladimir Savov from the Bulgarian Air Force Academy proposed the so-called ‘Rotoropter’ concept, using the same principle of the forced flapping

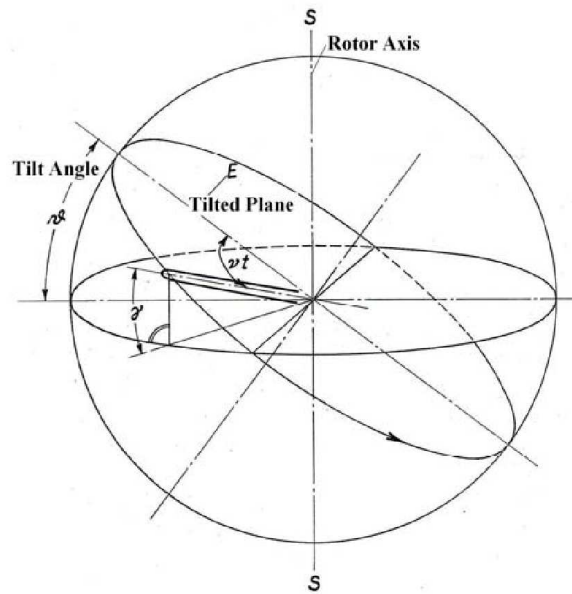


Figure 2.1: Sketch of blade movement [12]

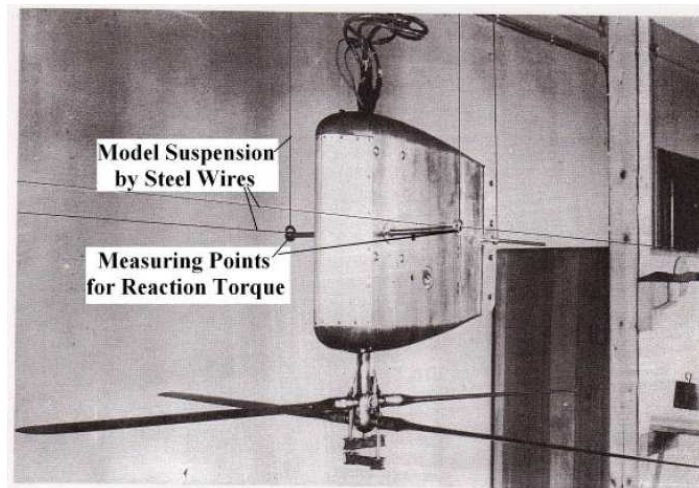
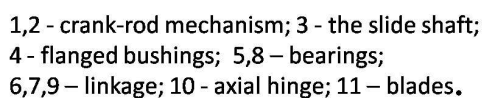


Figure 2.2: The windtunnel model developed by Küssner [11]

blades in order to eliminate the tail rotor. A mechanism was designed and patented by Savov, the so-called ‘freewheeling flapping wing’, as shown in Fig. 2.3 [2]. The blades can rotate freely and are forced to flap around the flapping hinge (component 7 in Fig. 2.3) by the crank-rod mechanism (1 and 2) and slide shaft (3). This flapping

9

2



2.1.2 The Ornicopter Concept

At Delft University of Technology, some research related to the Ornicopter has been performed. Initially, the basic Ornicopter principle was proposed, followed by feasibility analyses using a rotor model in hovering [32]. The principle of how to achieve the forced flapping motion on the Ornicopter was also defined later on [30, 37].

2.2 The Benchmark Helicopter

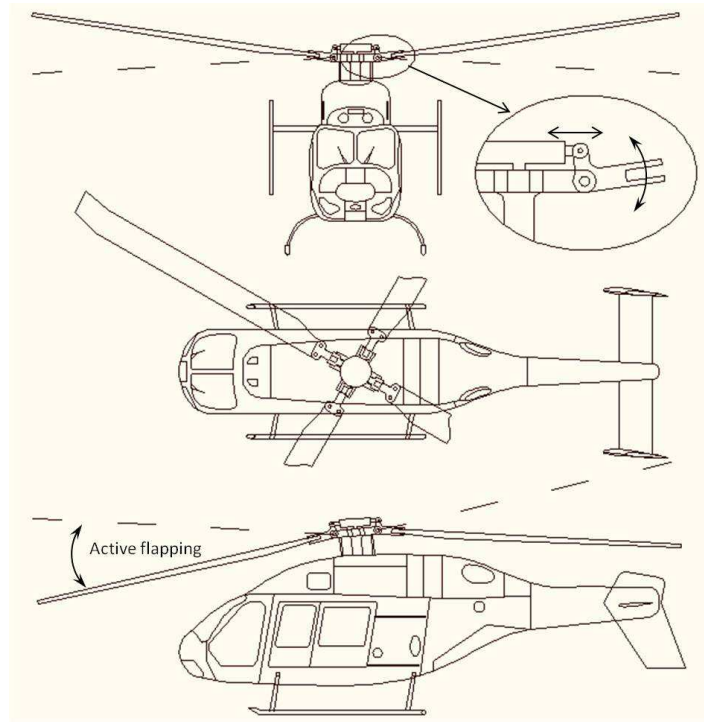


Figure 2.4: Sketch of a possible Ornicopter design

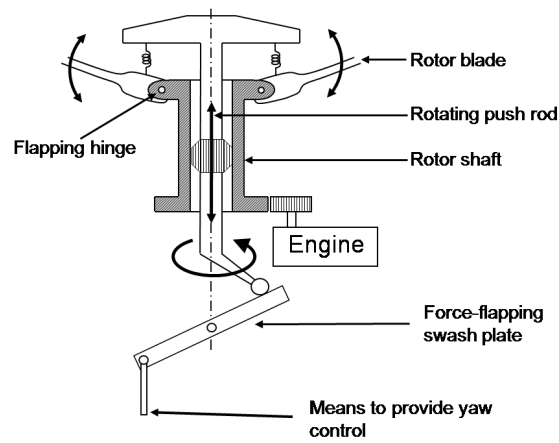


Figure 2.5: Principle of a forced flap mechanism using a push-pull rod and swashplate [33]

2.2 The Benchmark Helicopter

11

purpose, see Fig. 2.6.

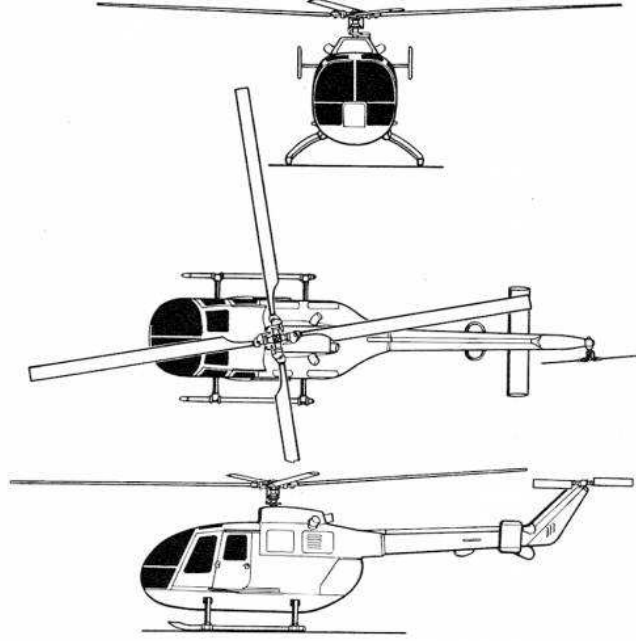


Figure 2.6: Three-view drawing of the Bo-105

As a widely used baseline helicopter in the rotorcraft community, the Bo-105 is a light, twin-engine, multi-purpose utility helicopter developed successfully in the 1970s in Germany. It has multiple variants, such as the Bo-105C (the initial version) and Bo-105S (the search and rescue version). Based on the DLR (German Aerospace Center) research helicopter Bo-105 S123 [10], a generic light Bo-105 configuration is used in this thesis. Some main design parameters are presented in Tab. 2.1. More detailed design parameters can be found in Appendix. B.

Table 2.1: Main design parameters of the Bo-105

Rotor radius	4.91 m	Blade chord	0.27 m
Solidity	0.07	Disk loading	29.05 kg/m ²
Tip velocity	218 m/s	Rotor RPM	424
Number of blades	4	Mass of helicopter	2200 kg
Tail rotor radius	0.95 m	Length (incl rotors)	11.86 m

Flight test data of the Bo-105 will be used to validate the flight mechanics model developed in Chapter 3. In Chapter 4, the Ornicopter using the same design as the Bo-105 will be compared with the Bo-105 from different respects.

2

Instead of the actual Bo-105 performance data, performance specifications from model prediction will be used in this thesis. The Bo-105 performance is determined using the following approach. The maximum speed (sea level) of the Bo-105 is assumed to be 150 knots. This is slightly higher than the real Bo-105 specification (145 knots [28]) due to the lower total weight. Based on the stall area and required power at 150 knots, the flight envelope of the Bo-105 is predicted. More detailed discussion can be found in Section 4.4. The main Bo-105 performance data from the Delcopter model (developed in Chapter 3) prediction is summarized in Tab. 2.2. These performance data will be used as the design requirement for the Ornicopter design in Chapter 5.

Table 2.2: Bo-105 performance predicted by Delcopter

Hovering ceiling	Service ceiling	Max. velocity
2815 m	5725 m	150 knots

2.3 The Basic Ornicopter Principle

2.3.1 The Vanished Reaction Torque

As stated previously, the Ornicopter flaps its blades like a bird. When a bird is flying, both a propulsive force - that pushes the bird to fly through the air - and a lift force - that will keep the bird airborne - are generated by its flapping wings (see Fig. 1.1 in the Introduction). Similarly, when the blades of a rotating rotor are actively flapping, both a lift force and a propulsive force are generated. In this case, the propulsive force will drive the rotor to rotate.

A very useful and simple understanding of how one can generate propulsive force with an Ornicopter blade is obtained by applying a constant pitch angle to the flapping blade. The movement of an Ornicopter blade during one revolution is illustrated in Fig. 2.7. During one revolution of the rotation, the blade will be forced to flap both up and down once, resulting in the undulating path shown in Fig. 2.7.

At 0° azimuth angle (ψ), the blade element passes through the neutral position with maximum upwards velocity. Due to the upwards flapping velocity, the overall speed (V) will rotate upwards, and hence the angle of attack of the blade element will decrease, resulting in relatively low lift force (L). At the same time, the lift force, which is perpendicular to the relative air flow vector, will follow the change of the incoming wind direction. Therefore, it tilts backwards with regard to the blade element.

After 90 degrees the blade reaches the maximum flapping deflection, where the flapping velocity is zero. The total velocity of the blade element is parallel to the flow direction in the case without flapping, i.e. as a normal helicopter blade. A similar situation can also be found when the blade reaches 270° . On the contrary, the blade reaches negative maximum flapping deflection at 270° azimuth angle.

Between 90° and 270° , the blade flaps downwards. In contrast to the upwards flapping discussed above, when the blade flaps down, the angle of attack of the blade

2.3 The Basic Ornicopter Principle

13

element will increase, and the increased lift force will tilt forward with regard to the blade element. This results in a positive thrust force, by which the blade is propelled.

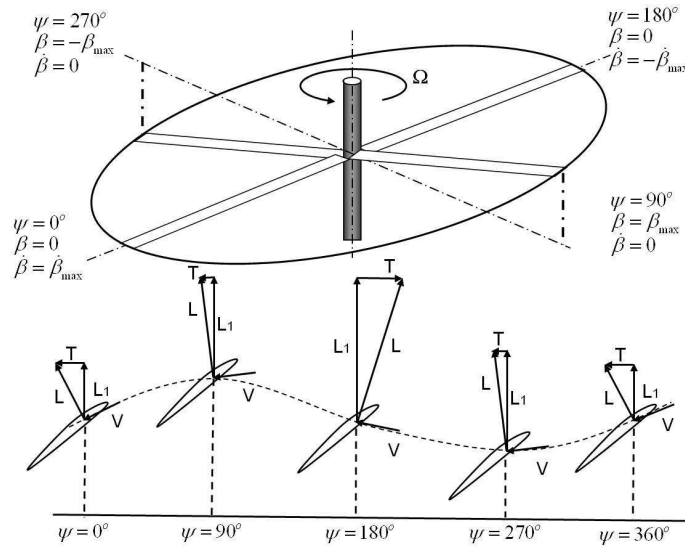


Figure 2.7: Lift and drag forces acting on an Ornicopter blade during one revolution when a constant pitch angle is applied

When a constant pitch angle is applied, the lift forces during one revolution will (averaged over one revolution) result in an upwards force and an average propulsive force. This average propulsive force is achieved because the forward horizontal component of the lift force that occurs when the blade is flapping downwards (from 90° to 270°) is much larger than the backwards horizontal component of the lift force that occurs when the blade is flapping upwards (from 0° to 90° and 270° to 360°). Thus, by setting all the Ornicopter blades at a constant pitch angle and flapping them up and down, a propulsive force is created that will rotate the blades around the rotor hub and an upwards force is created that will counteract gravity. The amount of propulsion force and the total thrust generated by the rotor are determined by the amplitude of flapping motion and the blade collective pitch. By choosing a proper combination of these two parameters, the desired forces can be achieved for trimmed flight or necessary control.

When the blades are propelled by a flapping motion one can demonstrate that the reaction torque acting on the fuselage will no longer exist. This can be explained by comparing a conventional helicopter to an Ornicopter, see Fig. 2.8 [30]. In a conventional helicopter the drag that acts on the rotor blades is counteracted by the shaft torque, which drives the rotor to rotate (see Fig. 2.8.a). As a result, there will also be a reaction torque from the rotor on the fuselage, and this reaction torque will have to be counteracted by an anti-torque device. For the Ornicopter configuration, the drag that acts on the rotor blades is counteracted by the propelling force produced by the forced flapping motion of the blades (see Fig. 2.8.b). There is thus no direct torque transferred

from the fuselage to the rotor to rotate the blades. As a consequence, there will not be a reaction torque from the rotor on the fuselage. Hence, an anti-torque device is no longer necessary.

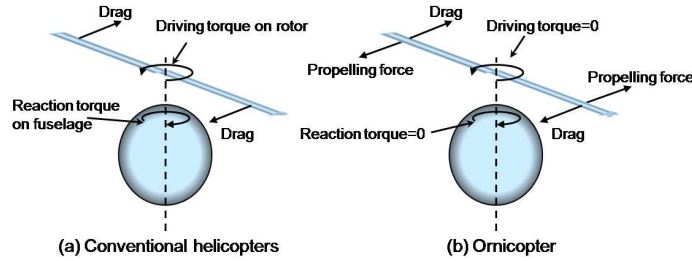


Figure 2.8: The forces and moments acting on a conventional helicopter and the Ornicopter [30]

It should also be mentioned that, for the Ornicopter design, the blade flapping motion has to be synchronized with the rotational speed of the rotor. In this manner, the forced flapping frequency can be kept close to the natural frequency of the blade flapping motion. Due to the resonance effect, the forced flapping motion can reach the maximum amplitude. In other words, in this situation, the minimum driving moment is needed for the forced flapping.

2.3.2 Controlling the Ornicopter

Yaw Control

In a conventional helicopter, yaw control is realized by the tail rotor. By increasing or decreasing the thrust of the tail rotor, the total yawing moment on the fuselage can be controlled. Since the Ornicopter obviously does not have a tail rotor, a different means for yaw control is needed.

By introducing a small amount of change in the forced flapping amplitude, the propelling force generated by the Ornicopter rotor can be controlled in order to achieve the desired yaw control moment. From Fig. 1.1, it can be seen that the propelling force is related to the amplitude of the plunge motion. By increasing the amplitude of the plunge motion (increasing h), the velocity of the vertical motion can be increased, which causes a higher effective angle of attack and larger thrust force. Similarly, the propelling force generated by the Ornicopter rotor can also be decreased when lower amplitude of the forced flapping is applied. In this manner, the Ornicopter can be controlled in the yaw direction, as shown in Fig. 2.9.

Figure 2.9.a presents the case when no yaw movement is desired (the flapping mechanism will be explained later). In this case the blades of the Ornicopter will be entirely propelled by blades flapping, and there will thus be no reaction torque acting on the fuselage. To realize this reactionless situation, a particular amplitude of the forced flapping motion will be necessary. All the engine power will be converted into the flapping

2.3 The Basic Ornicopter Principle

15

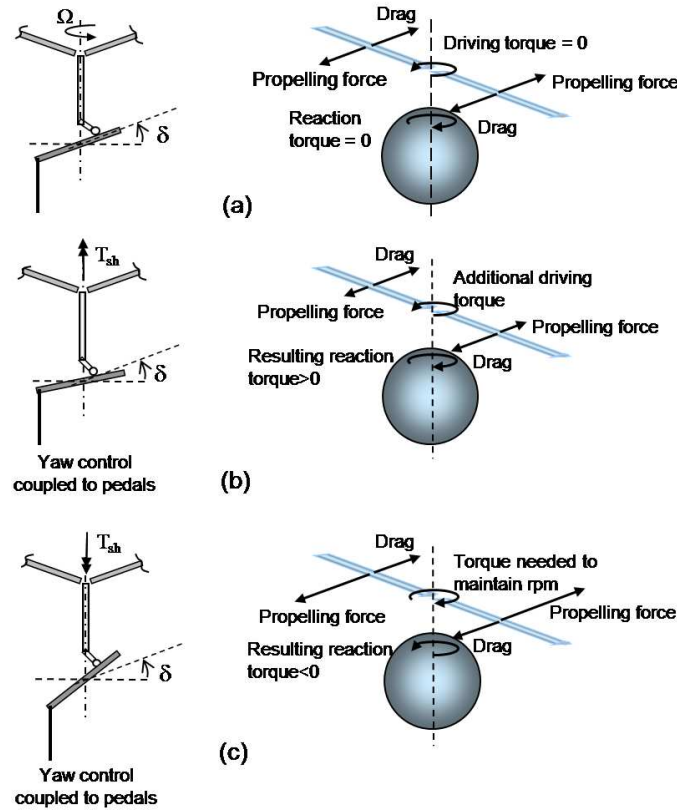


Figure 2.9: Schematic representation of yaw control by introducing a reaction torque

of the blades.

When, for the same situation, a small reduction of the flapping amplitude is chosen (Fig. 2.9.b), the propelling force generated by the active flapping will also be reduced. This implies that the flapping of the blades will not be sufficient to keep the rotor at its required rotational speed (the rotor will tend to slow down), and therefore some additional shaft torque will be needed. The same engine power is now used both for flapping of the blades and for applying some additional shaft torque. Since in this case shaft torque is directly transmitted from the fuselage to the rotor, there will also be a reaction torque acting on the fuselage. This reaction torque will cause yawing.

To yaw in the opposite direction, a larger amplitude of forced flapping motion of blades needs to be applied (Fig. 2.9.c). As a result of the larger flapping motion of the blades, the propelling force will increase and as a result the rotor will tend to speed up. In order to keep the rotor at its desired rotational speed, the rotor will have to be slowed down. The reaction torque caused by this is acting in the opposite direction as is the situation in Fig. 2.9.b, and will therefore cause a yaw movement in the opposite

2

direction, as shown in Fig. 2.9.c.

For a conventional helicopter, its tail rotor is loaded especially in hovering and low speed flight. In forward flight, the vertical fin, usually with a cambered airfoil and sometimes with a controllable surface, i.e. a rudder, provides almost all the yaw and sideslip controls. Hence, in forward flight the tail rotor of a conventional helicopter is usually unloaded. In the case of the Ornicopter, a rudder can also be used in forward flight. However, for simplicity, in this thesis it is assumed that the vertical fin is a fixed lift surface without only moveable parts. The yaw control for the Ornicopter is then achieved by changing the amplitude of the forced flapping motion on the blade.

Cyclic and Collective Control

The cyclic and collective controls for the Ornicopter are the same as those for conventional helicopters. A normal swashplate is used in the Ornicopter drive train. Using this conventional swashplate, the pitch angle of the blades can be controlled as per a conventional helicopter.

As each blade is forced to flap, their tip-path planes will be tilted in a certain direction according to the forced flapping moment. To minimise additional hub shears and moments, the average tip-path plane of all the blades should not be changed by the forced flapping motion. One possible way is to drive blades anti-symmetrically, as shown in Fig. 2.10.a [37]. These two tip-path planes tilt in opposite directions to maintain the average tip-path plane level. When the cyclic pitch control is applied, the tip-path planes of all the blades will tilt in the same way, as shown in Fig. 2.10.b. This is true for both the Ornicopter and normal helicopters.

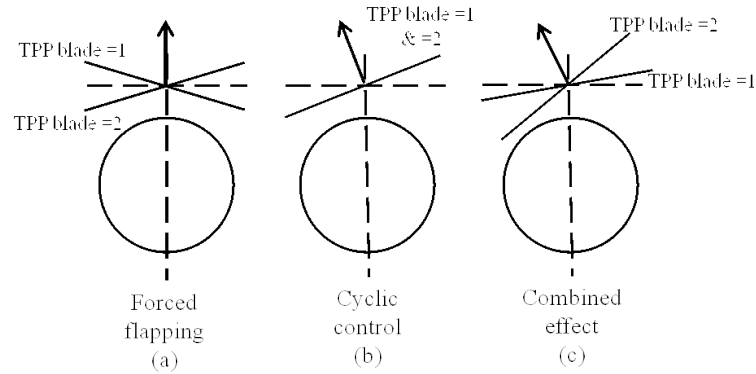


Figure 2.10: Cyclic control of Ornicopter [37]

It can thus be seen that each swashplate has a different effect on the tip-path planes of the blades. The combination of these two effects results in the total effect, as depicted in Fig. 2.10.c. Increasing the forced flapping angle and applying cyclic control are two effects that can be superimposed. Cyclic control can be achieved on top of the forced flapping motion and independent of the magnitude of this forced flapping motion. The

2.3 The Basic Ornicopter Principle

17

required cyclic control is thus not influenced by the forced flap and subsequently not influenced by the yaw control. In other words, there is a complete mutual decoupling of the cyclic and yaw control. In this manner, longitudinal and lateral control of the Ornicopter can be achieved.

As in conventional helicopters, a coupling does exist between collective control and yaw movement. If collective control is applied, the pitch angle of all the blades will increase, thereby providing more lift and also more drag. This increase in drag will tend to slow the rotor down, and thus some additional engine power will have to be transferred directly to the shaft. This causes a reaction torque which will cause the fuselage of the Ornicopter to yaw. This problem can be solved in exactly the same way as in conventional helicopters by applying yaw control in the opposite direction; however, instead of requiring a change in pitch angle of the tail rotor blades when the collective is used, in the Ornicopter configuration a change in the forced flapping angle is required. As a result the rotor will remain reactionless.

In conclusion, the Ornicopter changes the means of yaw axis control when compared to a conventional helicopter. In this new configuration, control of all axes is achieved through the main rotor.

2.3.3 Basic Flapping Configurations

For a fixed-wing Ornithopter, the optional flapping patterns are limited. Normally both sides of the flapping wing have to flap simultaneously. For a rotary wing Ornicopter, the flapping configuration can be designed, especially for a rotor that has a higher number of blades.

Some severe vibrations might occur due to the fact that within the rotor of an Ornicopter, blades (and thus masses) are moving up and down, and the magnitude of the lift vector is fluctuating and tilting backwards and forward. However, by choosing an appropriate number of blades and an appropriate flapping sequence of the blades most of these vibrations can be cancelled. Three rotor configurations for the Ornicopter have been proposed [34], including the double-teeter configuration, the 2×2 anti-symmetrical configuration (referred as 2×2 AS in what follows), and the third one, the so-called the 3-in-1-plane configuration, which generates high vibration loads. Therefore, the third configuration has never been used.

The Double Teeter Configuration

The principle of the double teeter configuration is depicted in Fig. 2.11 [34]. As indicated by its name, the rotor consists of two teetering rotors: the two opposite blades are connected like a see-saw, which means that if one blade is flapping upwards, the opposite blade is flapping downwards. All four of the blades are forced to flap with a 1/rev (once-per-revolution) frequency, which means the flapping motion achieves its maximum and minimum value once every rotor revolution. At the moment that one of the two teeters is at its maximum flapping angle, the other teeter will be in the neutral position, as shown in Fig. 2.11. The tip-path planes of the two teeters are anti-symmetrically tilted with respect to the shaft.

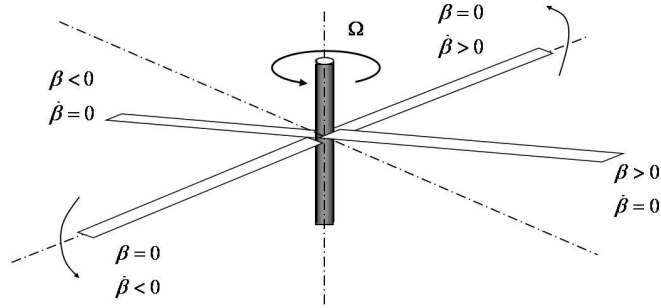


Figure 2.11: Principle of the four bladed double teeter rotor [34]

2×2 Anti-symmetrical Configuration

The rotor in the 2×2 AS configuration also consists of four blades. However, now the two opposite blades are flapping in the same direction. Consequently, (with reference to Fig. 2.12 [34]) when blade ($k = 0$) is flapping upwards, the opposite blade ($k = 2$) is flapping upwards as well, while at the same time the two other blades will be flapping downwards, and vice versa. The blades will pass through the neutral position at the same moment in time.

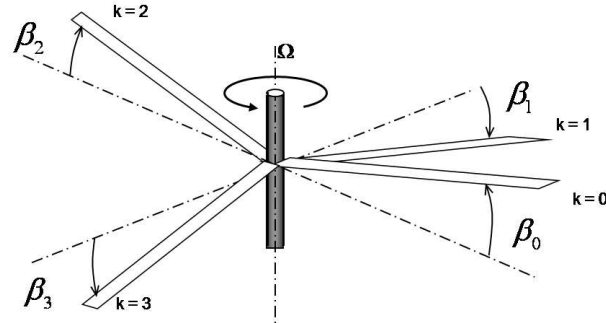


Figure 2.12: Principle of the 2×2 AS configuration [34]

Three Bladed 1-plane Configuration

For this three-bladed configuration, the three blades are always in one plane although each blade rotates in a different tip-path plane (see Fig. 2.13 [34]). The principle of 3-in-1-plane configuration is that when the first blade ($k = 0$) is at its maximum flapping angle, the other two blades ($k = 1, 2$) are at the $1/3$ negative maximum flapping angle. At this moment, the second blade is flapping upwards and the last one is flapping downwards.

The double teeter and 3-in-1-plane configurations have been chosen as concepts due

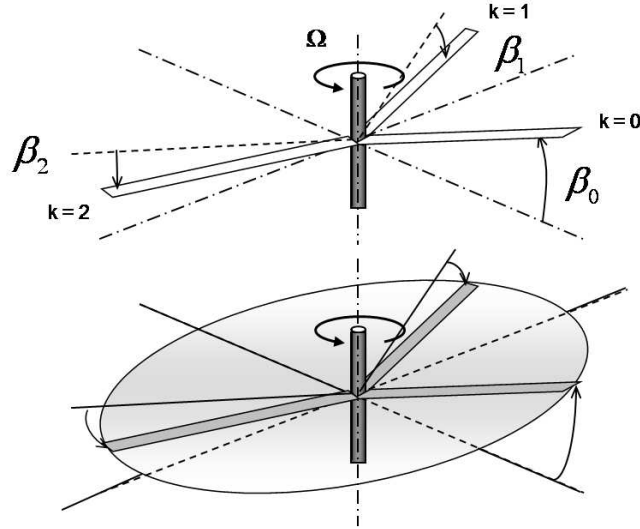


Figure 2.13: Principle of the three-bladed 1-plane rotor [34]

to their relative simplicity in the forced flapping mechanism. The double teeter was used for a wind tunnel test model [37]. However, the drawback of the first 2 mentioned configurations is that they will generate more vibratory loads on the rotor hub than the 2×2 AS configuration (more details about the vibratory loads will be discussed later, see Section 2.4.5). In this sense, although the forced flapping mechanism of the 2×2 AS configuration is more complicated, due to its expected favourable vibration characteristics, **the 2×2 AS is used as the baseline configuration for further Ornicopter analyses.**

2.4 Preliminary Theoretical Analyses

In this section, preliminary analytical calculations for Ornicopter will be introduced. The analyses for the required power, flapping moment and flapping amplitude performed in Ref [37] will be reviewed first. Afterwards, the theoretical analysis for Ornicopter is extended. The mathematical representations of flapping configurations will be explained, followed by analyses regarding Ornicopter control. At the end, vibratory loads [34] and effect of blade flexibility [35] will be briefly discussed.

A rotor model in hovering flight is developed for the above mentioned analyses. Chapter 3 develops a flight mechanics model for the Ornicopter in order to study its forward flight characteristics.

In this hovering rotor model, the blade flapping motion, rotor hub forces and moments are derived. The model is based on BET. It should be emphasized that the main purpose of developing this hovering model is to understand the basic principle of the Ornicopter concept. Therefore, some typical assumptions for the helicopter flight

2

dynamics modelling are used as follows:

1. The blades are rigid and centrally hinged;
2. The blades have uniform mass distribution;
3. The airfoil has a constant lift coefficient gradient and drag coefficient;
4. The inflow angle and blade flapping angle are small;
5. The stall effect is not considered;
6. The inflow is uniform.

A centrally-hinged rotor is considered in this model, as shown in Fig. 2.14. The Ornicopter blade is connected to the forced flapping mechanism through a spring. In this thesis, the stiffness of this spring is chosen to be the same as the equivalent flapping stiffness of the hingeless Bo-105 main rotor.

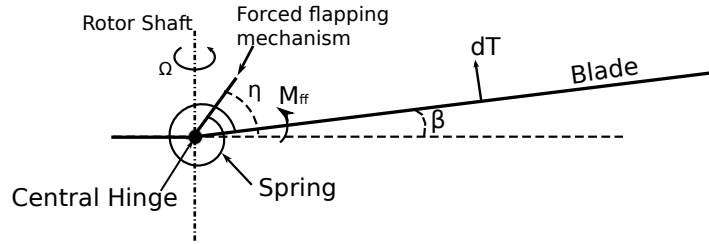


Figure 2.14: Blade configuration for the rotor model

The forced flapping mechanism moves at 1/rev frequency. Its motion (η) can be expressed similarly as the flapping motion of blades (β):

$$\begin{aligned}\eta &= \eta_{s1} \sin \psi + \eta_{c1} \cos \psi \\ \beta &= \beta_0 + \beta_{s1} \sin \psi + \beta_{c1} \cos \psi\end{aligned}\tag{2.1}$$

where β_0 , β_{s1} and β_{c1} are the blade coning, lateral and longitudinal flapping angles, η_{s1} and η_{c1} are the lateral and longitudinal flapping coefficients of the forced flapping mechanism, and ψ is the azimuth angle of blade. More detail on the derivation of the model can be found in Appendix A.

2.4.1 Power Requirement in Hover

One of the first questions that needs to be answered is related to the power consumption of the Ornicopter. Therefore, the average shaft power (P_{sh}) that is necessary to drive the rotor is derived. For this, the power needed to drive the blade element located at r_e radius position (see Fig. 2.15) is calculated, and integrated over the entire rotor blade.

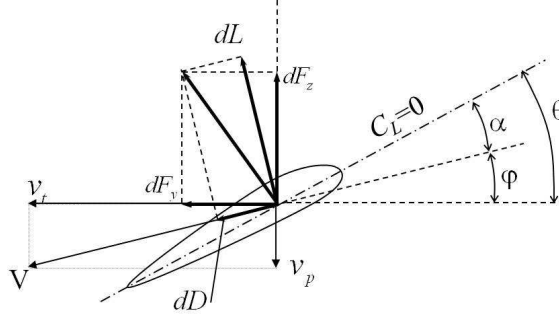


Figure 2.15: Aerodynamic environment at a typical blade element

In hovering, for a blade element shown in Fig. 2.15, the local tangential (v_t) and perpendicular (v_p) velocities can be expressed as:

$$\begin{aligned} v_p &= \dot{\beta} r_e + v_i \\ v_t &= \Omega r_e \end{aligned} \quad (2.2)$$

where $\dot{\beta}$ is the flapping velocity of blade, r_e is the radius location of the blade element, v_i is the induced velocity, and Ω is the rotational velocity of the rotor.

The induced angle at the blade element will be (see Fig. 2.15)

$$\varphi = \tan^{-1} \left(\frac{v_p}{v_t} \right) \quad (2.3)$$

The average required shaft power per blade can be calculated as:

$$P_{sh_s} = \frac{1}{2\pi} \int_0^{2\pi} d\psi \int_0^R (dL \sin \varphi + dD \cos \varphi) \Omega r_e dr_e \quad (2.4)$$

where dL and dD are the lift and profile drag force generated by a unit length of the blade element.

Assuming the induced angle is small and applying the small angle approximation results in

$$\varphi \approx \frac{v_p}{v_t} \quad (2.5)$$

$$P_{sh_s} \approx \frac{1}{2\pi} \int_0^{2\pi} d\psi \int_0^R (dL \varphi + dD) \Omega r_e dr_e \quad (2.6)$$

Substituting Eq. 2.2 and 2.5 into Eq. 2.6 results in:

$$\begin{aligned} P_{sh_s} &= \frac{1}{2\pi} \int_0^{2\pi} d\psi \int_0^R (dL v_i + dL \dot{\beta} r_e + dD \Omega r_e) dr_e \\ &= P_{i_s} + P_{p_s} + \frac{1}{2\pi} \int_0^{2\pi} M_{aero} \dot{\beta} d\psi \end{aligned} \quad (2.7)$$

where P_{i_s} is the blade induced power

$$P_{i_s} = \frac{1}{2\pi} \int_0^{2\pi} d\psi \int_0^R dL v_i dr_e \quad (2.8)$$

P_{p_s} is the blade profile power

$$P_{p_s} = \frac{1}{2\pi} \int_0^{2\pi} d\psi \int_0^R dD \Omega r_e dr_e \quad (2.9)$$

and M_{aero} is the flapping moment generated by the lift force, as:

$$M_{aero} = \int_0^R dL r_e dr_e \quad (2.10)$$

Equation 2.6 is a power equation that can be used for conventional helicopters, but note that the flapping angle (β) is negligible for a simple conventional helicopter rotor model during hover. To be able to add the mechanical flapping power to the shaft power, the equation of flapping motion for an Ornicopter blade is considered, i.e. with a mechanical flapping moment (M_{ff}) applied to the blade. The equation of blade motion in the hover can be expressed as:

$$I_\beta \ddot{\beta} = M_{aero} + M_{ff} - \Omega^2 \beta I_\beta \quad (2.11)$$

where $\ddot{\beta}$ is the flapping acceleration, I_β is the flap moment of inertia, as:

$$I_\beta = \int_0^R \rho_r r_e^2 dr \quad (2.12)$$

and $\Omega^2 \beta I_\beta$ is the flapping moment caused by the centrifugal force.

The flapping rate ($\dot{\beta}$) and acceleration ($\ddot{\beta}$) can be derived from Eq. 2.1, as:

$$\begin{aligned} \dot{\beta} &= \beta_{s1} \Omega \cos \psi - \beta_{c1} \Omega \sin \psi \\ \ddot{\beta} &= -\beta_{s1} \Omega^2 \sin \psi - \beta_{c1} \Omega^2 \cos \psi \end{aligned} \quad (2.13)$$

Combining Eq. 2.11 and Eq. 2.13, the relationship between M_{aero} and M_{ff} can be derived as:

$$M_{aero} = \Omega^2 \beta_0 I_\beta - M_{ff} \quad (2.14)$$

It should be noted that the M_{aero} and M_{ff} are functions of the blade flapping motion (β). They vary among the blade azimuth angle (ψ). Equation 2.14 is valid for all azimuth angles and it is used to derive the flapping coefficients of blades (β_0 , β_{s1} and β_{c1}) in App. A. In this section, the main interest is the required power of the Ornicopter concept, i.e. the average effects of the M_{aero} and M_{ff} in one rotation revolution. Therefore, the detailed expression of these two moments will not be considered at this moment.

Substituting Eq. 2.14 into Eq. 2.7 for blade shaft power gives:

$$\begin{aligned}
 P_{sh_s} &= P_{i_s} + P_{p_s} + \frac{1}{2\pi} \int_0^{2\pi} (\Omega^2 \beta_0 I_\beta - M_{ff}) \dot{\beta} d\psi \\
 &= P_{i_s} + P_{p_s} + \frac{1}{2\pi} \int_0^{2\pi} \Omega^2 \beta_0 \dot{\beta} d\psi - \frac{1}{2\pi} \int_0^{2\pi} M_{ff} \dot{\beta} d\psi \\
 &= P_{i_s} + P_{p_s} - P_{ff_s}
 \end{aligned} \tag{2.15}$$

where P_{ff_s} denotes the flapping power, i.e. the average power per revolution exerted by the forced flap mechanism on the blade:

$$P_{ff_s} = \frac{1}{2\pi} \int_0^{2\pi} M_{ff} \dot{\beta} d\psi \tag{2.16}$$

Summing the shaft power for all the blades, the Ornicopter rotor shaft power is:

$$\begin{aligned}
 P_{sh} &= \sum_{k=1} N_b P_{sh_s}^{(k)} \\
 &= \sum_{k=1} N_b P_{i_s}^{(k)} + \sum_{k=1} N_b P_{p_s}^{(k)} - \sum_{k=1} N_b P_{ff_s}^{(k)} \\
 &= P_i + P_p - P_{ff}
 \end{aligned} \tag{2.17}$$

where P_i , P_p and P_{ff} are the total rotor induced power, profile power and flapping power.

Equation 2.17 shows that if the flapping power (P_{ff}) is chosen to be sufficiently large, the shaft power can be reduced to zero. This means that if the rotor is driven by the forced flap mechanism, no additional shaft power will be needed (engine power, however, will still be needed to flap the blades). Moreover, the shaft power, in other words, the shaft torque, can be controlled by applying different flapping power. Therefore zero, positive and negative shaft torques can be achieved for yaw control.

It can also be seen that the flapping power just replaces the shaft power. In the torqueless condition ($P_{sh} = 0$), the flapping power will be the same as the sum of induced power and profile power ($P_{ff} = P_i + P_p$). The flapping power will thus not be larger than the power that is transferred to the rotor in conventional helicopters. As a matter of fact, the total power needed will be less for an Ornicopter than a conventional helicopter since the tail rotor, which normally consumes 5 – 10% of the total power, is no longer present.

2.4.2 Forced Flapping Moment and Angle

Integrating the lift force along the radial direction, the aerodynamic flapping moment can be expressed as (see Eq. A.22):

$$M_{aero} = \frac{\gamma I_\beta}{2} \Omega^2 \left(\frac{\theta}{4} - \frac{\lambda_i}{3} - \frac{\beta'}{4} \right) \tag{2.18}$$

where

$$\begin{aligned}\beta' &= \frac{\partial \beta}{\partial \psi} \\ &= \beta_{s1} \cos \psi - \beta_{c1} \sin \psi\end{aligned}\tag{2.19}$$

Defining the non-dimensional aerodynamic flapping moment (m_{aero}) and the non-dimensional mechanical flapping moment (m_{ff}) as:

2

$$\begin{aligned}m_{aero} &= \frac{M_{aero}}{\Omega^2 I_\beta} \\ m_{ff} &= \frac{M_{ff}}{\Omega^2 I_\beta}\end{aligned}\tag{2.20}$$

and substituting Eq. 2.18 into Eq. 2.14 gives the relation between the flapping angle (β) and the mechanical flapping moment (m_{ff}) as:

$$\frac{\gamma}{2} \left(\frac{\theta}{4} - \frac{\lambda_i}{3} - \frac{\beta'}{4} \right) = \beta_0 - m_{ff}\tag{2.21}$$

Assuming:

$$m_{ff} = C + A \sin \psi + B \cos \psi\tag{2.22}$$

results in Eq. 2.21 to be rewritten as:

$$\frac{\gamma}{2} \left(\frac{\theta}{4} - \frac{\lambda_i}{3} - \beta_0 \right) - \frac{\gamma}{8} (\beta_{s1} \cos \psi - \beta_{c1} \sin \psi) + C + A \sin \psi + B \cos \psi = 0\tag{2.23}$$

Collecting coefficients for constant and harmonic terms in Eq. 2.23 results in:

$$\frac{\gamma}{2} \left(\frac{\theta}{4} - \frac{\lambda_i}{3} - \beta_0 \right) + C + \left(\frac{\gamma}{8} \beta_{c1} + A \right) \sin \psi - \left(\frac{\gamma}{8} \beta_{s1} - B \right) \cos \psi = 0\tag{2.24}$$

The solution of the non-dimensional coefficients of mechanical flapping moment can be obtained by equating the constant and the harmonic coefficients of Eq. 2.24 to zero. This results in:

$$\begin{aligned}A &= -\frac{\gamma}{8} \beta_{c1} \\ B &= \frac{\gamma}{8} \beta_{s1} \\ C &= -\frac{\gamma}{2} \left(\frac{\theta}{4} - \frac{\lambda_i}{3} - \beta_0 \right)\end{aligned}\tag{2.25}$$

From Eq. 2.25 the relation can be found between the amplitude of the flapping angle ($\hat{\beta}$) and the amplitude of the non-dimensional flapping moment (\hat{m}_{ff}) is:

$$\hat{m}_{ff} = \sqrt{A^2 + B^2} = \frac{\gamma}{8} \hat{\beta}\tag{2.26}$$

Finally, substituting the flapping motion (Eq. 2.1) and the mechanical flapping moment (Eq. 2.22 and 2.25) into the expression of the flapping power (Eq. 2.16) gives:

$$\begin{aligned}
 P_{ffs} &= \frac{1}{2\pi} \int_0^{2\pi} \left(C - \frac{\gamma}{8} \beta_{c1} \sin \psi + \frac{\gamma}{8} \beta_{s1} \cos \psi \right) \Omega^2 I_\beta \\
 &\quad \times (\beta_{s1} \Omega \cos \psi - \beta_{c1} \Omega \sin \psi) d\psi \\
 &= \frac{I_\beta \Omega^3}{2} \frac{\gamma}{8} \hat{\beta}^2 \\
 &= \frac{I_\beta \Omega^3}{2} \frac{8}{\gamma} \hat{m}_{ff}^2
 \end{aligned} \tag{2.27}$$

2

For the Ornicopter, P_i and P_p can be calculated using BET (blade element theory) in the same way they are calculated for conventional helicopters. Therefore, the P_{ff} needed to reach the torqueless condition is known. Then Eq. 2.27 can be used to calculate the required amplitude of the flapping angle and mechanical flapping moment.

From Fig. 2.14, one can see that the forced flapping moment (M_{ff}) is:

$$M_{ff} = (\eta - \beta) K_\beta \tag{2.28}$$

where K_β is the stiffness of the spring which connects the forced flapping mechanism and the blade.

Substituting β and η (Eq. 2.1) into Eq. 2.28 and converting it into the non-dimensional form, one can get:

$$m_{ff} = \frac{K_\beta}{\Omega^2 I_\beta} [-\beta_0 + (\eta_{s1} - \beta_{s1}) \sin \psi + (\eta_{c1} - \beta_{c1}) \cos \psi] \tag{2.29}$$

Comparing Eq. 2.29 and 2.22, it can be found that:

$$\begin{aligned}
 A &= \frac{K_\beta}{\Omega^2 I_\beta} (\eta_{s1} - \beta_{s1}) = -\frac{\gamma}{8} \beta_{c1} \\
 B &= \frac{K_\beta}{\Omega^2 I_\beta} (\eta_{c1} - \beta_{c1}) = \frac{\gamma}{8} \beta_{s1}
 \end{aligned} \tag{2.30}$$

Defining the blade flap frequency ratio (λ_β) and stiffness number (S_β) as:

$$\begin{aligned}
 \lambda_\beta^2 &= 1 + \frac{K_\beta}{I_\beta \Omega^2} \\
 S_\beta &= \frac{\lambda_\beta^2 - 1}{\gamma/8}
 \end{aligned} \tag{2.31}$$

the motion of the forced flapping mechanism can be derived from Eq. 2.30 as:

$$\begin{aligned}
 \eta_{s1} &= -\frac{1}{S_\beta} \beta_{c1} + \beta_{s1} \\
 \eta_{c1} &= \frac{1}{S_\beta} \beta_{s1} + \beta_{c1}
 \end{aligned} \tag{2.32}$$

The required motion amplitude of the forced flapping mechanism ($\hat{\eta}$) can be calculated as:

$$\begin{aligned}\hat{\eta}^2 &= \eta_{s1}^2 + \eta_{c1}^2 \\ &= \frac{1 + S_\beta^2}{S_\beta^2} \hat{\beta}^2\end{aligned}\quad (2.33)$$

As an example of realistic values for the flapping angle and flapping moment, the Bo-105 helicopter is used. Calculating the amplitude of the dimensional flapping moment and the amplitude of the flapping angle gives:

$$\begin{aligned}\hat{M}_{ff} &= 34141 \quad \text{Nm} \\ \hat{\beta} &= 6.59 \quad \text{deg} \\ \hat{\eta} &= 18.1 \quad \text{deg}\end{aligned}\quad (2.34)$$

The amplitude of the forced flapping angle is thus very modest. It does not exceed the flapping angle limitation. For example, the lateral flapping limitation for most modern helicopters is about 10 deg [27, p. 154]. For the Bo-105 rotor (rotor radius is 4.91 m), the maximum flapping displacement at the blade tip is approximately 0.565 m corresponding to the flapping angle calculated above.

Regarding the forced flapping mechanism, the required motion amplitude is higher than that of the blades. This is due to the fact the mechanism is connected with the blade through a spring with limited stiffness. The motion of the forced flapping mechanism and the blade flapping motion will be identical if the spring is replaced by a rigid link, i.e. a spring with infinite stiffness. From the above example, one can see that for the Ornicopter rotor has the same flap stiffness as a hinge-less rotor, i.e. the Bo-105 rotor, the required motion amplitude of the forced flapping mechanism is also modest.

2.4.3 Flapping Configuration

The three proposed Ornicopter flapping configurations have been introduced in the previous section (see 2.3.3). For further analyses, a more detailed mathematical representation for flapping configurations is needed, which will be discussed in this section.

The motion of the forced flapping mechanism is similar to the flapping motion of blades:

$$\eta = \eta_{s1} \sin(\psi) + \eta_{c1} \cos(\psi) \quad (2.35)$$

Different coefficients (η_{s1} and η_{c1}) will be applied to each blade to form the desired flapping configuration, and these coefficients can be used as the parameter representing the flapping configuration. However, in this manner, too many parameters will be introduced, i.e. 8 coefficients for a rotor with 4 blades, and those coefficients do not directly represent the most important characteristics of the flapping motion, namely the amplitude and phase angle of the flapping motion.

2.4 Preliminary Theoretical Analyses

27

In this sense, Eq. 2.35 is next rewritten as:

$$\eta = \hat{\eta} \cos(\psi - \psi_\eta) \quad (2.36)$$

where the $\hat{\eta}$ is the amplitude of the flapping motion and the ψ_η is the azimuth angle where the flapping motion reaches the positive maximum displacement.

In this form, the physical meaning of parameters ($\hat{\eta}$ and ψ_η) is more clear. Meanwhile, as the flapping amplitude of the forced flapping mechanism is the same among all the blades, the number of parameters needed to describe the motion of forced flapping mechanism reduces to $N_b + 1$, i.e. N_b phase angles ($\psi_\eta^{(k)}$) and the flapping amplitude $\hat{\eta}$.

Moreover, the design of the flapping configuration (ψ_η) and the working condition ($\hat{\eta}$) can be separated. A series of ψ_η (one for each blade) will define the flapping configuration, as shown in Tab. 2.3. As discussed before, the amplitude of the forced flapping affects the rotor torque of the Ornicopter. Therefore, the flapping amplitude of forced flapping mechanism ($\hat{\eta}$) is the yaw control input for the Ornicopter. Its effects will be demonstrated by an hovering Ornicopter rotor model in the following discussions.

Table 2.3: Flapping sets for different configurations

Configuration	N_b	$\psi_\eta^{(k)} (\pi)$			
		1	2	3	4
Double Teeter	4	0	1	0	1
2×2 AS	4	0	3/2	1	1/2
3 bladed 1-plane	3	0	4/3	2/3	/

The coefficients (η_{s1} and η_{c1}) as used in the blade flapping EoM can be calculated with:

$$\begin{aligned} \eta_{s1} &= \hat{\eta} \sin(\psi_\eta) \\ \eta_{c1} &= \hat{\eta} \cos(\psi_\eta) \end{aligned} \quad (2.37)$$

2.4.4 Controlling the Ornicopter

In the previous section (see 2.3.2), control of the Ornicopter was generally discussed and some conclusions were drawn. In this section, with the Ornicopter model in hovering, those conclusions will be theoretically proved.

Average Tip Path Plane

From the hovering rotor model derived in Appendix A, one can see that the blade flapping motion is the superposition of forced flapping motion and the ‘conventional’ flapping motion (see Eq. A.32). Combining the flapping motion of all the blades, the

average tip-path plane of the Ornicopter rotor can be derived as (see Eq. A.35):

$$\begin{aligned}\vec{\beta}_{ave} &= \vec{\beta}_\theta + (\lambda_\beta^2 - 1) \mathbf{A}^{-1} \times [0, \bar{\eta}_{s1}, \bar{\eta}_{c1}]^\top \\ &= \vec{\beta}_\theta + \vec{\beta}_{ff}\end{aligned}\quad (2.38)$$

where \mathbf{A} is the coefficients matrix of the blade flapping EoM, as shown in Eq. A.28, $\bar{\eta}_{s1}$ and $\bar{\eta}_{c1}$ are the average flapping coefficients of the forced flapping mechanism:

2

$$\begin{aligned}\bar{\eta}_{s1} &= \sum_{k=1}^{N_b} \eta_{s1}^{(k)} \\ \bar{\eta}_{c1} &= \sum_{k=1}^{N_b} \eta_{c1}^{(k)}\end{aligned}\quad (2.39)$$

From Eq. 2.38 one can see that the average TPP of Ornicopter rotor is a linear combination of ‘conventional’ flapping ($\vec{\beta}_\theta$) and forced flapping ($\vec{\beta}_{ff}$).

The rotor hub pitch and roll moments are correlated with the average TPP. To minimise the impacts of forced flapping on these hub moments, the average TPP should not be affected by the active flapping. This can be achieved by choosing a certain flapping configuration, i.e. keeping the average flapping coefficients of forced flapping mechanism at zero ($\bar{\eta}_{s1} = 0$ and $\bar{\eta}_{c1} = 0$). In this manner, the average TPP of Ornicopter rotor will be the same as a conventional helicopter as shown in Fig. 2.10. This introduces one of the requirements of the flapping configuration design, namely **the average flapping coefficients of forced flapping mechanism should be zero** (referred to as the zero average flapping requirement in the following).

Recalling the three flapping configurations proposed in Section 2.3.3, one can see from Tab. 2.3 and Eq. 2.37 that all these three configurations satisfy the zero average flapping requirement proposed above.

Yaw Control

The yaw control of Ornicopter is one of the fundamental characteristics of this new concept. The relation between the amplitude of active flapping and the main rotor torque was discussed in Section 2.3.2. The theoretical analyses based on the Ornicopter hovering model will show the same result.

For a flapping configuration that matches the zero average flapping requirement ($\bar{\eta}_{s1} = 0$ and $\bar{\eta}_{c1} = 0$), the main rotor torque can be derived as (see Eq. A.44):

$$C_Q = C_T \lambda_i + C_{Q0} - \frac{1}{16} \sigma C_{L\alpha} c_{17} \hat{\eta}^2 \quad (2.40)$$

where c_{17} is a constant coefficient determined by the rotor design (see Appendix A for more details).

One can see from Eq. 2.40 that the main rotor torque of the Ornicopter consists of three parts: the induced torque caused by rotor thrust and induced velocity ($C_T \lambda_i$), the

2.4 Preliminary Theoretical Analyses

29

profile torque caused by profile drag (C_{Q0}) and the propulsive torque generated by active flapping ($\frac{1}{16}\sigma C_{L\alpha} c_{17}\hat{\eta}^2$). The former two parts are the same as those for conventional helicopters. The propulsive torque is proportional to the amplitude of flapping motion of the forced flapping mechanism ($\hat{\eta}$). In this sense, the $\hat{\eta}$ is the necessary yaw control input for the Ornicopter.

As the C_T and C_{Q0} are not affected by the cyclic pitch control (see Eq. A.13), the main rotor torque is not correlated with the cyclic pitch control. This indicates that the Ornicopter will not have an additional yaw coupling response to lateral and longitudinal control as discussed before.

The $\hat{\eta}$ is the yaw control input for the Ornicopter, as the tail rotor collective pitch (θ_{tr}) is in the case of conventional helicopters. In order to keep the consistency of control input notation, in this thesis the θ_{ff} will be used while discussing the Ornicopter yaw control.

Cyclic and Collective Pitch Control

The total hub forces and pitch/roll moments are also derived in Appendix A. Similarly to the yaw control, if the flapping configuration has $\bar{\eta}_{s1} = 0$ and $\bar{\eta}_{c1} = 0$, the rotor hub forces and pitch/roll moments will be uncoupled with the yaw control input and they will be the same as conventional helicopters, i.e.:

$$C_T = \frac{1}{2}\sigma C_{L\alpha} \left(\frac{\theta_0}{3} - \frac{\lambda_i}{2} \right) \quad (2.41)$$

$$C_H = \frac{1}{2}\sigma C_{L\alpha} (c_{11}\theta_{s1} + c_{12}\theta_{c1}) \quad (2.42)$$

$$C_S = \frac{1}{2}\sigma C_{L\alpha} (-c_{12}\theta_{s1} + c_{11}\theta_{c1}) \quad (2.43)$$

$$C_L = -\frac{1}{2}\frac{\lambda_\beta^2 - 1}{\gamma}\sigma C_{L\alpha} (c_5\theta_{s1} + c_3\theta_{c1}) \quad (2.44)$$

$$C_M = -\frac{1}{2}\frac{\lambda_\beta^2 - 1}{\gamma}\sigma C_{L\alpha} (-c_3\theta_{s1} + c_5\theta_{c1}) \quad (2.45)$$

where θ_0 , θ_{s1} and θ_{c1} are the collective, longitudinal and lateral cyclic control input respectively, and c_{11} , c_{12} , c_3 and c_5 are the coefficients derived in Appendix A, which are correlated to the rotor design, inflow ratio and collective pitch control.

Overall, for the Ornicopter concept, the $\hat{\eta}$ will be used as the yaw control input. By choosing a proper flapping configuration ($\bar{\eta}_{s1} = 0$ and $\bar{\eta}_{c1} = 0$), the yaw and cyclic/collective pitch controls of the Ornicopter can be decoupled, i.e. this revolutionary yaw control method will not affect the cyclic/collective pitch control of the Ornicopter, and they will be the same as those used in conventional helicopters.

2.4.5 Vibratory Loads

One may have noticed from Fig. 2.7 that the lift generated by the blade element varies during one revolution. This will likely cause vibratory loads on the rotor hub.

This kind of variation can cause both a $1/rev$ fluctuation and a $2/rev$ fluctuation on the hub forces and moments generated by a single blade. This will be explained below.

For example, the propelling force generated by the forced flap is equal to the lift times the inflow angle, while both the lift and inflow angle consist of a constant part and a $1/rev$ fluctuation. The $1/rev$ fluctuation on the propelling force is thus caused by the constant part of the lift multiplied by the fluctuating part of the inflow angle and by the constant part of the inflow angle multiplied by the fluctuating part of the lift. The $2/rev$ fluctuation on the propelling force occurs due to the multiplication of the fluctuating part of the lift with the fluctuating part of the inflow angle. This occurs in the case of hovering flight without cyclic control. In more realistic flight conditions, both flight velocity and cyclic control will introduce more harmonic components.

By choosing an appropriate number of blades and an appropriate flapping sequence between the different blades, the vibratory loads on the Ornicopter’s rotor can be minimized. In order to determine the configuration that causes the least vibrations, an exploratory study was performed for hovering using a rigid rotor model (see Ref [34]). All three Ornicopter configurations mentioned above were investigated from the vibratory point of view.

The vibratory characteristics of the three configurations are summarized in Tab. 2.4. One can see for example that the double teeter configuration has $2/rev$ harmonic components in horizontal (H) and sideways (S) in-plane hub forces, as well as $2/rev$ components in pitch (M) and roll (L) hub moments.

Table 2.4: Harmonic components on the rotor hub

		Forces($1/rev$)			Moments($1/rev$)		
		T	H	S	L	M	N
Configuration	Double teeter		2	2	2	2	
	2×2 AS						2
	3 bladed 1-plane		2	2	1,2	1,2	

Apparently, the 2×2 AS configuration is the one that generates the fewest harmonic forces and moments. In the meanwhile, taking into account the order of the magnitude of the vibration [34], it is concluded that the 2×2 AS configuration is the best choice for the Ornicopter from a vibratory point of view. Therefore, **the 2×2 AS configuration is used as the baseline configuration of the Ornicopter.**

2.4.6 The Effect of Blade Flexibility

The theory and the calculations performed so far are all based on the assumption of rigid rotor blades. A question that could arise is whether the introduction of flexible

blades will have an effect on any of the key characteristics of the Ornicopter, including the flapping power requirement, flapping angle, flapping moment, rotor torque, blade bending or rotor thrust.

The equations of motion for a flexible blade in forced vibration by the forced flapping mechanism were derived [35]. Subsequently, these equations were used to derive key characteristics of the Ornicopter with flexible blades. With one mode (rigid) and two mode (flexible) approximations, calculations have shown that the flexibility of the blades does not affect the key characteristics of the Ornicopter mentioned above, except for the flapping angle and flapping moment [35].

It was demonstrated that, despite the flexibility, it is still possible to achieve a propelling and lifting force by forced flapping of the blades, and it is thus still possible to realize a single rotor without reaction torque. Calculations show that the Ornicopter rotor with flexible blades requires the same power as a rotor with rigid blades, which means that no power is lost due to the flexibility of the blades.

The major influence of the flexible blades concerns the flapping angle at the blade root. Due to the flexibility, the flapping angle at the blade root of the flexible blade is larger than that of a rigid blade, as shown in Fig. 2.16 [35]. Different lines in Fig. 2.16 present the bending of a flexible blade at different azimuth angles during one revolution. An azimuth angle difference of $\pi/4$ occurs between two successive lines. One can see from Fig. 2.16 that due to deformation of the blade, the displacement of the outer part of the flexible blade is smaller than that of a rigid blade. On the contrary, at the inner part of the flexible blade, the displacement is higher than that of a rigid blade and a higher root flapping angle can be found for the flexible blade.

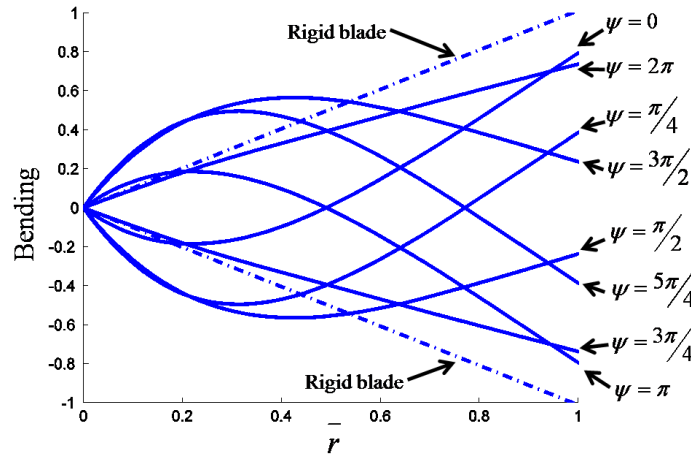


Figure 2.16: Bending of a flexible blade and a rigid blade for a given flapping power [35]

As a consequence of the larger blade root angle, the angular velocity of the flapping motion at the blade root will also be larger for a flexible blade. It appeared that, for

the same amount of power, a smaller flapping moment will be necessary for a flexible blade when compared to a rigid blade.

2.5 Practical Implementation and Test

2

2.5.1 Forced Flapping Mechanisms

Between 2002 and 2008, different forced flapping mechanisms have been proposed and tested in order to actively flap the Ornicopter’s blades [36]. All the flapping mechanisms are designed with the same basic principle, i.e. to generate an extra forced flapping moment on the blades. This moment needs to be adjustable for yaw control. The following flapping mechanisms were designed: 1) the swashplate mechanism, 2) the gearwheel mechanism, 3) the eccentric mechanism, and 4) the multiple disc mechanism.

The Swashplate Mechanism

Figure 2.5 shows the principle of the Ornicopter’s swash plate mechanism, which was patented by the TU Delft [33], including a force-flapping swashplate and a normal swashplate. When the rotor is rotating, the push rod will move up and down because of the force-flapping swashplate and hence the blades will be forced to flap. Since the push rod is driven by the swashplate, the frequency of its motion is the same as the rotation frequency of the rotor. Therefore, the forced flapping motion is synchronized with the rotation of the rotor.

The amplitude of the periodic vertical movement of the push rod depends on the tilt angle of the non-rotating swash plate. Therefore the amplitude of the forced flapping motion of the blades can be controlled by this forced flapping swashplate.

This mechanism was used for the wind tunnel tests see Fig. 2.17 [36]. For practical reasons, a modification was made to this mechanism, namely: the force-flapping swashplate was replaced by two thin section bearings. These two bearings have different diameters: one bearing fits within the other bearing. Looking at Fig. 2.17, one can see that each Ornicopter blade is connected to one of the bearings by a flapping link. When the swashplate has an inclination, the flapping link will glide along an inclined plane, thus forcing the blade, which it is connected to, to flap up and down with a $1/rev$ frequency.

The drawback of this modification is that the adjustment of the flapping mechanism is laborious and the orientation of the swashplates (to achieve larger or smaller flapping angles) can only be changed when the blades are not rotating [36]. However, the flapping mechanism in itself is relatively simple.

Incorporating a mechanism capable of adjusting the orientation of the swashplates while the blades are rotating would make the swashplate mechanism useful for a realistic application, although it would be more complicated.

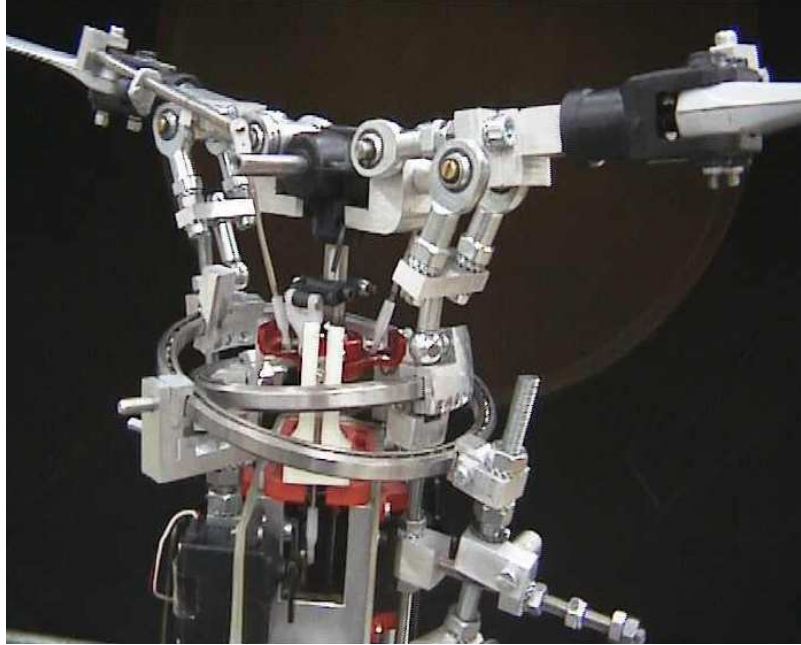


Figure 2.17: The windtunnel test model with swashplate mechanisms [36]

The Gearwheel Mechanism

The gearwheel mechanism was introduced and used for the Ornicopter demonstrator. The gearwheel mechanism was specifically designed for a four-blade rotor. However, the basic concept of this mechanism could be applied to a rotor with a different number of blades.

This mechanism has one or two sets of gearwheels, and each set consists of five gearwheels in a planetary system, as shown in Fig. 2.18 (only one rotating gearwheel is presented for clearance). This means that four of the gearwheels move around the middle gearwheel. A more detailed design is presented in Fig. 2.19 [16].

From Fig. 2.19 it can be seen that the middle gearwheel is attached to a solid shaft (the inner shaft) that is connected to the hull of the demonstrator model. The middle gearwheel will stay locked in the same position with respect to the hull. The outer four gearwheels are connected to the structure of the rotor head by smaller shafts. This structure is connected to a main shaft (the outer shaft) that rotates at the same speed as the normal rotor. This shaft is hollow, which allows the fixed shaft to run through. The rotor head therefore rotates with a normal RPM. This means that the rotor head structure and the four shafts of the outer gearwheels rotate around the fixed, middle gearwheel [36].

While the rotor is rotating, the rotating gearwheel will be driven by the fixed gear-

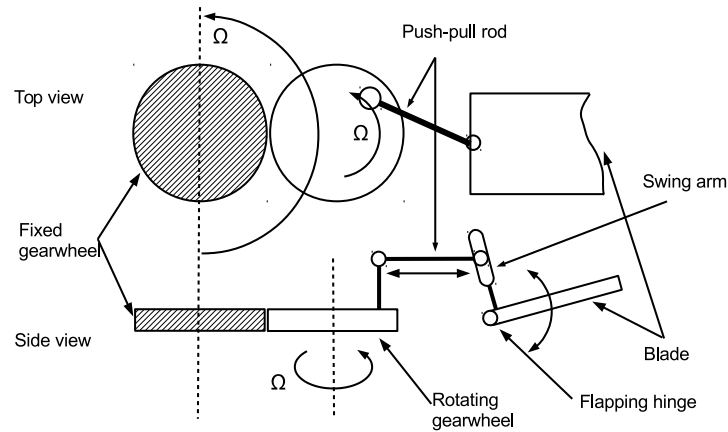


Figure 2.18: Sketch of the gearwheel mechanism

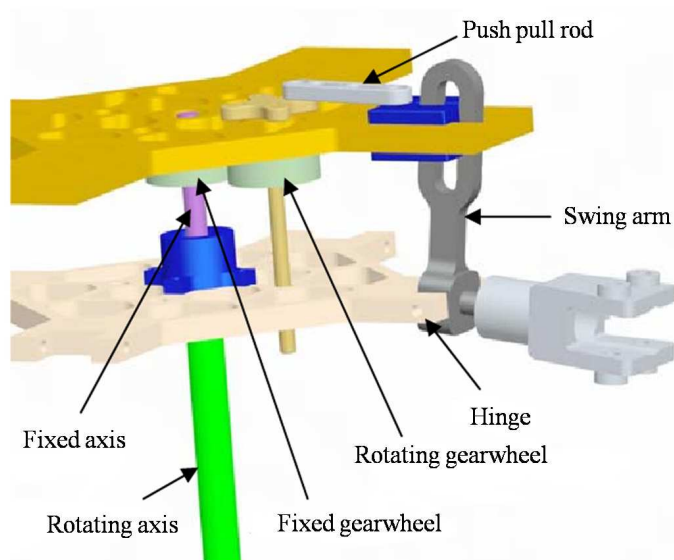


Figure 2.19: Detailed design of the gearwheel mechanism [16]

wheel to rotate. This rotational motion is converted to a reciprocal motion by the push-pull rod connected to the rotating gearwheel, and hence the blade will be forced to flap, see Fig. 2.19. The entire upper structure of the mechanism is moveable along the vertical axis. With this design, the vertical distance between the push -pull rod and

the flapping hinge can be adjusted to get a desired forced flapping angle. The higher the upper plate is, the smaller forced flapping angle will be generated.

The Eccentric Mechanism

The eccentric mechanism is designed for the double teeter configuration. As the name suggests, this mechanism is placed at a certain distance from the rotor axis (the eccentricity ‘ e ’), see Fig. 2.20. This mechanism consists of a cross, which can rotate around its own axis. All the blades are attached to the cross through a spring.

2

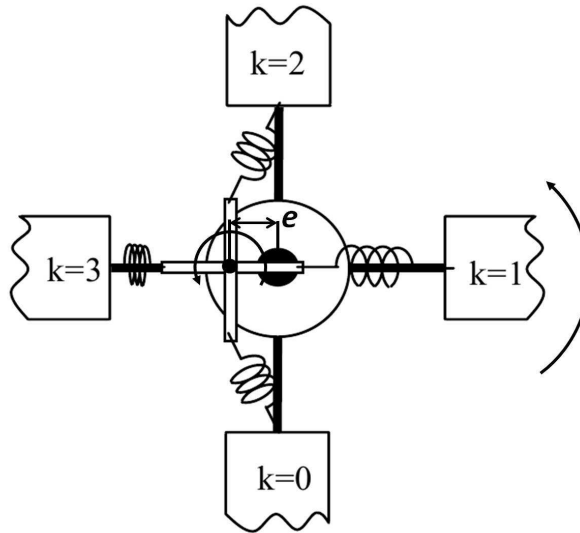


Figure 2.20: Principle of the eccentric mechanism [16]

From Fig. 2.20 one can see that during one revolution, the spring will be stretched ($k=1$) and compressed ($k=3$), and thus the blade will be forced to flap. Meanwhile, the magnitude of the forced flapping can be controlled by adjusting the eccentricity (e). Increasing the eccentricity will result in a larger forced flapping.

To apply this mechanism to the double teeter configuration, the two teeters are mounted on top of each other, and the eccentric mechanism is added in between, as shown in Fig. 2.21.

In Fig. 2.21, a spring will be stretched when the corresponding blade moves to the right-hand side of the rotor shaft. This will generate a downwards flapping moment on the top teeter, or a upwards flapping moment on the lower teeter. In this manner, the two teeters will be forced to flap in opposite directions and form a double teeter configuration.

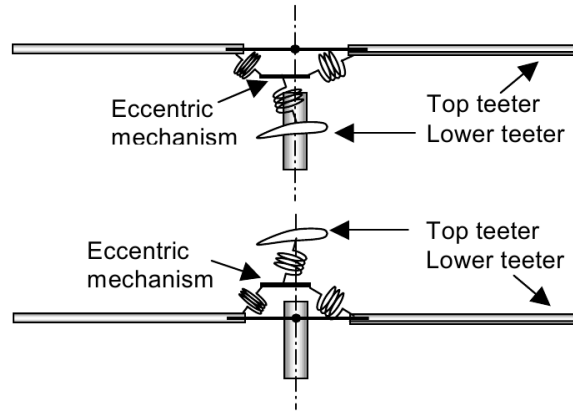


Figure 2.21: The eccentric mechanism for the double teeter configuration [16]

The Multiple Disc Mechanism

Similarly to the eccentric mechanism, this multiple disc mechanism also uses an eccentricity, however in a slightly different way. Recalling Fig. 2.21, it can be found that in the eccentric mechanism, two blades at opposite positions will be forced to flap in the same TPP as a teeter rotor. To achieve the 2×2 AS configuration, multiple eccentric mechanisms (multiple discs) are used as shown in Fig. 2.22.

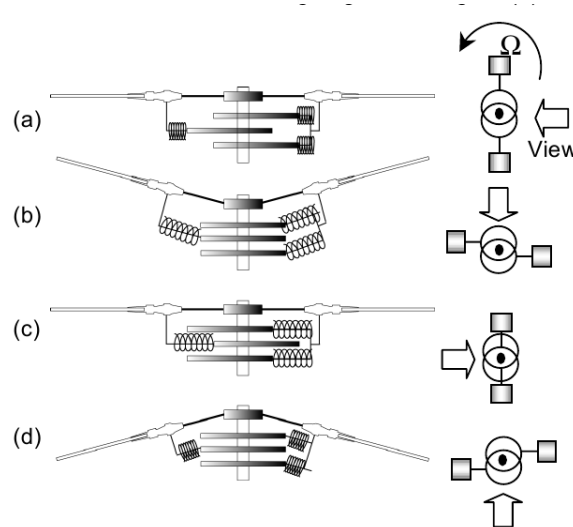


Figure 2.22: Principle of the multiple disc mechanism [16]

In this mechanism, those discs will be separated into two groups, and the eccentric-

ities of the two groups are in the opposite directions. In this manner, those two blades shown in Fig. 2.22 will flap ant-symmetrically.

To obtain the actual 2×2 AS configuration which consists of four blades, a second blade pair is connected to the first one by a diamond shaped frame, see Fig. 2.23. When the first blade pair (blade 1 and 3) is pushed to flap up, the frame will pull the second blade pair (blade 2 and 4) and force them to flap downwards. Thus the 2×2 AS configuration can be formed.

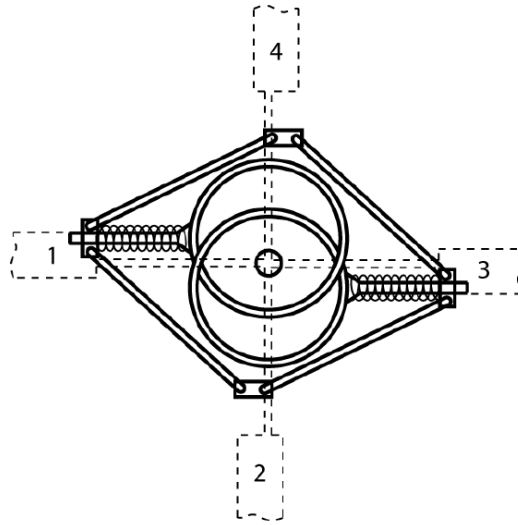


Figure 2.23: Multiple disc mechanism for 2×2 AS configuration [16]

2.5.2 Insight of the Shaft Torque

In Section 2.4, the theoretical analyses show that the Ornicopter rotor can drive itself to rotate by active flapping. However, for the flapping mechanisms introduced above, the engine still provides torque on the rotor shaft, which causes a reaction torque on the fuselage. This seems different from the fundamental of the Ornicopter concept. As a matter of fact, the forced flapping mechanism will generate a torque on the fuselage to counteract the reaction torque caused by the engine. Therefore the Ornicopter can reach a torque-less state.

The swashplate mechanism (Fig. 2.5) can be used as an example, as shown in Fig. 2.24. The push-pull rod slides on the force-flapping swash plate and drives the blades to flap. The total force (N) between the swash plat and the rod is perpendicular to the swash plat (friction is neglected). This force can be decomposed into a vertical force (F_1) and a horizontal force (F_2). The F_1 is the force that drives the blades to flap. The F_2 is the one that causes a torque on the forced flapping mechanism, and hence a torque on the fuselage.

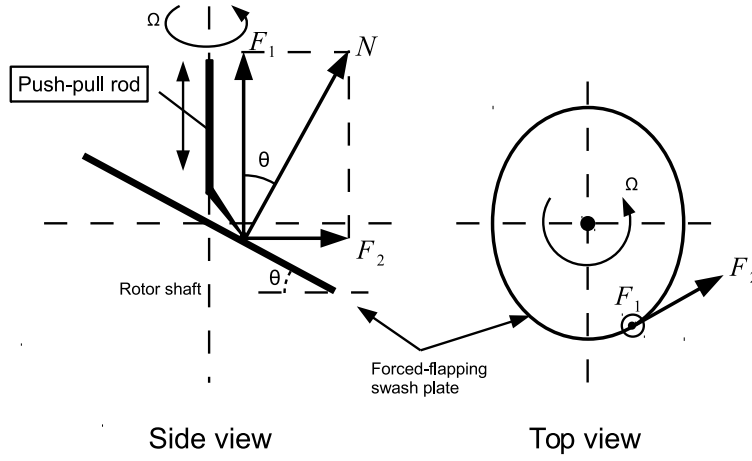


Figure 2.24: Forces on the forced-flapping swash plate

It should be emphasized that the push-pull rod can move only within the force-flapping swash plate, i.e. there is a bilateral constraint between the force-flapping swash plate and the push-pull rod. For clarity of the figure, the detailed mechanism designed to satisfy this bilateral constraint is not shown in Fig. 2.24.

These moments on the flapping mechanism and fuselage are internal moments for the whole Ornicopter system. In the following, they will be discussed in a general situation (see Fig. 2.25), in which the detailed design of the forced flapping mechanisms is not relevant.

The Ornicopter rotor system includes three sections as shown in Fig. 2.25. There are three external moments (only the rotation axis is considered) on the rotor system, namely: the aerodynamic moment on the blades (M_Q), the moment on flapping mechanism from the fuselage (M_{F2FM}), and the moment on the engine from the fuselage (M_{F2Eng}). Their positive directions are the same as the rotor rotation direction.

In the equilibrium condition, the following equation is valid:

$$M_Q + M_{F2FM} + M_{F2Eng} = 0 \quad (2.46)$$

The reaction moment on the fuselage (M_{ra}) generated by the rotor system will be:

$$\begin{aligned} M_{ra} &= M_{FM2F} + M_{Eng2F} \\ &= -M_{F2FM} - M_{F2Eng} \\ &= M_Q \end{aligned} \quad (2.47)$$

where M_{FM2F} is the moment on the fuselage caused by the flapping mechanism and M_{Eng2F} is the moment on the fuselage generated by the engine.

Equation 2.47 shows that the total moment on the fuselage (generated by the rotor system) is the same as the aerodynamic moment on the rotor blades. As discussed

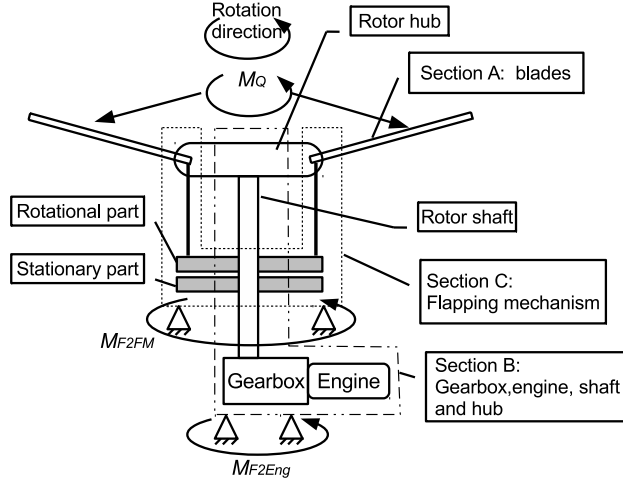


Figure 2.25: Sketch of the Ornicopter rotor components

before, by active flapping, the Ornicopter rotor can drive itself to rotate, i.e. the aerodynamic moment on the rotor (in the rotation direction) is zero ($M_Q = 0$). Therefore, the whole Ornicopter rotor system will not generate a reaction moment (torque) on the fuselage.

In the condition that $M_Q = 0$, Eq. 2.46 can be rewritten as:

$$M_{F2FM} = -M_{F2Eng} \quad (2.48)$$

This indicates that the forced flapping mechanism will generate a moment on the fuselage in the opposite direction of the moment generated by the engine. In other words, in the Ornicopter concept, the engine still provides a shaft torque and hence creates a reaction torque on the fuselage (M_{Eng2F}). This shaft torque (and hence the shaft power) is converted into a flapping moment (flapping power) to drive the blades to flap by the force flapping mechanism. During this conversion, a torque (M_{FM2F}) in the opposite direction is generated on the fuselage to counteract the reaction torque (M_{Eng2F}).

While applying yaw control input in the Ornicopter (changing the flapping amplitude), the M_{FM2F} will be changed. Using Fig. 2.24 as an example, to increase the forced flapping amplitude, the tilting angle (θ) should be increased. The larger flapping amplitude also requires higher F_1 to drive the blade. The combined effect will be a higher F_2 ($F_2 = F_1 \tan \theta$). This will change the total reaction torque on the fuselage and create the desired yawing moment.

These moments, such as M_{F2FM} and M_{F2Eng} , are internal moments. They will not affect the Ornicopter body motion dynamics. Therefore, the internal forces and

moments in the Ornicopter rotor system will not be studied in this thesis. The external forces and moments, i.e. the aerodynamic forces and moments on the Ornicopter rotor will be the main interest. They will be derived in the next chapter for the flight mechanics model.

2.5.3 Windtunnel Test

To prove his concept, in the 1930s Küssner conducted some windtunnel tests using the model shown in Fig. 2.2. The test section is shown in Fig. 2.26.

2

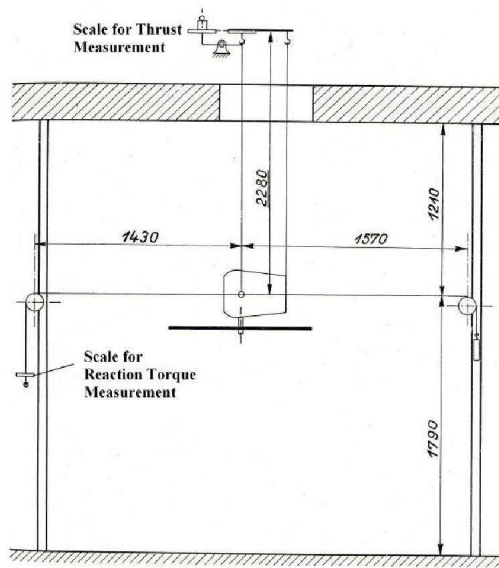


Figure 2.26: Side-view of the test section of Küssner's windtunnel test [11]

In his test, five different blade designs (such as the blade twist and airfoil) were tested in hovering for different RPMs (revolutions per minute) and collective pitch angles. The test results for blade design number five (V) will be presented in this section. This blade design is based on the cambered Joukowski airfoil Gö-541 with 10% thickness and 5% camber. The radius of the rotor is 0.5 m and the blade chord is 0.05 m.

Figure 2.27 presents the rotor torque and engine torque as a function of the forced flapping angle. It proves the feasibility of designing a single rotor without torque. The torqueless condition is achieved at the forced flapping angle between 9 deg and 10.5 deg (depending on RPM and collective pitch angle).

Windtunnel tests were also performed in 2004 at Delft University of Technology with an Ornicopter model, depicted in Fig. 2.28 [32]. To simplify the model development, the Vario Silence radio controlled helicopter was used as a starting point (rotor diameter: 1.5 m, number of blades: 2 (teeter rotor)) [3]. The forced flapping mechanism has been added to this helicopter. The swashplate mechanism as seen in Fig. 2.17 was used for

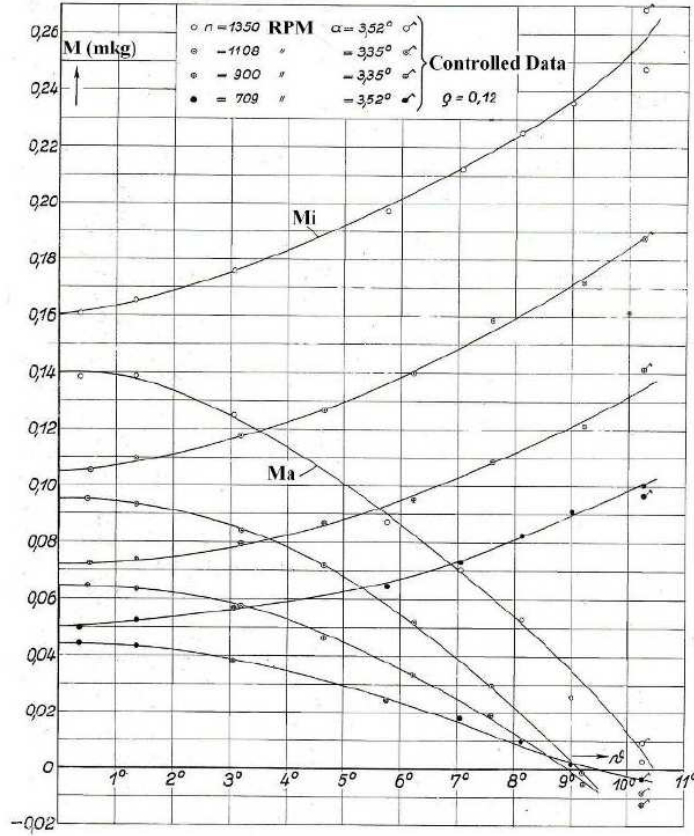


Figure 2.27: Variation of the rotor torque M_a and engine torque M_i with respect to the forced flapping angle [11]

this wind tunnel test. In the double teeter configuration, the modified Ornicopter rotor consists of four Vario blades with a rotor diameter equal to 1.65 m and a chord length of 0.53 m.

Since the windtunnel model does not contain vibration absorbers or dampers, in order to minimize the expected vibrations, the rotational speed of the rotor was kept low during the tests (with blade tip Mach numbers varying from 0.0397 to 0.132).

Using this windtunnel model, a series of tests in hovering were performed for different collective pitch and forced flapping angles. The rotor thrust, torque and power consumption were measured proving that the Ornicopter concept works.

Figure 2.29 [32] shows the relationship between the collective pitch input and the torque on the fuselage (M_z) and thrust (T). The flapping angle during this measurement was set at 12 degrees (at the blade root) in the hover configuration. It can be seen that the torque increases with absolute pitch, and, most importantly, that the torque on the

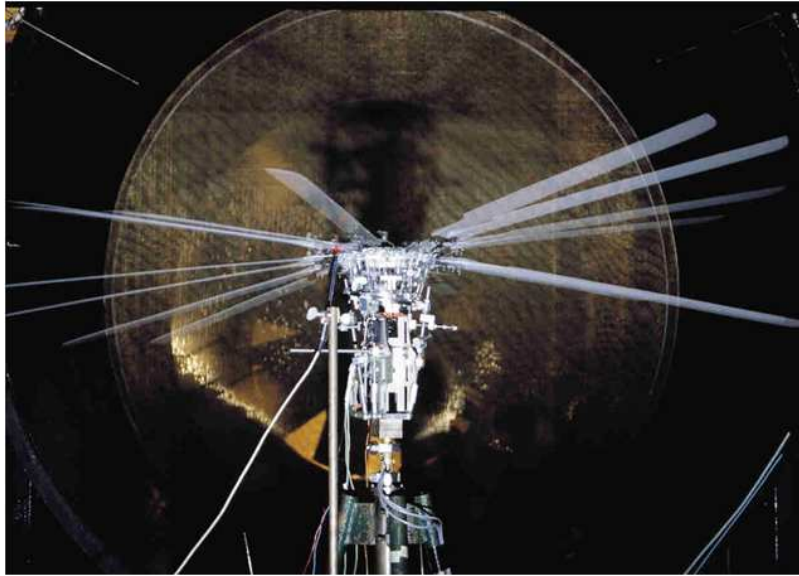


Figure 2.28: The Ornicopter windtunnel model [32]

Ornicopter’s fuselage equals zero at -2.7 degrees and 3.5 degrees pitch. This shows that it is possible to construct a single rotor without reaction torque. It also proves that both positive and negative reaction torque on the fuselage can be achieved. This confirms that the new means of helicopter yaw control is feasible, i.e. changing the main rotor torque directly in both a positive and negative direction.

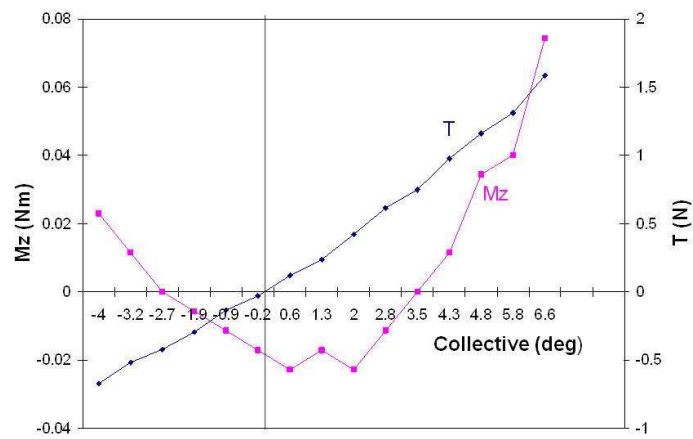


Figure 2.29: Rotor torque (M_z) and rotor thrust (T) as a function of collective pitch for a double teeter Ornicopter with twelve degrees of flapping [32]

Figure 2.30 [32] shows the comparison between the rotor thrust with and without the forced flapping. No noticeable impact can be found. The thrust response to the collective pitch input of the Ornicopter is the same as in conventional helicopters.

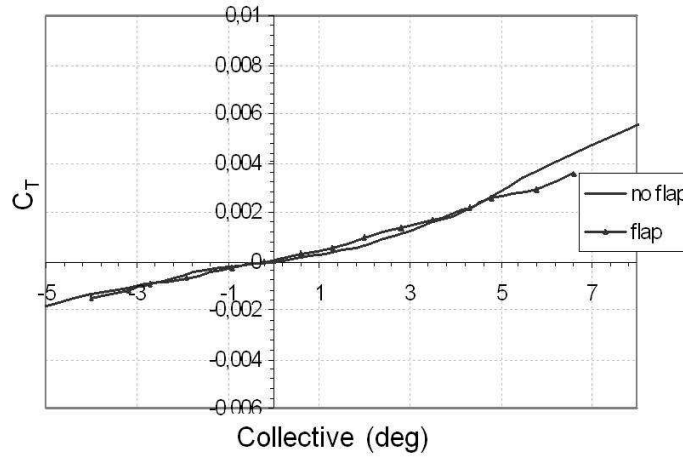


Figure 2.30: Rotor thrust as a function of the collective pitch for the Ornicopter with and without twelve degrees of flapping [32]

Figure 2.31 from reference [32] compares different forced flapping angles (i.e. maximum flapping angles). The figure shows that an increase in the flapping angle decreases the torque on the fuselage. At the same time, for certain collective pitch angles, by applying different forced flapping angles, positive, negative and zero shaft torque can be achieved. This is how the Ornicopter can be controlled in the yaw direction without a tail rotor.

When the active flapping is set to zero, the windtunnel model can be used as a conventional helicopter rotor. In this manner, the power consumptions of both the Ornicopter and conventional helicopter configurations were measured and compared, see Ref [32]. Figure 2.32 [32] shows the electric power input as a function of collective pitch input, for a conventional helicopter and for Ornicopter configuration. It should be noted that both curves differ by a constant value of 5 w.

This higher required power is partially caused by the friction in the flapping mechanism. The windtunnel model has not been optimized for friction in the forced flapping mechanism. A simple calibration showed that this friction consumed approximately 3 w to 5 w power [32]. Recalling Küssner’s test as shown in Fig. 2.27, it also shows an increasing engine torque (i.e. engine power) with increasing forced flapping angle. Although the preliminary theoretical analyses showed the Ornicopter concept requires the same power as conventional helicopter rotors, windtunnel tests suggest this conclusion may not be solid.

In conclusion, the windtunnel tests have shown that a single rotor without reaction torque can be designed and that both a negative and positive reaction torque can

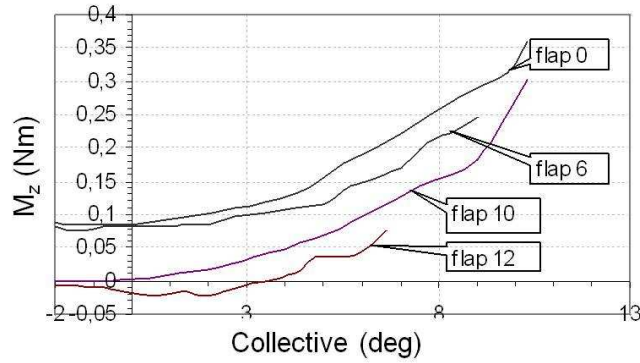


Figure 2.31: Rotor torque as a function of the collective pitch for various flapping values [32]

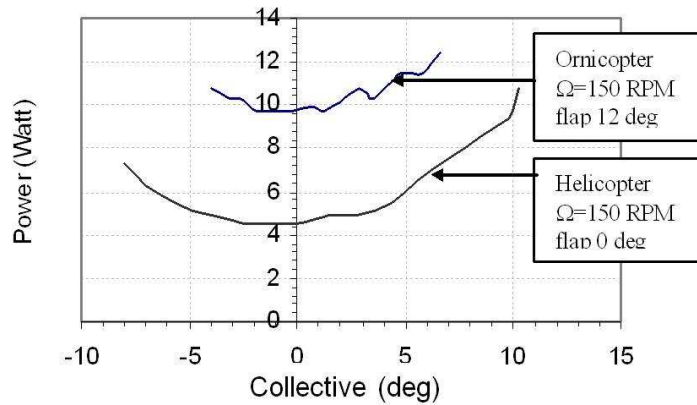


Figure 2.32: Power curves for a conventional helicopter and Ornicopter [32]

be deliberately introduced to provide yaw control. The tests also proved that the thrust achieved by the Ornicopter is equal to the thrust achieved by a conventional helicopter under the same circumstances. Additionally the tests demonstrated that only modest flapping angles are needed to arrive at a torqueless state. Regarding the power consumption, the windtunnel test showed higher required power for the Ornicopter. In the next chapter, more detailed analyses will be performed regarding the power efficiency of the Ornicopter.

2.5.4 The Demonstrator Model

A demonstrator model was developed and tested in 2006 to further prove the Ornicopter concept [15].

The Vario X-Treme [1] economic (max RPM 1500, rotor diameter 1.5 m, number of blades 2) helicopter kit was chosen to be rebuilt as a Ornicopter demonstrator, see Fig. 2.33 [15]. In this demonstrator, the gearwheel mechanism was applied, as shown in Fig. 2.19. The two-bladed Vario rotor was replaced by the four bladed Ornicopter rotor in the 2×2 AS configuration. The demonstrator model was tested on a 2 DoF base (vertical and yaw motion freedom) [17, 31].

2

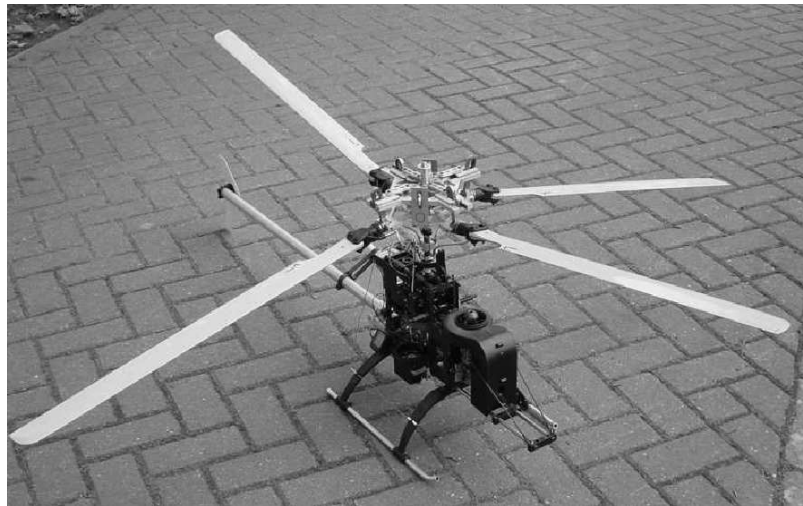


Figure 2.33: The Ornicopter demonstrator model [15]

The main goal of the demonstrator was to determine the lowest tip speed at which the Ornicopter could be operated properly in hover conditions. A low tip speed is important in order to limit the blade loads due to forced flapping. Proper operation in this respect implies that the demonstrator model can generate an amount of thrust that is at least sufficient for hover, and that the yaw motion can be fully controlled at this thrust level. Unfortunately, due to some mechanism failures and financial difficulties, the main goal of this test was not accomplished.

A secondary goal was to assess the yaw control response, in other words whether the Ornicopter had a good control authority. The tests proved again that the Ornicopter’s principle was valid. The stable torqueless state could be reached and the demonstrator had good control authority in yaw in the test conditions. However, this conclusion was mostly based on a qualitative assessment and visual observations of the yaw motion.

2.6 Conclusion

In this chapter, the basic Ornicopter concept was first explained. The Ornicopter rotor will not generate the reaction torque on the fuselage by actively flapping its blades, and hence the anti-torque device is no longer needed. While longitudinal and lateral cyclic control and collective control are achieved in exactly the same manner as in a conventional helicopter, the Ornicopter’s yaw control authority can be achieved by changing the amplitude of the active flapping.

2

Using a hovering rotor model, the feasibility of Ornicopter concept was proved. Calculations have shown that the required flapping moment and flapping angle are moderate, and this concept will not increase the required power of the helicopter rotor. By choosing a proper flapping configuration, the active flapping can be decoupled with the cyclic control. Therefore no additional control coupling will be introduced by the Ornicopter concept. Besides the theoretical research, the windtunnel test and the Ornicopter demonstrator model also confirmed that it is possible to reach a torqueless state for the Ornicopter rotor and both positive and negative yaw control moment can be generated.

3

The Ornicopter Model

In the previous chapter, the Ornicopter concept was analysed using a hovering rotor model. Analyses have been done for this concept regarding the required forced flapping angle and moment, required power, controlling the Ornicopter and vibratory loads.

To extend the analyses for the Ornicopter to the entire flight envelope, a mathematical model for the Ornicopter will be developed. For this purpose, in this chapter a model for conventional helicopters is developed first and validated. Afterwards, it is adapted for the Ornicopter concept.

This flight mechanics model is based on BET, as was the hovering rotor model used in previous chapter. Moreover, it considers more details of the rotor and all the components of the helicopter, such as the fuselage and stabilisers, and it can be used for all flight conditions instead of only for hovering.

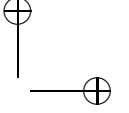
3.1 The Level of Modelling

The main rotor is the most important component of a helicopter, and the most difficult one for modelling. The momentum theory can provide a basic understanding for the rotor thrust and induced power. However, many details of the rotor are missing from this method. The state of art CFD (computational fluid dynamics) program can predict the flow field around the rotor, but demands high computational power. Between the above two methods, the BET and wake analysis (prescribed or free) are more common for flight mechanics models. Based on the different rotor complexity, three levels of modelling can be defined for different application areas, as shown in Tab. 3.1 [10].

The main applications of the helicopter flight mechanics model in this thesis correspond to the performance and handling qualities analyses within the flight envelope. From Tab. 3.1, one can see that the Level 1 model is sufficient for this purpose. Although its accuracy is inadequate for detailed rotor design, it is ideal for establishing a

Table 3.1: Levels of rotor modelling [10]

	Level 1	Level 2	Level 3
Aerodynamics	linear 2-D dynamic inflow, local momentum theory, analytically integrated loads	nonlinear (limited 3-D) dynamic inflow, local momentum theory, local effects of blade vortex interaction, unsteady 2-D compressibility, numerically integrated loads	nonlinear 3-D full wake analysis (free or prescribed), unsteady 2-D compressibility, numerically integrated loads
Dynamics	rigid blades (1) quasi-steady motion (2) 3 DoF flap (3) 6 DoF flap + lag (4) 6 DoF flap + lag + quasi-steady torsion	(1) rigid blades with options as in Level 1 (2) limited number of blade elastic modes	detailed structural representation as elastic modes or finite elements
Applications	parametric trends for flying qualities and performance studies, well within operational flight envelope, low bandwidth control	parametric trends for flying qualities and performance studies up to operational flight envelope, medium bandwidth, appropriate to high gain active flight control	rotor design, rotor limit loads prediction, vibration analysis, rotor stability analysis, up to safe flight envelope



3.2 The Generic Helicopter Flight Mechanics Model - Delcopter

49

fundamental understanding of the Ornicopter concept at this stage.

In this sense, a Level 1 classical 13 degrees of freedom (DoF) model will be first developed for conventional helicopters. It is developed in-house and is based on blade element theory. The model includes 6 DoFs for body motion, 3 DoFs for blade flapping motion, 3 DoFs for the Pitt-Peters dynamic inflow model and 1 DoF for the tail rotor inflow. In the following sections, this model will be referred as the **DelCopter** model.

3.2 The Generic Helicopter Flight Mechanics Model - Delcopter

3.2.1 Assumptions

To simplify the **DelCopter** model and keep focus on the main problem at this stage, some widely used assumptions and simplifications are implemented. The main assumptions and simplifications for different components of the helicopter are as follows:

For the main rotor:

1. Aerodynamic forces and moments are calculated using blade element theory;
2. The stall, compressibility effects and reversed flow effects are not considered;
3. The steady 2-D aerofoil model is adequate for the flight mechanics model. The aerofoil lift force is a linear function of the local blade angle of attack (α) and the drag force is a simple quadratic function of α , as:

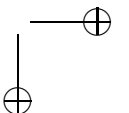
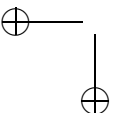
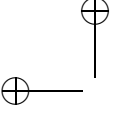
$$\begin{aligned} C_L &= C_{L_\alpha} \alpha \\ C_D &= C_{D0} + C_{D2} \cdot \alpha^2 \end{aligned} \quad (3.1)$$

4. The blades are rectangular;
5. The blades are assumed to be rigid;
6. The blade lead-lag motion is neglected;
7. A constant tip loss factor is used (0.97);
8. The blade gravitational forces are small compared to the aerodynamic, inertial and centrifugal forces;
9. Only the first order flapping motion is considered, i.e. the flapping angle is:

$$\beta = \beta_0 + \beta_{s1} \sin(\psi) + \beta_{c1} \cos(\psi) \quad (3.2)$$

10. The rotor blade has a uniform mass distribution;
11. The body motion acceleration is neglected in the blade flapping equation of motion;

3



12. The flapping and flow angles are small. Therefore, small angle approximations can be applied, such as $\sin \beta \approx \beta$ and $\cos \beta \approx 1$;
13. The rotor angular velocity is constant and is anticlockwise;

For the tail rotor:

1. A simplified rotor model is used for the tail rotor.
2. The flapping motion of the tail rotor blades is not considered.
3. A uniform inflow model is used for the tail rotor.
4. The torque generated by the tail rotor is neglected in the helicopter equations of motion.

3

For the other components:

1. From the aerodynamic aspect, the fuselage is considered as an equivalent plate that only generates drag force.
2. The pressure centre of the fuselage is assumed to be at the c.g., therefore the fuselage will not generate any moment on the c.g..
3. The horizontal stabilizer and vertical fin are considered as lifting plates with a constant lift coefficient slope. Drag forces generated by stabilizers are neglected.
4. The horizontal stabilizer and vertical fin are stationary. They do not have any control surface for either conventional helicopters or Ornicopter.
5. Interactions between different helicopter components are not taken into account.

3.2.2 Reference Frame

To derive the helicopter flight mechanic model, several reference frames are defined, including the body reference ($_b$), non-rotating reference ($_{nr}$), rotating reference ($_r$), flapping reference ($_\beta$) and non-rotating reference of the tail rotor ($_{tnr}$).

The body reference is the basic reference frame on the helicopter, which is fixed in the helicopter. Its origin is at the c.g. of the helicopter. The orientation of its coordinate axes is depicted in Fig. 3.1. The positive direction of the x_b axis towards the fuselage nose, and the positive z_b directed downward. The positive y_b axis is oriented towards the right side of the helicopter.

The non-rotating references for both the main rotor and tail rotor are also defined, see Fig. 3.1. Their origins are coincident with the centre of the main rotor and tail rotor respectively. For the main rotor non-rotating reference, its z_{nr} axis is aligned with the main rotor shaft and the x_{nr} axis is in the shaft plane and towards forward. The y_{nr} axis is perpendicular with the y_b axis. The tail rotator non-rotating reference is defined in the same way, except that the y_{tnr} axis is perpendicular to the z_b axis.

The main rotor non-rotating frame can be obtained from the body frame by rotating the body frame about the y_b axis through the shaft tilt angle (α_{sh} , positive for tilting

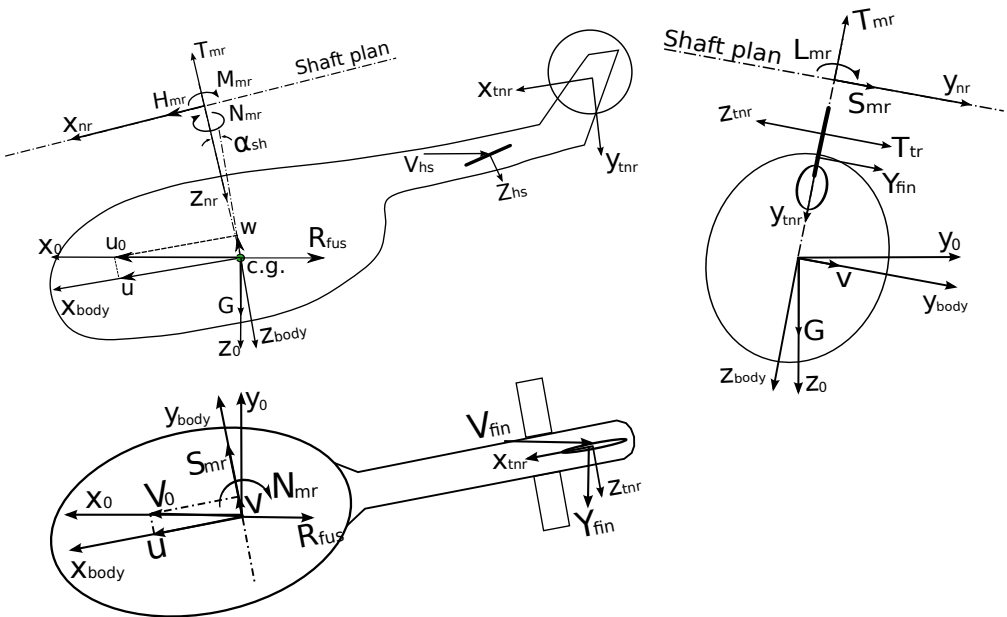


Figure 3.1: Forces and moments on helicopters



backwards). Similarly, rotating the body frame about the x_b axis through $\pi/2$ results in the tail rotor non-rotating frame. The transformation matrix can be written as:

$$\begin{aligned} \mathbf{T}_{b2nr} &= \begin{bmatrix} \cos(\alpha_{sh}) & 0 & -\sin(\alpha_{sh}) \\ 0 & 1 & 0 \\ \sin(\alpha_{sh}) & 0 & \cos(\alpha_{sh}) \end{bmatrix} \\ \mathbf{T}_{b2tnr} &= \begin{bmatrix} 1 & 0 & 0 \\ 0 & 0 & -1 \\ 0 & 1 & 0 \end{bmatrix} \end{aligned} \quad (3.3)$$

3

The main rotor rotating reference and flapping reference are defined as shown in Fig. 3.2. As its name suggested, the rotating frame rotates with the main rotor. The positive rotation direction is counter-clockwise (top view). It can be obtained by rotating the non-rotating frame about the z_{nr} axis for $(\pi - \psi)$. Afterwards, by rotating this reference frame about the y_r through the flapping angle (β , positive for flapping upwards), one can get the flapping reference, which is fixed on the blade.

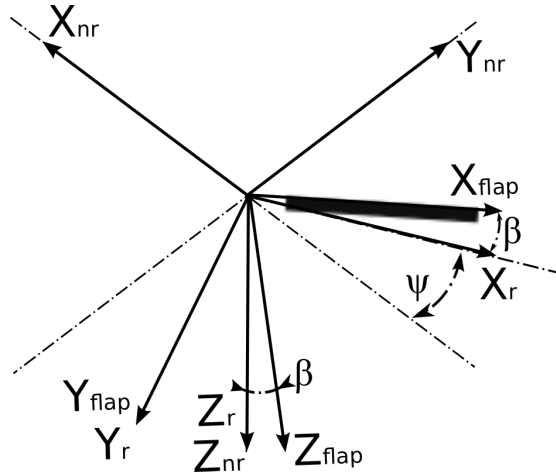


Figure 3.2: The rotor hub reference

The transformation matrix between the different rotor references are as follows:

$$\begin{aligned} \mathbf{T}_{nr2r} &= \begin{bmatrix} -\cos(\psi) & \sin(\psi) & 0 \\ -\sin(\psi) & -\cos(\psi) & 0 \\ 0 & 0 & 1 \end{bmatrix} \\ \mathbf{T}_{r2\beta} &= \begin{bmatrix} \cos(\beta) & 0 & -\sin(\beta) \\ 0 & 1 & 0 \\ \sin(\beta) & 0 & \cos(\beta) \end{bmatrix} \end{aligned} \quad (3.4)$$

3.2 The Generic Helicopter Flight Mechanics Model - Delcopter

53

To distinguish between the vectors in the different reference frames, the notation $\{V\}_{\{r\}}$ is defined. It indicates that the vector \mathbf{V} is defined in the reference r . The following notations are used for reference frames defined in this thesis:

- $\{b\}$: the body reference frame
- $\{nr\}$: the non-rotating reference frame
- $\{r\}$: the rotating reference frame
- $\{\beta\}$: the flapping reference frame

The coordinates of a vector in one reference frame can be converted into the coordinates in another one by left-multiplying the transformation matrix. For example, to convert the coordinate of \mathbf{V} in the non-rotating reference ($\{V\}_{\{nr\}}$) into the rotating reference ($\{V\}_{\{r\}}$), one can use:

$$\{V\}_{\{r\}} = \mathbf{T}_{nr2r} \times \{V\}_{\{nr\}} \quad (3.5)$$

3.2.3 The Component Models

In order to develop the flight mechanics model for helicopters, different helicopter components are first modelled, such as the main rotor, stabilizers and the inflow model. The detailed derivations for all the components are presented in Appendix D.

The derivation includes the following two main parts. Firstly, the forces (X , Y , Z) and moments (L , M , N) generated by different components on helicopter c.g. are derived. They will be used for the equation of body motion in the next section. Secondly, the component dynamics are derived, including: the flapping dynamics (Eq. D.45), the main rotor dynamics inflow model (Eq. D.66) and the tail rotor inflow dynamics (Eq. D.67).

3.2.4 The System of Equations of Motion

With the forces and moments generated by the different components derived, the total force and moment can be summed as:

$$\begin{aligned} X &= X_{mr} && + X_{fus} && + X_g \\ Y &= Y_{mr} &+ Y_{tr} &+ Y_{fus} && + Y_{fin} &+ Y_g \\ Z &= Z_{mr} && + Z_{fus} &+ Z_{hs} && + Z_g \\ L &= L_{mr} &+ L_{tr} && && + L_{fin} \\ M &= M_{mr} && &+ M_{hs} && \\ N &= N_{mr} &+ N_{tr} && && + N_{fin} \end{aligned} \quad (3.6)$$

For the subscripts used in the above equation, mr refers to the main rotor, tr refers to the tail rotor, fus refers to the fuselage, hs refers to the horizontal stabiliser, fin refers to the vertical fin and g refers to the gravity.

Those total forces and moments will be used for the Euler equations of the rigid-body motion [10]:

$$\begin{aligned}\dot{u} &= \frac{X}{M_a} + rv - qw \\ \dot{v} &= \frac{Y}{M_a} + pw - ru \\ \dot{w} &= \frac{Z}{M_a} + qu - pv\end{aligned}\tag{3.7}$$

3

$$\begin{aligned}\dot{p} &= \frac{I_z}{I_1}L + \frac{I_{xz}}{I_1}N + \frac{I_2}{I_1}pq + \frac{I_3}{I_1}qr \\ \dot{q} &= \frac{M}{I_y} + \frac{I_z - I_x}{I_y}pr + \frac{I_{xz}}{I_y}(r^2 - p^2) \\ \dot{r} &= \frac{I_{xz}}{I_1}L + \frac{I_x}{I_1}N + \frac{I_4}{I_1}pq - \frac{I_2}{I_1}qr\end{aligned}\tag{3.8}$$

where u , v and w are transitional velocities of the helicopter, p , q and r are rotational velocities of the helicopter, M_a is the mass of the helicopter, I_x , I_y and I_z are moments of inertia of the helicopter, I_{xz} is the product of inertia of the helicopter, and I_1 to I_4 are defined as:

$$\begin{aligned}I_1 &= I_x I_z - I_{xz}^2 \\ I_2 &= I_{xz}(I_x - I_y + I_z) \\ I_3 &= I_y I_z - I_z^2 - I_{xz}^2 \\ I_4 &= I_x^2 - I_x I_y + I_{xz}^2\end{aligned}\tag{3.9}$$

Besides the equations above, the relationship between the change rate of the Euler angles and the fuselage angular velocities in the body axis system is also needed. For the specific rotation sequence used in this thesis, i.e. rotating through yaw, pitch and roll in sequence, it has been derived as (p. 181 in Ref [10]):

$$\begin{aligned}p &= \dot{\Phi} - \dot{\Psi} \sin(\Theta) \\ q &= \dot{\Theta} \cos \Phi + \dot{\Psi} \sin(\Phi) \cos(\Theta) \\ r &= -\dot{\Theta} \sin(\Phi) + \dot{\Psi} \cos(\Phi) \cos(\Theta)\end{aligned}\tag{3.10}$$

where Ψ is the yaw angle, Θ is the pitch angle and Φ is the roll angle. From Eq. 3.10, the change rate of attitude angles can be derived as:

$$\begin{aligned}\dot{\Psi} &= r \frac{\cos(\Phi)}{\cos(\Theta)} + q \frac{\sin(\Phi)}{\cos(\Theta)} \\ \dot{\Theta} &= q \cos(\Phi) - r \sin(\Phi) \\ \dot{\Phi} &= p + r \tan(\Theta) \cos(\Phi) + q \tan(\Theta) \sin(\Phi)\end{aligned}\tag{3.11}$$

Combining the body motion dynamics (Eq. 3.7, 3.8 and 3.11) with flapping and inflow dynamics (Eq. D.45, D.66 and D.67), the mathematical model for conventional helicopters can be built in the form of a non-linear differential equation set, as:

$$\dot{\mathbf{X}} = \mathbf{F}(\mathbf{X}, \mathbf{U}) \quad (3.12)$$

where \mathbf{X} is the state vector and \mathbf{U} is the control input vector, as:

$$\begin{aligned} \mathbf{X} &= [\mathbf{X}_b, \mathbf{X}_\lambda, \mathbf{X}_\beta]^\top \\ \mathbf{X}_b &= [u, v, w, p, q, r, \Psi, \Theta, \Phi]^\top \\ \mathbf{X}_\lambda &= [\lambda_0, \lambda_{s1}, \lambda_{c1}, \lambda_{tr}]^\top \\ \mathbf{X}_\beta &= [\beta_0, \beta_{s1}, \beta_{c1}]^\top \\ \mathbf{U} &= [\theta_0, \theta_{s1}, \theta_{c1}, \theta_{tr}]^\top \end{aligned} \quad (3.13)$$

3

It should be noted that in a flight dynamics model, the flapping motion as seen from the reference frame rotating with the blade should be represented in the non-rotating reference frame which is fixed to the body. It is therefore essential to transform the blade flapping equations to the body frame. This will result in 3 rotor states in the non-rotating frame ($[\beta_0, \beta_{s1}, \beta_{c1}]^\top$) instead of 1 (β) in the rotating frame.

3.2.5 Model Linearisation

Thus far, a non-linear system of equations for a conventional helicopter has been developed. This will be used for further analyses, such as performance calculations and flight simulations.

At a certain trim point, the non-linear model can be linearised based on Taylor expansion. The linearised model has lower fidelity when compared with the non-linear model. However, it provides a more fundamental understanding of the behaviour of the helicopter, such as the stability derivatives and the natural modes of motion. In this sense, the linearised model has been developed for stability analyses of the Ornicopter concept. Using computer algebra software, derivatives of the complex non-linear equations can be derived analytically. Thus a numerical differential algorithm is not needed in this thesis.

The linearisation of the model with 6 body DoFs will be discussed in this section, and the same method can be applied to a model with more DoFs.

For the model only including the body DoFs, the non-linear system EoM can be written in the vector form as:

$$\dot{\mathbf{X}} = \mathbf{F}(\mathbf{X}, \mathbf{U}) \quad (3.14)$$

where:

$$\begin{aligned} \mathbf{X} &= [u, v, w, p, q, r, \Psi, \Theta, \Phi]^\top \\ \mathbf{U} &= [\theta_0, \theta_{s1}, \theta_{c1}, \theta_{yaw}]^\top \end{aligned} \quad (3.15)$$

Using the first order Taylor expansion, the above non-linear system can be rewritten in the perturbation form as:

$$\dot{\mathbf{X}} = \mathbf{F}(\mathbf{X}_0, \mathbf{U}_0) + \frac{\partial \mathbf{F}}{\partial \mathbf{X}}(\mathbf{X} - \mathbf{X}_0) + \frac{\partial \mathbf{F}}{\partial \mathbf{U}}(\mathbf{U} - \mathbf{U}_0) + \Delta \quad (3.16)$$

where \mathbf{X}_0 and \mathbf{U}_0 is the initial condition and Δ is the approximation error.

Choosing a equilibrium condition as the linearisation condition, i.e. $\mathbf{F}(\mathbf{X}_e, \mathbf{U}_e) = 0$ and neglecting the approximation error, one can get the linearised model as:

3

$$\dot{\mathbf{X}} = \mathbf{A}\delta\mathbf{X} + \mathbf{B}\delta\mathbf{U} \quad (3.17)$$

where $\delta\mathbf{X}$ and $\delta\mathbf{U}$ is the perturbation of the state and control from the equilibrium condition, and the state matrix \mathbf{A} and control matrix \mathbf{B} is given by

$$\begin{aligned} \mathbf{A} &= \left(\frac{\partial \mathbf{F}}{\partial \mathbf{X}} \right)_{\mathbf{X}=\mathbf{X}_e, \mathbf{U}=\mathbf{U}_e} \\ \mathbf{B} &= \left(\frac{\partial \mathbf{F}}{\partial \mathbf{U}} \right)_{\mathbf{X}=\mathbf{X}_e, \mathbf{U}=\mathbf{U}_e} \end{aligned} \quad (3.18)$$

The elements in matrix \mathbf{A} and \mathbf{B} are calculated as

$$\begin{aligned} A_{ij} &= \frac{\partial F_i}{\partial X_j} \\ B_{ij} &= \frac{\partial F_i}{\partial U_j} \end{aligned} \quad (3.19)$$

Recalling the system EoMs derived before (Eq. 3.7, 3.8 and 3.11), the state matrix \mathbf{A} and control matrix \mathbf{B} can be derived, see Eq. 3.20 and 3.21.

$$\mathbf{A} = \begin{bmatrix} X_u & X_v & X_w & X_p & X_q - w_e & X_r + v_e & 0 & -g \cos \Theta_e & 0 \\ Y_u & Y_v & Y_w & Y_p + w_e & Y_q & Y_r - u_e & 0 & -g \sin \Phi_e \cdot \cos \Theta_e & g \cos \Phi_e \cdot \cos \Theta_e \\ Z_u & Z_v & Z_w & Z_p - v_e & Z_q + u_e & Z_r & 0 & -g \cos \Phi_e \cdot \sin \Theta_e & -g \sin \Phi_e \cdot \cos \Theta_e \\ k_1 L_u + k_2 N_u & k_1 L_v + k_2 N_v & k_1 L_w + k_2 N_w & k_1 L_p + k_2 N_p & k_1 L_q + k_2 N_q & k_1 L_r + k_2 N_r & 0 & 0 & 0 \\ M_u & M_v & M_w & M_p & M_q & M_r & 0 & 0 & 0 \\ k_3 L_u + k_1 N_u & k_3 L_v + k_1 N_v & k_3 L_w + k_1 N_w & k_3 L_p + k_1 N_p & k_3 L_q + k_1 N_q & k_3 L_r + k_1 N_r & 0 & 0 & 0 \\ 0 & 0 & 0 & 0 & \frac{\sin \Phi_e}{\cos \Theta_e} & \frac{\cos \Phi_e}{\cos \Theta_e} & 0 & 0 & 0 \\ 0 & 0 & 0 & 0 & \cos \Phi_e & -\sin \Phi_e & 0 & 0 & 0 \\ 0 & 0 & 0 & 1 & \tan \Theta_e \sin \Phi_e & \tan \Theta_e \cos \Phi_e & 0 & 0 & 0 \end{bmatrix} \quad (3.20)$$

3

$$\mathbf{B} = \begin{bmatrix} X_{\theta_0} & X_{\theta_{s1}} & X_{\theta_{c1}} & X_{\theta_{yaw}} \\ Y_{\theta_0} & Y_{\theta_{s1}} & Y_{\theta_{c1}} & Y_{\theta_{yaw}} \\ Z_{\theta_0} & Z_{\theta_{s1}} & Z_{\theta_{c1}} & Z_{\theta_{yaw}} \\ k_1 L_{\theta_0} + k_2 N_{\theta_0} & k_1 L_{\theta_{s1}} + k_2 N_{\theta_{s1}} & k_1 L_{\theta_{c1}} + k_2 N_{\theta_{c1}} & k_1 L_{\theta_{yaw}} + k_2 N_{\theta_{yaw}} \\ M_{\theta_0} & M_{\theta_{s1}} & M_{\theta_{c1}} & M_{\theta_{yaw}} \\ k_3 L_{\theta_0} + k_1 N_{\theta_0} & k_3 L_{\theta_{s1}} + k_1 N_{\theta_{s1}} & k_3 L_{\theta_{c1}} + k_1 N_{\theta_{c1}} & k_3 L_{\theta_{yaw}} + k_1 N_{\theta_{yaw}} \\ 0 & 0 & 0 & 0 \\ 0 & 0 & 0 & 0 \\ 0 & 0 & 0 & 0 \end{bmatrix} \quad (3.21)$$

where

$$\begin{aligned} k_1 &= \frac{I_x I_z}{I_x I_z - I_{xz}^2} \\ k_2 &= \frac{I_z I_{xz}}{I_x I_z - I_{xz}^2} \\ k_3 &= \frac{I_x I_{xz}}{I_x I_z - I_{xz}^2} \end{aligned} \quad (3.22)$$

The derivatives of the forces and moments in the equations above can be expressed

in semi-normalized form as follows:

$$\begin{aligned}
 X_x &= \frac{\partial X/\partial x}{M_a} \left(\frac{1}{s}, \quad \frac{m}{\text{rad} \cdot s} \quad \text{or} \quad \frac{m}{\text{rad} \cdot s^2} \right) \\
 Y_x &= \frac{\partial Y/\partial x}{M_a} \left(\frac{1}{s}, \quad \frac{m}{\text{rad} \cdot s} \quad \text{or} \quad \frac{m}{\text{rad} \cdot s^2} \right) \\
 Z_x &= \frac{\partial Z/\partial x}{M_a} \left(\frac{1}{s}, \quad \frac{m}{\text{rad} \cdot s} \quad \text{or} \quad \frac{m}{\text{rad} \cdot s^2} \right) \\
 L_x &= \frac{\partial L/\partial x}{I_x} \left(\frac{\text{rad}}{m \cdot s}, \quad \frac{1}{s} \quad \text{or} \quad \frac{1}{s^2} \right) \\
 M_x &= \frac{\partial M/\partial x}{I_y} \left(\frac{\text{rad}}{m \cdot s}, \quad \frac{1}{s} \quad \text{or} \quad \frac{1}{s^2} \right) \\
 N_x &= \frac{\partial N/\partial x}{I_z} \left(\frac{\text{rad}}{m \cdot s}, \quad \frac{1}{s} \quad \text{or} \quad \frac{1}{s^2} \right)
 \end{aligned} \tag{3.23}$$

where $x \in \{u, w, v\}, \quad \{p, q, r\} \quad \text{or} \quad \{\Psi, \Theta, \Phi, \theta_0, \theta_{s1}, \theta_{c1}, \theta_{yaw}\}.$

3.2.6 The Control System

The Stability and Control Augmentation System

A stability and control augmentation system (SCAS) can be used to improve the helicopter handling qualities characteristics and reduce pilot workload. To investigate the impact of a SCAS system on handling qualities, a generic SCAS model is added to the DelCopter model.

The simple attitude and rate feedback algorithm is used in the longitudinal, lateral and yaw axes. This SCAS system can be written as follows:

$$\begin{aligned}
 \theta_0 &= \theta_0^{in} \\
 \theta_{s1} &= \theta_{s1}^{in} + K_q q + K_\Theta \delta \Theta \\
 \theta_{c1} &= \theta_{c1}^{in} + K_p p + K_\Phi \delta \Phi \\
 \theta_{yaw} &= \theta_{yaw}^{in} + K_r r + K_v \delta v
 \end{aligned} \tag{3.24}$$

where: θ_0^{in} , θ_{s1}^{in} , θ_{c1}^{in} and θ_{yaw}^{in} are the control input from the pilot, K_q , K_p , and K_v are the rate/velocity feedback gains, K_Θ and K_Φ are the attitude feedback gains, and $\delta \Theta$, $\delta \Phi$ and δv are perturbations of the pitch/roll attitude and side-slip velocity.

This SCAS system can also be written in the matrix format as:

$$\mathbf{U} = \mathbf{U}^{in} + \mathbf{K}\mathbf{X} \tag{3.25}$$

This SCAS model will be added to the linearised helicopter model (Eq. 3.17) together with an actuator model described in the following section.

The Actuator Model

Equation 3.25 defines the control signal generated by the SCAS system. These controls will be sent to the actuation system to finally apply the desired controls to the main rotor, as well as to the tail rotor for conventional helicopters.

The response of the actuation system is fast and it should be negligible for low frequency or smooth control input. However, for high frequency or rapid control input, such as a step input, the dynamic characteristics of actuators should be taken into account. Therefore, a first order actuator model is added to the DelCopter model.

The first order actuator model is defined as:

$$\tau \dot{U}_{act} = U - U_{act} \quad (3.26)$$

3

where: U is a certain control input to the actuator system, τ is the corresponding time constant of the actuator, U_{act} is the output of the actuator (which is the final control applied to the main rotor or tail rotor), and \dot{U}_{act} is the actuator motion rate.

In matrix form, the actuator model can be written as:

$$\begin{aligned} \dot{\mathbf{U}}_{act} &= \mathbf{A}_{act} \mathbf{U}_{act} + \mathbf{B}_{act} \mathbf{U} \\ \mathbf{B}_{act} &= \begin{bmatrix} \frac{1}{\tau_{col}} & & & 0 \\ & \frac{1}{\tau_{long}} & & \\ & & \frac{1}{\tau_{lat}} & \\ 0 & & & \frac{1}{\tau_{yaw}} \end{bmatrix} \\ \mathbf{A}_{act} &= -\mathbf{B}_{act} \end{aligned} \quad (3.27)$$

where τ_{col} , τ_{long} , τ_{lat} and τ_{yaw} are time constant of actuators for collective pitch, longitudinal cyclic, lateral cyclic and yaw control respectively. The time constants values used in this thesis are shown in Table 3.2.

Table 3.2: Time constants of the actuator

	Actuator time constants (sec)			
	τ_{col}	τ_{long}	τ_{lat}	τ_{yaw}
Bo-105	0.04	0.04	0.04	0.02
Ornicopter	0.04	0.04	0.04	0.04

Since the actuator model introduces new dynamics into the system, the state-space model needs to be extended. Combining the bare model (Eq. 3.17) and Eq. 3.27, one can get:

$$\begin{aligned} \dot{\mathbf{X}} &= \mathbf{A}\mathbf{X} + \mathbf{B}\mathbf{U}_{act} \\ \dot{\mathbf{U}}_{act} &= \mathbf{A}_{act}\mathbf{U}_{act} + \mathbf{B}_{act}\mathbf{U} \end{aligned} \quad (3.28)$$

3.3 Validation for the Generic Helicopter Model

61

Substituting Eq. 3.25 into Eq. 3.28, the extended state-space model can be derived as:

$$\begin{aligned}\dot{\mathbf{X}} &= \mathbf{A}\mathbf{X} + \mathbf{B}\mathbf{U}_{act} \\ \dot{\mathbf{U}}_{act} &= \mathbf{A}_{act}\mathbf{U}_{act} + \mathbf{B}_{act}(\mathbf{U}^{in} + \mathbf{K}\mathbf{X})\end{aligned}\quad (3.29)$$

$$\mathbf{X}^* = \begin{bmatrix} \mathbf{A} & \mathbf{B} \\ \mathbf{B}_{act}\mathbf{K} & \mathbf{A}_{act} \end{bmatrix} \begin{bmatrix} \mathbf{X} \\ \mathbf{U}_{act} \end{bmatrix} + \begin{bmatrix} 0 \\ \mathbf{B}_{act} \end{bmatrix} \mathbf{U}^{in} \quad (3.30)$$

where \mathbf{X}^* is the extended state vector as

$$\mathbf{X}^* = \begin{bmatrix} \dot{\mathbf{X}} \\ \dot{\mathbf{U}}_{act} \end{bmatrix} \quad (3.31)$$

3

Time Delay

So far, the new linearised model with a simple SCAS system and the first order actuator model have been derived.

Between the pilot control input and the control signal received by the SCAS, a time delay also exists. To simplify the model, constant time delays are applied, and it is assumed that all the control channels have the same time delay.

To model this time delay, the state-space model (Eq. 3.30) is transferred into the transfer functions as:

$$\mathbf{X}^*(s) = \mathbf{H}(s)\mathbf{U}^{in}(s) \quad (3.32)$$

where $\mathbf{H}(s)$ is the transfer function matrix.

By multiplying one term for the time delay, the system with a constant time delay is

$$\mathbf{X}^*(s) = \mathbf{H}(s)e^{-\tau s}\mathbf{U}^{in}(s) \quad (3.33)$$

where τ is the time delay. In this thesis, a common value (200 ms [29]) is used for all the controls of both the Ornicopter and Bo-105 helicopters.

3.3 Validation for the Generic Helicopter Model

3.3.1 The Trim

Trim values at different flight velocities are calculated using the DelCopter model and compared with flight test data. The results are shown in Fig. 3.3.

Figure 3.3 shows a comparison between a flight test and the theoretical model for four control inputs and two attitude angles for the Bo-105. It can be found that the model developed in this thesis has good accuracy with regard to collective pitch and longitudinal direction.

In the low speed region (forward velocity lower than 50 knots), the inflow increases the left cyclic control required, revealing a failing in the simple trapezoidal model of longitudinal inflow [10], as shown in Fig. 3.3. Also, the roll angle (Φ) is underestimated

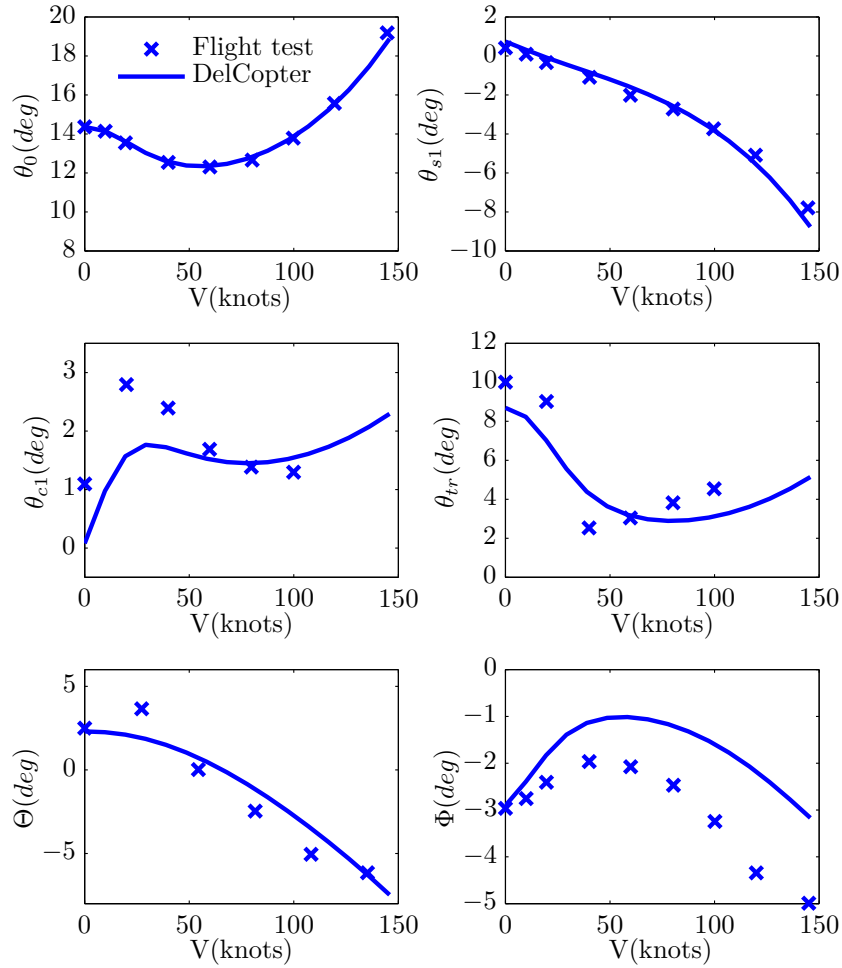


Figure 3.3: Trim values for the Bo-105

by the model, possibly caused by the fact that in this Level 1 model, the cross coupling between pitch and roll cannot be predicted very well. The tail rotor pitch is also usually under-predicted as a combined result of missing tail rotor losses and under-predicted main rotor torque, most noticeably at high speed [10].

3.3.2 The Main Rotor Torque

Figure 3.4 shows the main shaft torque of the Bo-105, which has the characteristic bucket profile as a function of forward speed. At high speed, non-linear rotor aerodynamic terms have a large effect on the collective pitch and power required, leading to gross errors with the simplified Level 1 modelling [10].

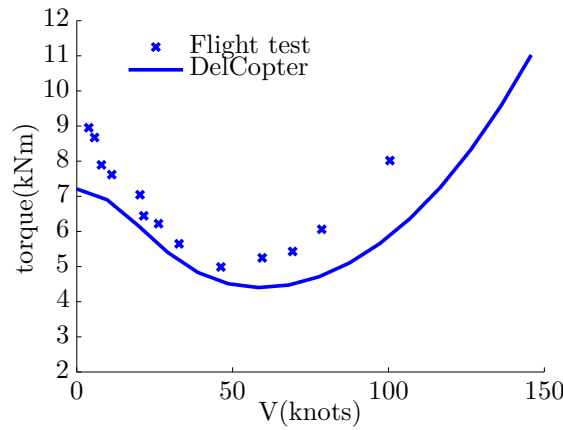


Figure 3.4: Main rotor torque of the Bo-105

3.3.3 The Dynamic Response

Besides the trim values and the shaft torque, in this thesis, the dynamic response of the helicopter to different control inputs are also used for model validation. Comparisons between test data and simulation for one test case are presented in Fig. 3.5. More comparisons for different test cases can be found in Appendix B:

Flight tests were conducted for all four control inputs of the helicopter. From the comparisons between the flight test and the numerical simulation, one can find that the theoretical model can predict the primary responses of the helicopter with good accuracy, especially in the yaw axis and the vertical direction. The longitudinal response to collective pitch input and lateral response to yaw input can be captured by the model. However, the pitch-roll cross coupling is missing from the simulation result, which is also a well known problem for the Level 1 model.

Comparisons in this section show that the DelCopter model can present the main characteristics of the helicopter. In the trim calculation, the main controls (collective and longitudinal inputs) can be captured with good accuracy. The main rotor shaft torque is underestimated with acceptable errors for concept analyses and conceptual design. Regarding the dynamic characteristics of the helicopter, the primary responses of the helicopter to different control inputs are well predicted by the model.

In the next chapter, this model will be used for different analyses. The main tasks

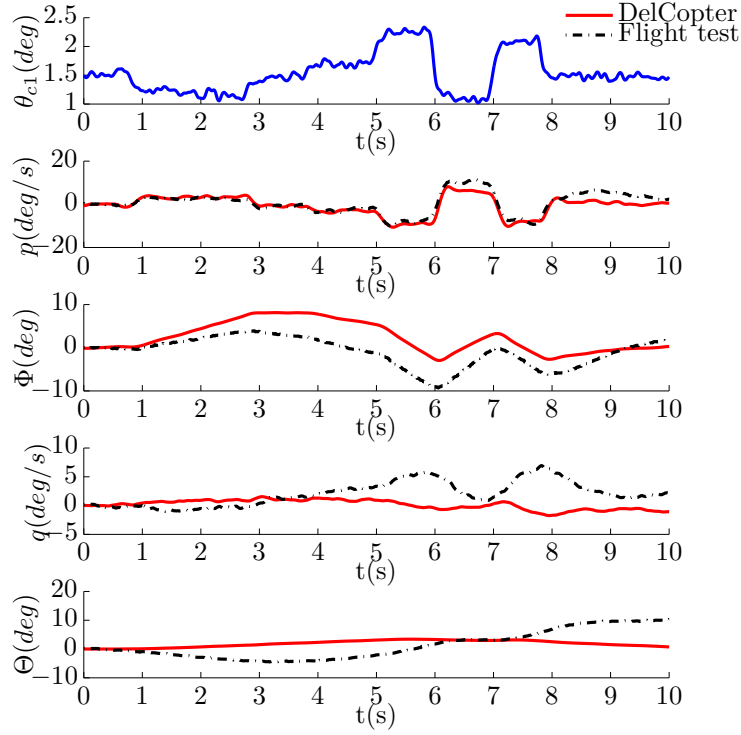


Figure 3.5: Flight test No. 9: positive longitudinal 3-2-1-1 input

will be the flight envelope prediction (which requires the trim calculation and power estimation), as well as the stability, controllability and handling qualities analyses (corresponding to the dynamic characteristics of the helicopter). the above comparison showed that the DelCopter model is valid for the research of this thesis.

3.4 Adaptations of the Delcopter to the Ornicopter Model

The DelCopter model was developed and validated in sections 3.2 and 3.3. This section will present the adaptations needed to develop the Ornicopter concept model, the so-called ‘ORNIcopter’ model.

3.4.1 The Forced Flapping Mechanism

The Ornicopter blades are driven by the forced flapping mechanism, as shown in Fig. 3.6, which is similar to the hovering rotor model for the Ornicopter used in Chapter 2 (see Fig. 2.14). In the Ornicopter flight mechanics model, the hinge offset is considered for a more generic blade configuration.

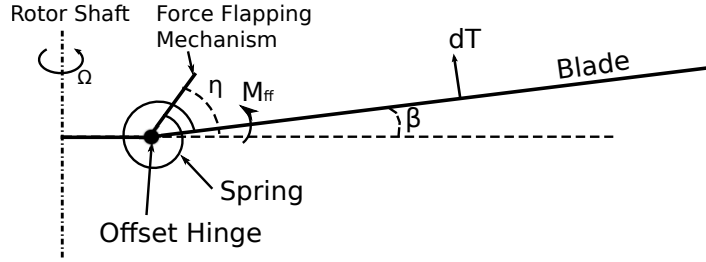


Figure 3.6: The blade hinge configuration of the Ornicopter

The flapping moment about the hinge generated by the forced flapping mechanism is:

$$M_{ff}(\psi) = K_{\beta}(\eta(\psi) - \beta(\psi)) \quad (3.34)$$

This moment will be used in the flapping EoM of the blade to calculate the blade motion, as well as the pitch and roll hub moments.

3.4.2 The Flapping Equation of Motion

The forced flapping mechanism generates a flapping moment on each Ornicopter blade, and hence, additional terms need to be added to the flapping equation of motion.

Recalling the Lagrangian equation (Eq. D.32), the generalized force for the Ornicopter is:

$$Q_{\beta} = M_{aero} + M_{ff} \quad (3.35)$$

and the kinetic energy of the blade for the Ornicopter is the same as that for conventional helicopters.

Substituting the forced flapping moment into the Lagrangian equation, one can derive three flapping equations for the Ornicopter, which is similar to those of a conventional helicopter model:

$$\mathbf{M}_{\beta} \ddot{\vec{\beta}} + \mathbf{A}_{\beta} \dot{\vec{\beta}} + \mathbf{N}_{\beta} + \mathbf{b}_{\beta} + \mathbf{b}_{\beta ff} = 0 \quad (3.36)$$

where \mathbf{M}_{β} , \mathbf{A}_{β} , \mathbf{N}_{β} and \mathbf{b}_{β} are the same as those for a conventional helicopter (see Eq. D.45), and $\mathbf{b}_{\beta ff}$ is the additional term introduced by the forced flapping moment, as:

$$\mathbf{b}_{\beta ff} = -\frac{\bar{K}_{\beta}}{\gamma} [0, \eta_{s1}, \eta_{c1}]^T \quad (3.37)$$

where \bar{K}_β is the normalized flapping, as:

$$\bar{K}_\beta = \frac{K_\beta}{\Omega^2 I_\beta} \quad (3.38)$$

Similarly to the hub forces and moments mentioned above, flapping equations are identical for each blade in conventional helicopter models. In the case of the Ornicopter, different equations can be derived for different blades, and the calculation for the flapping motion needs to be done N_b times in each interval.

The total number of flapping states and flapping equations of motion increase to $3 \times N_b$ for the Ornicopter. The flapping state vector is therefore:

$$\mathbf{X}_{\beta, Orni} = [\beta_0^{(1)}, \beta_{s1}^{(1)}, \beta_{c1}^{(1)}, \dots, \beta_0^{(N_b)}, \beta_{s1}^{(N_b)}, \beta_{c1}^{(N_b)}]^\top \quad (3.39)$$

3

3.4.3 The Forces and Moments Generated by One Blade

For the DelCopter model, the forces and moments generated by one blade are derived, including: three hub forces (T_s , H_s , S_s), three hub moments (M_{xs} , M_{ys} , M_{zs}), two aerodynamic moments for inflow model (M_{1s} , M_{2s}) and the first order harmonic components of thrust force (T_{ss1} , T_{sc1}) (see Eq. D.68 to D.75).

These forces and moments in the case of the Ornicopter are the same as for conventional helicopters, with the exceptions of pitch/roll hub moments (M_{xs} , M_{ys}). This does not mean that the Ornicopter rotor will have the same characteristics as conventional helicopter rotors. The impacts of the Ornicopter concept on hub forces and aerodynamic moments are embedded in the flapping motion of the blades ($\vec{\beta}$).

Due to the flapping moment generated by the forced flapping mechanism, the hub moments generated by the Ornicopter blades are different from those of conventional helicopters. Additional terms need to be added, as:

$$\begin{aligned} M_{xs, Orni}^{(k)} &= M_{xs}^{(k)} + \frac{1}{2} K_\beta \eta_{s1}^{(k)} \\ M_{ys, Orni}^{(k)} &= M_{ys}^{(k)} + \frac{1}{2} K_\beta \eta_{c1}^{(k)} \end{aligned} \quad (3.40)$$

where $M_{xs}^{(k)}$ and $M_{ys}^{(k)}$ are hub moments derived for conventional helicopters as shown in Eq. D.26, with the flapping motion of the blade replaced by the coefficients for the k^{th} blade of the Ornicopter.

3.4.4 The Total Hub Forces and Moments

It is assumed that all the blades of a conventional helicopter work identically and hence generate the same hub forces and moments. In the case of the Ornicopter, each blade is forced to flap differently, as discussed in Chapter 2. In this sense, each blade should be calculated separately with respect to the flapping motion, aerodynamic forces and moments, and hub forces and moments. Afterwards, these forces and moments can be

3.5 Validation of the Ornicopter Model

67

summed up for the total hub forces and moments, i.e.:

$$T_{mr} = \sum_{k=1}^{N_b} T_s(\vec{\beta}^{(k)}) \quad (3.41)$$

Similarly, calculating the roll hub moment of the Ornicopter rotor, one can obtain:

$$\begin{aligned} M_{x,Orni} &= \sum_{k=1}^{N_b} M_{x,Orni}^{(k)} \\ &= \sum_{k=1}^{N_b} M_x^{(k)} + \frac{1}{2} K_\beta \sum_{k=1}^{N_b} \eta_{s1}^{(k)} \\ &= \sum_{k=1}^{N_b} M_x^{(k)} + \frac{N_b}{2} K_\beta \bar{\eta}_{s1} \\ &= \sum_{k=1}^{N_b} M_x^{(k)} \end{aligned} \quad (3.42)$$

3

Recalling Eq. A.35 and the discussions in Section 2.4.4, the average flapping coefficients of the forced flapping mechanism ($\bar{\eta}_{s1}$ and $\bar{\eta}_{c1}$) should be zero to avoid introducing an additional titling angle of the average tip-path plane. In this sense, the motion of the forced flapping mechanism will not generate rotor hub moments, as shown in Eq. 3.42.

3.4.5 The Tail Rotor and Yaw Control

As the tail rotor is not needed for the Ornicopter, the force and moments generated by the tail rotor are removed from the generic flight mechanics model, as well as the inflow model for the tail rotor shown in Eq. D.67. The inflow state vector becomes:

$$\mathbf{X}_{\lambda,Orni} = [\lambda_0, \lambda_{s1}, \lambda_{c1}]^\top \quad (3.43)$$

The yaw control of the Ornicopter is achieved by varying the amplitude of the forced flapping motion. Therefore, the amplitude of the forced flapping mechanism motion (θ_{ff}) replaces the pitch control of the tail rotor in the control input vector \mathbf{U} , as:

$$\mathbf{U}_{Orni} = [\theta_0, \theta_{s1}, \theta_{c1}, \theta_{ff}]^\top \quad (3.44)$$

3.5 Validation of the Ornicopter Model

To prove that the assumptions made are correct at this stage of design, the ORNicopter model discussed above is validated against the test conducted by Küssner, which has been described in Section 2.5.3. Two test cases using the blade design number five (V) are used for the model validation. The rotor was tested in the hovering condition with different RPMs.

The propulsive shaft torque is extracted from the rotor torque data (M_a in Fig. 2.27). This is done by subtracting the rotor torque without active flapping ($\beta = 0$) from all the rotor torque data. Afterwards, the processed data is compared with the theoretical prediction, as shown in Fig. 3.7.

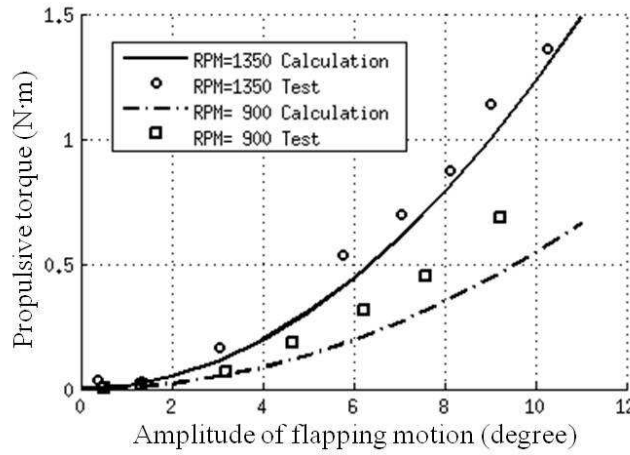


Figure 3.7: Propulsive torque as a function of the amplitude of flapping motion

From Fig. 3.7, it can be found that the theoretical prediction can match the test data with reasonable accuracy, especially for the test with high RPM. Decreasing the RPM reduces the accuracy of the model. The general trend of the propulsive shaft torque can be predicted. However, the propulsive torque is underestimated by the theoretical model and the difference between the test data and model prediction increases while a higher amplitude of flapping motion is applied. In the low RPM test condition, the test rotor encounters a low Re number close to the region where the lift enhancement caused by the LEV is essential for flapping wings [25]. This might be the reason causing the under-predicted propulsive torque.

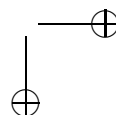
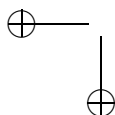
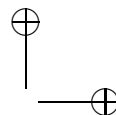
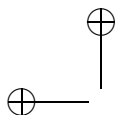
3.6 Conclusion

In conclusion, in this chapter, a Level 1 flight mechanics model is developed for conventional helicopters (the DelCopter model). It is an in-house classical 13 DoF flight mechanics model, including 6 DoF rigid body dynamics, 3 DoF blade flapping dynamics, 3 DoF main rotor inflow dynamics and 1 DoF tail rotor inflow dynamics. It also includes a simple SCAS, actuator model and control time delay. The model is validated against flight test data. Comparisons show that the model has good accuracy as a Level 1 model. After validation, the model is adapted for the Ornicopter concept to develop the Ornicopter flight mechanics model. The ORNIcopter model is compared with the windtunnel test in hovering condition. This shows that for the high RPM test case, the

3.6 Conclusion

69

ORNIcopter model can predict the propulsive torque (generated by the active flapping) with good accuracy.



4

Concept Analyses and Comparisons

4.1 Introduction

In Chapter 2, preliminary analyses for the Ornicopter concept were performed regarding the required forced flapping amplitude and flapping moment, as well as rotor hub forces and moments. Those analyses are limited to hovering using a simple Ornicopter rotor model.

In this chapter, the Ornicopter research is extended to various aspects in the forward flight condition. Using the Ornicopter flight mechanics model developed in Chapter 3, the Ornicopter concept will be analysed and compared with the conventional Bo-105 helicopter with respect to trim values, required power, flight envelope, autorotation, stability and controllability, handling qualities and vibrations. The comparisons will pinpoint the advantages and disadvantages of this concept. The reasons for these differences between the Ornicopter and conventional helicopters will be explored to provide further understanding of the Ornicopter concept.

In this chapter, all the Ornicopter design parameters will be kept the same as the baseline helicopter. As mentioned before, the conventional helicopter used as the baseline design is the Bölkow Bo-105.

4.2 The Trim Analysis

Using flight mechanics models, numerical algorithms can be applied to search the required control inputs and fuselage attitude angles (the trim values) to reach an equilibrium state in certain flight conditions. In this section, the trim values of the Ornicopter

and Bo-105 in level forward flight (standard sea level conditions) are calculated and compared. Figure 4.1 presents the trim values (four control inputs and two attitude angles) of the Ornicopter and Bo-105 as a function of forward flight speed.

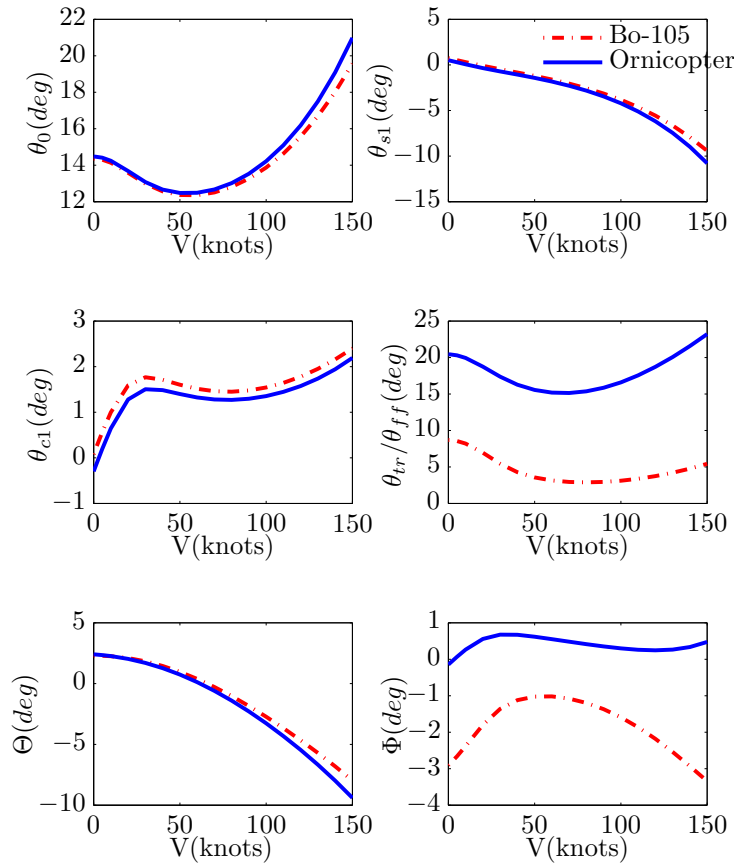


Figure 4.1: Trim values of the Ornicopter and Bo-105 in forward flight

From Fig. 4.1, one can see that the Ornicopter and Bo-105 have very similar trim values for collective pitch control, cyclic pitch controls and the fuselage pitch angle, which indicates similar characteristics for the Ornicopter rotor and conventional helicopter rotor with respect to generating thrust and hub moments. The main differences in the trim values between the Ornicopter and Bo-105 appear at the yaw control input

and the roll attitude angle.

The yaw control of the Ornicopter refers to the forced flapping mechanism motion, which is different from conventional helicopters. Despite this, the yaw control of the Ornicopter has a similar trend to that of the Bo-105. Both helicopters have a typical bucket shape for the yaw control due to the bucket-shaped collective pitch control input, i.e. the rotor shaft torque. At high forward speed, the required tail rotor collective pitch angle increases more gently than the Ornicopter yaw control. This is caused by the fact that the increasing air speed also increases the thrust generated by the tail rotor (see Eq. D.46). In the case of the Ornicopter, the forward flight speed is less influential on the propulsive moment generated by the Ornicopter rotor. In this sense, the Ornicopter yaw control needs to increase faster than the Bo-105 yaw control when the flight velocity is increasing.

The roll angle of the Ornicopter in trimmed flight is smaller than that of the Bo-105. This is caused by the absence of the tail rotor. The tail rotor generates a side force that needs to be balanced by tilting the thrust of the main rotor to the left (the main rotor rotates counter-clockwise), and hence causes a negative roll angle. Because the tail rotor, and hence the side force, no longer exists for the Ornicopter, the Ornicopter main rotor does not need to tilt to the left. Therefore, the roll angle of the Ornicopter is smaller than that of conventional helicopters, which is a favourable change caused by the Ornicopter concept. For the same reason, the lateral cyclic control of the Ornicopter in trimmed flight is also lower than that of the Bo-105.

For the collective pitch control, longitudinal cyclic control and pitch attitude angle, the Ornicopter has almost identical trim values as those of the Bo-105 at low flight velocity. Increasing the flight speed results in slightly increasing differences between the Ornicopter and Bo-105. The reason for this is the higher hub horizontal force (H) in the case of the Ornicopter. To balance this higher hub force, slightly higher rotor thrust is required, and the rotor needs to tilt further forward, resulting in a higher collective pitch, longitudinal cyclic control and nose-down pitch angle for the Ornicopter.

One simple example can be used to explain the higher horizontal force (H) of the Ornicopter, see Fig. 4.2. Two blades are considered in this case, of which one is tilting forward (TPP 1) and the other backward (TPP 2). As they are not in the shaft plane, their thrust forces (T_1 and T_2) can be decomposed into horizontal forces (H_1 and H_2).

The inflow conditions for the two blades are different due to the different tilting directions. As the blade 1 tilts forward, the incoming airflow (U_∞) has a larger impact on its thrust (T_1) due to the higher air flow perpendicular to the tip-path plane (u_i). In this sense, the thrust generated by blade 1 is smaller than that of blade 2, and hence blade 2 generates a higher horizontal force ($H_2 > H_1$).

This effect becomes stronger with increasing amplitude of the forced flapping. This additional horizontal force will not be generated if the active flapping is not applied, i.e. for a conventional helicopter. Therefore, the Ornicopter rotor generates a higher horizontal hub force (H) than in a conventional helicopter rotor.

The amplitude of the flapping motion of the Ornicopter blades required for steady forward flight is also calculated using the Ornicopter flight mechanics model, as shown in Fig. 4.3. The curve shows the bucket shape typical for the required power curve for

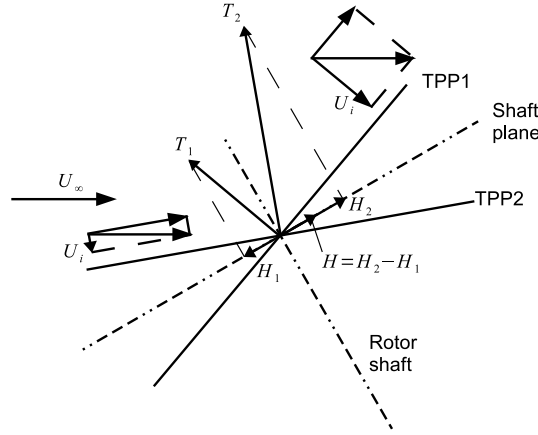


Figure 4.2: Hub horizontal force (H) of the Ornicopter in forward flight

4

helicopters in forward flight. This is caused by the fact that the required flapping amplitude is associated with the shaft torque, which is proportional to the required power (assuming the rotor RPM is constant). This calculation confirms that the Ornicopter only requires a modest flapping motion (less than 9°) to generate enough propulsive torque (in order to compensate for the shaft torque).

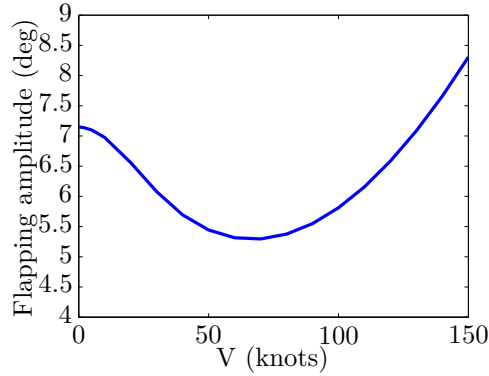


Figure 4.3: Average flapping amplitude of the Ornicopter blades as a function of forward velocity

One may have noticed that the flapping amplitude predicted by the hovering rotor model (see Eq. 2.34 in Section 2.4.2) is lower than the result from the Ornicopter flight mechanics model. This is caused by the relatively simple aerodynamic model used for the aerofoil in hovering, which has lower fidelity than the Ornicopter flight mechanics model. (In the hovering rotor model of the Ornicopter, a constant C_d is used for the

4.3 Efficiency and Required Power

75

blade element, while a quadratic function is used for the flight mechanics model as shown in Eq. 3.1.)

As discussed before, the active flapping of Ornicopter blades introduces a large variation in the blade element angle of attack. As in the flight mechanics model, the aerofoil profile drag is non-linear with regard to the AoA, and increasing the AoA variation will also increase the average profile drag of the blade element, as shown in Fig. 4.4. Therefore, the profile power of the Ornicopter rotor in hovering predicted by the flight mechanics model is higher than the values obtained with the hovering model. In this sense, a slightly higher amplitude of forced flapping (about 0.5°) is required to generate enough propulsive force (see Fig. 4.3 and Eq. 2.34).

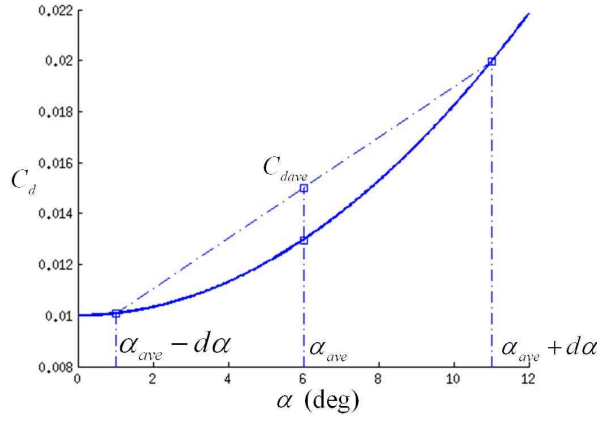


Figure 4.4: Higher average C_d with a larger AoA variation

4.3 Efficiency and Required Power

In this section the efficiency and the required power of the Ornicopter will be analysed and compared with the Bo-105 helicopter.

4.3.1 Power Calculation

The required power for conventional helicopters can be calculated as:

$$\begin{aligned} P &= Q_{mr}\Omega_{mr} + Q_{tr}\Omega_{tr} \\ &= P_{mr} + P_{tr} \end{aligned} \quad (4.1)$$

where Q_{mr} is the main rotor shaft torque, Ω_{mr} is the main rotor rotational velocity, Q_{tr} is the tail rotor shaft torque, Ω_{tr} is the tail rotor rotational velocity, P_{mr} is the main rotor power consumption, and P_{tr} is the tail rotor power consumption.

For the Ornicopter, blades are forced to flap and drive themselves to rotate. Therefore, the required power is consumed by the forced flapping mechanism. Recalling Eq. 3.34 and Fig. D.1, the moment required to drive the forced flapping mechanism will be the same as the forced flapping moment on the blade (M_{ff}), if the mass of the forced flapping mechanism is neglected. The instantaneous power consumed by the mechanism will be:

$$P_{ff}(\psi) = M_{ff}(\psi)\dot{\eta}(\psi) \quad (4.2)$$

where $\dot{\eta}(\psi)$ is the angular velocity of the forced flapping mechanism:

$$\begin{aligned} \dot{\eta}(\psi) &= \frac{d\eta(\psi)}{dt} \\ &= \eta_{s1}\Omega \cos(\psi) - \eta_{c1}\Omega \sin(\psi) \end{aligned} \quad (4.3)$$

Substituting Eq. 3.2 and 3.34 into Eq. 4.2 results in:

$$\begin{aligned} P_{ff}(\psi) &= K_\beta [(\eta_{s1} \sin(\psi) + \eta_{c1} \cos(\psi)) - (\beta_0 + \beta_{s1} \sin(\psi) + \beta_{c1} \cos(\psi))] \\ &\quad \times (\eta_{s1}\Omega \cos(\psi) - \eta_{c1}\Omega \sin(\psi)) \\ &= \frac{1}{2}K_\beta\Omega[\beta_{c1}\eta_{s1} - \beta_{c1}\eta_{s1} + 2\beta_0(\eta_{c1} \sin(\psi) - \eta_{s1} \cos(\psi)) \\ &\quad + (\eta_{s1}^2 - \eta_{c1}^2 - \beta_{s1}\eta_{s1} + \beta_{s1}\eta_{c1}) \sin(2\psi) \\ &\quad + (\eta_{s1}\eta_{c1} - \beta_{s1}\eta_{c1} + \beta_{c1}\eta_{s1}) \cos(2\psi)] \end{aligned} \quad (4.4)$$

The average power consumption can be calculated by integrating through the azimuth angle:

$$\begin{aligned} \bar{P}_{ff} &= \frac{1}{2\pi} \int_0^{2\pi} P_{ff}(\psi) d\psi \\ &= \frac{1}{2}K_\beta\Omega(\beta_{c1}\eta_{s1} - \beta_{c1}\eta_{s1}) \end{aligned} \quad (4.5)$$

As introduced before, the Ornicopter rotor can propel itself (to rotate). In other words, the propelling force generated by the active flapping motion can compensate for the resistant torque on the rotor (induced torque and profile torque).

In hovering, the total rotor torque should be zero to reach the equilibrium state. This indicates that no addition power is required to rotate the rotor except for the forced flapping power derived above. However, this is not necessarily true in forward flight. In forward flight, especially at high speed, the vertical fin can generate a yaw moment to compensate for a part of the main rotor torque. In this sense, the main rotor torque does not need to be zero. Due to the nonzero rotor torque, additional power is required to rotate the rotor, as:

$$P_r = Q_{mr}^{Orni}\Omega_{mr} \quad (4.6)$$

where P_r is the power consumed by the rotor torque and Q_{mr}^{Orni} is the main rotor torque of the Ornicopter rotor.

Similarly to the rotor hub forces, the active flapping power should be calculated for each Ornicopter blade separately, resulting in the required power for the Ornicopter as:

$$P^{(Orni)} = \sum_{k=1}^{N_b} \bar{P}_{ff}^{(k)} + P_r \quad (4.7)$$

where $\bar{P}_{ff}^{(k)}$ is the average flapping power consumption for the k^{th} blade.

4.3.2 The Figure of Merit

The Figure of Merit (FM) is defined as the ratio of the ideal power required to the actual power required of a hovering rotor, as shown in Eq. 4.8 [21]. It can be used as an indicator for how efficient the rotor is.

$$FM = \frac{\text{Ideal power required to hover}}{\text{Actual power required to hover}} < 1 \quad (4.8)$$

The ideal power is given by the momentum theory as [21]:

$$P_{ideal} = \frac{C_T^{3/2}}{\sqrt{2}} \quad (4.9)$$

4

and the actual required power is calculated by the DelCopter model using Eq. 4.1 (for the Bo-105) or the Ornicopter flight mechanics model using Eq. 4.7 (for the Ornicopter).

Figure 4.5 shows the Figure of Merit for the Bo-105 and the Ornicopter rotor as a function of thrust coefficient. It should be mentioned that the Ornicopter rotor is trimmed first for the nought shaft torque condition before the Figure of Merit is calculated.

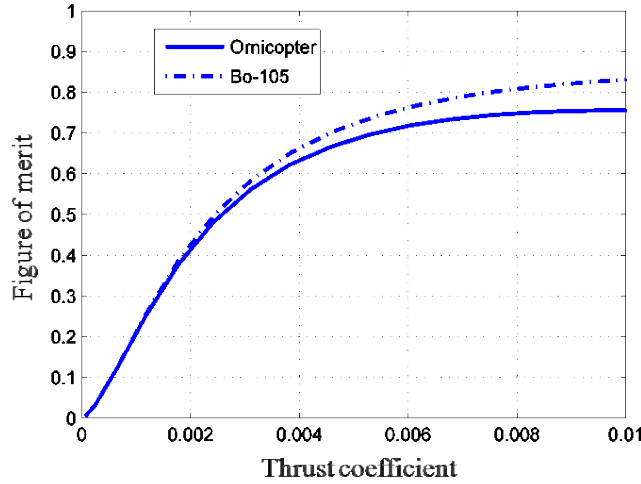
One can find out that the Figure of Merit of the Ornicopter is lower than that of the Bo-105 (around 8% lower when $C_T = 0.01$), i.e. the Ornicopter rotor is less efficient than the Bo-105 rotor. With increasing thrust coefficient, the difference between the two rotors increases.

The ideal power required for the Bo-105 and Ornicopter are identical for the same thrust coefficient. The lower efficiency of the Ornicopter rotor is caused by the higher blade profile power consumption.

As discussed before, the active flapping of the Ornicopter blades increases the average C_d of the blade elements. Therefore, the Ornicopter rotor consumes more profile power than a conventional helicopter rotor. Increasing the thrust coefficient results in a higher flapping amplitude needed to compensate for the higher shaft torque. Hence, a larger variation of AoA is introduced, which further increases the profile power consumption of the Ornicopter rotor. This causes the increasing difference between the Bo-105 main rotor and Ornicopter main rotor in terms of hovering efficiency.

4.3.3 Required Power

The calculation performed above shows the Ornicopter is less efficient than the Bo-105. However, the Figure of Merit does not take the tail rotor power consumption into



4

Figure 4.5: Figure of Merit predictions for the Bo-105 and Ornicopter rotor

account. The power consumed by the tail rotor is a relatively large portion of the total required power for conventional helicopters, especially in hovering. For the Figure of Merit calculation, the Ornicopter rotor has been trimmed for the nought shaft torque condition, and therefore no additional power is required for the Ornicopter.

For a more comprehensive comparison of the required power between the Ornicopter concept and the Bo-15, more detailed analyses are performed. The required power for the Ornicopter and Bo-105 helicopters is calculated as a function of the forward velocity, see Fig. 4.6. The required power is normalized by the Bo-105 total power requirement (power requirement for both main rotor and tail rotor), in order to have a more clear view of the different required power between the two helicopters.

While looking at the power required by the main rotor (curves *a* and *b* in Fig. 4.6), one can find that the Bo-105 main rotor is more efficient and needs less power than the Ornicopter rotor, as the Figure of Merit shows. This is the penalty that comes with flapping the blades in the Ornicopter concept. However, the tail rotor also consumes power in the case of conventional helicopters. The overall efficiency of the Ornicopter is slightly lower than that of the Bo-105. At low velocity, the total required power is slightly higher for the Ornicopter than the Bo-105 (about 1%). With increasing flight speed, the difference in power requirement between the Ornicopter and Bo-105 also increases slightly, and reaches approximately 3% at the maximum speed. Therefore, overall, there will not be a large increase in required power for the Ornicopter.

The statement has been made that the Ornicopter is more efficient than conventional helicopters due to the absence of a tail rotor [37]. The above calculation indicates different results. This is caused by the different aerofoil models, as mentioned in the trim analyses (Section 4.2).

In forward flight, the required power of helicopters consists of three parts: the in-

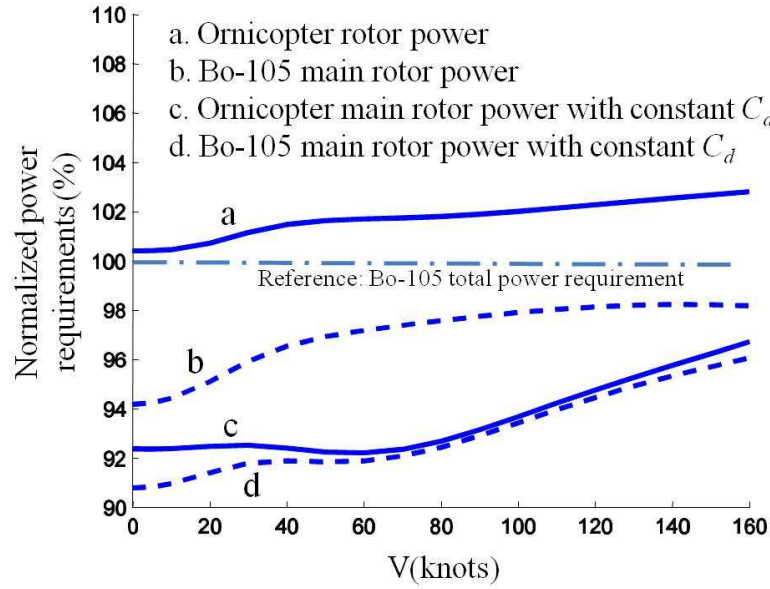


Figure 4.6: Power required of the Ornicopter and Bo-105

duced power, the profile power and the parasite power. The induced power is associated with the rotor thrust and the induced velocity, while the parasite power is only affected by the fuselage. As the Ornicopter is using the same design as the Bo-105, these two power components of both helicopters should be similar. The main reason for the higher required rotor power in the case of the Ornicopter is therefore related mainly to an increasing profile power.

Graphs *c* and *d* in Fig. 4.6 show the effect of the non-linearity of the C_D as a function of α . The rotor power requirements of the Ornicopter and Bo-105 with constant C_D were calculated. It can be found that, with constant C_D , the rotor power requirements of the Ornicopter and Bo-105 are almost identical. This confirms that the higher profile power of the Ornicopter rotor is caused by the non-linear drag coefficient and larger variation of the aerofoil AoA. As the profile power is a relatively small portion of the total power consumption, the total required power for the Ornicopter is only slightly increased.

4.4 The Flight Envelope

The flight envelope is the closed area in the altitude-velocity diagram, in which steady state flight is possible. It is determined by a large number of factors, such as weight, aerodynamics, engine system, structural dynamics and atmospheric conditions [9]. In this section, the flight envelopes of the Ornicopter and Bo-105 will be determined and compared. For this preliminary flight envelope prediction, simplified criteria are used,

including the power requirement and stall area.

4.4.1 The Calculation Criteria

Available Engine Power

To analyse the altitude performance of the Ornicopter, an engine model is required to predict the available engine power at different altitudes. As the main purpose of this analysis is to compare the performance of the Ornicopter and Bo-105 instead of to acquire accurate performance data, a simply engine model is used, [9]:

$$P_e \approx P_{e_0} \sigma_p^{1.35} \quad (4.10)$$

where P_e is the available engine power, P_{e_0} is the available engine power at sea level and σ_p is the relative air density.

Power Criterion

4

Inside the flight envelope, the engine should provide not only the required power for steady flight, but also some power margin for manoeuvrability. Therefore, the power criterion for each flight condition can be defined as:

$$P_0 \leq k_p P_e \quad (4.11)$$

where P_e is the maximum continuous power available from the engine in each flight condition, P_0 is the total required power of helicopters and k_p is the power margin factor considering the manoeuvrability margin and transmission loss.

In this thesis, the k_p is determined through an empirical way based on the Bo-105 specifications and model calculations. The required power of the Bo-105 at maximum velocity (sea level) is calculated using the DelCopter model and compared with the available engine power to determine the k_p , as:

$$k_p = \frac{P_0|_{V_{max}}}{P_{e_0}} \approx 0.846 \quad (4.12)$$

Stall Criterion

The effects of stall affect the performance of helicopters, e.g. the increase control loads and decrease control authority. For the preliminary Ornicopter analyses, a relatively simple criterion is defined based on the nondimensional total stall area (\bar{S}):

$$\bar{S} = \frac{S_{stall}}{\pi R^2} \leq \bar{S}_{max} \quad (4.13)$$

where S_{stall} is the average stall area of all the blades, R is the rotor radius and \bar{S}_{max} is the non-dimensional stall area boundary.

Similarly to the k_p , the stall boundary (\bar{S}_{max}) is also determined through the stall area prediction of the Bo-105 at maximum speed using the DelCopter model, as:

$$\bar{S}_{max} = \frac{S_{stall}|_{V_{max}}}{\pi R^2} \approx 8.93\% \quad (4.14)$$

4.4.2 Flight Envelopes of the Ornicopter and Bo-105

With the criteria defined above (Eq. 4.11 and 4.13), the flight envelopes (altitude vs. velocity) of the Ornicopter and Bo-105 are calculated and presented in Fig. 4.7. Two boundaries are drawn separately to show more details about the different characteristics of the Ornicopter and Bo-105.

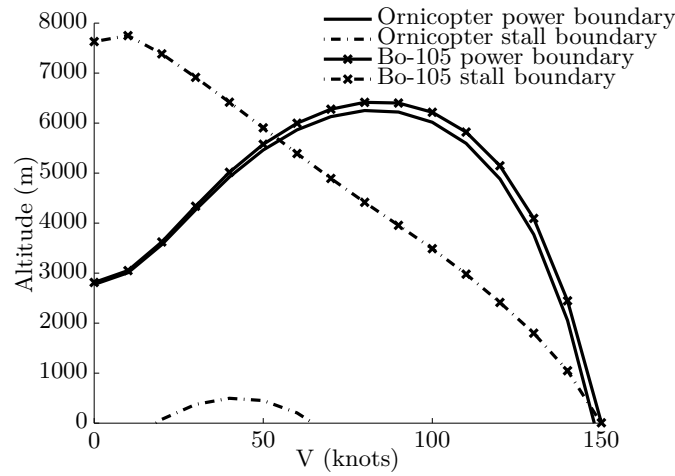


Figure 4.7: Flight envelope of the Ornicopter and Bo-105 defined by different criteria

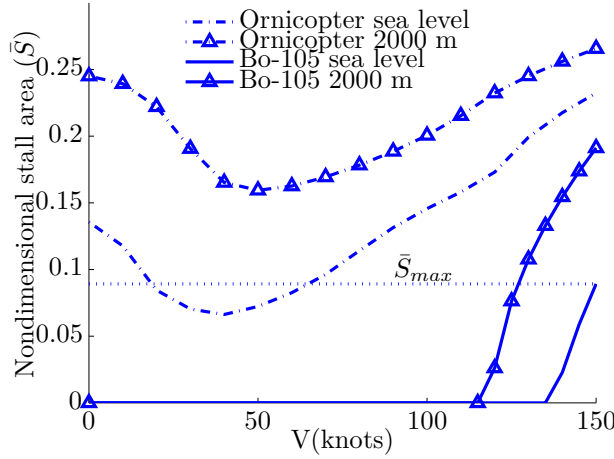
From Fig. 4.7 one can see that the boundaries determined by the power requirement for the Ornicopter and Bo-105 are very close to each other, due to the similar power required by both helicopters. The Ornicopter needs slightly more power than the Bo-105 (see Fig. 4.6), and therefore the power boundary of the Ornicopter is slightly smaller than that of the Bo-105.

The interesting difference corresponds to the stall boundaries. It can be found that the Ornicopter has a much smaller flyable region when compared to the Bo-105. This is due to the high stall area in both hovering and forward flight. The stall area of the Ornicopter and Bo-105 rotors at two altitudes (sea level and 2000 m) is presented in Fig. 4.8.

In forward flight, due to the blade longitudinal flapping and the longitudinal cyclic pitch control, stall occurs on the retreating side of the rotor, as shown in Fig. 4.9.

In the Ornicopter case, the additional active flapping motion enlarges the stall area of the Ornicopter rotor. Therefore, stall reaches the stall boundary earlier (around 65 knots) on the Ornicopter rotor than the Bo-105, as shown in Fig. 4.8. More details of the stall area on different Ornicopter blades are shown in Fig. 4.10.

Due to the fact that different blades are forced to flap in different phase angles, the stall area varies among blades. For different blades, the maximum AoA arises at different azimuth angles, where the blade flaps downwards. The blades No. 1 and 3



4

Figure 4.8: The rotor stall area of the Ornicopter and Bo-105 versus velocity

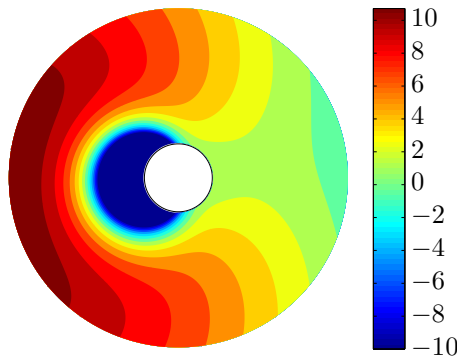


Figure 4.9: The angle of attack distribution on the Bo-105 rotor at 150 knots

are forced to flap laterally. Therefore, the impact of forced flapping on the stall area is relatively small, i.e. only slightly increased. In the case of blades No.2 and 4, which are forced to flap longitudinally, the stall area on blade changes dramatically. The blade No. 2 flaps up on the retreating side, which results in a large reduction of stall area, i.e. no stall occurs on this blade (the stall in the reversed area is not considered). On the contrary, the blade No. 4 encounters severe stalls.

One can see from Fig. 4.10 that the stall situation on the Ornicopter rotor is more complex than that of conventional helicopters. This should be considered in a more detailed research phase for the Ornicopter concept. In this thesis, only the average stall

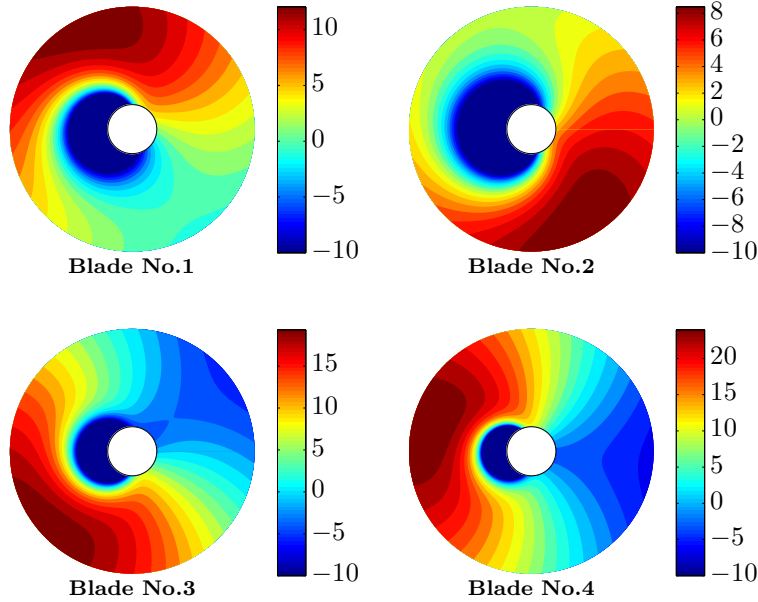


Figure 4.10: The angle of attack distribution on the Ornicopter rotor at 150 knots

area of all Ornicopter blades will be considered.

Figure 4.7 also shows that in hovering, the Bo-105 hovering ceiling is decided by the required power, while in the case of the Ornicopter, the stall effect is the most limiting factor. The stall area on the Ornicopter rotor is higher than the stall limitation in hovering at sea level, and increases with increasing altitude, as shown in Fig. 4.8.

In hovering flight, when the altitude is increasing, the air density decreases, and hence the induced velocity increases for the same rotor thrust. In this sense, higher collective pitch is needed, since higher induced velocity results in a lower angle of attack of the blade element and higher induced power. However, the total effect on the blade elements is only a slightly higher AoA. The AoA, and hence stall area, increase slowly with increasing altitude of the conventional helicopter rotor. Therefore, for conventional helicopters, the stall area will not reach the stall limitation in hovering until a very high altitude.

For the Ornicopter, some parts of its rotor encounter stall in hovering due to active flapping. The stall area is correlated with the amplitude of forced flapping motion. Recalling the trim values of the Ornicopter presented before, the yaw control input has a typical bucket shape. This results in similar bucket shape curves for the Ornicopter stall area as a function of velocity, as shown in Fig. 4.8.

To conclude, due to the active flapping, the blade angle of attack varies in a large

range for the Ornicopter rotor, and hence causes a large stall on the rotor of Ornicopter. This stall effect degrades the Ornicopter performance dramatically in terms of the flight envelope.

4.5 Autorotation

The autorotation performance of a helicopter depends on several factors, such as the rotor disk loading and the inertia of the rotor. To help the design process of a helicopter, the autorotation index (AI) is often used. One of the commonly used definitions is [21]:

$$AI = \frac{I_R \Omega^2}{2M_a DL} \quad (4.15)$$

where I_R is the rotor mass moment of inertia about the rotor shaft, M_a is the mass of the helicopter, and DL is the disc loading of the rotor.

For conceptual design, the Ornicopter's blade is assumed to have uniform mass distribution. The inertia of the rotor can be calculated as:

$$\begin{aligned} I_R &= N_b \int_0^R dm \cdot r^2 \\ &= N_b \int_0^R \rho_b S_a c^2 dr \cdot r^2 \\ &= \frac{1}{3} N_b \rho_b S_a c^2 R^3 \end{aligned} \quad (4.16)$$

where ρ_b is the density of blade, and S_a is the area of aerofoil with unit chord length.

Substituting Eq. 4.16 into the expression of autorotation index (Eq. 4.15) results in:

$$\begin{aligned} AI &= \frac{\frac{1}{3} N_b \rho_b S_a c^2 R^3 \Omega^2}{2M_a \frac{M_a g}{\pi R^2}} \\ &= \frac{\pi g \rho_b S_a V_t^2 R}{6N_b BL^2} \end{aligned} \quad (4.17)$$

where BL is the blade loading as $BL = (M_a g)/(N_b R c)$ and V_t is the tip velocity as $V_t = \Omega R$.

In this chapter, the Ornicopter is using the same design parameters as Bo-105. Therefore, they have the same AI. Equation 4.17 will be used again in the next chapter for the modified Ornicopter design.

It should be mentioned that in autorotation, the rotor works similarly to a wind turbine. It absorbs energy from the incoming airflow to drive itself to rotate. The main rotor torque is zero in autorotation and no reaction torque will be generated on the fuselage.

In this sense, the active flapping is not needed in the autorotation condition on the Ornicopter rotor. The amplitude of the forced flapping mechanism ($\hat{\eta}$) should be reduced to zero. For example, considering the swashplate mechanism (see Fig. 2.5), the

force flapping swashplate should be moved to the horizontal position in the autorotation. This requirement should be considered in the detailed mechanism design of the Ornicopter.

4.6 Stability and Controllability

From the full non-linear flight mechanics model, the linearized state-space model can be derived at trim points, as shown in Section 3.2.5.

The system matrix \mathbf{A} contains the derivatives of linear and angular accelerations of the body motion with regard to each state, such as $\partial\dot{w}/\partial u$, which indicates the effect of the perturbation of forward velocity (u) on the vertical acceleration (\dot{w}).

These derivatives can be calculated based on the system equations of motion (see Eq. 3.20 and 3.21), such as:

$$\begin{aligned}\frac{\partial\dot{u}}{\partial r} &= X_r + v_e \\ \frac{\partial\dot{p}}{\partial r} &= k_1 L_r + k_2 N_r\end{aligned}\tag{4.18}$$

where X_r , L_r and N_r are derivatives of the force and moment as defined in Eq. 3.23, v_e is the trim value of v , and k_1 and k_2 are inertial coefficients defined in Eq. 3.22.

It can be found that some of these derivatives, such as $\partial\dot{u}/\partial r$, consist of trim values of certain states, while other derivatives, such as $\partial\dot{p}/\partial r$, are affected by more than one total force or moment on a helicopter.

To get a more direct view of changes of forces and moments on the Ornicopter, the derivatives of total forces and moments with regard to all the states are used in the following comparisons. The force derivatives are normalized by the aircraft mass, and the moment derivatives are normalized by the moments of inertia (see Eq. 3.23), i.e.:

$$\begin{aligned}X_r &\equiv \frac{\partial X/\partial r}{M_a} \\ L_r &\equiv \frac{\partial L/\partial r}{I_x}\end{aligned}\tag{4.19}$$

These derivatives contain contributions from different components of the helicopter, including the main rotor, the tail rotor, fuselage and stabilizers. Since the Ornicopter has exactly the same design as the Bo-105 for the fuselage and stabilizers, these differences between the Ornicopter and Bo-105 are mainly generated by the new main rotor or the absence of a tail rotor.

To distinguish between the different contributions of the main and tail rotors to the derivatives, the derivatives for the Bo-105 helicopter have been calculated without the contribution of the tail rotor, the so-called Bo-105* configuration. In this way, differences between the derivatives of the Bo-105* and Ornicopter indicate only the effects of their different main rotors.

The 6 DoF body motion includes 9 states (6 states for body transitional and rotational velocities, 3 states for body Euler angles) and 4 control inputs (collective pitch,

longitudinal and lateral cyclic pitch and yaw control). The state matrix \mathbf{A} is a 9-by-9 matrix and the control matrix \mathbf{B} is 9-by-4, as shown in Eq. 3.20 and 3.21. Among these stability and control derivatives, some important derivatives of the Ornicopter and Bo-105/Bo-105* will be discussed, emphasizing the differences in behaviour between these two different helicopters.

4.6.1 Stability Derivatives

Force/Translational velocity derivatives X_u, Y_u, X_v, Y_v

The direct (X_u, Y_v) and the coupling force/velocity derivatives (X_v, Y_u) are presented in Fig. 4.11 as a function of forward flight velocity variation. The direct derivatives X_u and Y_v are due to the disc tilts aft and to the right (for a counter-clockwise rotor helicopter), following perturbations in u and v .

4

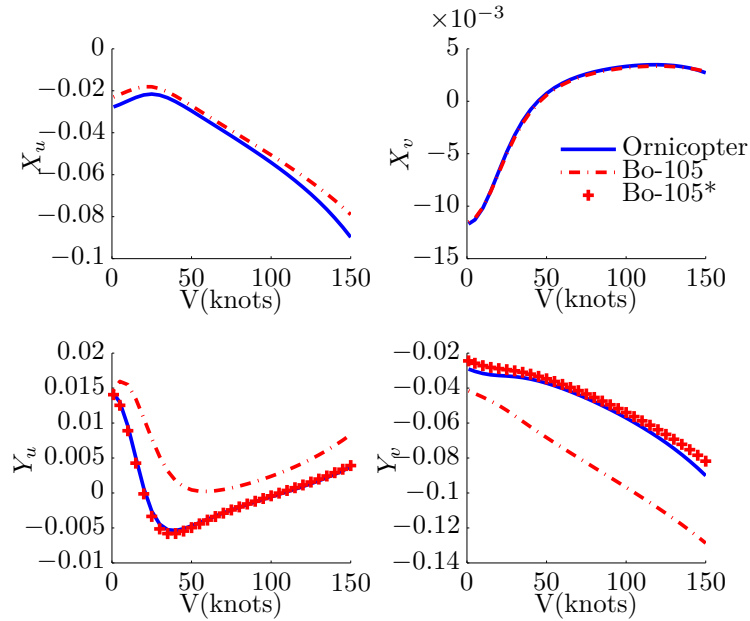


Figure 4.11: Direct and coupling force derivatives as a function of flight velocity

It can be found that in these derivatives of the X force - X_u and X_v , the values of the Ornicopter are nearly the same as in the case of the Bo-105, and the difference increases a little for high flight velocity. The tail rotor does not contribute to the X force and the curves for the Bo-105 and Bo-105* (the Bo-105 without a tail rotor) coincide.

However, for the Y force derivatives, the situation is different. Looking at Fig. 4.11, one can see that the Y force derivatives for the Ornicopter and Bo-105 have similar

trends, but their values are different. However, subtracting the tail rotor impact from the Y -derivative shows that the Y -derivatives for the Ornicopter and Bo-105* are almost identical. This indicates that the tail rotor is mainly responsible for the changes in the side force derivatives between the Ornicopter and Bo-105. It also indicates that the new main rotor configuration for the Ornicopter has the same lateral characteristics in the Y -forces as the Bo-105 rotor.

The speed and incidence static stability derivatives M_u and M_w

The speed and incidence static stability derivatives M_u and M_w give the static stability characteristics of the aircraft. The derivative M_u represents the change in pitching moment about the aircraft’s centre of mass when the aircraft is subjected to a perturbation in longitudinal velocity u . Figure 4.12 shows these two derivatives as a function of flight velocity.

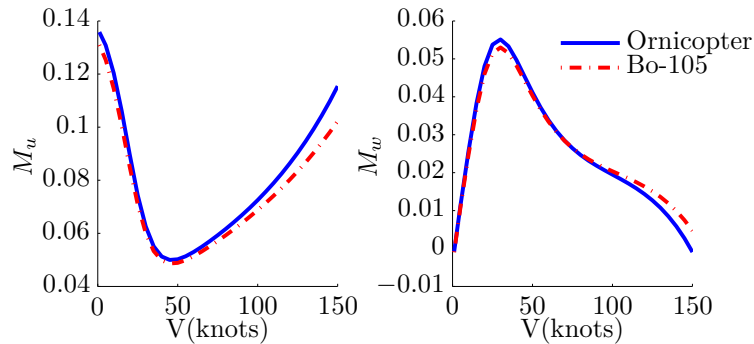


Figure 4.12: Variation of M_u and M_w with forward speed

Looking at this figure, only a slight difference can be found between the Ornicopter and Bo-105 static derivatives at high flight speed. The speed static derivative M_u of both helicopters exhibit static speed stability. An increase in forward speed causes the rotor disc to tilt back, as well as a higher lift force (downwards) on the horizontal stabilizer. This effect results in a nose-up pitching moment and a tendency to reduce speed. According to Padfield [10], this positive (apparent) speed stability is important for good handling qualities in forward flight but can degrade dynamic stability in both hover and forward flight.

Concerning the incidence static stability M_w , a negative M_w corresponds to a statically stable aircraft (a positive normal velocity perturbation results in a pitch-down moment). Looking at Fig. 4.12, one can see that M_w is positive for a large range of forward speeds. This is characteristic of most helicopters, as they are inherently unstable in pitch.

The heave damping derivative Z_w

The heave damping derivative Z_w gives the vertical response characteristics of a helicopter in response to a vertical gust. In the case of the heave damping derivative Z_w , the Ornicopter has the same damping as the Bo-105, as shown in Fig. 4.13. For hover, the value of Z_w is about $-0.33/s$, giving a heave motion time constant of about 3 seconds (this is a typical heave time constant for most helicopters in hover). With such a long time constant, the helicopter vertical response of both the Ornicopter and Bo-105 would seem more like an acceleration-control response than a velocity-control response, thus requiring more anticipation from the pilot’s point of view.

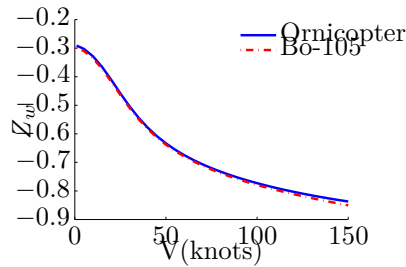


Figure 4.13: Variation of Z_w with forward speed

The sideslip derivatives L_v and N_v

The sideslip derivatives, i.e. the dihedral effect derivative L_v and the weathercock stability N_v , are significant for the lateral/directional DoFs. Figure 4.14 shows the variation of these two derivatives with forward speed for both the Bo-105/Bo-105* and the Ornicopter.

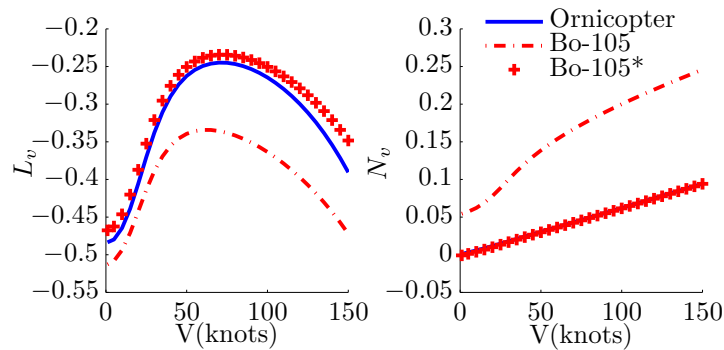


Figure 4.14: Variation of L_v and N_v with forward speed

Since the tail rotor contributes strongly to both derivatives, there are large discrep-

ancies in their values between the Ornicopter and Bo-105. The main reason for this is the tail rotor thrust. Once the tail rotor effect has been removed from the Bo-105 derivatives, the resulting Bo-105* configuration behaves very similar to the Ornicopter. In general, a positive value of N_v is stabilizing, while a negative value of L_v is stabilizing. Looking at Fig. 4.14, one can see that the Ornicopter has lower lateral/directional static stability.

The angular velocity derivatives

Figure 4.15 and Figure 4.16 shows the force/angular velocity derivatives X_q and Y_p , and the moment/angular velocities M_q , L_p , M_p and L_q for both the Ornicopter and Bo-105 helicopters. All these derivatives are contributed mainly by the main rotor. The M_q , L_p , M_p and L_q derivatives are also called direct and coupled damping derivatives. According to Padfield [10], the direct damping derivatives reflect short-term, small and moderate amplitude handling characteristics, while cross-damping derivatives play a dominant role in the level of pitch-roll and roll-pitch couplings. ‘They are the most potent derivatives in handling qualities terms, yet because of their close association with short-term rotor stability and response, they can also be unreliable as handling parameters.’ [10]

4

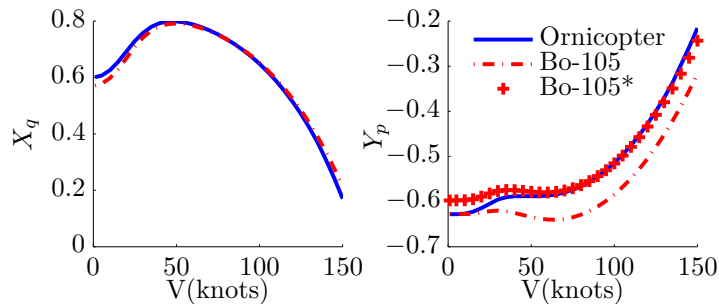


Figure 4.15: X_q and Y_p as a function of flight speed

Looking at Fig. 4.15 and Fig. 4.16, it appears again that the Ornicopter rotor has almost the same characteristics as a classical rotor system.

The derivatives N_r , L_r and N_p have a primary influence on the characteristics of the lateral/directional stability and control characteristics of the helicopter. As shown in Fig. 4.17, these three derivatives are also dominated by the tail rotor, which causes relatively large differences between the Ornicopter and Bo-105, especially in the yaw damping.

To conclude, there are major discrepancies between the stability characteristics of the Ornicopter and conventional helicopters. These differences can be attributed to the absence of the tail rotor on the Ornicopter. Its main rotor shows almost identical behaviour to that of the normal helicopter rotor. Derivatives dominated by the tail rotor are very different for the Ornicopter, including L_v , N_v , N_r , L_r and N_p . They will all

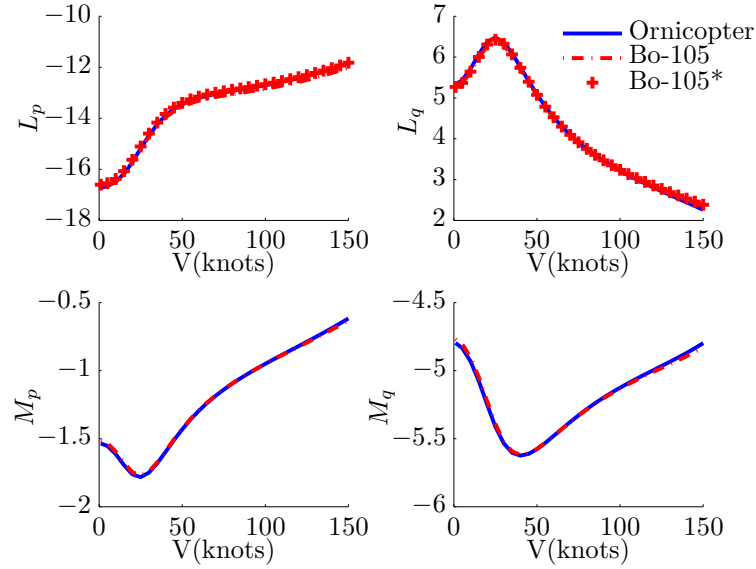


Figure 4.16: Variations of the direct and coupled damping derivatives

influence the lateral/directional stability and control characteristics of the Ornicopter. They will be further discussed in the handling qualities analyses (see Section 4.7).

4.6.2 The Natural Modes

The natural modes of motion for a helicopter can be calculated through the system matrix. Figure 4.18 shows the root loci of the Ornicopter and Bo-105 at different flight velocities (only for body motion DoFs). It can be found that the loci of the Ornicopter and Bo-105 are almost identical except for the Dutch roll mode.

Looking at this figure one can see that, assuming the same input data, the phugoid mode characteristics are almost identical for both helicopters, i.e. in hovering, the time to double the amplitude for Ornicopter is in the order of 2.8 seconds and 2.7 seconds for the Bo-105. An unstable phugoid mode is characteristic for most helicopters, and usually a horizontal stabilizer needs to be added to stabilize the mode. Also, the longitudinal pitch, heave subsidence and the lateral roll subsidence are very similar for both helicopters. The modes mentioned above are dominated by the characteristics of the main rotor in terms of generating thrust and pitch/roll moments. Similar modes show that the active flapping has very little impact on the main rotor thrust and hub moments.

As the Ornicopter is a tailless helicopter, the stability derivatives and natural modes dominated by the tail rotor change dramatically. This is mainly caused by the differ-

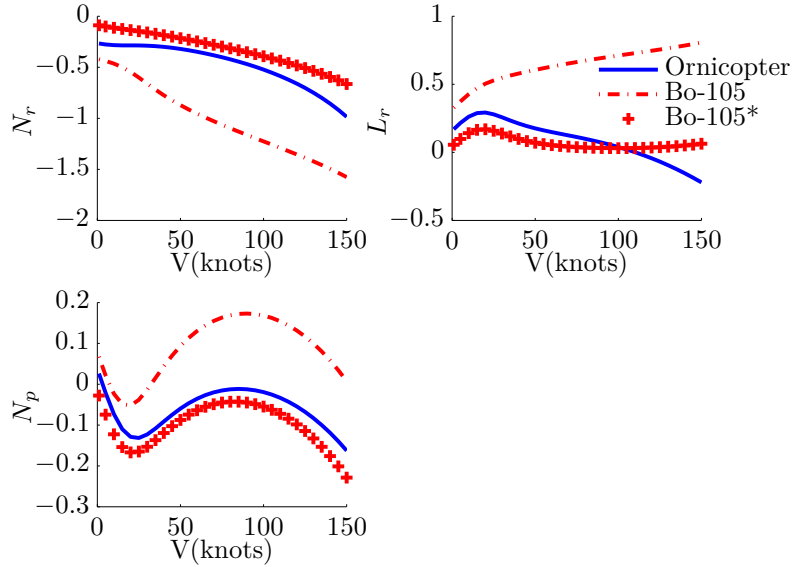


Figure 4.17: N_r , L_r and N_p as a function of flight speed

ence in yaw damping. For example, the combined roll-yaw motion of the Ornicopter represented by the Dutch roll mode is different from that of the Bo-105.

The Ornicopter’s Dutch roll mode is closer to the imaginary axis than that of the Bo-105. This indicates a lower Dutch roll damping. As is known, a low-damped Dutch roll is uncomfortable for passengers and is associated with high pilot workload especially in gusty conditions when trying to keep tracking a target. This shows that one will need to improve the Ornicopter’s Dutch roll characteristics either through redesign (incorporating for example endplate fins to the tail plane as in the MBB/Kawasaki BK117) or through the flight control system.

The time to half amplitude of the Dutch roll motion $t_{1/2}$ and the period of this periodic mode T can be calculated though the eigenvalues, as shown in Fig. 4.19.

It shows that the Ornicopter has a much higher half time than the Bo-105, especially at high velocity. This is due to the Ornicopter’s lower Dutch roll damping. The disturbances will need much more time to be damped off in the case of the Ornicopter, and this is not a favourable characteristic. This needs to be improved in the Ornicopter design. Solutions such as a bigger stabilizer or additional damping through controller design might be applied.

Meanwhile, the Ornicopter has a higher Dutch roll period (lower frequency) than the Bo-105. This longer period can reduce the number of oscillation cycles and may decrease pilot workload.

The eigenvectors of the system matrix also offer some useful information for the

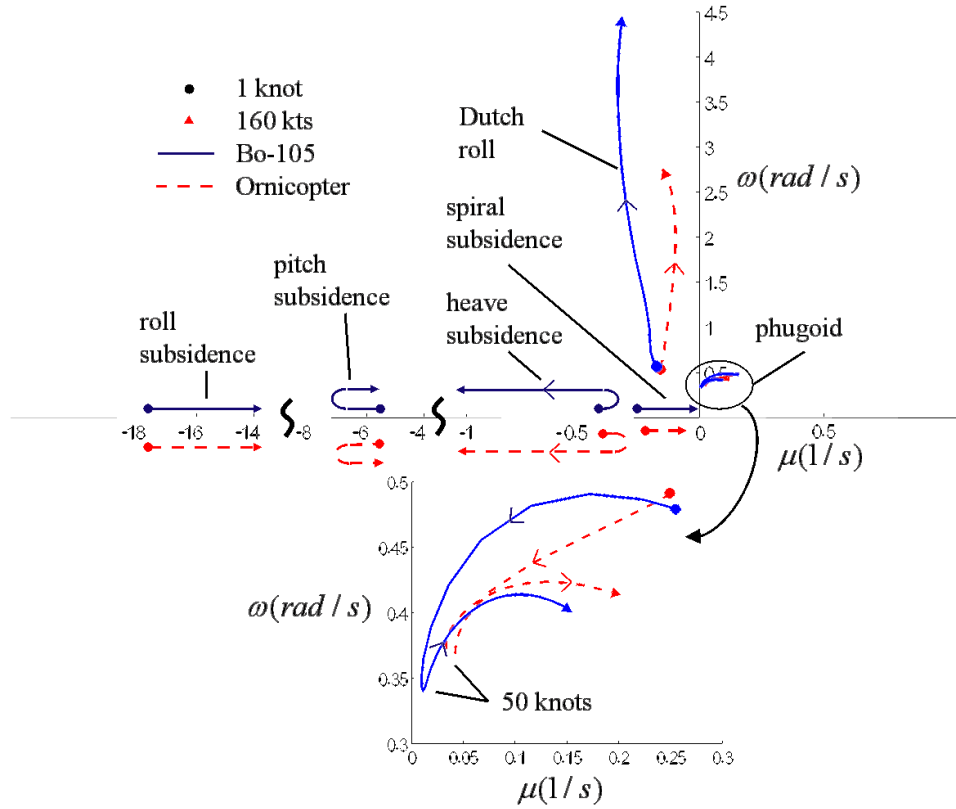


Figure 4.18: Loci of the Ornicopter and Bo-105 eigenvalues as a function of forward speed

amplitudes and phase angles of oscillations of each state. Table 4.1 presents the major part of the eigenvector for the Dutch roll mode at 80 knots. From this one can find that the phase angles for different motions are almost the same for the Ornicopter and Bo-105. However, the ratio of roll to yaw velocity is smaller in the case of the Ornicopter. Since the Ornicopter has a lower oscillation frequency, the roll attitude of the Ornicopter will reach a higher amplitude.

For the spiral mode, which is also a mode combined with roll and yaw motions, the Ornicopter and Bo-105 are surprisingly similar. This is caused by the fact that besides the yaw damping (N_r), the directional stability (N_v), the roll-to-sideslip derivative (L_v), the yaw-to-roll derivative (N_p) and the roll damping (L_p) also contribute to the spiral mode. The Ornicopter has different values for these derivatives (except the L_p) compared with the Bo-105. However, the combined effect of all the derivatives results in a similar spiral mode for both helicopters.

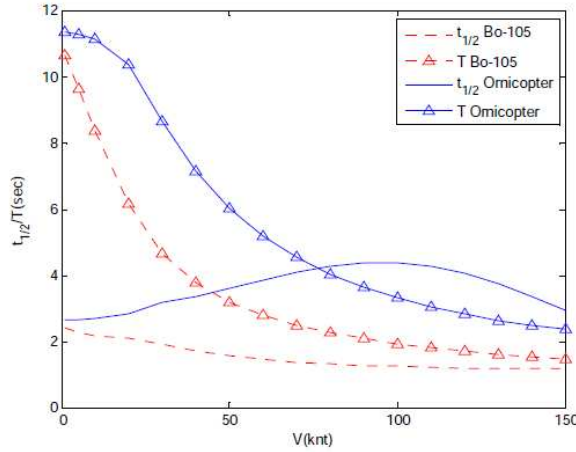


Figure 4.19: $t_{1/2}$ and T for Dutch roll

Table 4.1: Eigenvector for Dutch roll mode (partial)

		states			
		v	p	r	Φ
Bo-105	amplitude	1.0 m/s	1.1 deg/s	3.9 deg/s	0.40 deg
	phase(deg)	0	174	-79.7	68.8
Ornicopter	amplitude	1.0 m/s	0.94 deg/s	2.0 deg/s	0.61 deg
	phase(deg)	0	174	-83.4	74.8

4.6.3 Control Derivatives

Of the 24 control derivatives, characteristic of the 6 DoF model, 11 have been selected to be discussed in more detail in the following.

Figure 4.20 presents the first set of control derivatives corresponding to the derivatives of thrust with the main rotor collective θ_0 and longitudinal cyclic θ_{s1} , and the pitch and roll moments generated by the application of main rotor collective. The first two derivatives are primarily influenced by the blade loading and tip speed.

Figure 4.21 presents the second group of derivatives corresponding to the direct and coupled response for cyclic pitch control, including $L_{\theta_{s1}}$, $L_{\theta_{c1}}$, $M_{\theta_{s1}}$ and $M_{\theta_{c1}}$.

Since these two sets of derivatives are contributed primarily by the main rotor, no significant differences between the Ornicopter and Bo-105 helicopters can be found. These small differences are probably caused by the slightly different trim values of the Ornicopter.

Figure 4.22 presents the third set of control derivatives corresponding to the yaw control generated by applying collective pitch control of the tail rotor for the Bo-105,

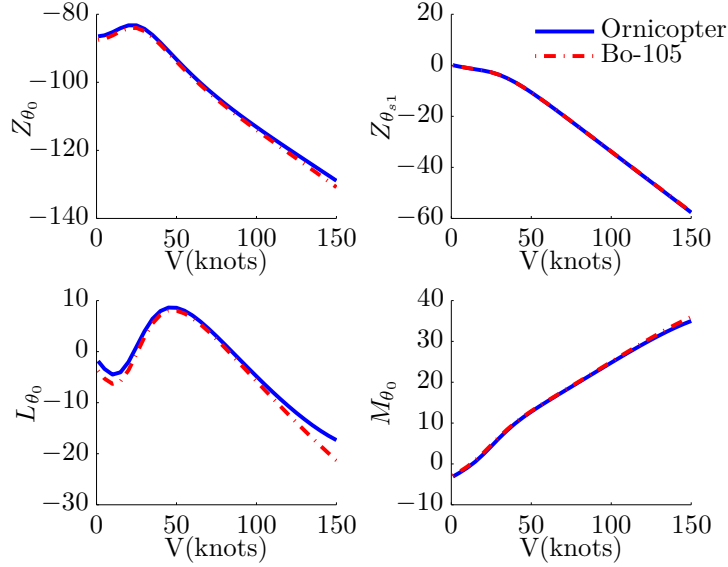


Figure 4.20: First set of control derivatives a function of flight speed

or in the case of the Ornicopter changing the amplitude of forced flapping motion. As the Ornicopter has a fundamental new method of yaw control, these control derivatives are very different from the Bo-105.

Looking at Fig. 4.22, it can be found that the Ornicopter’s coupled response for yaw control input is different from that of conventional helicopters. For the Bo-105, the yaw control causes relatively high side force and roll moment (Y_{yaw} and L_{yaw}), while these two coupling terms are nearly zero for the Ornicopter. This is caused by the fact that the Ornicopter yaw control is achieved by controlling the propulsive torque generated by the blade forced flapping motion. In this manner, the side force and the roll moment on the Ornicopter will not be affected while applying the yaw control.

At the same time, there are some additional coupling terms for the Ornicopter, i.e. X_{yaw} , Z_{yaw} and M_{yaw} . The additional terms are caused by the impacts of active flapping on the rotor thrust and horizontal force.

As discussed before (see Section 4.2), the active flapping increases the horizontal force (H) generated by the rotor in forward flight. While applying a perturbation (positive) on the Ornicopter yaw control, the amplitude of active flapping will be increased, and hence a larger hub horizontal force (H) will be generated. This additional force is in the negative direction of the x-axis, and therefore the Ornicopter has a negative X_{yaw} . The variation of the horizontal force will also cause a nose-up pitch moment ($dM > 0$). For this reason, a positive M_{yaw} can be found for the Ornicopter.

With increasing flight velocity, the additional horizontal hub force becomes higher

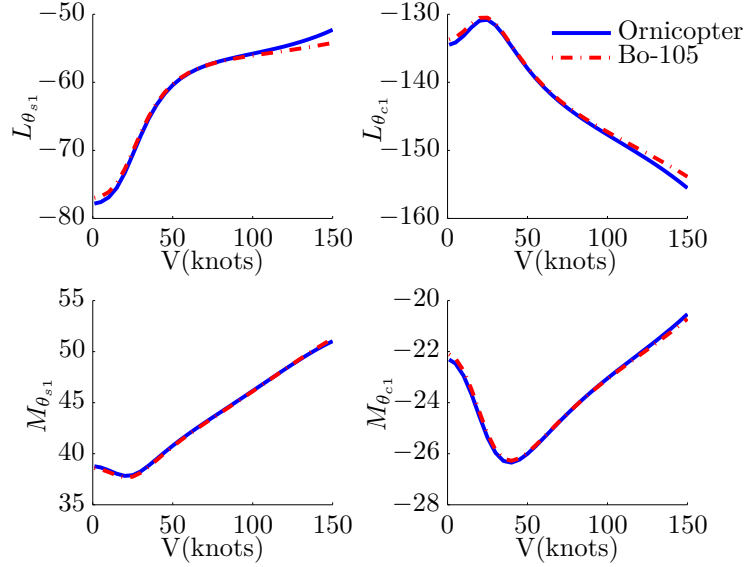


Figure 4.21: Variation of direct and coupling moment derivatives

due to the higher amplitude of the active flapping. Therefore, the values of X_{yaw} and M_{yaw} also increase when the flight velocity is increasing.

The coupled vertical acceleration (Z_{yaw}) is caused by the reduction of the main rotor thrust while applying yaw control. For a simple hovering example, considering one blade flapping with the amplitude of $\hat{\beta}$, the effective thrust (T_s) is:

$$T_s = L_s \cos(\hat{\beta}) \quad (4.20)$$

where L_s is the lift force of the blade perpendicular to the TPP. The effect of the flapping amplitude on the lift L_s is negligible. The variation of thrust while yaw control is applied will be:

$$\frac{dT_s}{d\hat{\beta}} = -L_s \sin(\hat{\beta}) \quad (4.21)$$

Recalling the relation between the blade flapping amplitude $\hat{\beta}$ and the yaw control input of Ornicopter, i.e. the motion amplitude of the forced flapping mechanism $\hat{\eta}$ (see Eq. 2.33), one can get:

$$\begin{aligned} \frac{dT_s}{d\hat{\eta}} &= \frac{dT_s}{d\hat{\beta}} \cdot \frac{d\hat{\beta}}{d\hat{\eta}} \\ &= -L_s \sin(\hat{\beta}) \sqrt{\frac{S_\beta^2}{1 + S_\beta^2}} \end{aligned} \quad (4.22)$$

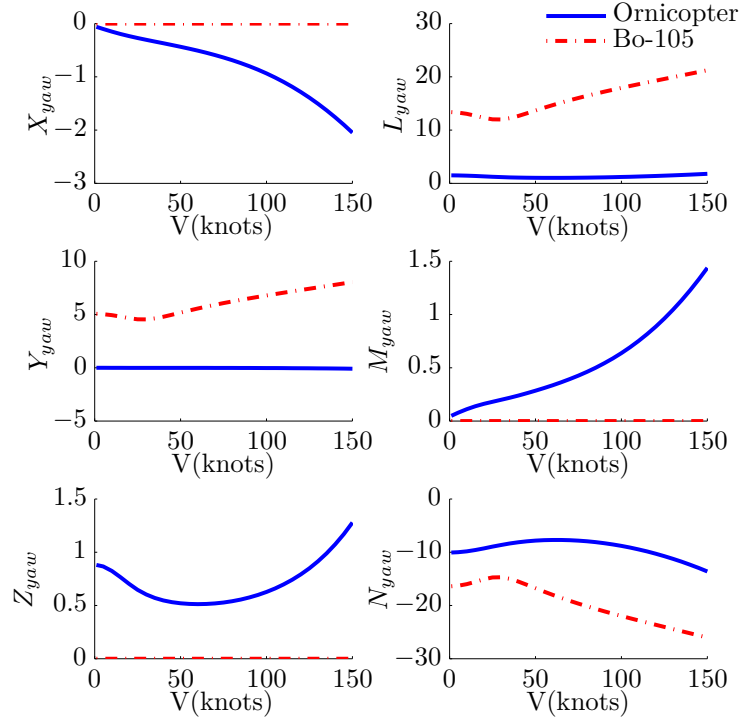


Figure 4.22: Yaw control derivatives as a function of flight speed

One can see from the above equation that increasing the yaw control of the Ornicopter will increase the amplitude of the active flapping, and hence decrease the total thrust generated by the Ornicopter rotor. This reduction is related to the amplitude of active flapping in trimmed flight. In this sense, the Z_{yaw} has a similar bucket shape similar to the flapping amplitude presented in Fig. 4.3.

Although the Ornicopter has some additional coupling responses to yaw control input, the derivatives are relatively small compared with the coupling terms of the Bo-105. In this sense, the Ornicopter has a lower coupling response to yaw control input and this is a positive characteristic of the Ornicopter as it reduces the workload of the pilot.

For the on-axis characteristics, since different yaw control mechanisms are used for the Ornicopter and Bo-105, the values of N_{yaw} derivatives cannot be compared directly. In the next section, handling qualities analyses will be performed, such as quickness and bandwidth parameters, to compare the yaw dynamic characteristics of Ornicopter and Bo-105.

Based on the comparisons in this section, some conclusions can be drawn. The Ornicopter rotor has stability and control characteristics very close to those of a conventional helicopter rotor in pitch and roll axes. Since the Ornicopter does not have a tail rotor, the stability derivatives dominated by the tail rotor change dramatically. This results in lower yaw damping and stability. These derivatives are significant for lateral/direction stability properties, and cause a large difference in the Ornicopter Dutch roll mode as compared to the Bo-105. Regarding yaw control, the Ornicopter has different coupling responses. However, those couplings are relatively small, and this is one of the favourable changes introduced by the Ornicopter concept.

4.7 Handling Qualities

In order to assess the handling qualities of the Ornicopter and Bo-105, the ADS-33 (Aeronautical Design Standard [4]) criterion is used. It is a widely used criteria in rotorcraft community, and defines different handling qualities parameters for helicopters, such as the bandwidth and phase delay. This thesis is concerned with those handling qualities that can be quantified, i.e. they can be calculated through theoretical analyses.

Using the Ornicopter flight mechanics model, simulation programs are developed for the attitude quickness calculation. The linearised model is used for bandwidth/phase delay and natural mode analyses.

The Bo-105 and Ornicopter are considered utility helicopters, and therefore the criteria for general mission task elements (MTEs) defined by the ADS-33 are used in this section, rather than target acquisition tasks or tracking tasks.

4.7.1 Yaw Control Power

The Ornicopter concept changes the helicopter yaw control method. Before further handling qualities analyses, the Ornicopter yaw control power is analysed to prove that this new concept is controllable.

In the ADS-33, the level of helicopters yaw control power is defined by the maximum achievable yaw rate in different flight conditions [4, p. 68]. To predict the maximum achievable yaw rate of helicopters, some details should be considered, such as the tail rotor stall and the mechanic limitations of control, which are not modelled in this thesis. The prediction for maximum achievable yaw rate may not be accurate enough for comparison.

Therefore, in this section, step yaw control inputs with different amplitudes are applied to both the Ornicopter and Bo-105 models. The maximum yaw rate caused by the yaw control is presented in Fig. 4.23 (curve a and b) as a function of the amplitude of the step input.

Comparing curve a and b in Fig. 4.23, one can see that the Ornicopter has a higher maximum yaw rate than the Bo-105 for the same yaw control input. It should also be considered that the yaw control input of the Ornicopter varies the motion amplitude of forced flapping mechanism ($\hat{\eta}$). The corresponding amplitude variation of the blade flapping motion is actually much smaller than the control input.

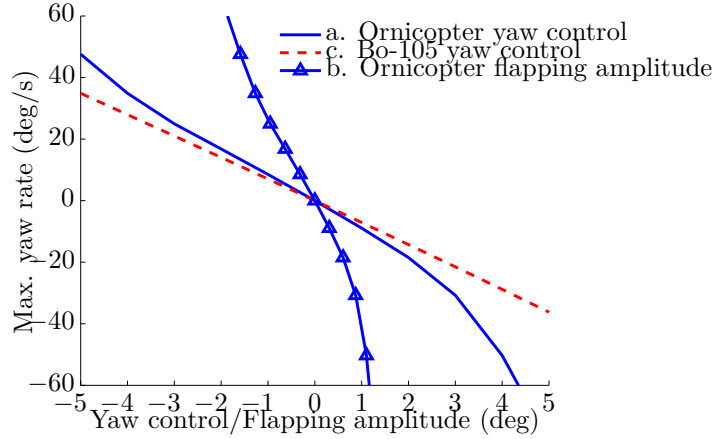


Figure 4.23: Maximum yaw rate for different yaw control inputs (40 knots)

4

In order to show this, the variation in the blade flapping amplitude caused by the yaw control input is also calculated, and plotted with the corresponding maximum yaw rate (curve c in Fig. 4.23). One can see that, to reach the same yaw rate, the change of blade flapping amplitude for the Ornicopter is less than 20% of the tail rotor cyclic variation in the case of the Bo-015.

Figure 4.23 indicates that the Ornicopter has higher yaw control power than the Bo-105. This is caused by the fact that the Ornicopter controls the main rotor torque directly instead of controlling the tail rotor thrust. In this sense, the Ornicopter can generate higher yaw moment on the fuselage than the Bo-105. It can also be considered from the power aspect point. With conventional helicopters, the tail rotor power consumption is less than 10% of the main rotor power. Therefore, by controlling the main rotor directly, the Ornicopter should have more control ‘power’ in the yaw direction. From this power aspect, it can also be concluded that for different helicopter weight catalogues, the Ornicopter will also have this advantage.

4.7.2 Bandwidth and Phase Delay

Parameter Definition

The bandwidth and phase delay is defined for short-term and small-amplitude attitude changes. It is based on the frequency response of the attitude angles (Ψ , Φ and Θ) to pilot control input. The Bode plot of the helicopter is used to determine these parameters, as shown in Fig. 4.24.

Some characteristic points (A to E in Fig. 4.24) are defined on the Bode plot to determine the bandwidth and phase delay of a helicopter. They are explained as follows:

- Point A is on the phase curve where the phase angle is -180° . The frequency at

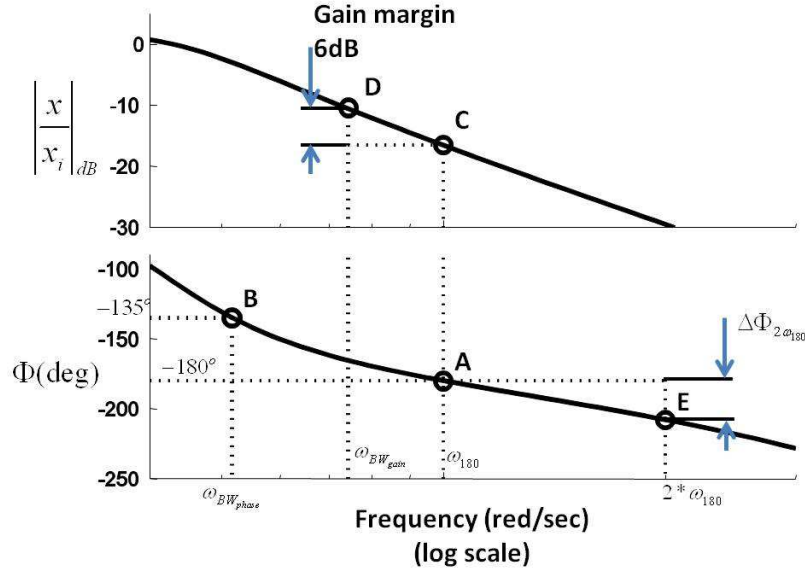


Figure 4.24: Bandwidth and phase delay definition

this point is defined as ω_{180} .

- Point B is on the phase curve where the phase angle is -135° . The frequency at this point is defined as $\omega_{BW_{phase}}$ (bandwidth for phase margin).
- Point C is on the magnitude curve, and corresponds to the same frequency as point A (ω_{180}).
- Point D is on the magnitude curve, and has a 6 dB higher magnitude response than point C. The frequency as point D is defined as $\omega_{BW_{gain}}$ (bandwidth for gain margin).
- Point E is on the phase curve, and corresponds to the frequency of $2\omega_{180}$. The phase difference between A and E is defined as $\Delta\Phi_{2\omega_{180}}$.

Since only a simple SCAS is implemented in the flight mechanics model to provide additional damping and stability, the helicopter analysed in this thesis can be considered as a rate response type. Based on the ADS-33, the bandwidth and phase are defined as:

$$\begin{aligned}\omega_{BW} &= \min(\omega_{BW_{gain}}, \omega_{BW_{phase}}) \\ \tau_p &= \frac{\Delta\Phi_{2\omega_{180}}}{57.3(2\omega_{180})}\end{aligned}\tag{4.23}$$

The Pitch and Roll Axes

It has been demonstrated that the values of the stability and controllability derivatives for the Ornicopter have almost identical characteristics in longitudinal and lateral directions when compared to the ones of the Bo-105 (with the assumption that the two helicopters are similar in dimensions). The bandwidth and phase delay calculations lead to the same conclusion, as seen in Fig. 4.25. For this calculation, all the SCAS gains are set to zero, while the actuator model and control time delay are applied.

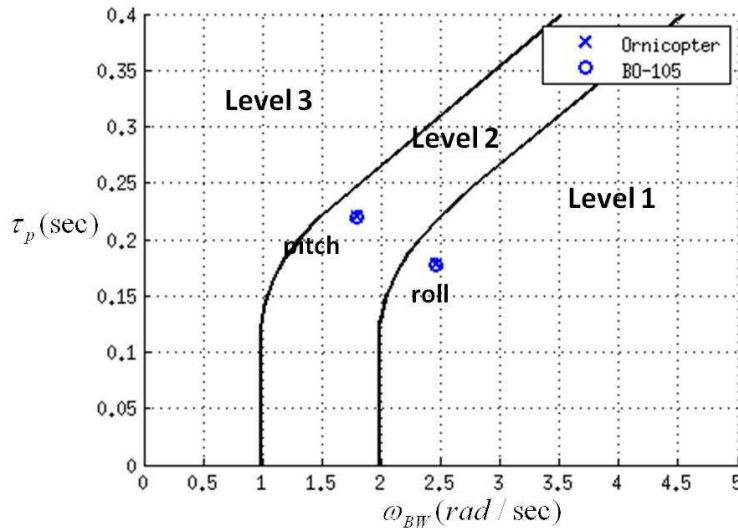


Figure 4.25: Bandwidth and phase delay in pitch and roll directions (5 knots)

Since the pitch and roll handling qualities of the Ornicopter and Bo-105 are very similar, they will not be discussed in detail in this thesis.

The Yaw Axis

Recalling the stability and controllability derivatives calculated in Section 4.6, the conclusion was that the main differences between the Ornicopter and Bo-105 appeared in the yaw direction (N_r) and lateral-yaw coupling terms (N_v and L_r). Therefore, differences between the Ornicopter and Bo-105 are expected in directional handling qualities.

For yaw direction, the bandwidth and phase delay without a SCAS are calculated between 1 knot and 90 knots flight velocity, as shown in Fig. 4.26 and 4.27.

It can be found that with increasing forward velocity, the bandwidth of both the Ornicopter and Bo-105 increases and the level of yaw handling quality follows an upward trend. However, the Ornicopter has a higher phase delay and lower bandwidth than the Bo-105 and hence it corresponds to one level lower for most of the velocities (10 knots to 90 knots with the interval of 10 knots), as seen in Fig. 4.27.

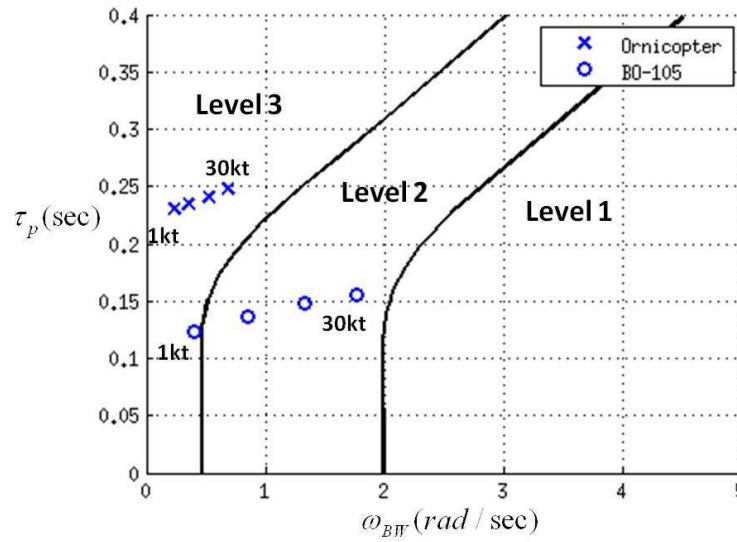


Figure 4.26: Bandwidth and phase delay in the yaw direction (hover and low speed)

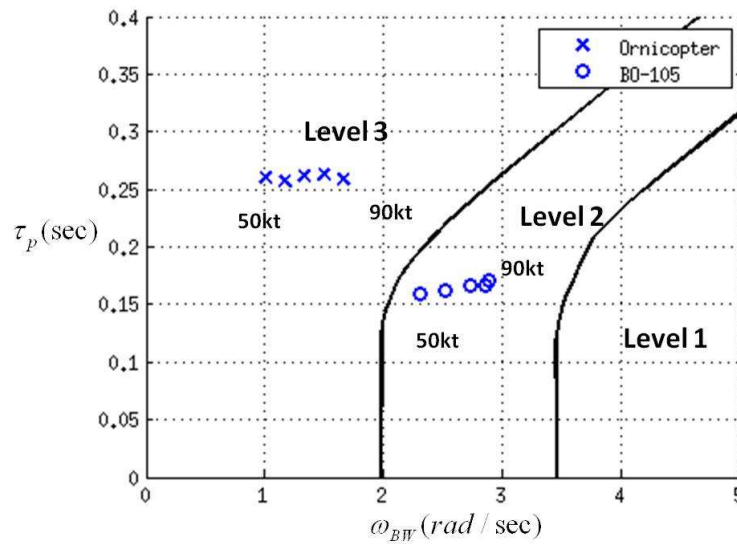


Figure 4.27: Bandwidth and phase delay in the yaw direction (forward flight)

To understand the reason for this drawback of the Ornicopter, flight mechanics models with different fidelities are extracted from the full mechanics model. Bode plots

for these models are made to show the impacts of different parts of the ORNIcopter model, as shown in Fig. 4.28.

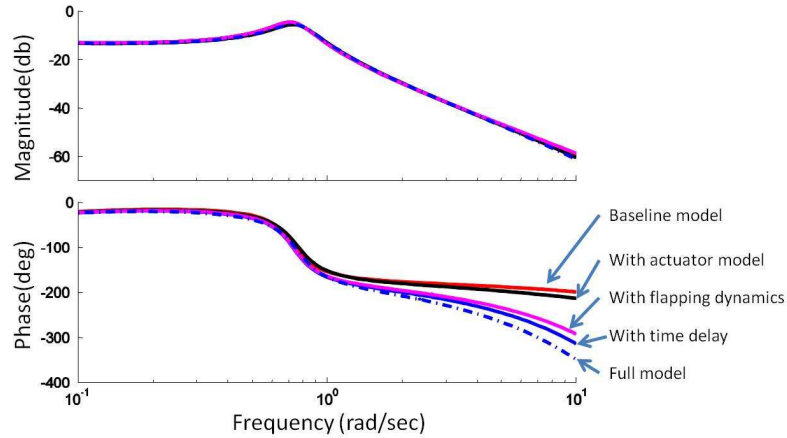


Figure 4.28: Magnitude and phase responses of different ORNIcopter models in the yaw direction (80 knots)

For the ‘baseline model’ used in Fig. 4.28, only the body motion degree-of-freedom is considered. The flapping dynamics and the inflow dynamics are not included. In other words, it is assumed that the flapping motion of the blades and induced velocities respond to the control input or changes in the body motion instantly. Moreover, time delay and the actuator model are also neglected in this baseline configuration. Obviously, this model cannot represent all the characteristics of Ornicopter with sufficient accuracy. However, it provides a reference for more detailed models.

Based on this ‘baseline model’, the flapping dynamics, the actuator dynamics and the control time delay are added to the baseline model separately. All these models are analysed and plotted in Fig. 4.28.

By comparing the different models, the impacts of each part mentioned above on the yaw bandwidth and phase delay can be determined qualitatively and some conclusions can be drawn.

Firstly, for all frequencies, the response magnitudes for all models are almost identical.

Secondly, at low frequencies (< 2 rad/s), additional dynamics and control time delay have very small impacts on phase angle. Therefore, the baseline model can predict the bandwidth for phase delay with good accuracy. The difference between bandwidths predicted by the baseline and the full model is less than 5% in the case shown in Fig. 4.28. This is caused by the fact that the time lags between the response of the helicopter and the control input (which are introduced by flapping dynamics, actuator dynamics or time delay) are relatively small when compared with the period of control input (> 3 s) at low frequency. Hereby, their impacts on the phase angle are negligible.

Thirdly, increasing the control frequency results in a higher impact of the additional

dynamics and control time delay on the phase response. Moreover, since the actuator model time constants are very small, the actuator dynamics have little impact on the phase angle response when compared with the control time delay and flapping dynamics. Comparing the ‘full model’ and the simplified model including only time delay, one can see that the control time delay has the highest impact on phase delay, and the flapping dynamics are of secondary importance.

Impact of the SCAS

In this section, the SCAS defined in Section 3.2.6 will be used. Its impacts on the Ornicopter yaw bandwidth and phase delay will be investigated.

As discussed above, the Ornicopter yaw direction bandwidth and phase delay is mainly impacted by the characteristics of the body motion DoFs, the control time delay and the flapping dynamics.

Since the yaw control of the Ornicopter is achieved by varying the amplitude of its active flapping blades, additional dynamics needs to be introduced in the yaw direction in comparison with the conventional helicopters. This is the inherent characteristic of the Ornicopter concept. It is not easy to reduce the impact of flapping dynamics on the phase delay, however it is less important when comparing with other dynamics affecting the yaw HQs characteristics. In order to improve yaw handling qualities of the Ornicopter with regard to bandwidth and phase delay, efforts should be made to reduce the control time delay and change the dynamic characteristics of body motion, i.e. the yaw damping.

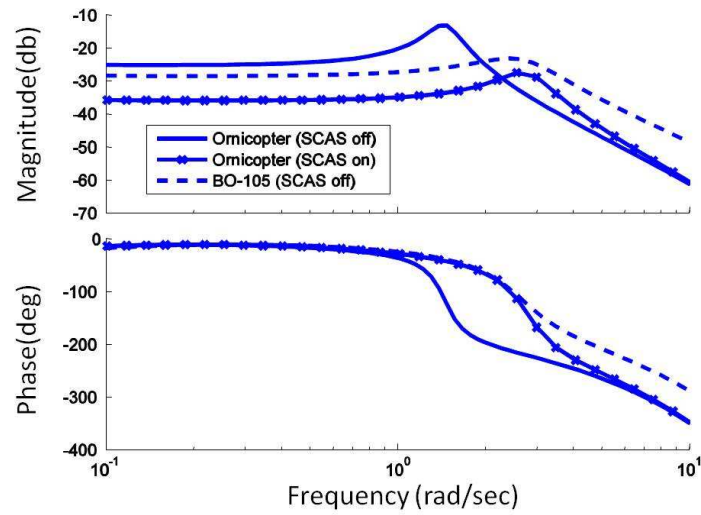
The values for the control time delays for the Ornicopter and Bo-105 are considered the same in this thesis. They should be reduced in order to improve the Ornicopter’s handling qualities. This issue is more related to the detailed design of the control system and is out of the scope of this thesis. Therefore, it will not be discussed.

By changing the design parameters of the Ornicopter, the stability derivatives can be tuned. However, it is more efficient to use the SCAS and tune the gains to investigate the influence of different dynamic characteristics of the body motion DoF on the yaw handling qualities at this stage. Therefore, the bandwidth and phase delay of Ornicopter are recalculated with different SCAS settings, in which only the gains for the yaw channel are set while all other gains are zero.

One of the bode plots is presented as Fig. 4.29, in which K_r is 0.15 and K_v is -0.015. It can be found that by applying yaw gains in the SCAS, the phase angle response of the Ornicopter can be improved considerably, especially at low frequency. The bandwidth for both the phase margin and phase delay can also be improved for the Ornicopter. However, at high frequency, the improvement caused by the SCAS is limited, since the high frequency response is dominated by the flapping dynamic and control time delay.

It should be noticed that the magnitude response of the Ornicopter reduces dramatically (about 10 dB) at low frequency. The bandwidth for gain margin in this case is not available. Hereby, the overall effects of using the SCAS to improve handling qualities for Ornicopter and more advanced SCAS algorithm design should be considered in further research.

To better understand the impacts of the SCAS on Ornicopter handling qualities,



4

Figure 4.29: Magnitude and phase responses of the Bo-105 and Ornicopter in the yaw direction (80 knots)

the bandwidth and phase delay parameters are calculated for different SCAS gains and plotted in Fig. 4.30.

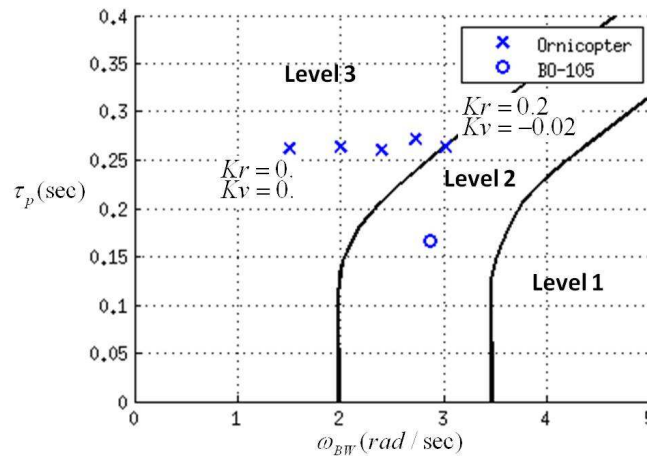


Figure 4.30: Bandwidth and phase delay in the yaw direction with different SCAS gains (80 knots)

Looking at this figure, one can see that the bandwidth of the Ornicopter can be improved from Level 3 to Level 2 handling qualities by using the SCAS, as the band-

width is determined by the low frequency response. Meanwhile, the SCAS only slightly influences the phase delay, which is dominated by a high frequency response by the system.

4.7.3 Attitude Quickness

Parameter Definition

For moderate-amplitude attitude changes, the ratio of the peak rotational rate (pitch, roll or yaw) to the maximum change of attitude angle should meet the limits specified by the ADS-33.

This quickness parameter ($q_{pk}/\Delta\Theta_{pk}$) is defined based on the time response of the helicopter to a rectangular step input. One example for the pitch axis is shown in Fig. 4.31.

The dynamic response of the helicopter will change with different control input settings, i.e. the amplitude and length of the step input. Therefore, multiple attitude quickness results can be obtained. In the following analysis, the length of the step input will vary from 1 s to 3 s, and an amplitude of 1° and 2° will be applied.

4

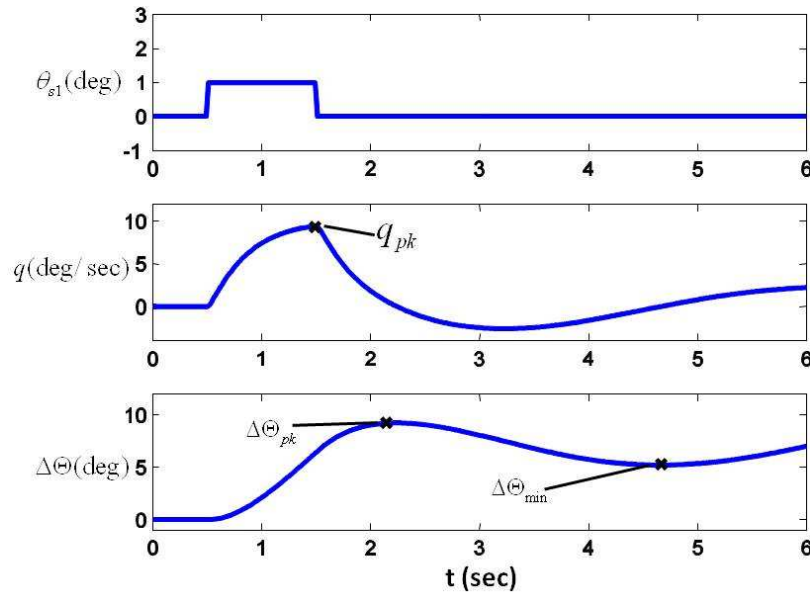


Figure 4.31: Attitude quickness definition

The Pitch Axis

As expected, in longitudinal and lateral directions, the attitude quickness of the Orni-copter and Bo-105 are very similar. Calculation results for the pitch channel at 30 knots

are presented in Fig. 4.32, from which one can see that the Ornicopter and Bo-105 have almost identical pitch attitude quickness. In this sense, the pitch and roll quickness will not be further discussed and the following section will focus on the yaw direction.

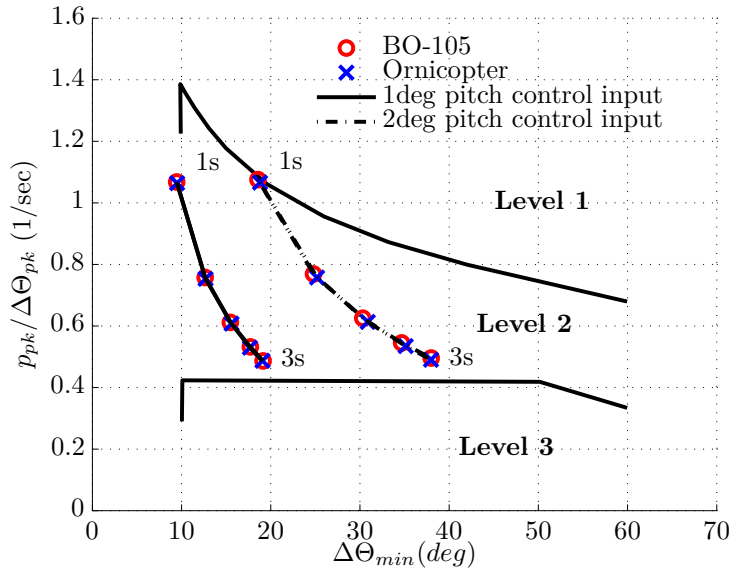


Figure 4.32: Pitch attitude quickness of the Bo-105 and Ornicopter (30 knots)

The Yaw Axis

Applying the same control input, the yaw attitude quickness of the Ornicopter and Bo-105 are also calculated, as shown in Fig. 4.33. This shows that the attitude quickness of the Ornicopter is lower than that of the Bo-105, especially for short control input. However, they are still graded as the same level of HQs for most cases, and the Ornicopter even reaches Level one for large yaw control input (2 deg input, longer than 2 s).

The attitude quickness and the minimum heading change of the Ornicopter follow the same trend as those of the Bo-105 when the control input is varying. However, the reduction of attitude quickness of the Ornicopter is smaller than that of the Bo-105. This leads to the result that the Bo-105 has much a higher yaw quickness than the Ornicopter for short control input, whereas they are close in quickness when longer controls are applied.

The yaw response of the Ornicopter and Bo-105 are presented in Fig. 4.34 in order to investigate the reason that causes the attitude quickness differences.

From the yaw rate response, one can see that after the yaw control is applied, the

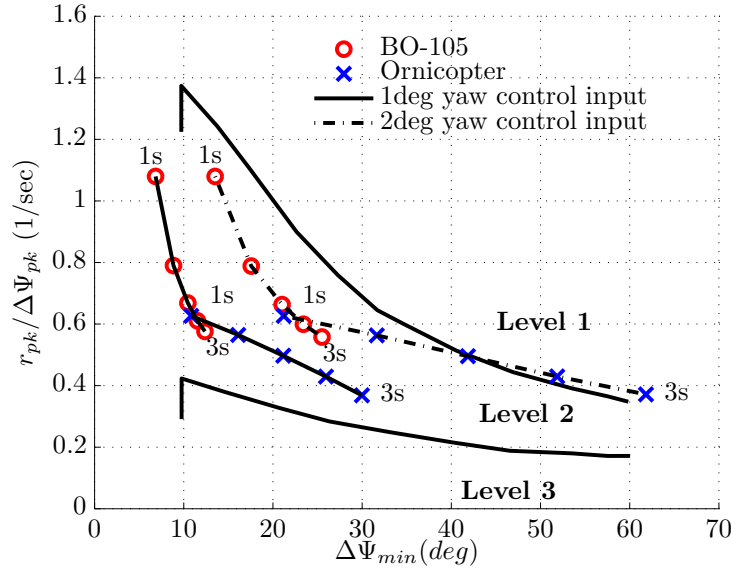


Figure 4.33: Yaw attitude quickness of Bo-105 and Ornicopter (30 knots)

Bo-105 can reach the maximum yaw rate very quickly (around 0.5 seconds), because of the relatively high yaw damping when compared with the Ornicopter. Afterwards, increasing the yaw angle further results in higher corresponding sideslip. This sideslip generates a counter yawing moment (N_v), and thus the helicopter intends to yaw back to the neutral position. This effect leads to the deceleration of yaw rate of the Bo-105 after the maximum yaw rate has been reached, and it lasts until the end of the step control input. After the yaw control returns to the trim position, the yaw rate decelerates and reverses very quickly, and meanwhile the yaw attitude reaches the peak heading change.

From the comparison of stability derivatives, the yaw damping (N_r) and sideslip derivative (N_v) of the Ornicopter are found to be lower than those of the Bo-105. Due to the Ornicopter’s low yaw damping and directional stability, its yaw rate will continue accelerating with an approximately constant gradient after the yaw control is applied. For the same reason, the yaw motion is slowly decelerated after the step input. In this sense, the peak heading change of the Ornicopter is much higher than that of the Bo-105. Despite the higher yaw peak rate, the high heading change peak results in lower attitude quickness for the Ornicopter, as well as higher minimum heading change.

From Fig. 4.34, it can also be found that the Ornicopter can be roughly considered as an acceleration control system in the yaw direction, whereas the Bo-105 is more close to a rate control system. Therefore, while step controls with the same amplitude and different time duration are given, the maximum yaw rate will keep constant for the

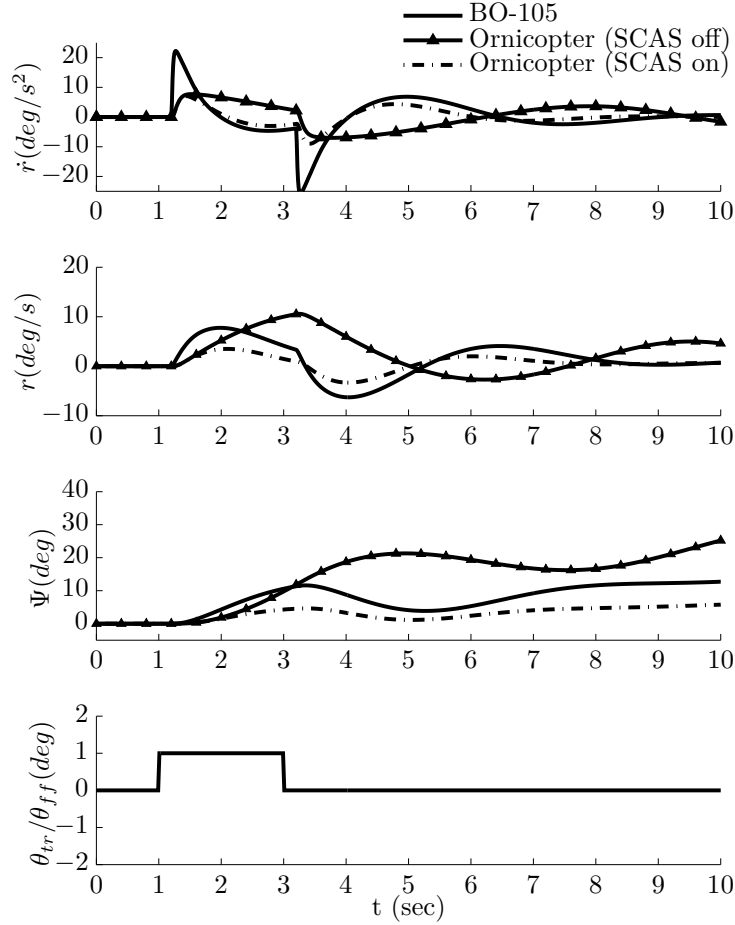


Figure 4.34: Yaw responses of the Bo-105 and Ornicopter for rectangular step control input

Bo-105, as long as the control input duration is longer than the rise time of the yaw response (which is about 0.5 seconds in the case shown in Fig. 4.34). At the same time, the peak and minimum heading changes will increase with an increase of the control input duration. Hence, the attitude quickness of the Bo-105 decreases greatly with the increasing of control input, see Fig. 4.33. In the case of the Ornicopter, since its characteristics correspond to an acceleration control system, the peak yaw rate, the peak and the minimum heading change will increase simultaneously. Therefore,

the attitude quickness of the Ornicopter declines only slightly in comparison with the Bo-105 helicopter.

Impact of the SCAS

The yaw attitude quickness of the Ornicopter can also be improved by applying the SCAS. The yaw response of the Ornicopter with the SCAS is calculated and shown in Fig. 4.35, in which K_r is 0.15 and K_v is -0.015.

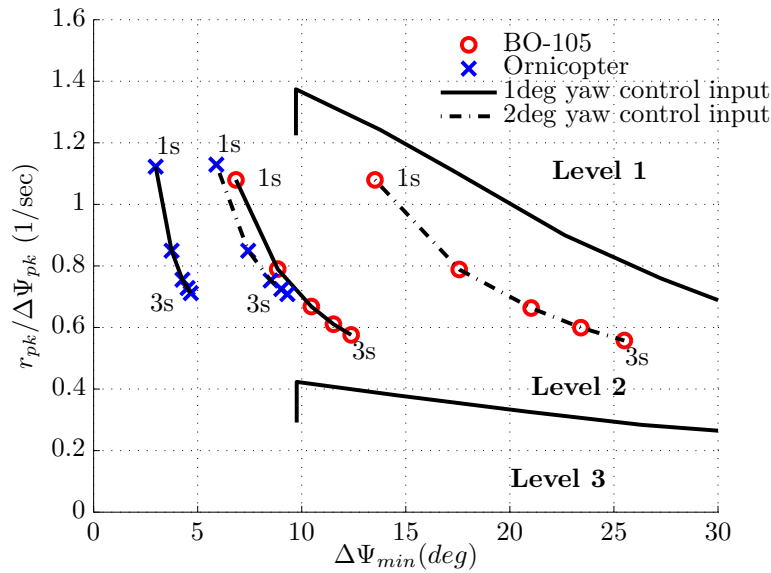


Figure 4.35: Yaw attitude quickness of the Bo-105 and Ornicopter with the SCAS (30 knots)

With the SCAS, the dynamic characteristics of the Ornicopter change rapidly. In this case, the Ornicopter has a very similar yaw response to the Bo-105 except a lower amplitude of the response (see Fig. 4.34). This is caused by the higher equivalent yaw damping and directional stability improved by the SCAS.

By using the SCAS, it is demonstrated that the Ornicopter’s yaw attitude quickness can be improved. Meanwhile, the effect of the SCAS on the yaw response corresponds with an amplitude reduction as shown in Fig. 4.34. This influence on attitude quickness is shown in Fig. 4.35. One can see that the yaw quickness of the Ornicopter is improved by the SCAS and it is even higher than that of the Bo-105. Moreover, the yaw attitude quickness curves move to the left, indicating lower attitude changes for the same control input.

4.7.4 Lateral-directional Oscillatory Requirement

The Dutch roll modes of the Ornicopter and Bo-105 are calculated and compared in Section 4.6.2. In this section, the impact of the SCAS on lateral-directional HQs as defined in ADS-33 are calculated, as presented in Fig. 4.36. As described before, the Dutch roll mode of the Ornicopter has lower damping and frequency than the Bo-105. From Fig. 4.36, one can see that with respect to the lateral-directional oscillation, the Ornicopter has poorer HQs than the Bo-105, while the locus of the Ornicopter is very close to the boundary between Level 2 and 3 (for other MTEs).

4

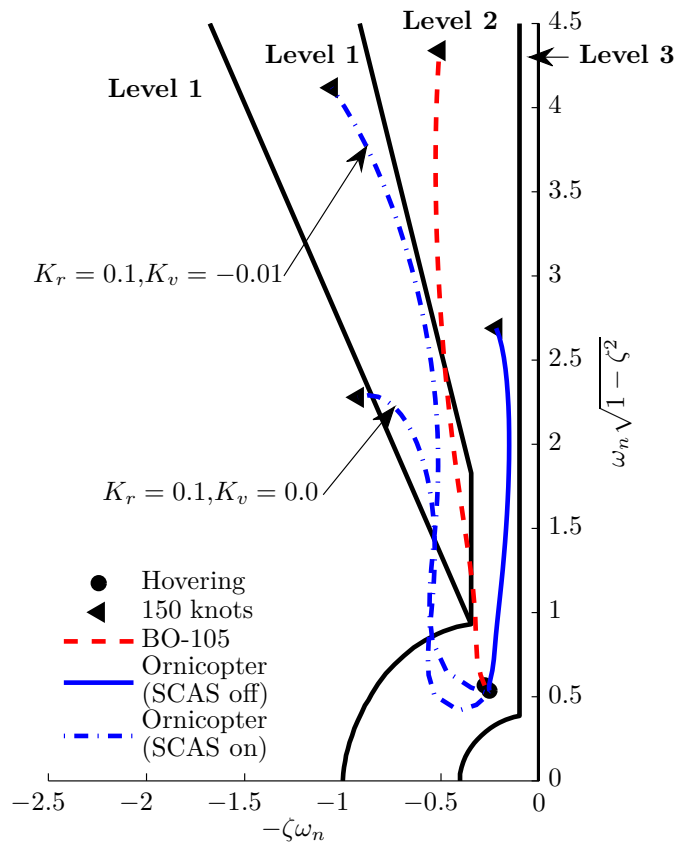


Figure 4.36: Lateral-directional oscillation grading

To improve the handling qualities of the Ornicopter, the SCAS is used. It can be found from Fig. 4.36 that by increasing the yaw damping through the SCAS, the

Ornicopter’s lateral-directional handling qualities can be improved from Level 2 to Level 1 handling qualities. Meanwhile, when the sideslip feedback is present, the frequency of the Dutch roll mode of the Ornicopter will increase. This effect is not beneficial for the handling qualities, as the locus moves towards the lower HQs regions. As discussed above, a higher directional stability is desired for bandwidth and attitude quickness. Therefore, detailed analyses should be done in further research to acquire an optimal control system design for the Ornicopter.

4.7.5 Yaw Control in Sideslip

In trimmed sideslip flight, the yaw control varies with the sideslip angle or sideslip velocity. A linear variation is desired for better handling qualities, since it is more predictable for the pilot.

As the yaw control method of the Ornicopter is completely different from that of a conventional helicopter, the yaw control in sideslip also changes, especially in sideward flight, as shown in Fig. 4.37 and Fig. 4.38.

Figure 4.37 shows the yaw controls of the Ornicopter and Bo-105 in pure sideward flight (no forward velocity). It can be found that the yaw control of the Bo-105 is almost a linear function of the sideward speed, whereas the Ornicopter requires highly non-linear yaw control, which has the same sign for both left and right sideward flight.

4

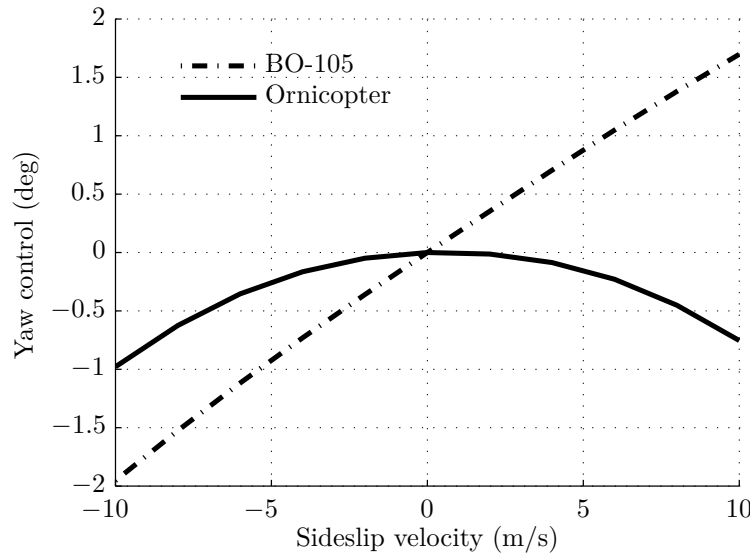


Figure 4.37: Yaw control deflection as a function of sideslip velocity ($u=0$ knot)

The reason for this non-linearity is that the variation in the main rotor torque is the dominating factor for the yaw control input of the Ornicopter in sideward flight.

From hovering, with the increasing of forward flight velocity, the main rotor torque reduces because of the reduction in induced torque, as shown in Fig. 3.4. This reduction is caused by the lower induced velocity due to the increasing inflow velocity. As the flight direction is not relevant, the same phenomenon can be found in sideward flight, i.e. in both directions of sideward flight (up to modest velocity), the main rotor torque will be lower than the torque corresponding to hovering.

For the Bo-105, in sideward flight, the inflow condition of the tail rotor changes dramatically, and hence is the main reason for the variation in yaw control. The relative airflow reduces the tail rotor thrust in right sideward flight, which results in a large tail rotor collective pitch. The opposite situation can be found in left sideward flight. In this case, the yaw control of the Bo-105 has the same sign as the sideward flight speed and is almost linear with the speed.

In the case of the Ornicopter, which does not have a tail rotor, the main rotor torque is the dominating factor for yaw control, and hence the same direction of yaw control deflections is needed for both sides of sideward flight. Since the main rotor torque is not linear with the flight velocity, the yaw control of the Ornicopter in sideward flight is also non-linear with regard to the sideward flight speed.

Figure 4.38 shows the yaw control deflections for different sideslip angles in forward flight. The forward flight velocity is kept constant (80 knots). In this case, the vertical fin can generate a relatively large yaw moment in sideslip (due to the high dynamic pressure), and the sideward velocity is less influential on the tail rotor thrust in fast forward flight. Hereby, the Ornicopter has a similar yaw control deflection with different sideslip angles to the Bo-105.

In conclusion, for the yaw control in the sideslip condition, high non-linearity can be found for the Ornicopter at hovering and low flight velocity, which will change the pilot’s control strategy. This should be considered in the control system design in order to keep the yaw control deflection the same sign as the sideslip angle. In forward flight, this effect does not appear since the vertical fin is more effective. Moreover, in the flight conditions discussed above (50 to 90 knots), the yaw control of the Ornicopter is less than that of the Bo-105. This is beneficial for Ornicopter as this new concept may have more control margin in the yaw direction.

4.8 Vibratory Loads and Preliminary Solutions

In Chapter 2, the vibratory problem of the Ornicopter was briefly analysed in hovering flight. Based on the harmonic components on the rotor hub, the three basic flapping configurations were compared, i.e. double teeter configuration, 2×2 AS configuration and 3-in-1-plane configuration. Some unfavourable harmonic forces and moments were found for all of these configurations. Based on this, the 2×2 AS configuration was found to be the best one with regard to vibration [34].

This section will investigate the cause of the Ornicopter’s vibratory problem and extend the previous hovering case analysis to trimmed forward flight. In order to reduce the Ornicopter’s vibratory loads, new flapping configurations will be proposed.

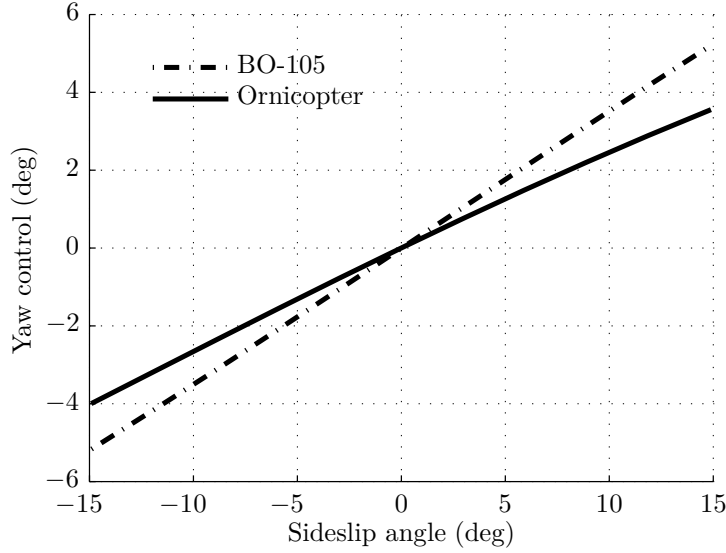


Figure 4.38: Yaw control deflection as a function of the sideslip angle (u=80 knots)

4.8.1 The Cause of Vibratory Loads

In the development of the Ornicopter flight mechanics model, the hub forces and moments generated by one blade were derived (see Eq. D.28), which can be written in the form of a Fourier series. For instance, the thrust of the k^{th} blade can be written as (for constant and $1/rev$ component):

$$T_s^{(k)}(\psi) = T_{s0}^{(k)} + T_{ss1}^{(k)} \sin(\psi^{(k)}) + T_{sc1}^{(k)} \cos(\psi^{(k)}) \quad (4.24)$$

Using the azimuth angle of the first blade as reference, the total thrust is:

$$\begin{aligned} T(\psi) = \sum_{k=1}^{N_b} T_{s0}^{(k)} + \sum_{k=1}^{N_b} T_{ss1}^{(k)} \sin\left(\psi^{(1)} + \frac{2(k-1)}{N_b}\pi\right) \\ + \sum_{k=1}^{N_b} T_{sc1}^{(k)} \cos\left(\psi^{(1)} + \frac{2(k-1)}{N_b}\pi\right) \end{aligned} \quad (4.25)$$

Equation 4.25 can be simplified when N_b is known, which is 4 for the Bo-105 helicopter and Ornicopter. Therefore, for a 4-blade helicopter, it becomes

$$T(\psi) = T_0 + T_{s1} \sin(\psi^{(1)}) + T_{c1} \cos(\psi^{(1)}) \quad (4.26)$$

where:

$$\begin{aligned} T_0 &= \sum_{k=1}^4 T_{s0}^{(k)} \\ T_{s1} &= T_{ss1}^{(1)} - T_{sc1}^{(2)} - T_{ss1}^{(3)} + T_{sc1}^{(4)} \\ T_{c1} &= T_{sc1}^{(1)} + T_{ss1}^{(2)} - T_{sc1}^{(3)} - T_{ss1}^{(4)} \end{aligned} \quad (4.27)$$

For higher order components, similar equations can be derived, except the N_b/rev component. For the 4-blade helicopter, the coefficients are:

$$\begin{aligned} T_{s4} &= T_{ss4}^{(1)} + T_{ss4}^{(2)} + T_{ss4}^{(3)} + T_{ss4}^{(4)} \\ T_{c4} &= T_{sc4}^{(1)} + T_{sc4}^{(2)} + T_{sc4}^{(3)} + T_{sc4}^{(4)} \end{aligned} \quad (4.28)$$

Thus far, all the harmonic components for rotor thrust from $1/rev$ to N_b/rev are derived. Similar derivations can be applied to other hub forces and moments, i.e. H , S , M_x , M_y and M_z .

For conventional helicopters, it is assumed that all the blades are working in an identical condition, i.e. coefficients (such as T_{ssn} and T_{scn}) are constant among blades. Therefore, except for the N_b/rev component, harmonic components generated by different blades can cancel each other out (see Eq. 4.27). For the Ornicopter, the situation is more complex because each blade is forced to flap individually. As the coefficients vary with blades, they cannot be cancelled and they cause harmonic vibratory loads starting from $1/rev$ to N_b/rev .

The Ornicopter’s harmonic forces and moments are derived analytically above. Numerical results will be presented below in order to get the feeling of their order.

Figure 4.39 and 4.40 show the amplitudes of the periodical components of rotor thrust and shaft moment as a function of flight velocity for the 2×2 AS configuration.

Looking at Fig. 4.39 and 4.40, it can be found that, for the Ornicopter, there are harmonic components from $1/rev$ to $4/rev$, while normally only a $4/rev$ component exists for a conventional helicopter with 4 blades. Meanwhile most of the components rise dramatically with increasing flight velocity.

4.8.2 New Configurations

As demonstrated in Figs. 4.39 and 4.40, periodical forces and moments on the hub are relatively large and therefore need attention during design. One possible solution is to design new hub configurations that are different from the three configurations proposed in Section 2.4.3.

One simple solution is to increase the number of blades to reduce vibration. Moreover, having more blades denotes that it is possible to design more forced flapping patterns for the Ornicopter, which may be favourable with regard to vibration.

In order to solve the vibratory problem, 4 new configurations with an increased number of blades are proposed. These are: $3 \times \text{Teeter}$ ($3 \times T$), 3×2 AS, $4 \times \text{Teeter}$ ($4 \times T$) and 4×2 AS configuration. The flapping motion of each configuration is presented in

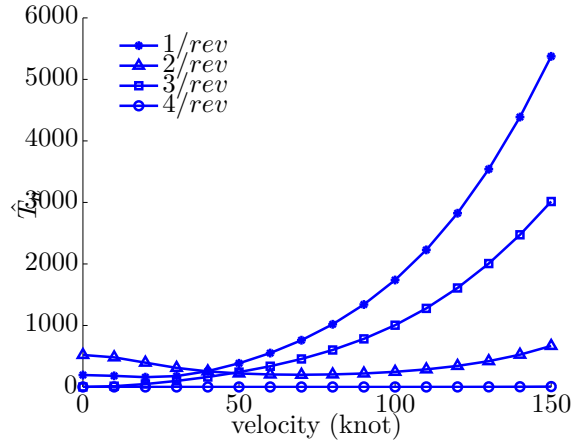


Figure 4.39: Amplitudes of harmonic components of the Ornicopter rotor thrust

4

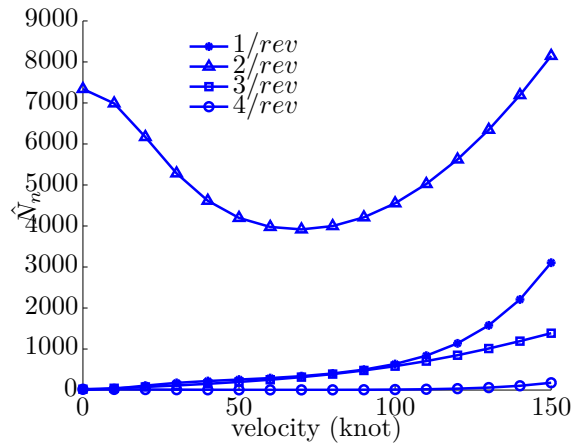


Figure 4.40: Amplitudes of harmonic components of the Ornicopter rotor torque

Tab. 4.2. In this table, the flapping configuration is defined by the azimuth angles where the forced flapping mechanism reaches the maximum flapping angle for each blade, as discussed in Section 2.4.3.

The proposed configurations are similar, as the 2×2 AS and the double teeter configuration explained in Section 2.4.3. Each of them has several pairs of blades which are at opposite azimuth positions. In the $n \times 2$ AS configurations, two blades in each pair flap anti-symmetrically, while they flap as a teeter in the $n \times$ Teeter configurations.

Table 4.2: Flapping sets for different configurations

Configuration	N_b	$\psi_\eta^{(k)}(\pi)$							
		1	2	3	4	5	6	7	8
2×2 AS	4	0	$3/2$	1	$1/2$	/	/	/	/
$3 \times T$	6	0	$4/3$	$2/3$	0	$4/3$	$2/3$	/	/
3×2 AS	6	0	1	0	1	0	1	/	/
4×2 AS	8	0	$5/4$	$1/2$	$7/4$	1	$1/4$	$3/2$	$4/3$
$4 \times T$	8	0	1	0	1	0	1	0	1

Vibratory Level

In order to compare different flapping configuration designs, the coefficients for harmonic forces and moments need to be transformed into a simple form. A parameter for vibratory level needs to be defined for this purpose. As a detailed vibratory analysis is not the main task of this thesis, this parameter is defined by using a simple form similarly as in Ref [13]. In this thesis, all the hub force and moment components from $1/rev$ to N_b/rev are taken into account, while only the N_b/rev oscillatory hub shears and moments are considered in Ref [13]. The vibratory level is defined as:

$$v_l = \sum_{n=1}^{N_b} \left(w_f \left(\hat{T}_n + \hat{H}_n + \hat{S}_n \right) + w_{mx} \hat{L}_n + w_{my} \hat{M}_n + w_{mz} \hat{N}_n \right) \quad (4.29)$$

where w_f , w_{mx} , w_{my} , w_{mz} are weighting factors for amplitudes of hub forces and moments. They are chosen with regard to the total weight and inertial moment of the Ornicopter, as:

$$\begin{aligned} w_f &\equiv \frac{1}{M_a} \\ w_{mx} &\equiv \frac{1}{I_x} \\ w_{my} &\equiv \frac{1}{I_y} \\ w_{mz} &\equiv \frac{1}{I_z} \end{aligned} \quad (4.30)$$

Impacts of Flapping Configurations

Considering that the Ornicopter’s vibration is caused by the active forced flapping motion, the flapping configuration should be a crucial factor for the vibration. Figure 4.41 shows the vibratory level for five configurations as a function of forward flight velocity.

It is clear that the number of blades and the flapping configuration have a large impact on the Ornicopter vibratory level. By using more blades and different flapping

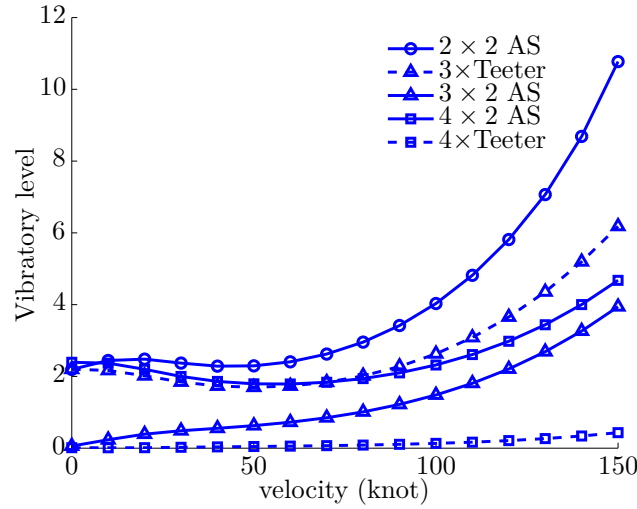


Figure 4.41: Vibratory level of the Ornicopter as a function of velocity and configurations

configurations, the vibration of the Ornicopter can be reduced to a similar level as the Bo-105. As shown in Fig. 4.41, regarding the 4×Teeter configuration, which has 8 blades, the vibratory level is $O(0.5)$, while the value for the Bo-105 predicted by the same model is $O(0.3)$.

In addition, Figure 4.41 also shows an interesting conclusion, namely that by increasing the flight velocity, the vibratory level does not simply rise up. For the 2×2 AS, the $3 \times T$ and 4×2 AS configurations, the vibratory level first decreases with the increasing of flight speed and reaches the minimum vibratory level around 80 knot before it starts increasing. Although the 4×2 AS configuration has a higher number of blades than the $3 \times T$ configuration, it generates higher vibratory loads than the $3 \times T$ configuration, especially in hovering.

Recalling the discussion about autorotation (see Section 4.5), using a higher number of blade will reduce the autorotation index of the Ornicopter rotor (see Eq. 4.17). In this sense, the AI of the Ornicopter rotor should be checked while increasing the number of blades.

4.9 Conclusion

In this chapter the Ornicopter was analysed and compared with the Bo-105 helicopter for various aspects. It was demonstrated that the Ornicopter has similar trim values and required power as the Bo-105. The current Ornicopter rotor needs slightly more power than a conventional helicopter rotor due to the increased profile power caused by the

forced flapping motion. Regarding the dynamic characteristics (stability, controllability and handling qualities), the Ornicopter is very similar to the Bo-105 in pitch, roll and heave axes.

Comparisons showed that the Ornicopter has two major deficiencies, namely a higher stall area of main rotor and worse yaw stability and handling qualities.

The active flapping of the Ornicopter rotor blades increases the stall area in forward flight and introduces stall even in hovering. This effect is the strongest limitation of the Ornicopter performance, and sharply reduces the flyable region of the Ornicopter. Different characteristics of this concept should be considered in the design process in order to extend the flight envelope of the Ornicopter.

Since the Ornicopter does not have a tail rotor, the stability derivatives dominated by a tail rotor change dramatically. This results in lower yaw damping and directional stability of the Ornicopter, and hence degrades the handling qualities of the Ornicopter in the yaw direction with regard to bandwidth and phase delay, attitude quickness, lateral-directional oscillation and yaw control in steady sideslip.

Two favourable changes found in the Ornicopter are that it has higher yaw control power and lower coupling responses while applying yaw control as compared to the Bo-105. This is due to the fact that the yaw control is achieved by controlling the main rotor torque directly on the Ornicopter.

Due to the stall effect, the fidelity of the ORNIcopter model is degraded for some flight conditions. This may result in a lower accuracy for the Ornicopter analyses and comparisons, such as the power calculation, the stability and controllability, and the handling qualities. However, these analyses still provide some fundamental understandings of the characteristics of the Ornicopter concept and the corresponding physical reasons, which is the main interest of this chapter.

5

The Ornicopter Design

In Chapter 4, the Ornicopter concept was analysed and compared with the Bo-105 conventional helicopter. The comparisons provided more details of the characteristics of this new concept. These showed that the Ornicopter has a very small flight envelope compared with Bo-105 when it uses the same design parameters as the Bo-105.

One of the reasons causing these drawbacks of the Ornicopter is that the design parameters are not optimized for the Ornicopter concept. Based on the new understanding, in this chapter, some design parameters of the Ornicopter will next be unfrozen and optimized to improve the Ornicopter’s performance. Afterwards, the optimized design will be compared with the Bo-105 to answer the main research question, i.e. how can an Ornicopter with comparable or improved flight performance be designed as compared to the Bo-105.

5.1 Design Requirements and Method

Due to the active flapping and the absence of a tail rotor, two major drawbacks of the Ornicopter are found in the previous chapter, including a small flight envelope and low yaw stability and handling qualities. Because it is a first attempt to optimize the Ornicopter design, the handling qualities will not be considered as design requirements in this thesis.

As mentioned in the research questions, the performance is the main interest of the Ornicopter design process. In this sense, the flight envelope of the Bo-105 (as predicted in Fig. 4.7) will be used as the design requirements of the Ornicopter. The main performance specifications are summarized in Tab. 2.2.

To predict the flight envelope of a helicopter, a numerical method needs to be used to search the boundaries of flyable region in the altitude-velocity diagram, i.e. analyses need to be performed at multiple altitudes and velocities. This requires high computa-

tional power, especially in the optimization process.

To reduce the calculation cost, not the entire flight envelope boundary of the Ornicopter will be calculated for the design optimization. Two specifications will be considered as shown in Tab. 2.2, including the hovering ceiling and the maximum velocity. First, the Ornicopter design will be optimized based on this simplified requirement. Afterwards, the entire flight envelope of the new Ornicopter design will be calculated and compared with the Bo-105 to verify if the design matches the design requirement.

The following procedure will be used for the Ornicopter design:

1. A sensitivity analysis will be performed with regard to design parameters. This is done in order to pinpoint important parameters for the Ornicopter design and their influences on Ornicopter performance.
2. Based on the parameters selected, a design database will be created which contains a large number of Ornicopter designs. Using the database, the general trend of a feasible Ornicopter design will be analysed.
3. The optimization problem for the Ornicopter will be defined and optimal designs will be attained.
4. The optimized design of the Ornicopter will be compared with the Bo-105 design to verify if it matches the design requirements and answer the main research questions.

5

The detailed design of the forced flapping mechanism for full-scale helicopters has not been considered. It is very difficult to estimate the weight of these mechanisms accurately at this stage. Therefore, it is assumed that the forced flapping mechanism has the same weight as the tail rotor system, i.e. the Ornicopter has the same gross weight as the Bo-105. This assumption introduces some error for the weight of the Ornicopter. However, it is considered to be negligible.

It should be mentioned that the Ornicopter design in this thesis is the initial concept design. This design process is based on the initial estimation of the total weight of the Ornicopter, which is the same as the Bo-105 helicopter. After a new Ornicopter design has been obtained, the weight of Ornicopter should be re-calculated to verify whether all the design requirements are satisfied. Multiple iterations of the design process might be needed before the final converged design result is acquired.

The main purpose of the Ornicopter design research in this thesis is to unmask the general design trends of this new concept and further understand its characteristics compared with a conventional helicopter. The initial design process can provide a relatively good result for this purpose. In this sense, the following design process will not be looped for the final converged result. The weight estimation for the Ornicopter is not considered in this thesis. The influence of varying design parameters on the gross weight of the Ornicopter is neglected, i.e. the Ornicopter total weight is assumed constant.

5.2 The Design Parameters

5.2.1 Rotor Sizing

The main rotor is the most important component of the helicopter. Proper design of the rotor is critical to meet the performance requirements for the helicopter as a whole. The Ornicopter introduces the additional flapping motion to the rotor, and hence leads to different characteristics for the Ornicopter as discussed before. In this sense, the main rotor design will be the main concern of the Ornicopter design research in this chapter.

The conceptual and preliminary design of the main rotor generally encompasses the following parts [21]:

1. The general sizing, i.e. the rotor diameter and the rotor tip velocity.
2. The geometric platform of the blade which includes the chord, solidity, number of blades, blade twist and tip shape.
3. The choice of airfoil(s).

In this thesis, only the general sizing and the blade chord will be discussed as this is decisive for the performance. Other main rotor design elements will be kept constant, such as the number of blades and blade twist.

It should be mentioned that some parameters for the helicopter rotor are correlated to each other. Two sets of them will be presented before the sensitivity analysis, and these are:

1. Rotor radius, tip velocity and rotor rotational speed, as:

$$V_t = R\Omega \quad (5.1)$$

2. Rotor radius, solidity and blade area, as:

$$\sigma = \frac{A_b}{\pi R^2} \quad (5.2)$$

In the following research, the rotor radius R , tip velocity V_t and blade area A_b are chosen as design variables. In this sense, the rotational speed Ω and solidity σ will not be constant and vary according to the three chosen design variables.

5.2.2 Vertical Fin

In Chapter 4, the performances of the Ornicopter and Bo-105 were compared, which showed some drawbacks of the Ornicopter due to stall (this was directly related to the average AoA and the variation of the AoA). In forward flight, the vertical fin design can be modified to reduce the rotor stall area, and hence improve the performance of the Ornicopter.

The oscillation amplitude of the AoA is determined by both ‘conventional’ flapping and the forced flapping motion. When a larger fin size (S_{vs}) and/or a higher incidence angle (β_0^{fin}) is used, the fin can generate higher yaw moment in forward flight to balance a part of the shaft torque, especially at high velocity. In this case, the active flapping motion needs to compensate for a smaller partition of the shaft torque, and hence the forced flapping motion can be reduced. In this manner, the Ornicopter performance can be improved.

In the steady forward flight condition, the sideways velocity (v) is very small and the rotational velocities (p, q, r) are zero. Therefore, the yaw moment generated by the vertical fin (Eq. D.59) can be simplified as:

$$N_{fin} = \frac{1}{2} \rho u^2 S_{fin} C_{l_\alpha}^{fin} \beta_0^{fin} x_{fin} \quad (5.3)$$

Defining the equivalent fin area, as:

$$S_e = S_{fin} \beta_0^{fin} x_{fin} \quad (5.4)$$

gives the yaw moment generated by the vertical fin as:

$$N_{fin} = P_{dyn} S_e C_{l_\alpha}^{fin} \quad (5.5)$$

where P_{dyn} is the dynamic pressure ($P_{dyn} = \frac{1}{2} \rho u^2$).

One can see that in steady forward flight the moment generated by the vertical fin is proportional to the equivalent fin area. For different fin designs which have a different fin size (S_{vs}), incidence angle (β_0^{fin}) or fin location (x_{fin}), the yaw moment generated will be the same in steady forward flight, as long as they have the same equivalent fin area.

In this chapter, the purpose of changing the vertical fin design is to partially compensate for the rotor torque, and hence to reduce the amplitude needed for the blade forced flapping motion. The ability to generate a yaw moment is the main point of interest in this context. In this sense, the equivalent fin area will be considered as a main design parameter in the sensitivity analysis. To keep it simple, only the fin area will be varied next.

5.2.3 Pitch Flap Coupling

As discussed in Section 2.3, the Ornicopter blades are forced to flap with a constant pitch angle. Meanwhile, all the examples of flapping-wing propulsion in nature combine pitching and flapping motions. The combined pitch-plunge flapping wing has been studied in the flapping wing community and research shown that the flapping wing thrust efficiency can be increased by using a combined pitch-plunge motion [26]. Therefore, pitch-flap coupling should also be considered for the Ornicopter concept. It is modelled by two coupling terms as shown in Eq. D.20, and their effects on the Ornicopter design will be analysed next.

Figure 5.1 shows the impacts of pitch flap coupling terms on the blade pitch angle (assuming cyclic control is not applied). The pitch flap angle coupling is common for

conventional helicopters. The flapping motion of the blade will slightly change the blade pitch angle if the pitch control rod is not located on the flapping axis. A positive $k_{\theta 1}$ indicates that the pitch angle will be increased when the flapping angle (β) is positive, as shown in Fig. 5.1.b. In the case of pitch flap rate coupling, the change in the pitch angle is associated with the blade flapping rate. A positive $k_{\theta 2}$ indicates that the pitch angle will be increased when the blade is flapping upwards ($\dot{\beta} > 0$), see Fig. 5.1.c.

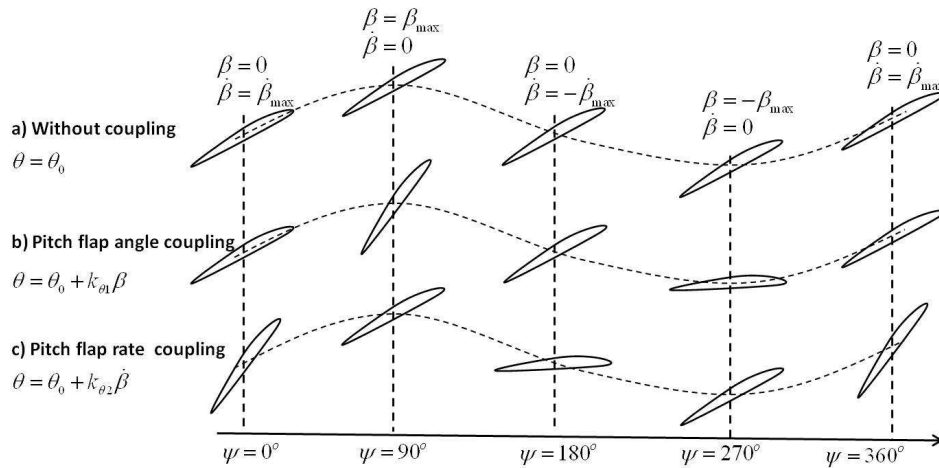


Figure 5.1: Sketch for blade pitch flap coupling

5.3 Sensitivity Analyses

The following design parameters will be investigated in the following sensitivity analyses: the rotor radius, blade area, rotor tip velocity, the fin size and the pitch-flap coupling.

The sensitivities of the required power and the stall area with respect to the above chosen design parameters will be investigated. Calculations will be performed for two flight conditions, including hovering and fast forward flight at 120 knots.

In the following figures, the required power is normalized by the maximum continuous engine power, and the stall area is normalized by the rotor disk area. All the design parameters are normalized by their values in the baseline design (Bo-105) respectively, except the pitch flapping coupling parameters (both $k_{\theta 1}$ and $k_{\theta 2}$) (their values in the baseline design are zero).

5.3.1 The Rotor Radius

The effects of changing the rotor radius on the Ornicopter’s performance are shown in Fig. 5.2 with regard to the non-dimensional stall area \bar{S} and the required power \bar{P} .

One can see the large improvements in the Ornicopter performance with the increase in the rotor radius in hovering. When a larger rotor is used, lower power is required

and a smaller rotor area encounters stall (in percentage). In forward flight, the required power can also be reduced by using a larger rotor, while the stall area will be slightly increased.

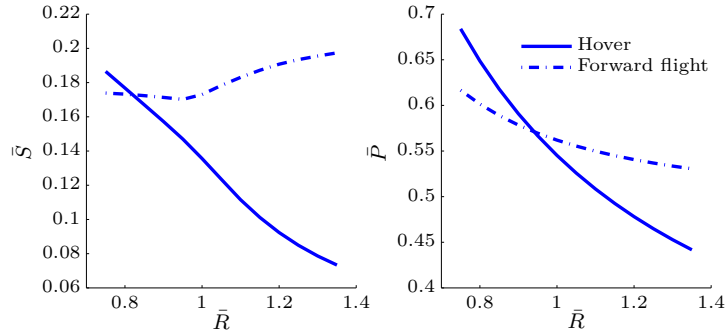


Figure 5.2: Impact of the rotor radius on the stall area and required power

5

By increasing the rotor radius, the induced velocity can be reduced, and hence lower induced power is required. As the induced power is the major part of the required power of helicopters in hovering, using a larger rotor can dramatically reduce the total required power of the Ornicopter. In forward flight, it is less beneficial to increase the rotor radius as the parasitic power is the dominant factor at high speed.

From the preliminary analyses, one can see that the amplitude of active flapping is associated with the forced flapping power (see Eq. 2.27). By reducing the required power i.e. the forced flapping power, the amplitude of the active flapping can be reduced.

The simple Ornicopter rotor model in hovering (see Appendix A) can be used for more detailed analyses. In the trimmed hovering condition, the shaft torque coefficient should be zero. Equation. A.13 can be rewritten as (cyclic pitch control is not considered):

$$0 = \frac{1}{2}\sigma_s C_{l_\alpha} \alpha_e \lambda_i + \frac{1}{8}\sigma_s C_{d0} - \frac{1}{16}\sigma_s C_{l_\alpha} \hat{\beta}^2 \quad (5.6)$$

in which the effective angle of attack α_e is :

$$\alpha_e = \frac{\theta_0}{3} - \frac{\lambda_i}{2} \quad (5.7)$$

The required flapping amplitude can be calculated as:

$$\hat{\beta}^2 = 8\alpha_e \lambda_i + 2 \frac{C_{d0}}{C_{l_\alpha}} \quad (5.8)$$

Rewriting the main rotor thrust (see Eq. A.7) gives:

$$\begin{aligned}
 T &= \frac{1}{6} \rho (N_b c R) C_{l_\alpha} (\Omega R)^2 \theta_0 - \frac{1}{4} \rho (N_b c R) C_{l_\alpha} (\Omega R)^2 \frac{v_i}{\Omega R} \\
 &= \frac{1}{6} \rho A_b C_{l_\alpha} V_t^2 \theta_0 - \frac{1}{4} \rho A_b C_{l_\alpha} V_t^2 \frac{v_i}{V_t} \\
 &= \frac{1}{2} \rho A_b V_t^2 C_{l_\alpha} \left(\frac{\theta_0}{3} - \frac{\lambda_i}{2} \right) \\
 &= \frac{1}{2} \rho A_b V_t^2 C_{l_\alpha} \alpha_e
 \end{aligned} \tag{5.9}$$

In hovering, the thrust of the main rotor equals the total weight, which is assumed to be constant. Therefore, the α_e will keep constant as the blade area and tip velocity are constant while the rotor radius is varying. Meanwhile, the inflow ratio (λ_i) will decrease with the increase in the rotor radius. Combining these effects, one can find that increasing the rotor radius will decrease both the collective pitch (see Eq. 5.7) and the active flapping amplitude (see Eq. 5.8) in hovering, as shown in Fig. 5.3.

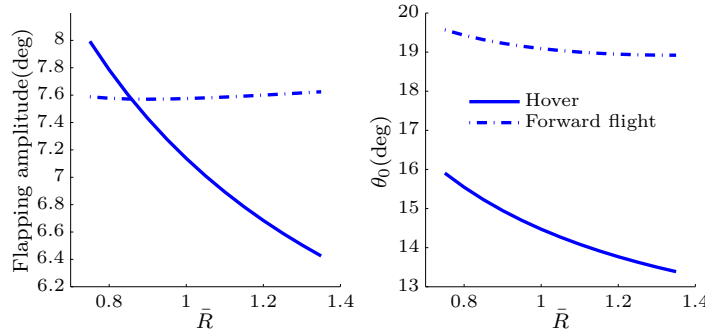


Figure 5.3: Flapping amplitude and collective pitch as a function of the rotor radius

As discussed before, the reason why the Ornicopter’s rotor encounters stall in hovering is that the active flapping introduces an additional variation of the blade angle of attack. By reducing the active flapping and collective pitch, both the mean angle of attack and the variation of the angle of attack can be reduced, and hence the stall area can also be reduced. Hereby, with regard to stall, the Ornicopter performance can be improved by increasing the rotor radius.

In forward flight, the numerical calculations can show the effects of varying rotor radius on the active flapping and collective pitch control. Figure 5.3 shows that changing the rotor radius has less effect on the amplitude of active flapping and collective pitch control in forward flight than in hovering. As the induced power is a small part of the total required power in forward flight, the active flapping is almost constant while varying rotor radius. Due to the slightly reduced induced velocity, the collective pitch control also reduces slightly.

The increasing rotor radius also changes the flapping dynamics of the Ornicopter rotor. With a larger rotor, a higher negative longitudinal cyclic pitch control (θ_{s1}) is required for trimmed forward flight, which increases the blade pitch angle on the retreating side. This will increase the stall on the retreating blades. Therefore, the stall area will increase with an increase in the rotor radius in forward flight.

5.3.2 The Blade Area

Figure 5.4 shows the impact of the blade area on the Ornicopter performance. As the rotor radius is constant in this case, the rotor solidity will also change proportionally with the blade area.

The blade area is directly related to the blade loading (M_{ag}/A_b). By increasing the blade area, the blade loading will be smaller, and the local blade element angle of attack can be reduced for both hovering and forward flight. Recalling Eq. 5.9, the equivalent angle of attack (α_e) is inversely proportional to the blade area, i.e. it will decrease with an increase in the blade area. The blade area will not affect the induced velocity, i.e. the inflow ratio is constant. In this sense, the required collective pitch angle reduces in line with an increase in the blade area (see Eq. 5.7). From Eq. 5.8, one can see that the amplitude of the flapping motion also drops off for a lower equivalent blade angle of attack (α_e). The variation in the active flapping amplitude and collective pitch with the blade area is presented in Fig. 5.5. Due to the effects discussed above, increasing the blade area results in the stall area dropping off dramatically.

5

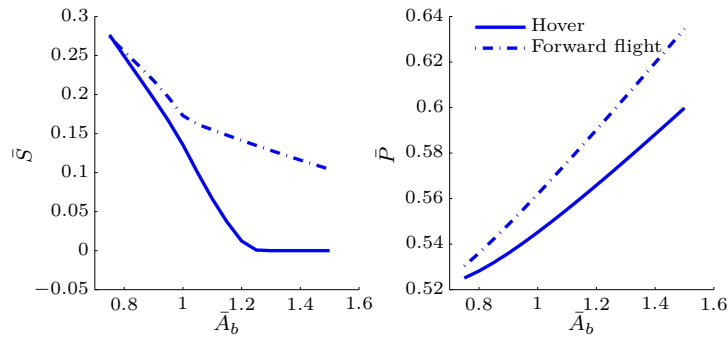


Figure 5.4: Impact of the blade area on the stall area and required power

This is accompanied by higher power consumption due to the higher profile power, which is proportional to the blade area. In forward flight, more additional profile power is required because of higher local velocity on the blade element.

5.3.3 The Tip Velocity

In the case of tip velocity, its effect on performance is similar to that of the blade area. The higher the tip velocity is, the more dramatically the stall area drops and the

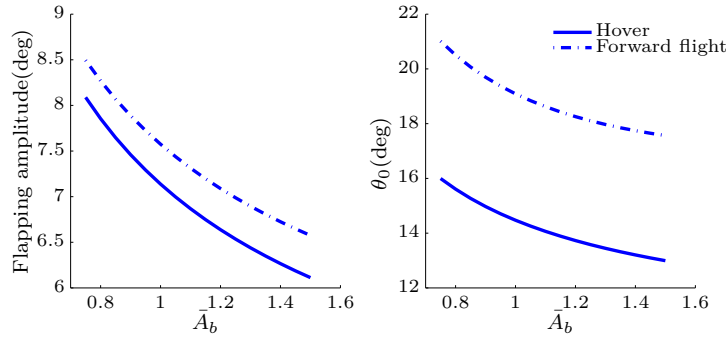


Figure 5.5: Impact of the blade area on the flapping amplitude and collective pitch

required power increases, see Fig. 5.6.

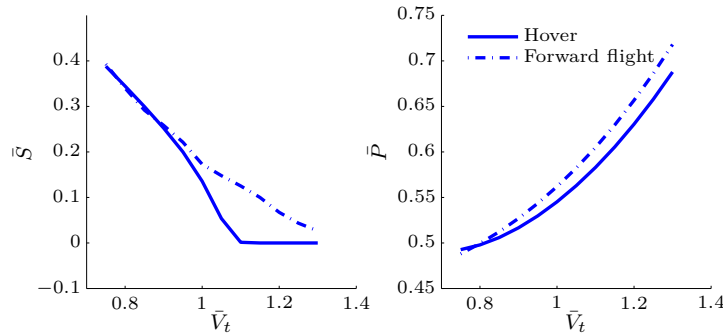


Figure 5.6: Impact of the tip velocity on the stall area and required power

The reduction of the stall area with increasing tip velocity is also caused by the lower flapping amplitude and collective pitch, similarly to the case of the blade area. However, varying the tip velocity has a greater effect on the Ornicopter’s performance than changing the blade area. This is due to the fact that aerodynamic forces are affected by the square of velocity (V_t^2). In hovering, using about a 10% higher tip velocity can eliminate the stall area, while it requires about a 20% larger blade area to obtain the same effect.

5.3.4 The Fin Size

The yaw moment generated by the vertical fin is negligible at low speed. In this sense, the vertical fin will only affect the performance of the Ornicopter in forward flight, as shown in Fig. 5.7 and 5.8.

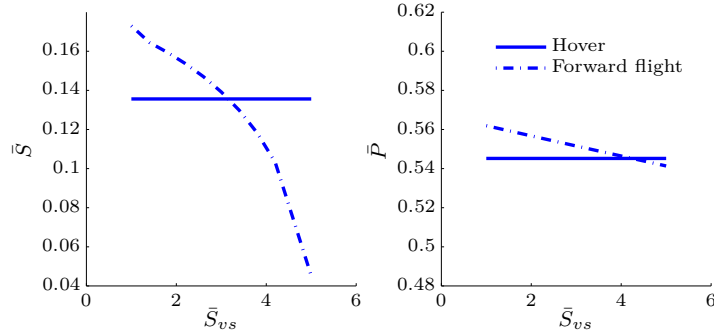


Figure 5.7: Impact of the fin size on the stall area and required power

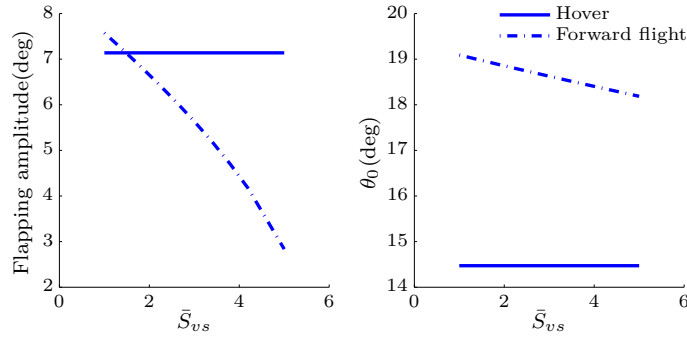


Figure 5.8: Impact of the fin size on the flapping amplitude and collective pitch

By using the vertical fin to compensate for a part of the shaft torque, less propulsive torque generated by the active flapping is required, and hence the amplitude of the forced flapping motion can be reduced, as shown in Fig. 5.8. In this way, the stall area in forward flight can be limited and the flight envelope of the Ornicopter can be extended. By reducing the active flapping, the rotor profile power can be reduced. As the profile power is not the main part of the total power in forward flight, a modest reduction in the required power can be found while increasing the fin size.

In the trim value comparison (see Fig. 4.1), it has been discussed that the Ornicopter rotor requires a higher collective pitch input than the Bo-105 in forward flight, which is caused by the higher horizontal hub force (H). Since a larger vertical fin can reduce the amplitude of active flapping (in other words the Ornicopter can fly more ‘like’ a conventional helicopter), the additional collective pitch control for the Ornicopter can be reduced. This results in a lower collective pitch when the fin size is increasing, as shown in Fig. 5.8.

5.3.5 The Pitch Flap Coupling

As shown in Eq. D.20, two pitch flap couplings are considered in the flight mechanics model developed in this thesis, including the pitch flap angle coupling ($k_{\theta 1}$) and the pitch flap rate coupling ($k_{\theta 2}$).

The Pitch Flap Angle Coupling

Figure 5.9 presents the impacts of the pitch flap angle coupling on the stall area and the required power of the Ornicopter. One can see that this coupling term has a relatively small effect on the stall area (it only varies by around 3%) and it will not noticeably affect the Ornicopter’s required power either in hovering or forward flight.

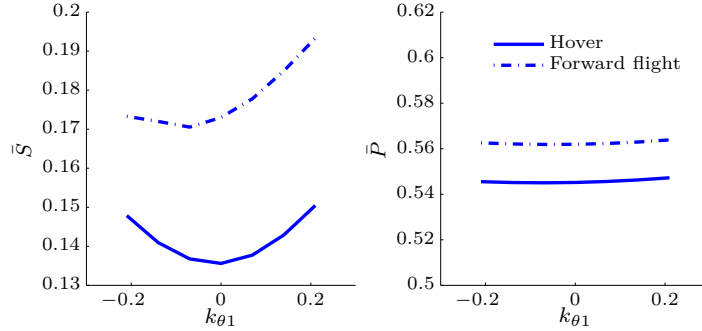


Figure 5.9: Impact of the pitch flap angle coupling on the stall area and required power

As mentioned above, the pitch flap angle coupling will change the blade pitch angle when the blade is not at the neutral position (in the flapping direction). This additional pitch angle will slightly enlarge the the angle of attack variation amplitude on the blade elements. For example, considering a hovering Ornicopter rotor without cyclic control, the angle of attack of a blade element is:

$$\alpha = \theta - \varphi \quad (5.10)$$

Substituting the pitch angle (Eq. D.20) and the induced angle (Eq. 2.5) into Eq. 5.10, one can get:

$$\begin{aligned} \alpha = & \theta_0 + \theta_{tw} \bar{r} + \frac{\lambda_i}{\bar{r}} + k_{\theta 1} \beta_0 \\ & + (k_{\theta 1} \beta_{s1} + \beta_{c1}) \sin(\psi) + (k_{\theta 1} \beta_{c1} - \beta_{s1}) \cos(\psi) \end{aligned} \quad (5.11)$$

The angle of attack variation amplitude is then:

$$\begin{aligned} \hat{\alpha} = & \sqrt{(k_{\theta 1} \beta_{s1} + \beta_{c1})^2 + (k_{\theta 1} \beta_{c1} - \beta_{s1})^2} \\ = & \sqrt{k_{\theta 1}^2 + 1} \sqrt{\beta_{s1}^2 + \beta_{c1}^2} \end{aligned} \quad (5.12)$$

From Eq. 5.12 one can see that the variation of the blade angle of attack will be enlarged by both the positive and negative values of the pitch flap angle coupling, assuming that the flapping motion is not affected by $k_{\theta 1}$. Calculations also show that this coupling term has no influence on the active flapping amplitude, as shown in Fig. 5.10. In this sense, when the $k_{\theta 1}$ is zero, the stall area has its minimum value, and increases for both positive and negative $k_{\theta 1}$.

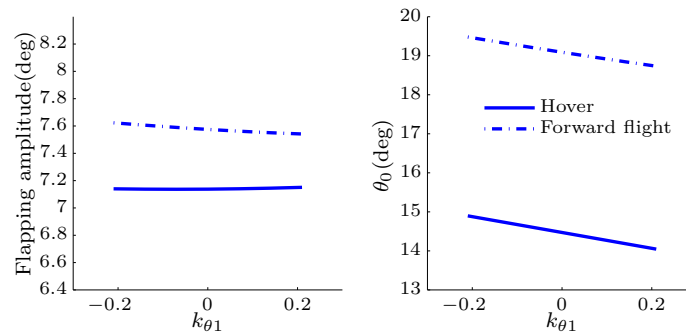


Figure 5.10: Impact of the pitch flap angle coupling on the flapping amplitude and collective pitch

5

In forward flight, similar impacts of $k_{\theta 1}$ as in hover can be found. However, due to the unsymmetrical airflow, positive and negative $k_{\theta 1}$ have slightly different impacts on the stall area. The stall area will reach its minimum value when $k_{\theta 1}$ is around -0.05 .

The Pitch Flap Rate Coupling

Recalling the basic concept of the Ornicopter (Chapter 2), while the blade is flapping downwards, the blade element angle of attack will be increased due to the flapping motion. This higher angle of attack will increase the stall area of the Ornicopter rotor. By using a positive pitch flap rate coupling, the blade angle of attack can be reduced as the pitch angle is reduced by the pitch flap rate coupling term.

In hovering, this effect can reduce the angle of attack variation on blade elements, as well as the maximum angle of attack. Therefore, the stall area can be reduced (see Fig. 5.11). Due to the lower local angle of attack, the average profile drag will also be lower. In this sense, the required power in hovering reduces slightly in line with the increasing $k_{\theta 2}$.

This coupling effect also reduces the propulsive force generated by the active flapping. During the down stroke, where the propulsive force is produced, the pitch angle is reduced by the pitch flap rate coupling, and hence less lift and propulsive fore are generated. On the other hand, the drag force increases in the upstroke due to the higher pitch angle. Therefore, the average propulsive force drops off, which requires the amplitude of active flapping to be increased, as shown in Fig. 5.12.

5.3 Sensitivity Analyses

131

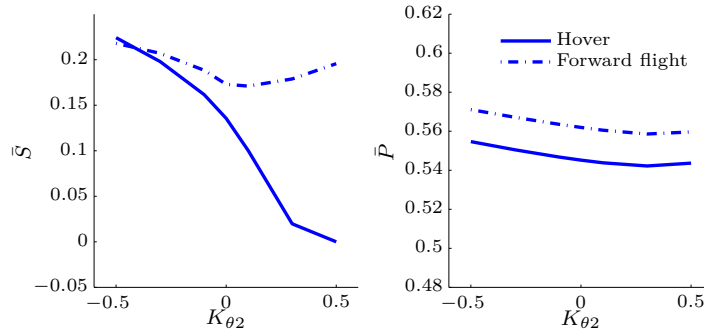


Figure 5.11: Impact of the pitch flap rate coupling on the stall area and required power

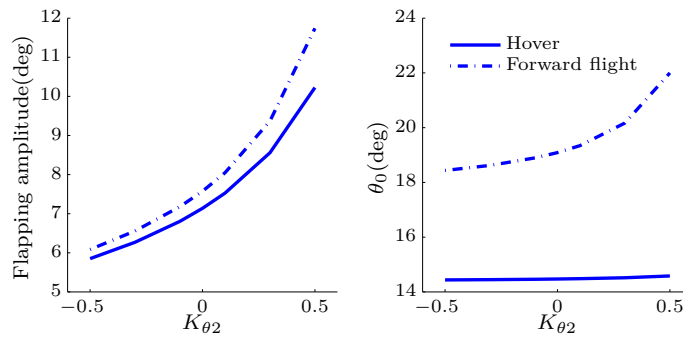


Figure 5.12: Impact of the pitch flap rate coupling on the flapping amplitude and collective pitch

It should be mentioned that though the amplitude of active flapping increases while higher $k_{\theta 2}$ is used, the local angle of attack on the blade element will increase more gradually. A higher flapping amplitude also indicates a higher flapping rate. As the change of pitch angle due to the pitch flapping rate coupling is proportional to the flapping rate, a higher flapping amplitude also means a larger reduction of pitch angle when the blade is flapping downwards ($k_{\theta 2} > 0$).

It can also be found that the collective pitch control will not be affected by this coupling effect in hovering, as shown in Fig. 5.12. In hovering, as there is no unsymmetrical incoming airflow, the average impact of the coupling on the rotor thrust in one revolution is zero. Hereby, the collective pitch control will be kept constant for different $k_{\theta 2}$ in hovering.

Overall, the total effect of a positive $k_{\theta 2}$ is a strong reduction of the stall area in hovering, as shown in Fig. 5.11.

For forward flight, the situation is different. The amplitude of active flapping will

increase while increasing $k_{\theta 2}$, similar to in hovering. However, the collective pitch control will increase in this case.

From Fig. 5.12, one can see that when negative $k_{\theta 2}$ is used, the collective pitch is increasing slowly with increasing $k_{\theta 2}$. Meanwhile, the gradient of the curve also increases, resulting in a rapidly increasing collective pitch when $k_{\theta 2}$ is close to 0.5.

As discussed in the previous chapter (see Section 4.2), the blades’ active flapping will cause a higher negative horizontal hub force (H), and hence a larger nose-down pitch angle and collective pitch control. This effect becomes stronger as a higher amplitude of active flapping is required. Therefore, increasing $k_{\theta 2}$ increases the collective pitch in forward flight.

Combining the two effects from above, the variation in the stall area in forward flight as a function of $k_{\theta 2}$ is characterised by a bucket shape. While $k_{\theta 2}$ is negative, the stall area can be reduced by increasing $k_{\theta 2}$, similar to in hovering. When $k_{\theta 2}$ is positive, increasing collective pitch becomes the dominant effect, and causes a higher stall area.

5.3.6 Conclusion

From the above analyses, some conclusions can be made:

1. By increasing the rotor radius, the performance of the Ornicopter in hovering can be improved. In forward flight, the required power can also be reduced, while a smaller rotor will have better stall characteristics.
2. Using a higher blade area and tip velocity can reduce the stall area dramatically, but consumes more profile power.
3. By using a larger vertical fin, both the stall area and the required power of the Ornicopter in forward flight can be improved. This parameter should be used as the main approach to improve the Ornicopter performance in forward flight.
4. The pitch flap angle coupling will degrade the performance of the Ornicopter, and it should be kept at zero.
5. The pitch flap rate coupling has different effects on the Ornicopter in hovering as compared to forward flight. This parameter can be used to tune the performance of the Ornicopter for overall optimal design.

The impacts of different design parameters on the Ornicopter are summarized in Tab. 5.1. The rotor radius, blade area, tip velocity and fin size will be considered as the main design variables in the next section. Different combinations will be analysed, in order to form a design database.

5.4 The Design Database

In the previous section, analyses were performed that varied only one design parameter at one time. Analyses for combinations of multiple design parameters can show

Table 5.1: Impacts of the design parameters on the Ornicopter stall area and required power

Design variation		Stall		Power	
		Hovering	Forward flight	Hovering	Forward flight
R	\nearrow	\downarrow	\nearrow	\downarrow	\searrow
	\searrow	\uparrow	\rightarrow	\uparrow	\nearrow
A_b	\nearrow	\Downarrow	\downarrow	\nearrow	\uparrow
	\searrow	\Uparrow	\uparrow	\searrow	\downarrow
V_t	\nearrow	\Downarrow	\downarrow	\nearrow	\uparrow
	\searrow	\Uparrow	\uparrow	\searrow	\downarrow
S_{vs}	\nearrow	\rightarrow	\downarrow	\rightarrow	\searrow
	\searrow	\rightarrow	\uparrow	\rightarrow	\nearrow
$k_{\theta 1}$	\nearrow	\nearrow	\nearrow	\rightarrow	\nearrow
	\searrow	\nearrow	\nearrow	\rightarrow	\nearrow
$k_{\theta 2}$	\nearrow	\Downarrow	\nearrow	\searrow	\searrow
	\searrow	\Uparrow	\nearrow	\searrow	\searrow

$\nearrow, \uparrow, \Uparrow$ = small, modest, large increase
 $\searrow, \downarrow, \Downarrow$ = small, modest, large decrease
 \rightarrow = not affected

more information regarding the Ornicopter characteristics. In this sense, a database consisting of a large number of different Ornicopter designs is desired.

As mentioned above, four parameters were chosen for the design database, and their values are shown in Tab. 5.2. Most of the design combinations from Tab. 5.2 are included in the database, resulting in more than 1×10^4 designs.

Table 5.2: Variation of the design parameters

Parameter	Baseline design	Minimum		Maximum		Number of designs	Unit
		value	%	value	%		
R	4.91	3.68	75	6.63	135	13	m
A_b	5.30	3.98	75	7.95	150	16	m^2
V_t	218	164	75	283	130	12	m/s
S_{vs}	0.710	0.710	100	3.55	500	6	m^2

For each design, different performance and handling qualities analyses are carried out, including:

1. Trim process for different flight velocities (hovering to 150 knots) and altitudes (0 m to 5000 m) combinations;
2. Required power calculation for each trim point;
3. Stall area analyses for fast forward flight (130 knots to 160 knots) at sea level and hovering at different altitudes (0 m to 4000 m);
4. Linearised models derived for handling qualities analyses;
5. Bandwidth and attitude quickness calculations for sea level forward flight (40 knots).

The calculation flow chart for one design case is shown in Fig. 5.13. For each Ornicopter design, the non-linear flight mechanics model will be linearised using *Maple*, from which corresponding *Matlab* code files will be generated. For these code files, all the design parameters are embedded into the codes, i.e. these files will not take the Ornicopter design parameters as input data, and they are only valid for one specific Ornicopter design. In this manner, the calculation cost of the code file can be reduced dramatically, which is beneficial for the large amount of analyses desired in the database. Using this code, an analysis program can perform the analyses mentioned above, and save all the data into the database.

5

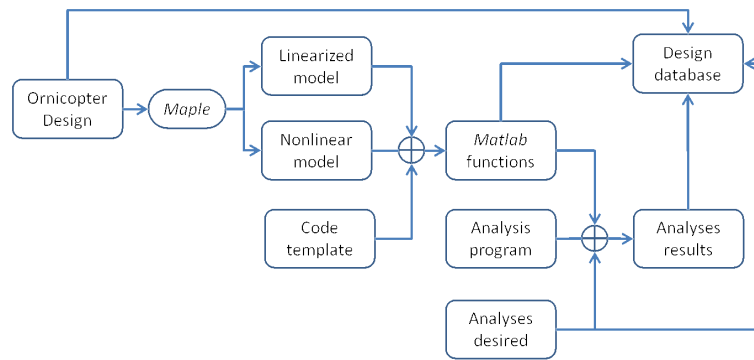


Figure 5.13: Flow chart for the design database

5.5 The Design Process

5.5.1 Design Space

Using the design database, more analyses can be performed for the Ornicopter concept. One of the important applications is to find a feasible design space for certain design

requirements. In this section, the feasible design space for the Ornicopter based on the Bo-105 performance shown in Tab. 2.2 will be investigated.

Defining the Design Criteria

The design requirements are defined based on the performance specification in Tab. 2.2, i.e. the hovering ceiling and maximum velocity. They can be converted into the required power and stall area limitations in certain flight conditions to reduce the calculation cost.

For example, to predict the maximum speed of a helicopter limited by the stall area, numerical methods will be used to search for the velocity at which the rotor stall area reaches the maximum value allowed. This means that analyses need to be performed for several velocities. The stall area increases with increasing flight velocity. Therefore, if the stall area of one design does not reach the maximum stall allowed at the maximum speed requirement (V_{max}^{req}), it can fly faster than V_{max}^{req} , i.e. it satisfies the design requirement. In this way, the stall analysis only needs to be performed once, and the computation cost can be reduced dramatically.

To get more understanding of the influences of different designs on the Ornicopter performance, the sea level hovering condition is also considered in this section. In this sense, three flight conditions are chosen for the analyses: hovering at sea level (referred to as hovering in the following), maximum speed forward flight (150 knots) at sea level, and hovering ceiling (2815 m).

The required power and stall area will be analysed for each condition and the analysis results for the Bo-105 helicopter will be used as design requirements for the Ornicopter design. In other words, the Ornicopter design should have the same or lower power consumption and stall area than the Bo-105 helicopter.

It should be noticed that the Bo-105 rotor does not encounter stall in hovering, while the Ornicopter concept introduces stall in hovering due to active flapping. The same stall area requirement will be applied to the Ornicopter in hovering conditions (both sea level and hovering ceiling) as for forward flight.

All the design requirements with regard to stall and power (in non-dimensional form) are summarized in Table. 5.3.

Table 5.3: Design requirements

Flight condition	Velocity	0	0	150 knots
	Altitude	0	2815 m	0
Maximum stall		0.0893	0.0893	0.0893
Maximum power		0.543	0.584	0.846

Results from the Design Database

Based on these design requirements discussed above, a feasible design space for the Ornicopter can be determined. As the four design parameters vary, the feasible design

space will be a four-dimensional space, which is difficult to visualise. To have a better view of the design space and the impacts of varying parameters on it, the feasible rotor sizing (i.e. rotor radius and blade area) is presented for different tip velocities and vertical fin size. Besides the stall and power requirements mentioned above, the allowable blade aspect ratio (R/c) is also limited, for example by the blade structure design. In the following figures, the aspect ratio limitation is also presented ($14 < R/c < 20$).

Figure 5.14 shows the feasible rotor design boundary for different tip velocities based on the sea level hovering requirements.

For the stall requirement, the feasible design space is on the top-right side of the boundary, due to the fact that a higher rotor radius and blade area can reduce the stall area. In the case of the required power, a higher rotor radius and lower blade area will be beneficial. Therefore, the feasible design space is on the bottom-right side of the boundary.

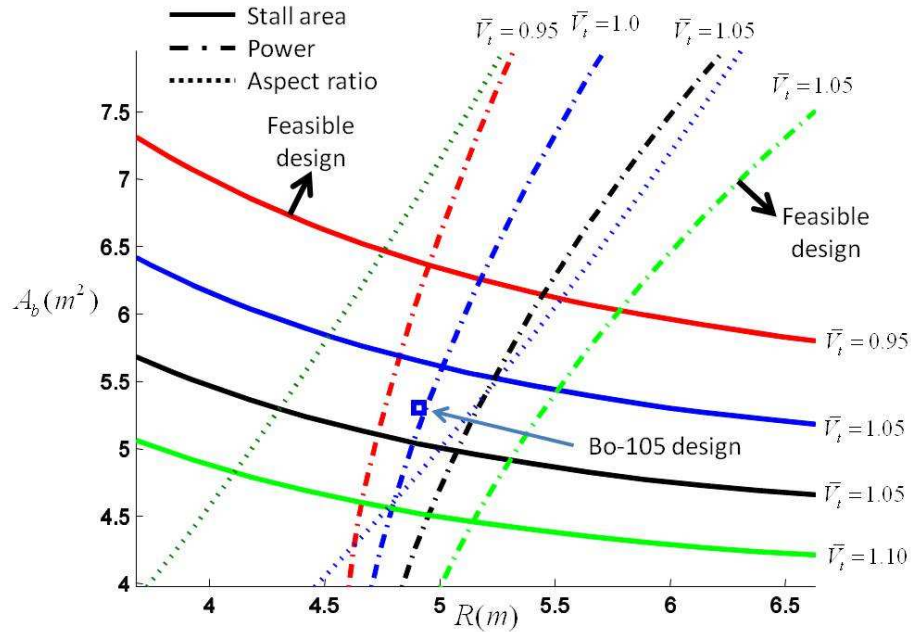


Figure 5.14: Design space with different tip velocities for hovering ($\bar{S}_{vs} = 5$)

Increasing the tip velocity, both the boundaries for stall and power will shift. As increasing the tip velocity dramatically reduces the stall area, a lower blade area and rotor radius are required to keep the stall area lower than the design requirement. The stall boundary moves towards the bottom-left side and the feasible design area for stall requirement is enlarged. Meanwhile, the higher the tip velocity is, the larger the profile power required. To maintain the same total power consumption, a higher rotor radius should be used to reduce the induced power or the blade area should be lower to reduce

the profile power. This effect moves the power boundary towards the right-hand side and reduces the feasible design space.

The design boundaries change with the variation in the tip velocity. For all the tip velocities presented in Fig. 5.14, a design space can be found that fulfils both the stall and power requirements. This feasible design space moves from the top-right corner to bottom-right when the tip velocity is increasing.

Similar results can be found for the hovering ceiling requirement, as shown in Fig. 5.15. Two major differences can be found when comparing this to the sea level hovering condition.

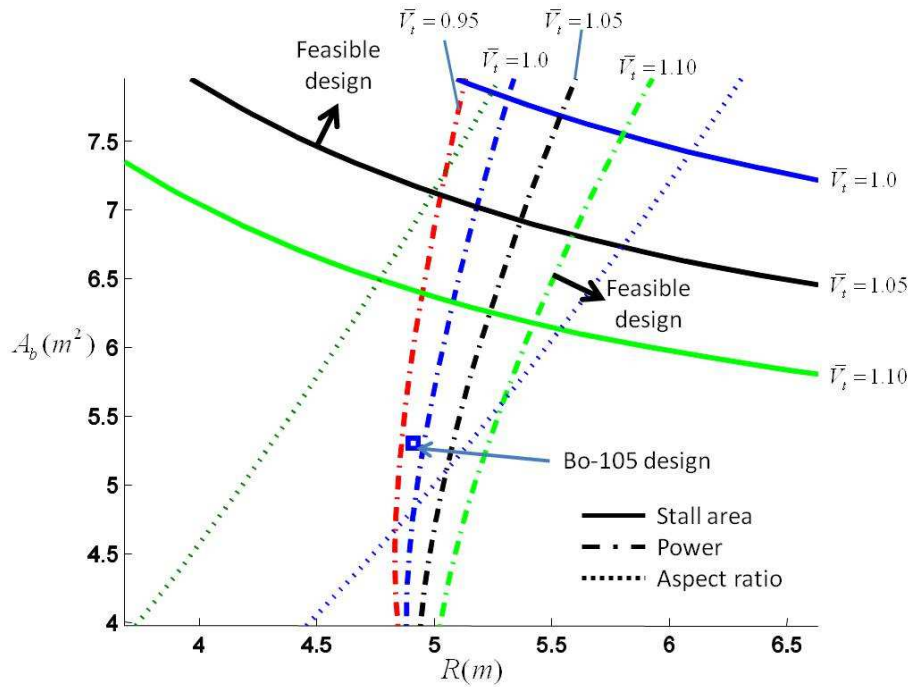


Figure 5.15: Design space with different tip velocities for the hovering ceiling condition ($\bar{S}_{vs} = 5$)

First, the stall boundary shifts to the top-right corner of the plot. This is caused by a higher stall area with an increased altitude. At high altitude, the air density becomes lower. To generate the same thrust, the rotor needs to accelerate more air (in volume), in other words, the induced velocity and inflow ratio will be higher. Meanwhile, the thinner air will also increase the required equivalent blade angle of attack, see Eq. 5.9. Recalling Eq. 5.8, the increasing α_e and inflow ratio will require a higher amplitude of active flapping for the same thrust. Combining these effects, the stall area of the Ornicopter rotor will increase with increasing altitude. Because of the higher stall area, a higher blade area and rotor radius are needed to match the stall design requirement,

and hence the stall boundary moves.

Secondly, the power boundary slightly rotates and is more close to a vertical line when compared with the sea level hovering condition. The impact of tip velocity on the power constraint becomes smaller. This is caused by the fact that with increasing altitude, the profile power becomes a smaller part of the total required power. As the tip velocity only affects the profile power, it has less impact on the power constraint. Similarly, the blade area also has a small effect on the total required power. The rotor radius is the dominant factor for power requirement in this flight condition.

In fast forward flight, the design boundaries are different from hovering, as shown in Fig. 5.16

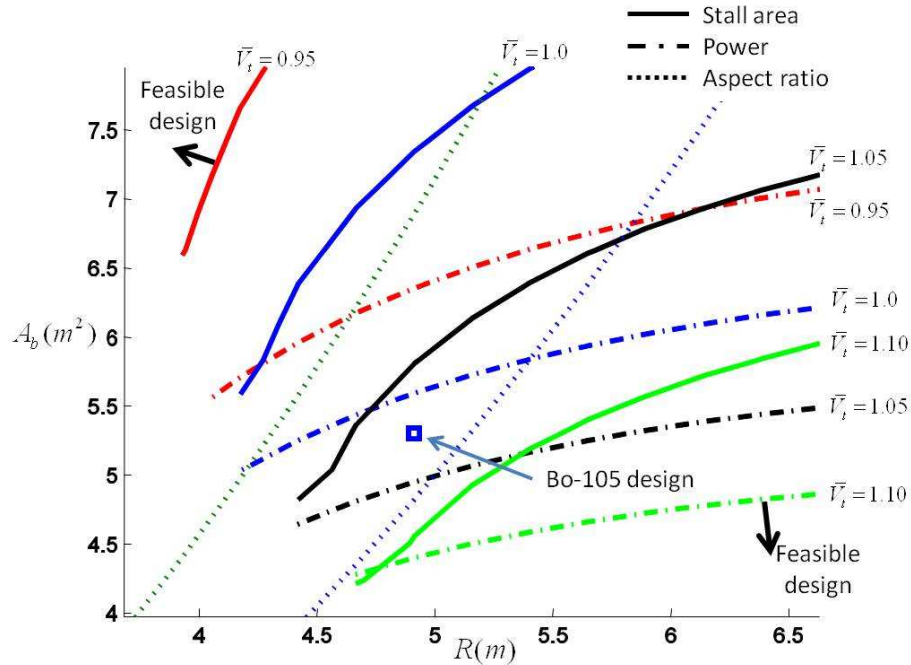


Figure 5.16: Design space with different tip velocities for forward flight ($\bar{S}_{us} = 5$)

For the power requirement, the feasible design space is still on the bottom-right side of the boundary, which indicates that a smaller blade area and smaller rotor radius are preferable with regard to power consumption. In forward flight, the parasite power is the main part of the required power and it is determined by the fuselage design. The profile power is secondary and the induced power is the smallest proportion of the total required power. In this sense, the power boundary is relatively flat, i.e., the required power is more sensitive to the blade area than to the rotor radius.

Some major changes can be found on the stall boundaries. In the forward flight condition, the feasible design space is located on the top-left side of the stall boundary instead of the top-right side, which indicates the trend to use a smaller rotor. This can

also be found from the sensitivity analysis, as Fig. 5.2 shows a slightly increase in the stall area with an increase in rotor radius in forward flight.

One may have noticed that there is no intersection between the feasible design spaces defined by stall and power requirement respectively. This demonstrates that no feasible design space can be found for the Ornicopter in forward flight. While the tip velocity is increasing, both stall and power boundaries are shifting to the bottom-right side of the graph. The feasible design cannot be achieved by changing rotor tip velocity.

As discussed in the previous chapter, the Ornicopter active flapping blade will increase the stall area and the profile power of the main rotor. To reduce the stall area, a larger blade area or higher tip velocity should be used. However, those solutions will further increase the rotor profile power. In hovering, while the induced power is the major part of the total required power, by using a larger rotor radius, the required power can be reduced. At a certain point, the reduction in induced power can overcome the increasing of the profile power necessary for the stall requirement, resulting in a feasible Ornicopter design. In forward flight, the impact of the rotor radius on the required power is very small. Therefore, the power and stall requirements cannot be satisfied at the same time.

So far, the impacts of vertical fin size on the feasible design space have not been discussed. As the vertical fin does not generate any force or moment in hovering, it will not affect the Ornicopter performance in hovering. In this sense, only the design boundaries in the forward flight condition will be shown, see Fig. 5.17.

The general shape of the stall boundaries is similar to those boundaries drawn while changing tip velocity. By increasing the fin size, the Ornicopter’s feasible design space can be greatly enlarged.

For the power boundary, the vertical fin size is less influential. However, increasing the vertical fin size is beneficial for the power boundary. Though a feasible design space cannot be found for the fin designs shown in Fig. 5.17, the stall and power boundaries are moving towards each other. At a certain point, when the vertical fin is large enough, a feasible design will be found. This will happen when the vertical fin compensates for all the main rotor shaft torque. The active flapping will not be needed. In this case, the Ornicopter rotor will work as a conventional helicopter rotor. The stall area and required power should be very close to those of a conventional helicopter. Meanwhile, the tail rotor does not exist on the Ornicopter. The Ornicopter total required power can be smaller than that of the Bo-105 helicopter. This results in a feasible design space for the Ornicopter in the forward flight condition.

However, this will require a large equivalent fin area (S_e), which will cause other drawbacks. One of them is a lack of yaw control. If the vertical fin compensates for all the shaft torque and the amplitude of the active flapping is zero, the Ornicopter rotor will work as a conventional helicopter rotor, and hence it will not be able to generate a yaw control moment in both directions. An additional yaw control method is needed, such as the use of a rudder. Meanwhile, a large vertical fin may also cause some problems regarding the structure or weight. More research should be carried out for a proper fin design in future work.

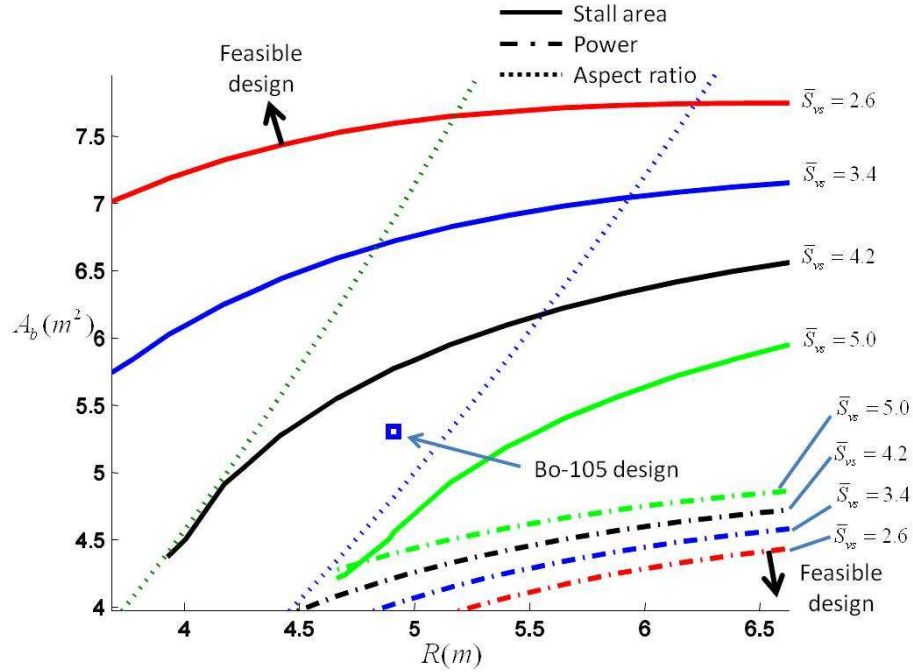


Figure 5.17: Design space with different vertical fin sizes for forward flight ($\bar{V}_t = 1.1$)

Compromised Design Requirements

As shown above, a design space for the Ornicopter that fulfils the requirements for all three flight conditions cannot be found. The most critical condition is at the maximum forward flight velocity. This indicates that the final Ornicopter design will have a higher power consumption and/or smaller flight envelope.

In this sense, the design requirements should be modified. Some requirements have to be compromised to achieve a satisfactory design.

For the power requirement, the allowed power consumption can be increased for each flight condition. This results in an Ornicopter design that has higher required power than the Bo-105 helicopter. Figure 5.18 shows all the design boundaries in all three flight conditions. The maximum power consumption in this case is increased by 10%. A feasible design space can now be found.

It can be found that the feasible Ornicopter design will have a higher blade area and tip velocity to reduce the stall area. This will also increase the profile power of the rotor. Therefore, the rotor radius will also be increased to reduce the induced power. However, reducing the induced power cannot compensate for all the additional profile power, resulting in a higher total required power for the Ornicopter.

In the case of the stall requirements, a similar calculation as for the power requirement is performed, as shown in Fig. 5.19. In this case the stall area limitations are

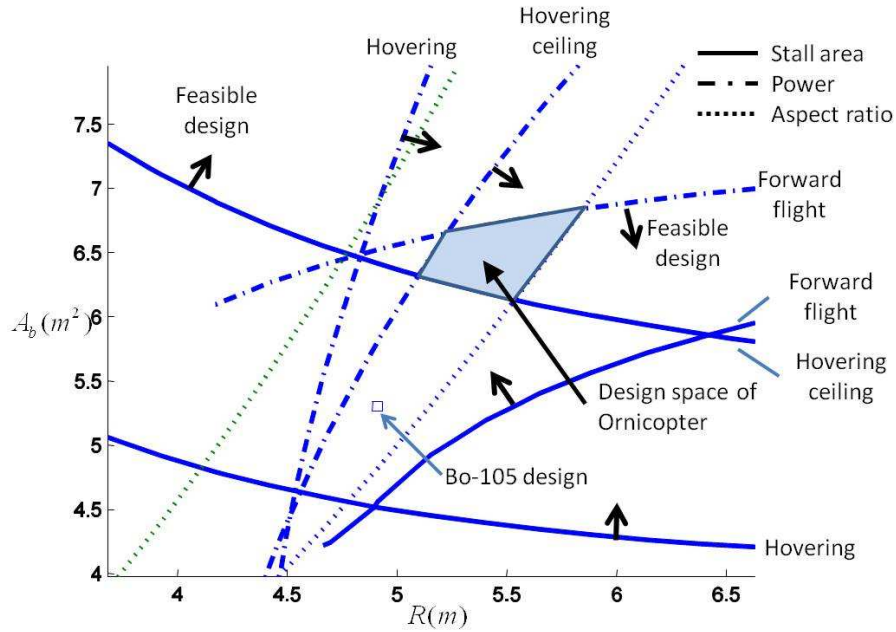


Figure 5.18: Feasible design space (10% higher power, $\bar{V}_t = 1.1$, $\bar{S}_{vs} = 5.0$)

increased by 20%.

From Fig. 5.19 one can see that with the higher allowable stall area, the design boundaries for the stall requirements shift only slightly. Hence, no feasible design space can be found in this case.

Comparing Fig. 5.18 and 5.19, it can be found that the design boundaries of the power requirements are significantly more sensitive to the design requirements than the stall boundaries.

This is caused by the fact that these design parameters have higher impacts on the stall area than on the required power. For example, recalling the sensitivity analyses shown in Fig. 5.4, the stall area varies by about 100% of the initial value in forward flight, while the variation in required power is only about 20%.

In this sense, while changing the stall design requirements, the stall design boundaries only move slightly. Therefore, no feasible design space can be found when increasing the allowed stall area by 20%.

In order to obtain a feasible design, the stall requirements need to be further relaxed, which means a very small flight envelope. In this way, the required power of the Ornicopter can be kept the same as the Bo-105. However, the small flight envelope will be a major drawback for this design.

In conclusion, from the above analyses, it appears that the power requirements should be relaxed to enable a feasible Ornicopter design, and the stall requirements can be kept the same as proposed before. The resulting Ornicopter design will have a

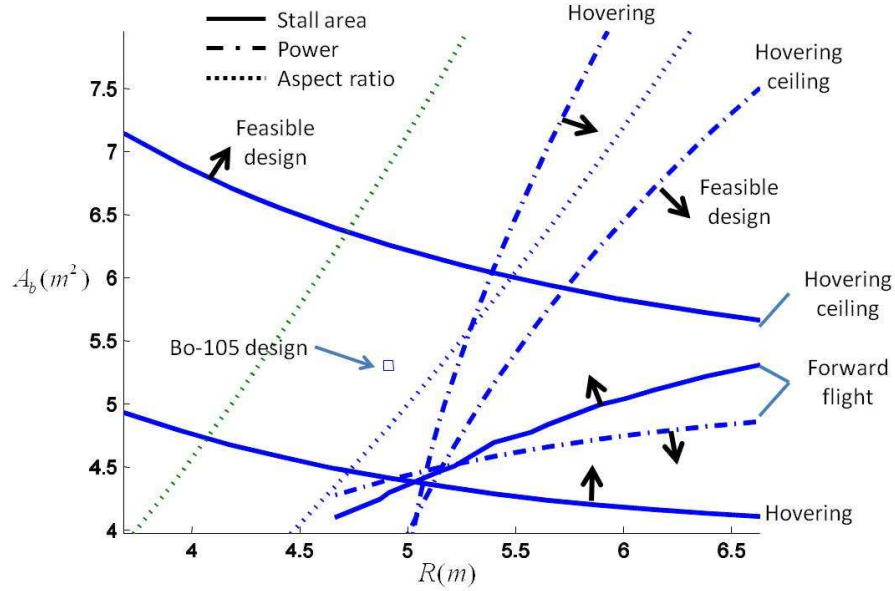


Figure 5.19: Feasible design space (20% larger stall area, $\bar{V}_t = 1.1$, $\bar{S}_{vs} = 5$)

5

similar flight envelope as the Bo-105 helicopter but a higher power consumption.

5.5.2 Design Optimization

From the design database, the general trend of a feasible Ornicopter design can be found. However, the design variation is limited by the computational cost, and it cannot provide an optimal design of the Ornicopter. In this sense, the design optimization will be performed in this section to obtain the optimal Ornicopter design.

Four design parameters are chosen for the design database, including the rotor radius, the blade area, the tip velocity and the vertical fin size. Out of these parameters, increasing the vertical fin size is the most efficient way to improve the Ornicopter performance. In the Ornicopter flight mechanics model, the vertical fin is only considered as a lifting plate. Possible drawbacks of using a larger vertical fin, such as the higher weight, are not modelled. If the vertical fin size is chosen as a design variable, the optimization result will reach the upper limit of the optimization boundary. Therefore, the vertical fin size will be kept constant, i.e. the maximum value used in the design database ($\bar{S}_{vs} = 5.0$), for the following design optimization.

Looking at the feasible design space presented in Fig. 5.18, one can see that the feasible design space is determined by the power requirements of hovering ceiling and forward flight conditions, the stall requirements at the hovering ceiling, as well as the maximum blade aspect ratio. The stall design boundary for the forward flight is still relatively far away from the feasible design space. This indicates that there is a stall

margin for forward flight condition, which can be traded for the hovering performance. In this sense, if a certain design can reduce the Ornicopter stall area in hovering and increase the stall area in forward flight, it can be used to tune the Ornicopter performance in different flight conditions, and may improve the overall performance.

From the sensitivity analyses for the different design parameters, it was found that the pitch flap rate coupling ($k_{\theta 2}$) has the desired impacts on the Ornicopter. Therefore, it will be included in the design variables used for optimization.

Hereby, the design variables which will be optimized include the rotor radius, blade area, tip velocity and the pitch flap rate coupling. The boundaries of these design parameters are shown in Tab. 5.4. In the following part, the optimization problem will be defined and the optimization results will be presented.

Table 5.4: Boundaries of the design parameters

	$R(m)$	$V_t(m/s)$	$A_b(m^2)$	$k_{\theta 2}$
Minimum	4.0	200	4	-0.2
Maximum	9.0	260	10	1.2

Defining Cost Function and Constraints

From the analyses of the design space, it was concluded that to maintain the same required power as the Bo-105 helicopter, the Ornicopter has to compromise its flight envelope. It will be a better option to design an Ornicopter with a similar flight envelope to the Bo-105, while requiring slightly more power. Therefore, the stall requirement will be considered as design constraints and the required power will be used as the optimization objective.

As discussed before, the stall area on the Ornicopter rotor in hovering will increase with increasing altitude. Therefore, for a certain design, the stall area in the hovering ceiling condition will always be larger than that of sea level hovering. The maximum allowed stall areas are the same for all flight conditions. Therefore, a design will be satisfactory with regard to the stall requirement at sea level if it satisfies the stall requirement at high altitude. It is not necessary to include the stall requirement in hovering at sea level as design constraints of the optimization.

In this sense, the main constraints of the design include the stall area at the hovering ceiling and in forward flight (150 knots), as well as the blade aspect ratio limitation, as:

$$\begin{aligned}\bar{S}_{hc} &< 0.0893 \\ \bar{S}_f &< 0.0893 \\ 14 &\leq R/c \leq 20\end{aligned}\tag{5.13}$$

The optimization objective is the Ornicopter’s required power in the three flight conditions used before. As there are multiple flight conditions, the results should be combined to form one scalar objective function. The following weight factor is used for

this purpose:

$$F = w_f \bar{P}_f + \frac{1 - w_f}{2} (\bar{P}_h + \bar{P}_{hc}) \quad (5.14)$$

where w_f is the weight factor for required power in forward flight, \bar{P}_f , \bar{P}_h and \bar{P}_{hc} are the normalized required power in three flight conditions (forward flight, sea level hovering and hovering ceiling respectively), which represent the ratio of the required power of the Ornicopter to that of the Bo-105 helicopter, as:

$$\begin{aligned} \bar{P}_f &\equiv \frac{P_f^{(Orni)}}{P_f^{(Bo)}} \\ \bar{P}_h &\equiv \frac{P_h^{(Orni)}}{P_h^{(Bo)}} \\ \bar{P}_{hc} &\equiv \frac{P_{hc}^{(Orni)}}{P_{hc}^{(Bo)}} \end{aligned} \quad (5.15)$$

By tuning the weight factor, optimal designs can be obtained for different flight conditions. The value of the weight factor will depend on the desired Ornicopter applications. For example, the Ornicopter designed for troop transportation will mainly fly at high velocity, and hence a large w_f should be considered ($0.5 < w_f < 1.0$). To investigate the impacts of the weight factor on the final Ornicopter design, different values are tested. The optimization results will be presented in the following section.

5

Optimized Designs

The optimization tool provided by *Matlab* (*fmincon*) is used for the design optimization. This can find the minimum value of the constrained non-linear multi-variable function. The interior point algorithm provided by *fmincon* is used for the following optimization. It will not be further discussed in detail as it is a standard method. More details of the algorithm were discussed in Ref [6, 7].

The design optimizations are performed with different weight factors w_f , ranging from 0 to 1.0. In this sense, a series of optimal designs are obtained.

Before presenting all the optimization results, the optimization history data for one case ($w_f = 0.5$) is presented. Figure. 5.20 shows the history of design parameters with their upper (UL) and lower limits (LL). In Fig. 5.21, the design constraints (blade aspect ratio and rotor stall area) are presented.

The optimization starts with the Bo-105 design. It is not satisfactory due to the high stall area. The optimization algorithm first searches for a feasible design, resulting in a very high tip velocity. From this design, the search direction follows the trend of using a larger rotor radius and blade area, lower tip velocity and a small negative $k_{\theta 2}$.

From Fig. 5.20 and 5.21, one can see that the design parameters do not reach the limitations, and the active constraints for this optimization case are the blade aspect ratio and stall area in forward flight.

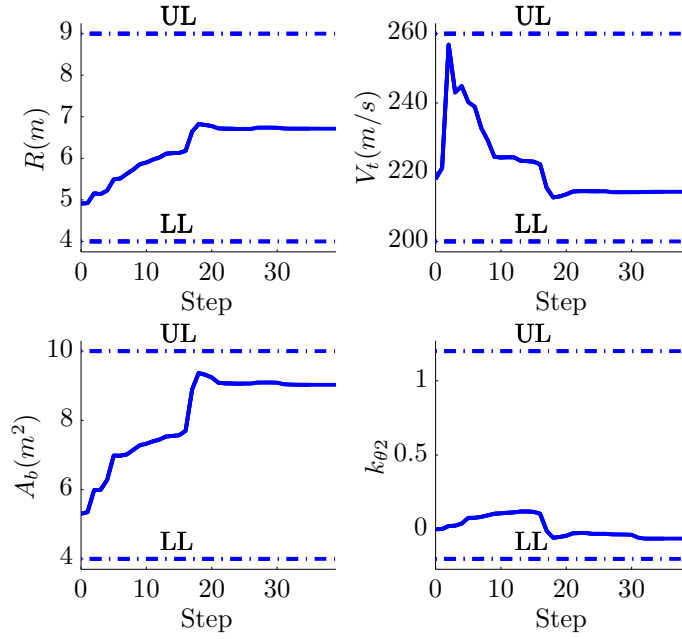


Figure 5.20: Design parameter history for $w_f = 0.5$

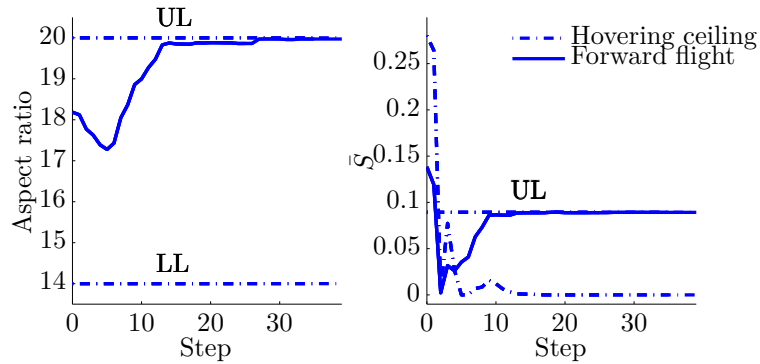


Figure 5.21: Design constraints for $w_f = 0.5$

To understand the trend of the optimized Ornicopter design and the active constraints, all the optimization results ($0.0 \leq w_f \leq 1.0$) are analysed together. The physical reasons causing these results will be investigated.

Figure 5.22 presents the normalized power requirement of the optimal Ornicopter

designs with different w_f . It clearly shows that the required power in the hovering condition and forward flight are contradictory.

With a low weight factor, the Ornicopter design can be optimized mainly for hovering, resulting in approximately 7% less required power in hovering and 15% power requirement reduction at the hovering ceiling, when compared to the Bo-105. The drawback that comes with this design is the higher required power in forward flight, which is about 11% higher than that of the Bo-105 helicopter.

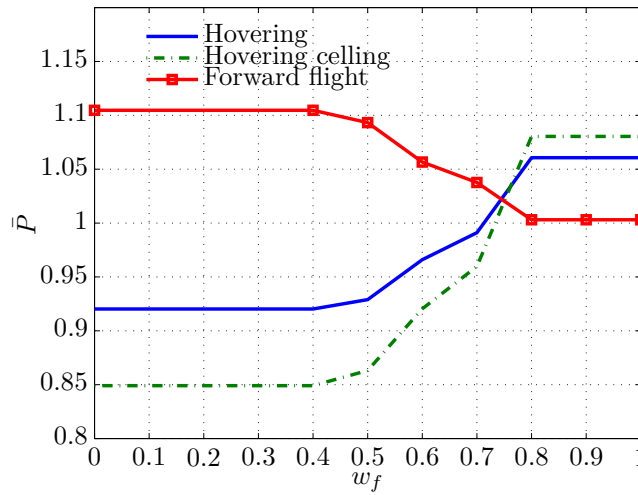


Figure 5.22: Normalised required power of the optimal Ornicopter design as a function of w_f

Similar results can be found for the high w_f cases, in which the forward flight performance is the main optimization objective. However, the optimal Ornicopter design will still have higher required power than the Bo-105 in forward flight (approximately 1%), and the required power in hovering will be increased dramatically (close to 8%). In other words, to reduce the Ornicopter power consumption in forward flight, the hovering performance needs to be compromised to a large extent.

From Fig. 5.22, one can also find that the impact of w_f on the hovering performance is much higher than in the forward flight condition. The change of normalized power requirement at the hovering ceiling is nearly 25%, while the required power in forward flight varies by only around 10%.

This is caused by the fact that the induced power is the dominant part in the total required power in hovering, and it is very sensitive to the design parameters considered in the above optimization, especially the rotor radius. In forward flight, the fuselage parasitic power is the main part of the total required power, which is not affected by the rotor design parameters.

Figure 5.22 also shows that the optimal design is not affected for low and high weight factors, i.e. the w_f is influential mainly in the range of 0.4 to 0.8. For a better understanding of Ornicopter’s the optimization results, the variations in the optimal design parameters (as a function of w_f) are presented in Fig. 5.23, and Fig. 5.24 shows the blade aspect ratio and rotor stall area of the optimal designs.

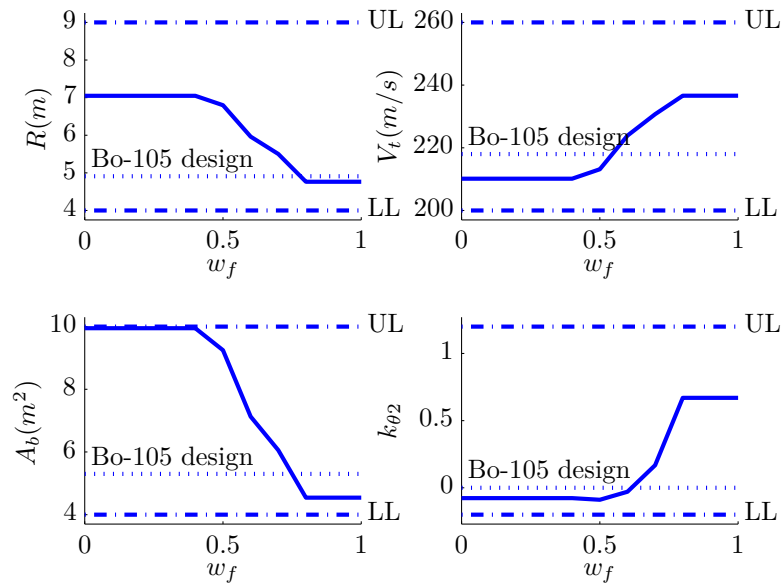


Figure 5.23: Optimal designs for different w_f

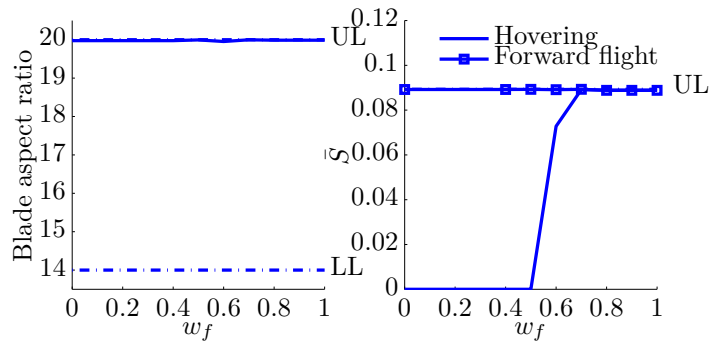


Figure 5.24: Design requirements at different w_f

From Fig. 5.23 and 5.24, one can see that the optimal design reaches the boundary (boundary for design parameters or stall boundary) when w_f is lower than 0.4 or higher than 0.8.

When w_f is low, the design is optimized mainly for hovering, where a higher rotor radius is desired to reduce the induced power. Due to the design constraint of the maximum blade aspect ratio, the blade chord length also needs to be increased. At the point where w_f is 0.4, the blade area reaches the maximum value allowed. In this sense, the required power in hovering cannot be further reduced when lowering w_f .

Increasing w_f (between 0.4 and 0.8), the required power for forward flight becomes a larger part of the optimization objective. To reduce the forward flight power consumption, the blade area needs to be reduced, in order to minimize the profile power. Due to the blade aspect ratio constraint, the rotor radius should also be reduced. This will increase the induced power consumption. However, the induced power is very small in forward flight, and thus the total required power can be reduced by using a smaller rotor. Meanwhile, as shown before, a lower blade area also means a higher stall area. Therefore, the rotor tip velocity should be increased to delay the stall.

For the low w_f cases, due to the high blade area and rotor radius, the stall will not occur in the hovering ceiling condition (see Fig. 5.24). Increasing w_f , the optimal rotor radius and blade area decrease. This causes more stall in hovering. Therefore, the optimal pitch-flapping coupling will also increase, as this can reduce the stall area in hovering (see Fig. 5.11).

After w_f reaches 0.8, its effect on the optimal Ornicopter design becomes very small. This is due to the fact that the stall area reaches the design requirements in both hovering and forward flight conditions. In this situation, any design variation which can reduce the forward flight power consumption, such as a smaller rotor or a lower tip velocity, will increase the stall area and results in an unsatisfactory design.

Overall, the weighing factor w_f will affect the final optimal Ornicopter design, and this plays an important role between the range of 0.4 and 0.8. The higher w_f is, the better the forward flight performance, which requires a smaller rotor size and blade area, as well as a higher tip velocity and pitch flapping rate coupling to reduce the stall area.

The final optimal Ornicopter design will depend on the potential applications of the helicopter. In this sense, it is not the intention of this thesis to determine the ‘best’ Ornicopter design.

In this thesis, the purpose of the Ornicopter design process is to find a design that has a similar performance to the reference helicopter Bo-105 and to investigate the potential of this new concept. Therefore, the optimization results which have similar required power to the Bo-105 for both hovering and forward flight should be considered as the Ornicopter design candidates.

Recalling Fig. 5.22, this shows that the Ornicopter concept is not a good solution for fast forward flight. Its minimum required power in forward flight is still higher than the power consumption of the Bo-105, while the cost to reduce it is very high (i.e. the required power in hovering increases dramatically). Meanwhile, to reduce the stall area, the rotor tip velocity should be increased, see Fig. 5.23. This will also degrade

the Ornicopter high speed performance due to compressibility effects on the advancing side.

Overall, the optimal Ornicopter design corresponding to $w_f = 0.7$ has been chosen. The design parameters are presented in Tab. 5.5. The Ornicopter design has almost identical required power in hovering as the Bo-105 ($\bar{P}_h = 0.9911$) and lower required power at the hovering ceiling ($\bar{P}_{hc} = 0.9598$). As discussed before, the required power of the Ornicopter will be higher than that of the Bo-105. For the chosen Ornicopter design, it requires about 4% more power at 150 knots forward flight ($\bar{P}_f = 1.038$).

Table 5.5: Optimized Ornicopter rotor design

	Design parameters					
	R (m)	A_b (m ²)	V_t (m/s)	$k_{\theta 2}$	c (m)	Ω (rad/s)
Ornicopter	5.50	6.06	230.7	0.168	0.275	41.9
Bo-105	4.91	5.30	218.0	0	0.270	44.4

It should be mentioned that the vertical fin size used in the optimization is relatively high (\bar{S}_{vs}), in order to increase the equivalent vertical fin size (S_e). To limit the vertical fin size to a practical value, while keeping the same equivalent vertical fin size, the vertical fin size and the incidence angle are both increased for the following comparisons. The incidence angle (β_0^{fin}) is increased to 8° ($\bar{\beta}_0^{fin} = 1.72$) and the \bar{S}_{vs} equals 2.91.

5.6 Comparisons with the Bo-105

In this section, the new optimized Ornicopter design will be compared with the Bo-105 helicopter. The comparisons will be done for the flight envelope, the natural modes and handling qualities.

5.6.1 The Flight Envelope

The flight envelope of the new Ornicopter design as compared with the Bo-105 is presented in Fig. 5.25. The same criteria used in the previous chapter are applied to the calculation.

It can be found that the Ornicopter stall boundary is greatly extended when compared to the baseline design. For this new Ornicopter design, the flight envelope will be similar to that of the Bo-105 helicopter.

Looking at the stall boundary, one can see that the stall effect still has a large impact on the Ornicopter hovering performance when compared with the Bo-105. However, this optimized Ornicopter has dramatically increased the hovering ceiling defined by the stall effect.

Increasing the air speed, the stall service altitude of the Ornicopter will increase first until it reaches the maximum altitude at around 50 knots flight speed. Afterwards, it

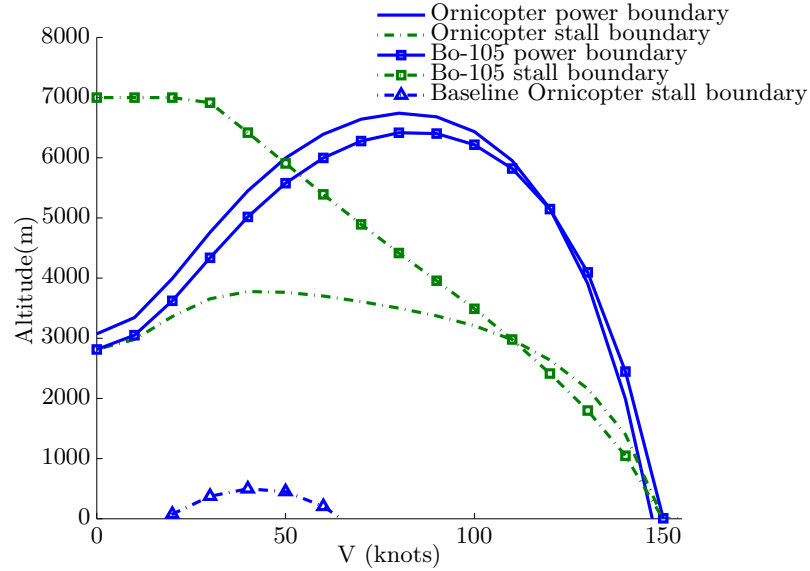


Figure 5.25: The flight envelope of the optimal Ornicopter and Bo-105

5

will decrease with the increase in speed. In the Bo-105 case, the stall service altitude will keep decreasing as the velocity increases.

This is caused by the fact that the stall area on the Ornicopter rotor consists of two parts: 1) the ‘conventional’ stall area caused by the blades’ longitudinal flapping, the longitudinal cyclic control and the unsymmetrical local air flow, and 2) the stall introduced by the active flapping.

The amplitude of the active flapping has a bucket shape as the required power for helicopters (see Fig. 4.3). This indicates that the stall caused by the active flapping will also have a bucket shape, which makes the stall boundary of the Ornicopter have a ‘reversed’ bucket shape as seen in Fig. 5.25.

One can also see that at high forward speed (around 130 knots), the Ornicopter has a higher stall service altitude than the Bo-105 helicopter. This shows that, in forward flight, the stall area on the Ornicopter rotor is less sensitive to altitude compared with a conventional helicopter main rotor.

For the same flight speed, increasing the altitude will increase the ‘conventional’ stall area on both the Ornicopter rotor and conventional helicopter rotor. For the Ornicopter, the stall area caused by the active flapping is associated with the required power. In fast forward flight, increasing the altitude decreases the air density, and hence the power required by the Ornicopter reduces (as the parasite power is the major part of the total required power). In this sense, the amplitude of active flapping will decrease as the altitude increases, as well as the stall area. Combining these two effects, the

5.6 Comparisons with the Bo-105

151

development of the stall area on the Ornicopter rotor is more gradual than that of the Bo-105 while the altitude is increasing. Therefore, in forward flight, the Ornicopter has a slightly higher service altitude than that of the Bo-105.

In hovering, the situation is reversed. Now the induced power is the main part of the required power. Increasing the induced power at higher altitude requires an increase in the amplitude of active flapping which causes a larger stall area. In this sense, the Ornicopter rotor stall area in hovering will increase very fast when the altitude is increasing resulting in much lower stall hovering ceiling than the Bo-105.

For the power boundaries, the Ornicopter shows a similar trend to conventional helicopters. At low and modest speed, the Ornicopter has a slightly higher service altitude than the Bo-105, while its maximum speed which is limited by the available power is lower.

This is also caused by the different compositions of required power in hovering and forward flight. Due to the stall effect, the Ornicopter needs a rotor with a higher radius, blade area and tip velocity. This design modification will reduce the induced power, while increasing the profile power. In this sense, compared with the Bo-105, the Ornicopter has lower required power in hovering, when induced power is the dominant part of the total required power, and higher required power in forward flight, when the profile power is higher than the induced power.

Combining stall and power boundaries, one can see that the Ornicopter will have a slightly better performance in hovering and low speed. Due to the higher stall area, the Ornicopter has a lower service ceiling when compared to the Bo-105. For high speed flight, the Ornicopter performance is worse than the Bo-105 due to the higher required power.

5.6.2 Autorotation

In Chapter 4, the autorotation index (AI) of a helicopter main rotor was derived as:

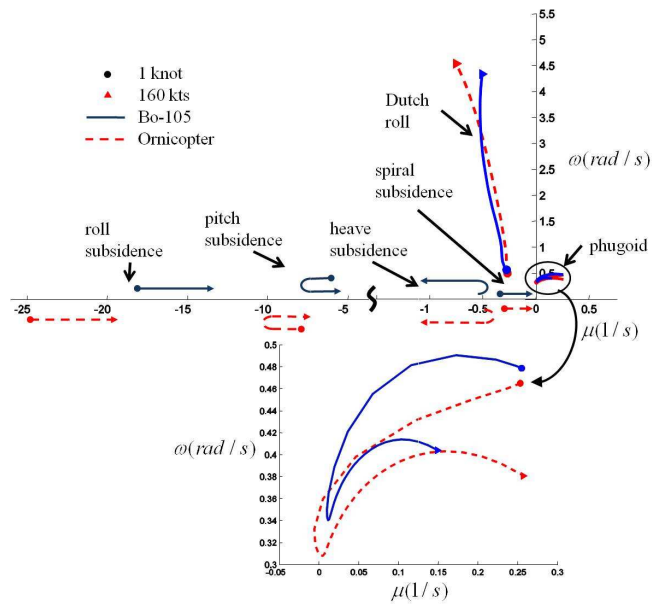
$$AI = \frac{\pi g \rho_b S_a V_t^2 R}{6 N_b B L^2} \quad (5.16)$$

From the design research for the Ornicopter above, it is showed that the stall effect is the most critical issue for the Ornicopter concept. To reduce the stall area, the Ornicopter's blade loading should be reduced, and a higher rotor tip velocity is preferable. Meanwhile, a larger rotor disk size (larger radius) is required to reduce the induced power. All the design modifications will increase the AI of the Ornicopter rotor. As the ρ_b and S_a are assumed to be constant at the preliminary stage, the optimized Ornicopter rotor will have a higher AI as compared to the Bo-105. Substituting the optimized design of the Ornicopter (see Tab. 5.5) into Eq. 5.16, one can get that the AI of the Ornicopter is 67.6% higher than that of the Bo-105.

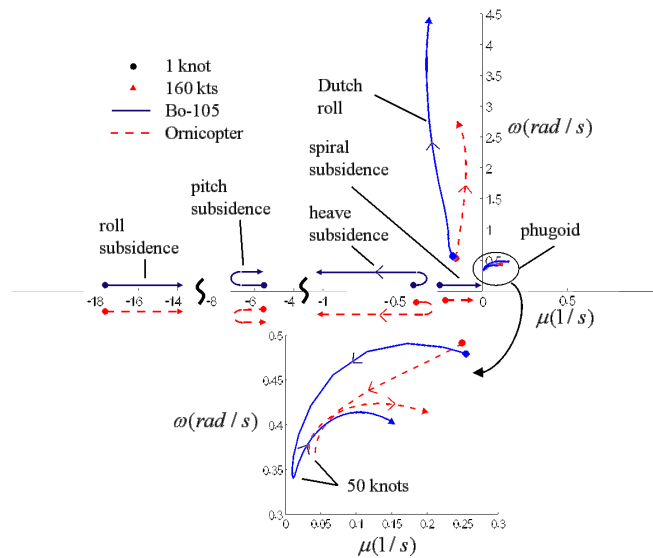
5.6.3 Natural Modes of Motion

The new Ornicopter design also changes the flight dynamics of the helicopter. Those impacts can be found from the natural modes of the body motion DoF. Figure 5.26(a)

presents the eigenvalues of this new Ornicopter design, together with the eigenvalues of the Bo-105.

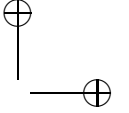


(a) The optimized Ornicopter design and the Bo-105



(b) The baseline Ornicopter design and the Bo-105

Figure 5.26: Comparisons of natural modes for the Ornicopter and the Bo-105



5.6 Comparisons with the Bo-105

153

The figure shows that the general trends of the modes are kept the same for the new Ornicopter design. The main differences between the new and baseline Ornicopter design corresponds to pitch/roll subsidence and the Dutch roll modes (see Fig. 5.26(b)).

Comparisons in Chapter 4 showed that the baseline Ornicopter design has almost identical dynamic characteristics as the Bo-105 in the pitch and roll axes, since they have the same design. For the new design, the pitch and roll subsidence modes shift to the left hand side, indicating higher pitch and roll dampings. These higher dampings will make the Ornicopter more stable and may improve its handling qualities.

This change is caused by the larger (and heavier) blades used for the new design. With the heavier blades, this new rotor can generate higher hub moments, and hence the new Ornicopter design has higher pitch and roll damping.

The most interesting change is related to the Dutch roll mode. The baseline Ornicopter has a very different Dutch roll mode when compared to the Bo-105. Both the Dutch roll damping and frequency of the baseline Ornicopter are lower than that of the Bo-105. This is caused by the low Ornicopter yaw damping and directional stability.

The new design uses a bigger vertical fin to compensate for part of the shaft torque. Meanwhile, the bigger vertical fin also improves the yaw damping and the directional stability, especially at high velocities. Therefore, the Dutch roll mode of the new Ornicopter design is similar to that of the Bo-105.

For a clearer view, the Dutch roll modes of the Ornicopter and Bo-105 are also presented with the handling qualities rating defined in ADS-33 [4], see Fig. 5.27.

From Fig. 5.27 one can see that for the new design, the Ornicopter has the same handling qualities rating as the Bo-105. The differences between them are very small. As for the baseline design, the SCAS system can be used to improve the Ornicopter handling qualities. the calculation shows that for the new design, the improvements with regard to the Dutch-roll mode achieved by using the SCAS system is less than that for the baseline design.

5

5.6.4 Handling Qualities

The changes in the Ornicopter dynamic characteristics also affect handling qualities. In the following, the attitude quickness and the bandwidth/phase delay will be presented for pitch and yaw directions.

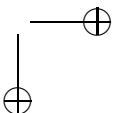
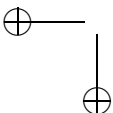
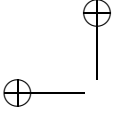
The Pitch Axis

Since the impacts of the new Ornicopter design on pitch and roll axes are similar, only the pitch axis is analysed and presented in this thesis, as shown in Figs. 5.28 and 5.29.

According to the discussion for the yaw handling qualities in the previous chapter, higher damping can improve the Ornicopter’s yaw handling qualities. Similar effects can also be found in the pitch axis.

The new Ornicopter design increases the pitch and roll damping of the helicopter, as shown in Fig. 5.26(a), resulting in a higher pitch bandwidth and better attitude quickness response.

The pitch bandwidth and delay is affected by pitch damping, as well as by flapping



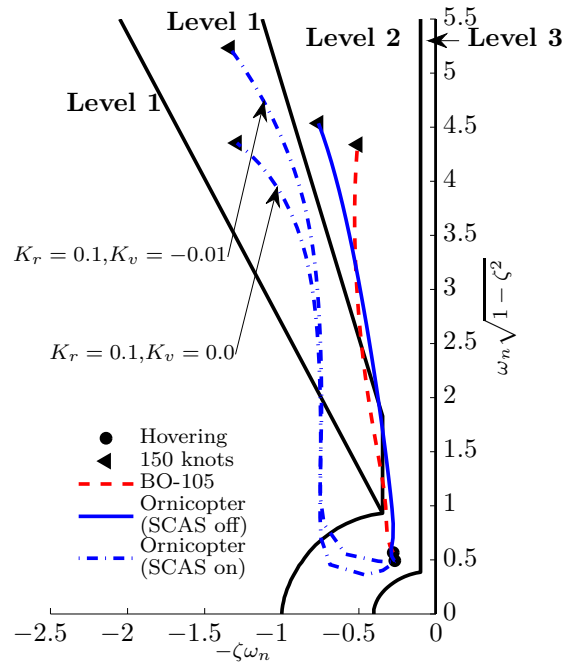


Figure 5.27: Dutch roll mode with the handling qualities rating

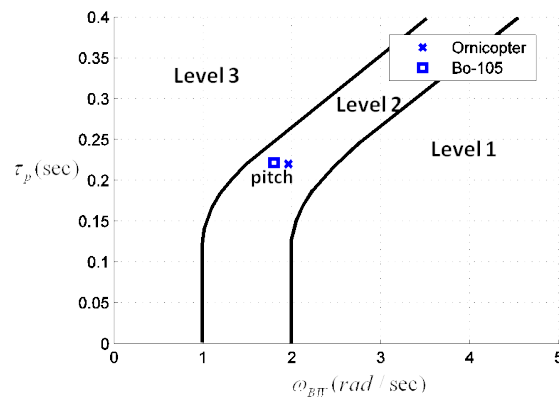


Figure 5.28: The pitch bandwidth and phase delay

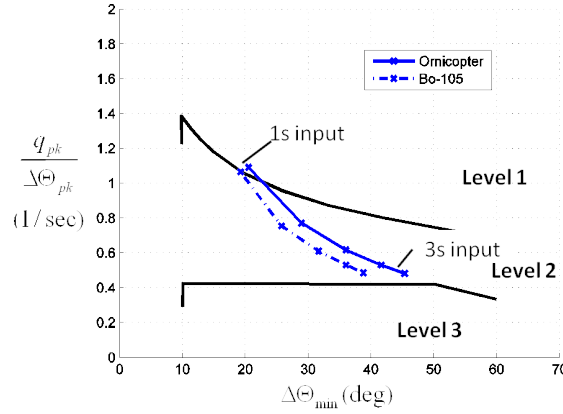


Figure 5.29: The pitch attitude quickness

dynamics and inflow dynamics. Therefore, though the pitch damping of the new Ornicopter design is greatly increased, the improvement in pitch bandwidth and delay is relatively small.

For pitch attitude quickness, the improvement is also limited. This new Ornicopter design has almost identical pitch quickness as the Bo-105 and slightly higher minimum attitude change ($\Delta\Theta_{min}$). The calculation results shift slightly towards the Level 1 region. However, the Ornicopter and Bo-105 still have the same level of handling qualities with regard to quickness.

The Yaw Axis

Due to the additional yaw damping and directional stability provided by the larger vertical fin, the new Ornicopter design has better yaw handling qualities, as shown in Fig. 5.30 to 5.32.

From Fig. 5.30, one can see that the general trend in the yaw bandwidth and delay of the new Ornicopter design is the same as the baseline Ornicopter and Bo-105. The bandwidth of the Ornicopter is improved by the new design, especially at a high velocity. This is caused by the fact that the vertical fin is more influential at higher air speed. At fast forward flight (130 knots), the Ornicopter has almost the same yaw bandwidth as the Bo-105.

However, the larger vertical fin affects only the dynamics of the body motion DoF. The higher phase delay of the Ornicopter, which is mainly caused by the control time delay and flapping dynamics, cannot be improved in this new Ornicopter design. This is the inherent characteristic of the Ornicopter concept, and cannot be easily overcome. The flight control system should be considered to solve this drawback of the Ornicopter.

Figure 5.32 shows the yaw attitude quickness of the new Ornicopter and the Bo-105. One can see that the new design has similar quickness parameters as Bo-105, while the minimum heading change is smaller. This change causes the curve for the Ornicopter

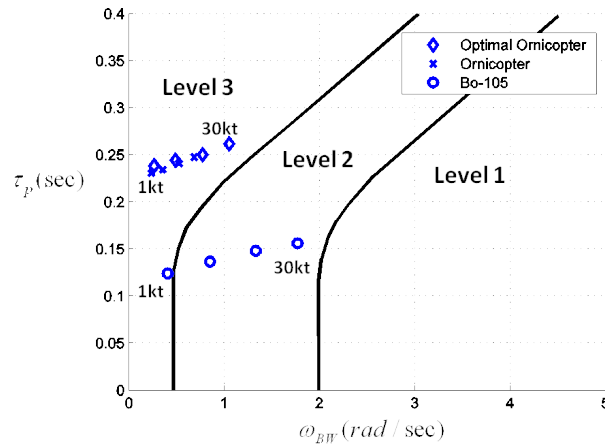


Figure 5.30: The yaw bandwidth (hovering and low speed)

5

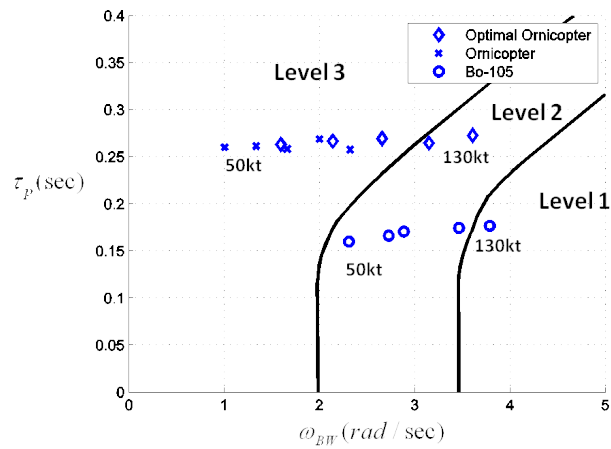


Figure 5.31: The yaw bandwidth (forward flight)

to move a little away from the Level 1 boundary when compared with the baseline Ornicopter design, which indicates slightly worse handling qualities. However, the yaw response of this new design should be more similar to conventional helicopters, which is favourable for the pilot workload.

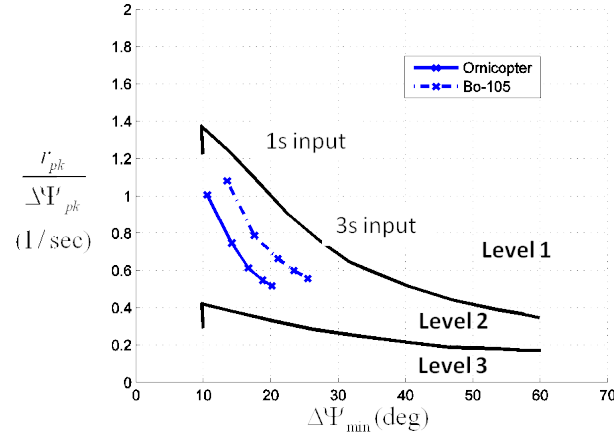


Figure 5.32: The yaw altitude quickness

5.7 Discussion

5.7.1 Weight Prediction

During the design process, the weight of the Ornicopter is assumed to be the same as that of the Bo-105. From the design database and design optimization, one can see that the optimal Ornicopter tends to use a larger blades and a bigger vertical fin.

As previously discussed, the design process in this thesis does not include a weight analysis. The reason for this is that the main focus of the research relates to the Ornicopter's performance with the additional consideration of rotor design parameters that can improve this performance. The design modifications identified in the present thesis will increase the weight of the Ornicopter when the rest of the parameters remain unchanged.

With a higher weight, the Ornicopter performance will be degraded, i.e. higher required power and stall area. In forward flight, the fuselage parasite power is the dominant factor for helicopter performance. Consequently, the forward flight of the Ornicopter will be less influenced by the increased weight compared to the hovering performance.

5.7.2 Influence of the Helicopter Size

In this thesis, only one benchmark helicopter is considered. Possible influences of the gross weight on the Ornicopter are not considered.

The gross weight does not affect the stall characteristics of helicopters directly. The blade loading coefficient (C_T/σ) combining the helicopter's weight and rotor design parameters is more representative regarding rotor stall. It can be calculated as (in

hovering):

$$\begin{aligned} C_T/\sigma &= \frac{T}{\rho V_T^2 \pi R^2} \frac{\pi R^2}{A_b} \\ &= \frac{M_a g}{\rho V_T^2 A_b} \end{aligned} \quad (5.17)$$

The statistic data shows that most helicopters have a blade loading coefficient (in hovering) of about 0.08 at their MGTOW (maximum gross takeoff weight) [22], as shown in Fig. 5.33. A stall margin is required for the rotor to produce enough thrust force in forward flight and to conduct flight manoeuvres.

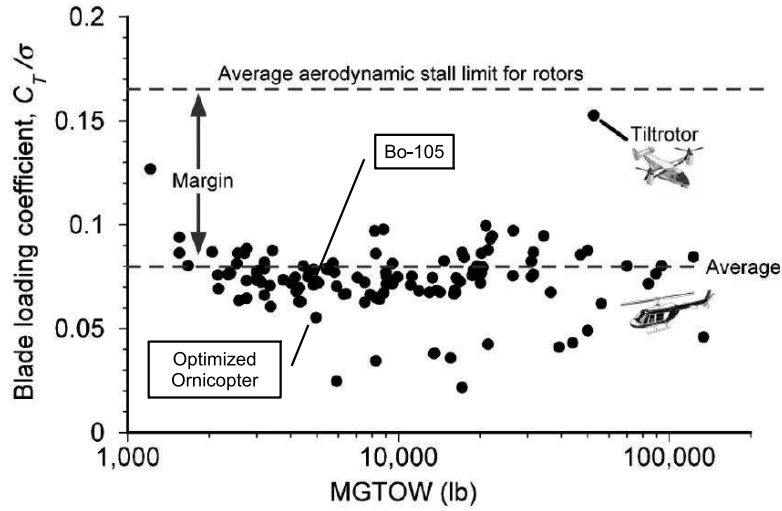


Figure 5.33: Trends of blade loading coefficient versus MGTOW [22]

As the Ornicopter enlarges the rotor stall due to active flapping, the stall margin needed for the Ornicopter is higher than that of conventional helicopters, i.e. the Ornicopter should have lower blade loading coefficient. The design optimization has shown this trend.

As one can see in Fig. 5.33, the blade loading coefficient is very similar for helicopters with different weights. The Ornicopter design should also have the same trend, i.e. the weight of the helicopter will not be the main factor for the differences between the optimized Ornicopter design and conventional helicopter designs.

Regarding the required power, the Ornicopter only increases the rotor profile power, which is a relatively small portion of the total required power. Increasing the gross weight increases the required power of the helicopter. However, the composition of the required power (induced power, profile power and parasite power) should be similar for different sizes of helicopter. In this sense, using different benchmark helicopters should result in a similar increase of required power for the Ornicopter (in percentage terms).

5.7.3 Different Design Requirements

In this thesis, the flight envelope of the benchmark helicopter (Bo-105) is used as the design requirements of the Ornicopter. Design optimization showed the Ornicopter has worse performance than the Bo-105. Using a different benchmark helicopter (and hence different design requirements) might affect the final conclusion. Different kinds of flight envelope should be considered in future research.

To reduce the rotor stall, the Ornicopter design tends to increase the main rotor profile power. In fast forward flight, the parasite power is the dominant part of the total required power, and it increases very fast with increasing air speed. The profile power becomes a smaller proportion of the total required power at higher speed. In this sense, the additional profile power on the Ornicopter will be less detrimental while a higher maximum velocity is required, i.e. the difference of the Ornicopter and conventional helicopters will be smaller (in percentage) regarding the required power in forward flight. It should be considered that at higher speed, the compressibility effects on the advancing side of the rotor become stronger. Therefore, a higher maximum velocity requirement might be favourable for the Ornicopter concept before the compressibility effects become the main limitation of the maximum speed.

In hovering, as the helicopter performance is more sensitive to the main rotor design than in forward flight, the Ornicopter design can be optimized and have the same or even better performance than the Bo-105. In this sense, the hovering ceiling requirement is less influential for the differences between the Bo-105 and optimized Ornicopter.

From the flight envelope calculations, as shown in Fig. 5.26(a), one interesting result can be found that the general shape of the Ornicopter flight envelope is different from that of the Bo-105. The service ceiling of Bo-105 (5725 m) is much higher than its hovering ceiling (2815 m). This results in a parabolic top of the Bo-105 flight envelope. In the case of the Ornicopter, its flight envelope has a more flat top. These different shapes are correlated to the different characteristics of the two helicopters. Similar requirements for the hovering ceiling and the maximum service might be favourable for the Ornicopter concept, as they fit the characteristics of the Ornicopter better.

5.8 Conclusion

In this chapter, some design parameters of the Ornicopter are modified based on its characteristics. The new optimized Ornicopter design is determined.

Sensitivity analyses are performed first to investigate the impacts of different design parameters on the Ornicopter performance. Based on the analyses results, four parameters are chosen to build a design database, including: the rotor radius, the blade area, the tip velocity and the vertical fin size.

Combining the different values of these four parameters, a design database is formed. From the database, it can be found that no feasible design can be found for the Ornicopter to satisfy both the design requirements, i.e. the stall area requirements and the required power requirements.

Using the optimization method, the optimal Ornicopter designs concerning different

flight conditions (hovering or forward flight) are identified. The results show that the hovering performance of Ornicopter can be better than that of the Bo-105, with the cost of poorer forward flight performance. However, the optimal forward flight performance of the Ornicopter is always inferior to that of the Bo-105 due to the active flapping. This indicates that the Ornicopter concept might be more suitable for low and mid-range velocity applications.

From the series of optimal Ornicopter designs, the one with similar hovering performance to the Bo-105 is chosen as an example design, and compared with the Bo-105 in means of the flight envelope and handling qualities.

Comparisons show that the new Ornicopter design can greatly improve the limited flight envelope of the baseline Ornicopter design. The new design has a better altitude performance at low speed and fast forward flight, while having lower maximum speed due to the higher required power.

This new Ornicopter design also improves the handling qualities, and it has better handling qualities in pitch and roll axes than the Bo-105. Although its yaw handling qualities are improved, this new design is still slightly worse than the Bo-105 in a few of its handling qualities.

6

Conclusions and Recommendations

The goal of the present dissertation was to understand how and why the Ornicopter concept behaves differently when compared with conventional helicopters, and to investigate the feasibility of the Ornicopter design.

In this context, the Ornicopter concept was first mathematically modelled and analysed. Comparisons with the Bo-105 helicopter using the same design parameters were performed. The main characteristics of the Ornicopter, such as required power, flight envelope and handling qualities, were found and served as an important guide for the following Ornicopter design. Based on sensitivity analyses and a design database, some important design parameters for the Ornicopter were pinpointed and optimized. The optimized Ornicopter was again compared with the Bo-105 to answer the research questions of the thesis.

6.1 Conclusions

6.1.1 Impacts of the Ornicopter Concept

Question 1:

As compared to a conventional helicopter, what are the characteristics of the Ornicopter regarding performance, stability, controllability, and handling qualities?

The Ornicopter concept introduces two fundamental changes to conventional helicopters. They are active flapping blades and the absence of a tail rotor. Based on comparisons between the baseline Ornicopter design (the same as the Bo-105) and the Bo-105, those two changes will affect the Ornicopter in the following ways.

The active flapping blades mainly affect the Ornicopter performance. This is due to a large variation in the blade angle of attack. This large variation will increase the stall area on the Ornicopter rotor, as well as the profile power. The increased stall area of the Ornicopter is the major drawback of the Ornicopter concept, especially when the Ornicopter is using the same design as the Bo-105. The flight envelope of the Ornicopter is strongly limited by the stall effect. The maximum velocity and service ceiling of the Ornicopter reduce dramatically because of the stall, i.e. the Ornicopter maximum speed is 50% lower than that of the Bo-105 helicopter, and the Ornicopter service ceiling is about 500 m.

The active flapping causes higher profile power which reduces the efficiency of the Ornicopter rotor. Approximately 6% more power than of a conventional helicopter rotor is required. As the Ornicopter does not need the tail rotor, the total required power of the Ornicopter will be similar to the Bo-105 in hovering, and about 5% more than that of the Bo-105 in forward flight. It should be mentioned that the above power calculations were done with the assumption that the stall effects are neglected. Considering the large stall area on the Ornicopter rotor, the actual required power of the baseline Ornicopter will be higher. The power comparisons between the optimized Ornicopter (stall area is limited) and Bo-105 is more accurate.

The active flapping also generates higher hub vibratory loads. As all blades are forced to flap in sequence, the harmonic components of hub forces and moments generated by different blades cannot cancel each other, resulting in vibratory loads in the range of $1/rev$ to N_b/rev . The most efficient way to reduce the Ornicopter’s vibratory problem is by using a higher number of blades and new flapping configurations, such as the 3×2 AS configuration or the $4 \times$ Teeter configuration.

The absence of the tail rotor affects the stability and the handling qualities of the Ornicopter in the yaw direction. The Ornicopter does not have the yaw damping or the directional stability offered by a conventional tail rotor. Therefore, the Ornicopter yaw handling qualities are inferior to conventional helicopters, with respect to bandwidth and delay, attitude quickness and lateral-directional oscillation. Without a tail rotor, the Ornicopter yaw control is achieved by controlling the main rotor torque directly. Two advantages can be found for this yaw control method, namely the higher yaw control power and the lower coupling responses for yaw control input.

6

6.1.2 Ornicopter Design

Question 2:

As compared to a conventional helicopter, how can an Ornicopter with comparable or improved flight performance be designed?

The comparisons between the Ornicopter concept and conventional helicopters have shown some drawbacks of the Ornicopter concept. Some of them can be overcome by modifying the Ornicopter design.

The sensitivity analyses showed the impacts of different design parameters on the Ornicopter concept. Most of these parameters have contradictory effects on the stall

area and required power.

One exception is the vertical fin size. In forward flight, by using the vertical fin to compensate for the main rotor torque, the amplitude of the forced flapping can be reduced. In this way, both the stall area and required power can be reduced. Considering that a larger vertical fin also improves the yaw stability and handling qualities, the Ornicopter design will tend to have a larger vertical fin when compared with conventional helicopters.

To have a better view on the different combinations of design parameters, a design database was created with more than 10^4 Ornicopter designs. Analyses showed that no Ornicopter design can be found in the database that has the same or lower stall area and required power as Bo-105 helicopter.

This is caused by the fact that the stall area and required power are contradictory requirements. Trying to reduce the stall area will most probably increase the power consumption. Recalling that the Ornicopter concept will increase both the stall and required power of the main rotor, it will be difficult to reduce both of them by changing some design parameters. In this sense, the Ornicopter design was optimized for the power consumption, the stall area being used as design a constraint.

The design optimization showed the general trend in the design parameters for different optimization objectives. For the Ornicopter having a similar hovering performance as the Bo-105, it was found that it requires about 4% more power in forward flight. This design has a larger blade area (A_b) and tip velocity (V_t) to reduce the stall area and a larger rotor radius (R) to reduce the required power in hovering. It uses a positive pitch flap rate coupling ($k_{\theta 2}$) to improve the hovering performance and a larger vertical fin to improve the forward flight performance.

The new Ornicopter design was compared with the Bo-105 for the flight envelope and handling qualities. The calculations showed a large improvement for the Ornicopter’s flight envelope compared with the baseline design, as well as better handling qualities.

From all the analyses and comparisons that have been done, the different characteristics of the Ornicopter concept when compared with conventional helicopters can be summarized, as shown in Tab. 6.1. It should be emphasised that the advantages/disadvantages are based on an Ornicopter design which is similar to the Bo-105. Some of them will vary with the design trade off.

Overall, this thesis extended the research for the Ornicopter concept to a more detailed stage. Multidisciplinary analyses have been performed, such as performance, stability and handling qualities analysis, and the thesis gives a more comprehensive understanding of the characteristics of this concept. The research in this thesis showed that the Ornicopter has worse performance (smaller flight envelope and higher required power) due to its inherent characteristics, i.e. the active flapping blades. The thesis also investigated the application of a design database and design optimization in the conceptual design phase of a new configuration. The design method applied in the thesis has shown its effectiveness to unmask the general design trend of a new concept and its potential to be a tool for general conceptual design applications.

Table 6.1: Characteristics of the Ornicopter concept

	Advantages	Disadvantages
Power	Lower required power in hovering	Higher required power in forward flight
Stall		Higher stall area, stall in hovering flight
Flight envelope		Lower maximum service ceiling
Stability		Lower yaw damping and directional stability
Controllability	Higher yaw control power	
Handling qualities	Lower coupling responses for yaw control input	Slightly worse yaw handling qualities
Other	Higher autorotation index	Higher vibratory loads

6.2 Recommendations

6

6.2.1 Improving the Model

The flight mechanics model developed in this thesis is a classical Level 1 [10] model using blade element theory. Some assumptions (Section 3.2.1) and simplifications were made while developing the model. Improving this model will provide more fundamental understanding of the Ornicopter.

Some preliminary analyses have been done for the effects of elastic blades on the Ornicopter. However, those analyses were only done for hovering. Those analyses showed a relatively large deformation of the blades due to the active flapping. These elastic effects will change the local air flow condition on blade elements, which may change the characteristics of the Ornicopter. The elastic blade model throughout the flight envelope should be considered in further research.

One of the major impacts of the active flapping of blades is the larger angle of attack variation. In this sense, unsteady aerodynamics and a dynamic stall model should be considered to improve the hub forces and moments prediction.

In the design process, the total weight of the Ornicopter is assumed to be constant. The weight of additional forced flapping mechanics should be estimated, as well as the weight reduction caused by the absence of the tail rotor. Meanwhile, the impacts of design parameters, such as a larger rotor and vertical fin, on the weight of the Ornicopter should be also considered.

6.2.2 Analyses for More Disciplines

Research has been done in this thesis mainly in the field of performance and flight dynamics. For the Ornicopter, its main propose is to eliminate the tail rotor from the helicopter. As mentioned before, the tail rotor has some drawbacks with respect to safety, noise, and control authority. In this sense, the Ornicopter concept should also be studied with regard to other disciplines, such as safety, reliability, lifecycle cost and environmental impacts.

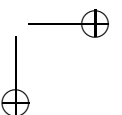
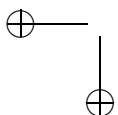
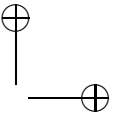
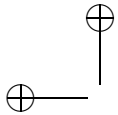
One of the critical issues for the Ornicopter is, as in the case of any helicopters, related to safety. Eliminating the tail rotor results in the increasing reliability of a helicopter. However, the Ornicopter concept introduces additional complexities on the main rotor. The effect of this revolutionary rotor concept on the helicopter’s reliability requires a more detailed rotor hub design and should be considered in further analyses. Likewise, the Ornicopter’s behaviour after the failure of the forced flapping mechanism should also be investigated.

6.2.3 Hybrid Concept

Some drawbacks have been found with the Ornicopter in this thesis. By design optimization, the performance of the Ornicopter can be improved. However, the improvement is limited by the inherent characteristics of this concept. By combining the Ornicopter concept with other new technologies, some disadvantages of the Ornicopter might be overcome.

One promising configuration is to use the vertical fin to compensate for all the shaft torque in forward flight. In this case, the active flapping will not be needed in forward flight and the Ornicopter rotor will work as a conventional helicopter rotor. The yaw control will be achieved by using a rudder, like a fix-wing aircraft. At low speed, the blades will be forced to flap again like the original Ornicopter concept.

Besides the above configuration, some other new technologies, such as the HHC (high harmonic control), IBC (individual blade control) and variable RPM rotor, may also improve the Ornicopter concept, and should be considered in future research.



A

The Ornicopter Rotor Model in Hovering

In this appendix, a simple rotor model for the Ornicopter in hovering will be derived using blade element theory. A central hinged rotor is considered in this model, as shown in Fig. A.1.

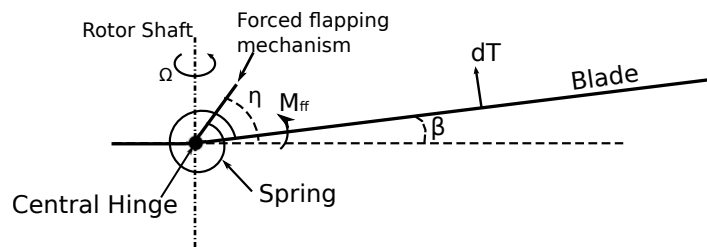


Figure A.1: Blade configuration for the rotor model

A.1 Hub Force and Moment for One Blade

The lift and drag forces on the blade element shown in Fig. A.2 are:

A

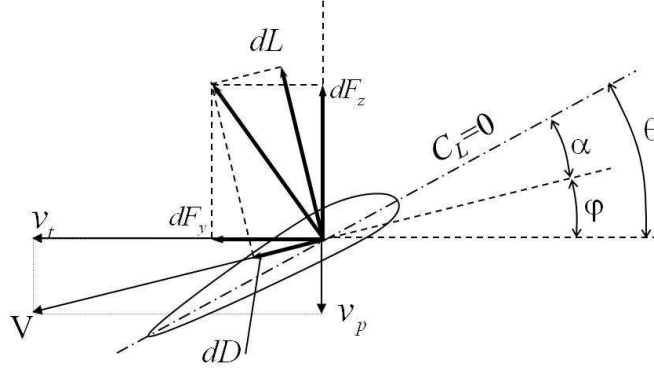


Figure A.2: Aerodynamic environment at a typical blade element

$$\begin{aligned}
 dL &= \frac{1}{2} \rho (v_p^2 + v_i^2) C_l c dr \\
 &\approx \frac{1}{2} \rho v_i^2 C_l c dr \\
 dD &= \frac{1}{2} \rho (v_p^2 + v_i^2) C_d c dr \\
 &\approx \frac{1}{2} \rho v_i^2 C_d c dr
 \end{aligned} \tag{A.1}$$

in which:

$$\begin{aligned}
 C_l &= C_{l_\alpha} \alpha \\
 &= C_{l_\alpha} (\theta - \varphi) \\
 C_d &= C_{d0}
 \end{aligned} \tag{A.2}$$

where θ is the pitch angle of the blade defined as:

$$\theta = \theta_0 + \theta_{s1} \sin \psi + \theta_{c1} \cos \psi \tag{A.3}$$

The blade twist is not considered in this model.

The lift and drag forces can be expanded as;

$$\begin{aligned}
 dL &= \frac{1}{2} \rho C_{L_\alpha} c (\theta \Omega^2 r_e^2 - \Omega r_e (\dot{\beta} r_e + v_i)) dr_e \\
 dD &= \frac{1}{2} \rho \Omega^2 r_e^2 C_{d0} c dr_e
 \end{aligned} \tag{A.4}$$

Assuming that the induced angle is small, one can obtain:

$$\begin{aligned}
 dF_y &\approx dD + dL \varphi \\
 dF_z &\approx -dL
 \end{aligned} \tag{A.5}$$

A.1 Hub Force and Moment for One Blade

169

Similarly, these forces can be transformed into the rotor shaft reference, thus in order to calculate the total hub force and moment generated by the rotor:

$$\begin{aligned} dT &\approx dL \\ dH &= -dF_y \sin \psi + dF_z \beta \cos \psi \\ dS &= -dF_y \cos \psi - dF_z \beta \sin \psi \\ dN &\approx dF_y r \end{aligned} \tag{A.6}$$

A

where T is the rotor thrust, H is the horizontal hub force, S is the sideways hub force and N is the shaft torque.

Integrating through the blade radius and rotor azimuth angle gives the total hub forces and torque generated by one blade. The blade thrust is then:

$$\begin{aligned} T_s &= \frac{1}{2\pi} \int_0^{2\pi} \int_0^R dT \\ &= \frac{1}{6} \rho c C_{l_\alpha} \Omega^2 R^3 \theta_0 - \frac{1}{4} \rho c C_{l_\alpha} \Omega R^2 v_i \end{aligned} \tag{A.7}$$

It can also be written in non-dimensional form as:

$$\begin{aligned} C_{T_s} &= \frac{T_s}{\rho (\Omega R)^2 \pi R^2} \\ &= \frac{1}{2} \sigma_s C_{l_\alpha} \left(\frac{\theta_0}{3} - \frac{\lambda_i}{2} \right) \end{aligned} \tag{A.8}$$

where σ_s is the solidity of a single blade, i.e.:

$$\sigma_s = \frac{c}{\pi R} \tag{A.9}$$

and λ_i is the inflow ratio:

$$\lambda_i = \frac{v_i}{\Omega R} \tag{A.10}$$

The Ornicopter’s horizontal hub force, sideways hub force and shaft torque coeffi-

cients can be derived in the same way, and this gives:

$$C_{H_s} = \frac{1}{2} \sigma_s C_{l_\alpha} \left(\frac{\theta_0}{3} - \frac{\lambda_i}{2} \right) \beta_{c1} - \frac{1}{8} \sigma_s C_{l_\alpha} \lambda_i (\theta_{s1} + \beta_{c1}) + \frac{1}{12} \sigma_s C_{l_\alpha} \beta_0 (\theta_{c1} - \beta_{s1}) \quad (\text{A.11})$$

$$C_{S_s} = -\frac{1}{2} \sigma_s C_{l_\alpha} \left(\frac{\theta_0}{3} - \frac{\lambda_i}{2} \right) \beta_{s1} - \frac{1}{8} \sigma_s C_{l_\alpha} \lambda_i (\theta_{c1} - \beta_{s1}) - \frac{1}{12} \sigma_s C_{l_\alpha} \beta_0 (\theta_{s1} + \beta_{c1}) \quad (\text{A.12})$$

$$\begin{aligned} &= -C_{T_s} \beta_{s1} - \frac{1}{8} \sigma_s C_{l_\alpha} \lambda_i (\theta_{c1} - \beta_{s1}) - \frac{1}{12} \sigma_s C_{l_\alpha} \beta_0 (\theta_{s1} + \beta_{c1}) \\ C_{Q_s} &= \frac{1}{2} \sigma_s C_{l_\alpha} \left(\frac{\theta_0}{3} - \frac{\lambda_i}{2} \right) \lambda_i + \frac{1}{8} \sigma_s C_{d0} \\ &\quad - \frac{1}{16} \sigma_s C_{l_\alpha} (\beta_{s1}^2 + \beta_{c1}^2 + \beta_{c1} \theta_{s1} - \beta_{s1} \theta_{c1}) \\ &= C_{T_s} \lambda_i + C_{Q0_s} - \frac{1}{16} \sigma_s C_{l_\alpha} (\hat{\beta}^2 + \beta_{c1} \theta_{s1} - \beta_{s1} \theta_{c1}) \end{aligned} \quad (\text{A.13})$$

As the blade is centrally hinged, the pitch and roll moments are generated only by the flapping spring, which connects the blade and the forced flapping mechanism as shown in Fig. 2.14). Therefore, the pitch and roll moments generated by one blade are:

$$\begin{aligned} dL_s &= M_{ff} \sin \psi \\ dM_s &= M_{ff} \cos \psi \end{aligned} \quad (\text{A.14})$$

where M_{ff} is the flapping moment generated by the forced flapping mechanism on the blade:

$$M_{ff} = (\eta - \beta) K_\beta \quad (\text{A.15})$$

Substituting the forced flapping mechanism motion (η) and the blade flapping motion (β) (see Eq. 2.1) into Eq. A.15 and integrating through the azimuth angle results in the average roll hub moment:

$$\begin{aligned} L_s &= \frac{1}{2\pi} \int_0^{2\pi} ((\eta_{s1} \sin \psi + \eta_{c1} \cos \psi) - (\beta_0 + \beta_{s1} \sin \psi + \beta_{c1} \cos \psi)) K_\beta \sin \psi d\psi \\ &= \frac{1}{2} K_\beta \eta_{s1} - \frac{1}{2} K_\beta \beta_{s1} \end{aligned} \quad (\text{A.16})$$

Similarly, the pitch hub moment is:

$$M_s = \frac{1}{2} K_\beta \eta_{c1} - \frac{1}{2} K_\beta \beta_{c1} \quad (\text{A.17})$$

The non-dimensional pitch and roll moments coefficients can also be derived as:

$$\begin{aligned}
 C_{L_s} &= \frac{L_s}{\rho (\Omega R)^2 \pi R^3} \\
 &= \frac{1}{2} \frac{\lambda_\beta^2 - 1}{\gamma} \sigma_s C_{l_\alpha} (\eta_{s1} - \beta_{s1}) \\
 C_{M_s} &= \frac{M_s}{\rho (\Omega R)^2 \pi R^3} \\
 &= \frac{1}{2} \frac{\lambda_\beta^2 - 1}{\gamma} \sigma_s C_{l_\alpha} (\eta_{c1} - \beta_{c1})
 \end{aligned} \tag{A.18}$$

where λ_β is the flapping natural frequency ratio and γ is the blade Lock number. They are defined as:

$$\begin{aligned}
 \lambda_\beta^2 &= 1 + \frac{K_\beta}{I_\beta \Omega^2} \\
 \gamma &= \frac{\rho c C_{L_\alpha} R^4}{I_\beta}
 \end{aligned} \tag{A.19}$$

A.2 Forced Flapping Motion

For a rotor in hovering, the flapping blade equation of motion is [10]:

$$I_\beta \ddot{\beta} + I_\beta \Omega^2 \beta = M_{flap} \tag{A.20}$$

For conventional helicopters, the flapping moment on one blade (M_{flap}) contains only the aerodynamic moment (the gravity of blade is neglected). In the case of the Ornicopter, an additional forced flapping moment is applied. Therefore, the flapping moment is:

$$M_{flap} = M_{aero} + M_{ff} \tag{A.21}$$

Using Eq. A.4, the aerodynamic flapping moment M_{aero} can be derived as:

$$\begin{aligned}
 M_{aero} &= \int_0^R dL r_e \\
 &= \frac{1}{2} \rho C_{L_\alpha} c \Omega^2 R^4 \left(\frac{\theta}{4} - \frac{\dot{\beta}}{4\Omega} - \frac{v_i}{3\Omega R} \right) \\
 &= \frac{1}{2} \gamma I_\beta \Omega^2 \left(\frac{\theta}{4} - \frac{\beta'}{4} - \frac{\lambda_i}{3} \right)
 \end{aligned} \tag{A.22}$$

where

$$\begin{aligned}
 \beta' &= \frac{d\beta}{d\psi} \\
 &= \beta_{s1} \cos \psi - \beta_{c1} \sin \psi \\
 &= \frac{\dot{\beta}}{\Omega}
 \end{aligned} \tag{A.23}$$

Substituting the flapping moment into the flapping equation of motion gives:

$$\beta_0 = \frac{1}{2}\gamma \left(\frac{\theta}{4} - \frac{\beta'}{4} - \frac{\lambda_i}{3} \right) + (\eta - \beta)(\lambda_\beta^2 - 1) \quad (\text{A.24})$$

A

Expanding Eq. A.24 and collecting terms for the constant and first harmonic coefficients (which should be zero), three equations can be derived for the three flapping coefficients (β_0 , β_{s1} and β_{c1}):

$$\begin{aligned} -\beta_0 + \frac{1}{8}\gamma\theta_0 - \frac{1}{6}\lambda_i - \beta_0(\lambda_\beta^2 - 1) &= 0 \\ \frac{1}{8}\gamma\theta_{s1} + \frac{1}{8}\gamma\beta_{c1} + (\eta_{s1} - \beta_{s1})(\lambda_\beta^2 - 1) &= 0 \\ \frac{1}{8}\gamma\theta_{c1} - \frac{1}{8}\gamma\beta_{s1} + (\eta_{c1} - \beta_{c1})(\lambda_\beta^2 - 1) &= 0 \end{aligned} \quad (\text{A.25})$$

The flapping equations of motion (A.25) can also be written in matrix form as:

$$\mathbf{A} \times \vec{\beta} = \mathbf{b} \quad (\text{A.26})$$

where:

$$\vec{\beta} = [\beta_0, \beta_{s1}, \beta_{c1}]^\top \quad (\text{A.27})$$

$$\mathbf{A} = \begin{bmatrix} \lambda_\beta^2 & 0 & 0 \\ 0 & \lambda_\beta^2 - 1 & -\frac{1}{8}\gamma \\ 0 & \frac{1}{8}\gamma & \lambda_\beta^2 - 1 \end{bmatrix} \quad (\text{A.28})$$

$$\begin{aligned} \mathbf{b} &= \begin{bmatrix} \left(\frac{\theta_0}{8} - \frac{\lambda_i}{6} \right) \gamma \\ \frac{\theta_{s1}}{8}\gamma + \left(\lambda_\beta^2 - 1 \right) \eta_{s1} \\ \frac{\theta_{c1}}{8}\gamma + \left(\lambda_\beta^2 - 1 \right) \eta_{c1} \end{bmatrix} \\ &= \begin{bmatrix} \theta_0 - \frac{4\lambda_i}{3} \\ \theta_{s1} \\ \theta_{c1} \end{bmatrix} \frac{\gamma}{8} + \begin{bmatrix} 0 \\ \eta_{s1} \\ \eta_{c1} \end{bmatrix} (\lambda_\beta^2 - 1) \end{aligned} \quad (\text{A.29})$$

$$= \frac{\gamma}{8} \vec{\theta} + (\lambda_\beta^2 - 1) \vec{\eta}$$

$$\vec{\theta} = \left[\theta_0 - \frac{4\lambda_i}{3}, \theta_{s1}, \theta_{c1} \right]^\top \quad (\text{A.30})$$

$$\vec{\eta} = [0, \eta_{s1}, \eta_{c1}]^\top \quad (\text{A.31})$$

The blade flapping motion can be calculated as:

$$\begin{aligned} \vec{\beta} &= \mathbf{A}^{-1} \times \mathbf{b} \\ &= \frac{\gamma}{8} \mathbf{A}^{-1} \times \vec{\theta} + (\lambda_\beta^2 - 1) \mathbf{A}^{-1} \times \vec{\eta} \\ &= \vec{\beta}_\theta + \vec{\beta}_{ff} \end{aligned} \quad (\text{A.32})$$

where $\vec{\beta}_\theta$ is the flapping angle caused by the pitch control input and the inflow, which is the same for both the Ornicopter and conventional helicopters, and $\vec{\beta}_{ff}$ is the flapping motion introduced by the forced flapping mechanism.

Substituting Eq. A.27 to A.31 into Eq. A.32, the flapping coefficients become:

$$\begin{aligned}\beta_0 &= c_1 + c_2\theta_0 \\ \beta_{s1} &= c_5\theta_{s1} + c_3\theta_{c1} + c_4\eta_{s1} + c_5\eta_{c1} \\ \beta_{c1} &= -c_3\theta_{s1} + c_5\theta_{c1} - c_5\eta_{s1} + c_4\eta_{c1}\end{aligned}\tag{A.33}$$

where:

$$\begin{aligned}c_1 &= -\frac{\gamma}{2\lambda_\beta^2} \frac{\lambda_i}{3} \\ c_2 &= \frac{\gamma}{8\lambda_\beta^2} \\ c_3 &= \frac{\gamma^2}{64(\lambda_\beta^2 - 1)^2 + \gamma^2} \\ c_4 &= \frac{64(\lambda_\beta^2 - 1)^2}{64(\lambda_\beta^2 - 1)^2 + \gamma^2} \\ c_5 &= \frac{8(\lambda_\beta^2 - 1)\gamma}{64(\lambda_\beta^2 - 1)^2 + \gamma^2}\end{aligned}\tag{A.34}$$

The average flapping motion of all the Ornicopter’s blades are then:

$$\begin{aligned}\vec{\beta}_{ave} &= \frac{1}{N_b} \sum_{k=1}^{N_b} (\vec{\beta}_\theta^{(k)} + \vec{\beta}_{ff}^{(k)}) \\ &= \vec{\beta}_\theta + \frac{1}{N_b} \sum_{k=1}^{N_b} \vec{\beta}_{ff}^{(k)} \\ &= \vec{\beta}_\theta + \frac{1}{N_b} (\lambda_\beta^2 - 1) \mathbf{A}^{-1} \times \left[0, \sum_{k=1}^{N_b} \eta_{s1}^{(k)}, \sum_{k=1}^{N_b} \eta_{c1}^{(k)} \right]^T \\ &= \vec{\beta}_\theta + (\lambda_\beta^2 - 1) \mathbf{A}^{-1} \times [0, \bar{\eta}_{s1}, \bar{\eta}_{c1}]^T\end{aligned}\tag{A.35}$$

A.3 The Total Hub Forces and Moments

Substituting the flapping coefficients (Eq. A.33) into the hub forces and moments for a single blade (Eq. A.8, A.11 to A.13 and A.18) results in the total hub forces and moments on a hovering Ornicopter rotor.

As the thrust (thrust coefficient) is not affected by the active flapping and cyclic pitch controls, the total Ornicopter rotor thrust coefficient will be the same as that of conventional helicopters, i.e.:

A

$$\begin{aligned}
 C_T &= \sum_{k=1}^{N_b} C_{T_s}^{(k)} \\
 &= N_b C_{T_s} \\
 &= \frac{1}{2} N_b \sigma_s C_{l_\alpha} \left(\frac{\theta_0}{3} - \frac{\lambda_i}{2} \right) \\
 &= \frac{1}{2} \sigma C_{l_\alpha} \left(\frac{\theta_0}{3} - \frac{\lambda_i}{2} \right)
 \end{aligned} \tag{A.36}$$

The Ornicopter’s in-plane hub forces and moments will vary among each blade due to the different flapping motions of blades, i.e. η_{s1} and η_{c1} will vary on each blade, while the collective and cyclic pitch control will be the same for all the blades. In this sense, the hub forces and moments generated by the different blades should be calculated separately and summed up for the total rotor hub forces and moments.

Substituting Eq. A.33 into the horizontal force coefficient (Eq. A.11) results in:

$$C_{H_s} = \frac{1}{2} \sigma_s C_{l_\alpha} (c_{11} \theta_{s1} + c_{12} \theta_{c1} + c_{13} \eta_{s1} + c_{14} \eta_{c1}) \tag{A.37}$$

where:

$$\begin{aligned}
 \alpha_{ef} &= \frac{\theta_0}{3} - \frac{\lambda_i}{2} \\
 c_{11} &= -\frac{1}{6} c_1 c_5 - \frac{1}{6} c_2 c_5 \theta_0 - \left(\alpha_{ef} - \frac{1}{4} \lambda_i \right) c_3 - \frac{1}{4} \lambda_i \\
 c_{12} &= \frac{1}{6} (1 - c_3) (c_1 + c_2 \theta_0) + \left(\alpha_{ef} - \frac{1}{4} \lambda_i \right) c_5 \\
 c_{13} &= -\frac{1}{6} c_4 (c_1 + c_2 \theta_0) - \left(\alpha_{ef} - \frac{1}{4} \lambda_i \right) c_5 \\
 c_{14} &= -\frac{1}{6} c_5 (c_1 + c_2 \theta_0) + \left(\alpha_{ef} - \frac{1}{4} \lambda_i \right) c_4
 \end{aligned} \tag{A.38}$$

A.3 The Total Hub Forces and Moments

175

Then the Ornicopter’s rotor horizontal force can be derived as:

$$\begin{aligned}
 C_H &= \sum_{k=1}^{N_b} C_{H_s}^{(k)} \\
 &= \frac{1}{2} \sigma_s C_{l_\alpha} \sum_{k=1}^{N_b} (c_{11} \theta_{s1} + c_{12} \theta_{c1} + c_{13} \eta_{s1} + c_{14} \eta_{c1}) \\
 &= \frac{1}{2} \sigma_s C_{l_\alpha} \left(c_{11} \theta_{s1} N_b + c_{12} \theta_{c1} N_b + c_{13} \sum_{k=1}^{N_b} \eta_{s1}^{(k)} + c_{14} \sum_{k=1}^{N_b} \eta_{c1}^{(k)} \right) \\
 &= \frac{1}{2} \sigma_s C_{l_\alpha} (c_{11} \theta_{s1} N_b + c_{12} \theta_{c1} N_b + c_{13} N_b \bar{\eta}_{s1} + c_{14} N_b \bar{\eta}_{c1}) \\
 &= \frac{1}{2} \sigma C_{l_\alpha} (c_{11} \theta_{s1} + c_{12} \theta_{c1} + c_{13} \bar{\eta}_{s1} + c_{14} \bar{\eta}_{c1})
 \end{aligned} \tag{A.39}$$

As mentioned before (see Section 2.4.4), to avoid the effect of forced flapping motion on the average tip-path plane of the rotor, the average forced flapping coefficient ($\bar{\eta}_{s1}$, $\bar{\eta}_{c1}$) should be zero. In this sense, the horizontal force generated by the Ornicopter rotor will not be affected by the active flapping, and the rotor horizontal force coefficient will be a function of cyclic pitch control, i.e.:

$$C_H = \frac{1}{2} \sigma C_{l_\alpha} (c_{11} \theta_{s1} + c_{12} \theta_{c1}) \tag{A.40}$$

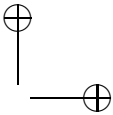
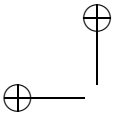
Similarly, the rotor side hub force (C_S), the pitch and roll hub moments (C_M and C_L) and the shaft torque (C_Q) can be derived as:

$$\begin{aligned}
 C_S &= \frac{1}{2} \sigma C_{l_\alpha} (-c_{12} \theta_{s1} + c_{11} \theta_{c1} - c_{14} \bar{\eta}_{s1} + c_{13} \bar{\eta}_{c1}) \\
 &= \frac{1}{2} \sigma C_{l_\alpha} (-c_{12} \theta_{s1} + c_{11} \theta_{c1})
 \end{aligned} \tag{A.41}$$

$$\begin{aligned}
 C_L &= \frac{1}{2} \frac{\lambda_\beta^2 - 1}{\gamma} \sigma C_{l_\alpha} (\bar{\eta}_{s1} - c_5 \theta_{s1} - c_3 \theta_{c1} - c_4 \bar{\eta}_{s1} - c_5 \bar{\eta}_{c1}) \\
 &= -\frac{1}{2} \frac{\lambda_\beta^2 - 1}{\gamma} \sigma C_{l_\alpha} (c_5 \theta_{s1} + c_3 \theta_{c1})
 \end{aligned} \tag{A.42}$$

$$\begin{aligned}
 C_M &= \frac{1}{2} \frac{\lambda_\beta^2 - 1}{\gamma} \sigma C_{l_\alpha} (\bar{\eta}_{c1} + c_3 \theta_{s1} - c_5 \theta_{c1} + c_5 \bar{\eta}_{s1} - c_4 \bar{\eta}_{c1}) \\
 &= -\frac{1}{2} \frac{\lambda_\beta^2 - 1}{\gamma} \sigma C_{l_\alpha} (-c_3 \theta_{s1} + c_5 \theta_{c1})
 \end{aligned} \tag{A.43}$$

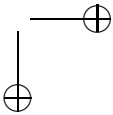
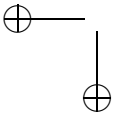
$$\begin{aligned}
 C_Q &= C_T \lambda_i + C_{Q0} - \frac{1}{16} \sigma C_{l_\alpha} ((c_{15} \theta_{s1} + c_{16} \theta_{c1}) \bar{\eta}_{s1} \\
 &\quad + (-c_{16} \theta_{s1} + c_{15} \theta_{c1}) \bar{\eta}_{c1} + c_{17} \hat{\eta}) \\
 &= C_T \lambda_i + C_{Q0} - \frac{1}{16} \sigma C_{l_\alpha} c_{17} \hat{\eta}^2
 \end{aligned} \tag{A.44}$$



where:

$$\begin{aligned} c_{15} &= 2c_3c_5 + 2c_4c_5 - c_5 \\ c_{16} &= 2c_3c_4 - 2c_5^2 - c_4 \\ c_{17} &= c_4^2 + c_5^2 \end{aligned} \tag{A.45}$$

A



B

Bo-105 Data

B.1 Bo-105 Design Data

Bo-105 data according to Ref [10].

Table B.1: Bo-105 data

Notation	Description	Value	Unit
R	Radius of the main rotor	4.91	m
c	Blade chord	0.27	m
N_b	Number of blades	4	
σ	Main rotor solidity	0.07	
θ_{tw}	Blade twist	-0.14	rad
k_r	Radius location of the first aerodynamic section on the blade (nondimensional)	0.224	
k_l	Tip loss factor	0.97	
e_f	Nondimensional flapping hinge offset	0.02	
I_β	Flapping moment of inertia	142	$kg \cdot m^2$
M_β	First moment of mass of blade	51.1	$kg \cdot m$
K_β	Flapping stiffness	94025	Nm/rad

Continued on next page

B

Table B.1 – continued from previous page

Notation	Description	Value	Unit
γ	Lock number of blade	8.47	
λ_β	Flapping natural frequency ratio	1.112	
Ω	Rotation speed of the main rotor	44.4	rad/s
C_{l_α}	Airfoil lift coefficient slope	6.24	rad^{-1}
C_{d0}	Airfoil drag coefficient	0.0103	
C_{d2}	Airfoil drag coefficient	0.147	rad^{-2}
α_{sh}	Main rotor shaft tilt angle	-0.0524	rad
x_{mr}	Main rotor position in the body reference	-0.03	m
y_{mr}		0	
z_{mr}		-1.48	
$k_{\theta 1}$	Pitch flap angle coupling	0	
$k_{\theta 2}$	Pitch flap rate coupling	0	
F_0	Equivalent drag area of the fuselage	1.3	m^2
M_a	Mass of the helicopter	2200	kg
I_x	Moments of inertia of the helicopter about the x-, y- and z-axes	1433	$kg \cdot m^2$
I_y		4973	
I_z		4099	
I_{xz}	Product of inertia of the helicopter about the x- and z-axes	660	$kg \cdot m^2$
$C_{l_\alpha}^{hs}$	Lift coefficient slope of the horizontal stabilizer	3.16	rad^{-1}
α_0^{hs}	Incidence angle of the horizontal stabilizer	0.0698	rad
S_{hs}	Size of the horizontal stabilizer	0.8	m^2
x_{hs}	Horizontal stabilizer position in the body reference	-4.59	m
y_{hs}		0	
z_{hs}		-0.6	
$C_{l_\alpha}^{vs}$	Lift coefficient slope of the vertical fin	2.29	rad^{-1}
x_{vs}	Vertical fin position in the body reference	-5.45	m
y_{vs}		0	
z_{vs}		-0.6	

Continued on next page

Table B.1 – continued from previous page

Notation	Description	Value	Unit
β_0^{vs}	Incidence angle of the vertical fin	0.08816	rad
S_{vs}	Size of the vertical fin	0.8	m^2
R_{tr}	Radius of the tail rotor	0.95	m
c_{tr}	Tail rotor blade chord	0.179	m
N_b^{tr}	Number of blades of the tail rotor	2	
$k_{r_{tr}}$	Tail rotor nondimensional root cut	0.2	
Ω_{tr}	Rotation speed of the tail rotor	233	rad/s
$C_{l_\alpha}^{tr}$	Airfoil lift coefficient slope of the tail rotor	6.16	rad^{-1}
C_{d0}^{tr}	Airfoil drag coefficient of the tail rotor	0.0069	
C_{d2}^{tr}	Airfoil drag coefficient of the tail rotor	0.2062	rad^{-2}
x_{tr}	Tail rotor position in the body reference	-6.03	m
y_{tr}		-0.32	
z_{tr}		-1.72	

B

B.2 Flight Test Data

The flight tests were conducted in 1987 using the DLR research helicopter Bo-105 S123 for system identification and simulation validation purposes. The initial trimmed condition for flight tests was a steady level flight at 80 knots and at a density altitude of 3000 feet standard atmosphere. The flight tests consist of:

1. Positive and negative doublet inputs for each of the four controls (Tests No. 1 to 8)
2. Positive and negative modified 3-2-1-1 inputs for each of the four controls (Tests No. 9 to 16)
3. Pilot generated frequency sweeps for each of the four controls (Tests No. 17 to 20)

Among these tests, four tests applying 3-2-1-1 input are chosen for the model validation, as shown in Fig. 3.5 and Figs. B.1 to B.3.

B

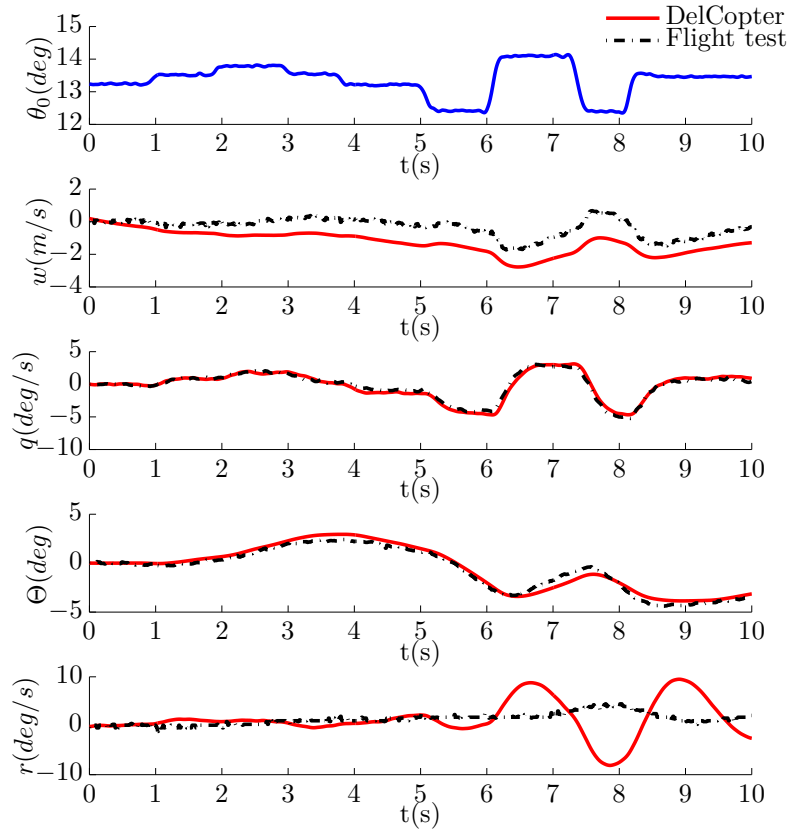


Figure B.1: Flight test No. 11: positive lateral 3-2-1-1 input

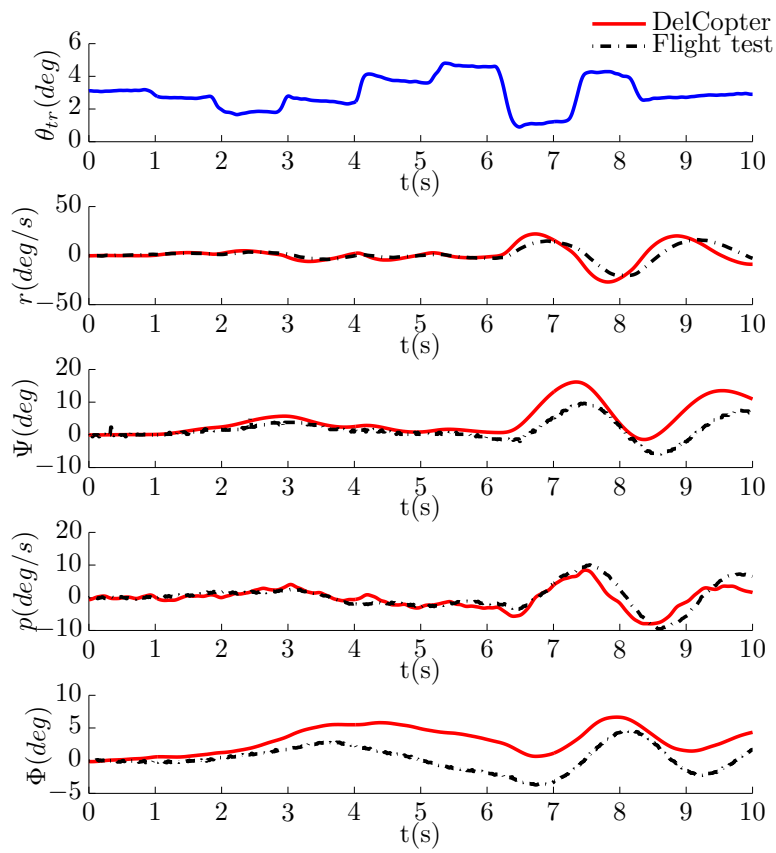


Figure B.2: Flight test No. 13: positive collective 3-2-1-1 input

B

B

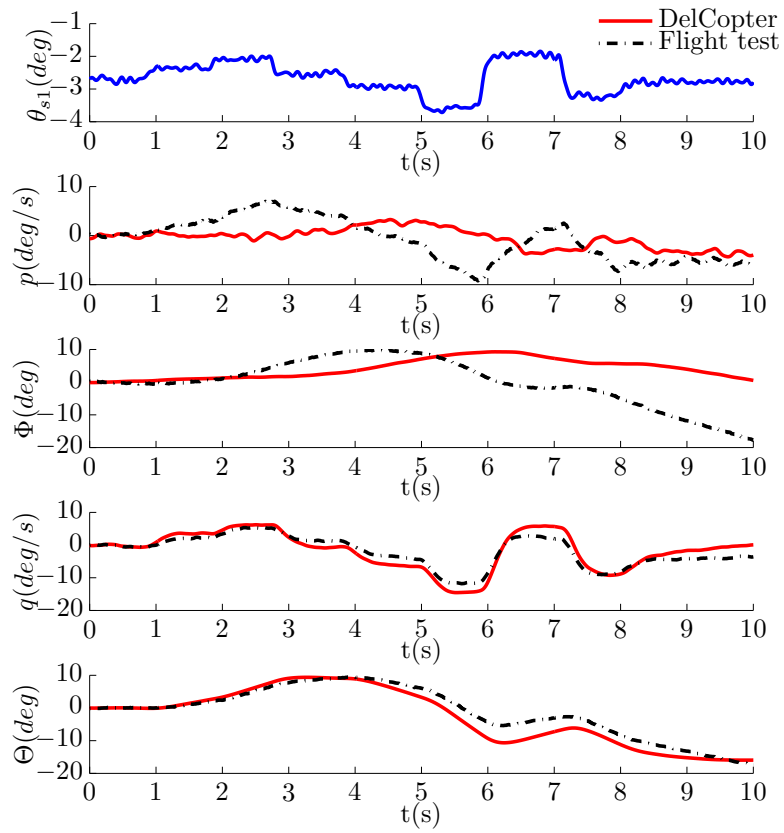


Figure B.3: Flight test No. 15: positive pedal 3-2-1-1 input

C

An Ordering Scheme for Model Simplification

While developing the conventional helicopter flight mechanics model, the question was raised of how to simplify the model while keeping it as accurate as possible. Some assumptions and simplifications have been applied to the model, such as the small angle assumption for the blade flapping angle. However, analytical expressions in the flight mechanics model were still complex and needed to be simplified without harming the accuracy.

In this dissertation, the symbolic algebra software *Maple* is used for the flight mechanics model development. *Maple* is capable of handling extremely long expressions (i.e. a polynomial having more than 10^5 terms can be processed using *Maple* on a regular personal computer). However, to extend the flight mechanics model to such complexity is not always beneficial as this will increase the computational cost dramatically and the improvements might be limited.

To balance the complexity and accuracy of the model, a simplification scheme was developed based on an ordering scheme of all variables involved in the model. It is applied to the developments of the DelCopter and Ornicopter flight mechanics model in this thesis.

C.1 Simplification Method

The basic principle of the simplification scheme is to determine the order of all the terms in the polynomial expressions (such as Eq. D.11 and D.12) and neglect the small terms.

To do so, the O notation is defined first. One can say that:

$$y(\mathbf{X}) = O(\epsilon^n), \quad 0 < \epsilon < 1 \quad (\text{C.1})$$

if and only if there exists a positive number δ that:

$$|y(\mathbf{X})| \leq \epsilon^n \quad \text{while} \quad |\mathbf{X} - \mathbf{X}_0| < \delta \quad (\text{C.2})$$

When the condition (C.2) is satisfied, one can say that the $y(\mathbf{X})$ is in the order of n (with the basis ϵ).

In the case of the flight mechanics model, y can be any variable in the model. \mathbf{X} is the flight condition and \mathbf{X}_0 is the trimmed condition. For the model variables, their ranges correspond to the trimmed states. For example, the amplitude of forced flapping motion of the Ornicopter blade has been proven to be modest (see Eq. 2.34). One can obtain:

$$\begin{aligned} \beta &\leq 0.2 \\ &< 0.5^2 \\ &= O(\epsilon^2) \quad (\epsilon = 0.5) \end{aligned} \quad (\text{C.3})$$

As the basis ϵ is less than 1, the higher the order is, the smaller the variable will be. In this sense, some higher order terms in a polynomial can be neglected. It should be noticed that the order of the variable also depends on the choice of ϵ . In this thesis, 0.5 is used for model simplification. The orders of the different model variables are shown in Tab. C.1.

Table C.1: Ordering scheme

Variable		Min	Max	Order
Normalized helicopter transitional velocities	μ_x	-0.1	0.4	$O(\epsilon)$
	μ_y	-0.1	0.1	$O(\epsilon^3)$
	μ_z	-0.1	0.1	$O(\epsilon^3)$
Normalized helicopter rotational velocities	\bar{p}	-0.02	0.02	$O(\epsilon^5)$
	\bar{q}	-0.02	0.02	$O(\epsilon^5)$
	\bar{r}	-0.02	0.02	$O(\epsilon^5)$
Inflow ratio	λ_0	0.01	0.06	$O(\epsilon^4)$
	λ_{s1}	-0.02	0.02	$O(\epsilon^5)$
	λ_{c1}	-0.02	0.03	$O(\epsilon^5)$
Blade flapping angle	β	-0.25	0.35	$O(\epsilon)$
Blade coning, lateral and longitudinal flapping angles	β_0	0	0.1	$O(\epsilon^3)$
	β_{s1}	-0.25	0.25	$O(\epsilon^2)$
	β_{c1}	-0.25	0.25	$O(\epsilon^2)$

Continued on next page

Table C.1 – continued from previous page

Variable		Min	Max	Order
Collective, longitudinal and lateral cyclic control	θ_0	0	0.25	$O(\epsilon^2)$
	θ_{s1}	-0.2	0.2	$O(\epsilon^2)$
	θ_{c1}	-0.2	0.2	$O(\epsilon^2)$
Normalized air foil drag coefficients	\bar{C}_{d0}	0.001	0.0025	$O(\epsilon^8)$
	\bar{C}_{d2}	0.02	0.03	$O(\epsilon^5)$
Flap hinge offset	e_f	0	0.1	$O(\epsilon^3)$
Pitch flap coupling coefficients	$k_{\theta 1}$	-0.4	0.4	$O(\epsilon)$
	$k_{\theta 2}$	-0.4	0.4	$O(\epsilon)$
Blade root cut ratio	r_c	0	0.2	$O(\epsilon^2)$
Tip loss factor	k_l	0.95	1	$O(\epsilon^0)$
Blade twist angle	θ_{tw}	-0.2	0	$O(\epsilon^2)$

When the order of each variable is known, the order of the different terms in a polynomial expression can be calculated. For a general term, its order can be derived as (assuming that the basis ϵ is consistent):

$$\begin{aligned}
 Y(\mathbf{X}) &= \prod y_i^{p_i} \\
 &\leq \prod (\epsilon^{n_i})^{p_i} \\
 &\leq \epsilon^{\sum n_i p_i} \\
 &= O(\epsilon^{\sum n_i p_i})
 \end{aligned} \tag{C.4}$$

For example, based on Tab. C.1, one can get:

$$\begin{aligned}
 \frac{1}{2}\beta_0^2\mu_z &= O(\epsilon)O(\epsilon^{3\cdot 2})O(\epsilon) \\
 &= O(\epsilon^8)
 \end{aligned} \tag{C.5}$$

Applying the above calculation to all the flight mechanics model terms, one can obtain the distribution of orders in the range between the minimum (largest terms) and maximum order (smallest terms). Based on this, one can decide up to which order the terms should be kept in the flight model model. In general, with $\epsilon = 0.5$, terms which are 5 orders higher than the minimum order are very small compared with the largest ones (less than 4%), and they are negligible.

It should also be mentioned than the number of orders that should be kept in a model is not fixed. This will depend on the acceptable computation cost and the desired model accuracy.

C.2 Demonstration

To demonstrate the method, one example is used, which is the perpendicular velocity (v_p) on the blade element, see Eq. D.11.

Substituting the blades flapping motion (Eq. 3.2) into Eq. D.11, the non-dimensional perpendicular velocity can be derived as:

$$\begin{aligned}
 \bar{v}_p = & \frac{1}{2}\beta_0^2\mu_z - \frac{1}{2}\beta_0\beta_{c1}\lambda_{c1}\bar{r}_e - \mu_z - \frac{1}{2}\beta_{s1}\mu_y - \frac{1}{4}\lambda_0\beta_{c1}^2 \\
 & + \lambda_0 + \frac{1}{4}\beta_{s1}^2\mu_z - \frac{1}{4}\lambda_0\beta_{s1}^2 + \frac{1}{4}\beta_{c1}^2\mu_z + \frac{1}{2}\beta_{c1}\mu_x - \frac{1}{2}\lambda_0\beta_0^2 \\
 & + \left(-\bar{p}\bar{r}_e + \beta_0\beta_{s1}\mu_z - \frac{1}{4}\beta_{s1}\beta_{c1}\lambda_{c1}\bar{r}_e + e_f\beta_{c1} - \beta_{c1}\bar{r}_e - \beta_0\mu_y - \lambda_0\beta_0\beta_{s1} + \lambda_{s1}\bar{r}_e \right) \sin(\psi) \\
 & + \left(\beta_{s1}\bar{r}_e + \lambda_{c1}\bar{r}_e - \frac{1}{8}\beta_{s1}^2\lambda_{c1}\bar{r}_e - \lambda_0\beta_0\beta_{c1} + \beta_0\beta_{c1}\mu_z - \frac{3}{8}\beta_{c1}^2\lambda_{c1}\bar{r}_e - e_f\beta_{s1} + \beta_0\mu_x \right. \\
 & \quad \left. - \frac{1}{2}\beta_0^2\lambda_{c1}\bar{r}_e - \bar{q}\bar{r}_e \right) \cos(\psi) \\
 & + \left(-\frac{1}{2}\beta_{c1}\mu_y + \frac{1}{2}\beta_{s1}\mu_x + \frac{1}{2}\beta_{s1}\beta_{c1}\mu_z - \frac{1}{2}\beta_0\beta_{s1}\lambda_{c1}\bar{r}_e - \frac{1}{2}\lambda_0\beta_{s1}\beta_{c1} \right) \sin(2\psi) \\
 & + \left(\frac{1}{4}\lambda_0\beta_{s1}^2 + \frac{1}{4}\beta_{c1}^2\mu_z + \frac{1}{2}\beta_{c1}\mu_x - \frac{1}{4}\beta_{s1}^2\mu_z + \frac{1}{2}\beta_{s1}\mu_y - \frac{1}{4}\lambda_0\beta_{c1}^2 \right. \\
 & \quad \left. - \frac{1}{2}\beta_0\beta_{c1}\lambda_{c1}\bar{r}_e \right) \cos(2\psi) \\
 & - \frac{1}{4}\beta_{s1}\beta_{c1}\lambda_{c1}\bar{r}_e \sin(3\psi) + \left(-\frac{1}{8}\beta_{c1}^2\lambda_{c1}\bar{r}_e + \frac{1}{8}\beta_{s1}^2\lambda_{c1}\bar{r}_e \right) \cos(3\psi)
 \end{aligned} \tag{C.6}$$

One can see from Eq. C.6 that it consists of 24 terms, among which the lowest order is 2 and the highest order is 10.

To investigate the impacts of simplification up to different orders, 7 simplified expressions are extracted from the complete v_p expression, as shown in Tab. C.2. For example, the expression including the lowest 4 orders (from the order of 2 to 5) will consist of 16 terms, and other 8 terms in higher orders will be neglected. All simplified expressions are compared with the full expression in a coordinated turning condition (flight velocity 80 knots, load factor 1.5).

Since the v_p is a function of the azimuth angle ψ and the blade element radius position r_e , the root-mean-square error (RMSE) during one revolution at $0.7R$ radius position is calculated to show the impacts of simplification on model accuracy. In order to investigate the impacts of model simplification on computational cost, the calculation time of each expression (normalized by the calculation time of the full expression) is also shown in Tab. C.2.

Table C.2: Results of simplifications with different highest orders

Order	Terms in this order	Terms kept	RMSE (m/s)	Calculation time (%)
2	2	2	5.23	9.037
3	3	5	4.38	22.93
4	2	7	1.63	27.42
5	9	16	1.28×10^{-2}	67.50
6	1	17	1.25×10^{-3}	72.98
7	1	18	1.23×10^{-3}	81.97
8	5	23	3.72×10^{-4}	99.95
9	0	23	3.72×10^{-4}	99.95
10	1	24	0.00	100.0

C

One can see that increasing the highest order kept after simplification results in an increase of model accuracy, as well as the computational cost. The simplification error (in logarithmic scale) is approximately linear with regard to the computational cost, as shown in Fig. C.1. It indicates that, for the same amount of accuracy improvement, the additional calculation cost to be needed will increase dramatically as the model fidelity increases.

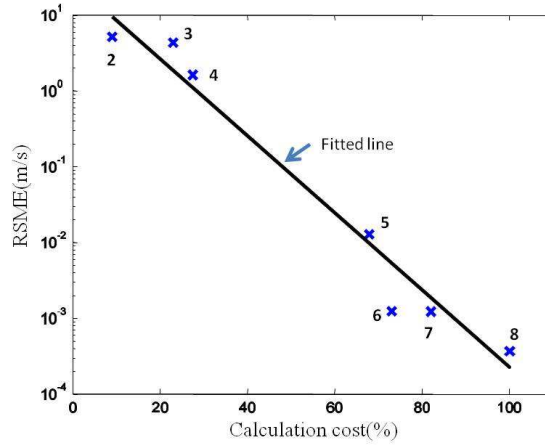


Figure C.1: RMSE as a function of calculation time

Based on the accuracy and calculation cost, the expression consists of the lowest 4 orders can be chosen as the required final result of the simplification, as shown in Eq. C.7.

It should be mentioned that the simplification performed in this appendix is only a demonstration of the simplification method. During the model development, the model was not simplified during the intermediate steps. This simplification scheme was applied only to the final output, such as the rotor hub forces (T , H , S), in order to minimize the error introduced by the simplification. The terms in the lowest 7 orders are kept during the model simplification.

$$\begin{aligned}
 \bar{v}_p = & \frac{1}{2}\beta_0^2\mu_z + \lambda_0 - \mu_z + \frac{1}{4}\beta_{c1}^2\mu_z + \frac{1}{4}\beta_{s1}^2\mu_z + \frac{1}{2}\beta_{c1}\mu_x - \frac{1}{2}\beta_{s1}\mu_y \\
 & + (e_f\beta_{c1} + \beta_0\beta_{s1}\mu_z - \beta_0\mu_y + \lambda_{s1}\bar{r}_e - \bar{p}\bar{r}_e - \beta_{c1}\bar{r}_e)\sin(\psi) \\
 & + (\beta_0\beta_{c1}\mu_z + \beta_0\mu_x - e_f\beta_{s1} + \beta_{s1}\bar{r}_e + \lambda_{c1}\bar{r}_e - \bar{q}\bar{r}_e)\cos(\psi) \\
 & + \left(-\frac{1}{2}\beta_{c1}\mu_y + \frac{1}{2}\beta_{s1}\beta_{c1}\mu_z + \frac{1}{2}\beta_{s1}\mu_x\right)\sin(2\psi) \\
 & + \left(-\frac{1}{4}\beta_{s1}^2\mu_z + \frac{1}{4}\beta_{c1}^2\mu_z + \frac{1}{2}\beta_{s1}\mu_y + \frac{1}{2}\beta_{c1}\mu_x\right)\cos(2\psi)
 \end{aligned} \tag{C.7}$$

D

Development of the Generic Flight Mechanics Model

In this appendix, different components of the generic flight mechanics model will be developed. They are used to form the helicopter system EoM as discussed in Chapter 3.

D.1 Generic Model Components

D.1.1 The Main Rotor Model

In this thesis, the main rotor blade is considered as an offset hinged blade with a spring, as shown in Fig. D.1. While the blade is flapping, a moment will be generated by the spring as:

$$M_k(\psi) = -K_\beta \beta(\psi) \quad (D.1)$$

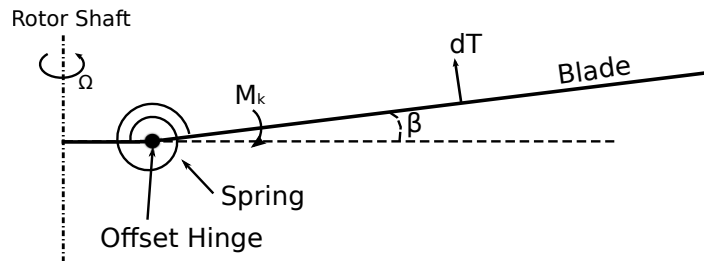


Figure D.1: Blade hinge configuration

Forces and Moments

The location of the blade element in the flapping reference can be expressed as:

$$\{\mathbf{r}_e\}_{\{\beta\}} = \left\{ [r_e - R_{ef} (1 - \cos \beta), 0, R_{ef} \sin \beta]^\top \right\}_{\{\beta\}} \quad (\text{D.2})$$

Considering the flapping angle and hinge offset are relatively small, the equation above can be simplified as:

$$\{\mathbf{r}_e\}_{\{\beta\}} \approx \left\{ [r_e, 0, 0]^\top \right\}_{\{\beta\}} \quad (\text{D.3})$$

Transforming the coordinates into the non-rotating and rotating reference results in:

$$\begin{aligned} \{\mathbf{r}_e\}_{\{r\}} &= \mathbf{T}_{r2\beta}^{-1} \{\mathbf{r}_e\}_{\{\beta\}} \\ &= r_e \left\{ \begin{bmatrix} \cos(\beta) \\ 0 \\ -\sin(\beta) \end{bmatrix} \right\}_{\{r\}} \end{aligned} \quad (\text{D.4})$$

$$\begin{aligned} \{\mathbf{r}_e\}_{\{nr\}} &= \mathbf{T}_{nr2r}^{-1} \{\mathbf{r}_e\}_{\{r\}} \\ &= r_e \left\{ \begin{bmatrix} -\cos(\psi) \cos(\beta) \\ \sin(\psi) \cos(\beta) \\ -\sin(\beta) \end{bmatrix} \right\}_{\{nr\}} \end{aligned} \quad (\text{D.5})$$

The relative air flow velocity at the blade element consists of contributions from four parts: the motion of the rotor hub (u, v, w, p, q, r), the rotation of the blade among the rotor shaft (Ω), the flapping motion of the blade ($\dot{\beta}$) and the inflow (v_i), as:

$$\{\mathbf{V}_{air}\}_{\{\beta\}} = - \left(\{\mathbf{V}_m\}_{\{\beta\}} + \{\mathbf{V}_\Omega\}_{\{\beta\}} + \{\mathbf{V}_{flap}\}_{\{\beta\}} \right) + \{\mathbf{V}_\lambda\}_{\{\beta\}} \quad (\text{D.6})$$

The $\{\mathbf{V}_m\}_{\{\beta\}}$ is caused by the motion of the rotor hub, which is affected by both the translation and rotation of the hub. It can be calculated in the non-rotating reference first and transformed into the flapping reference, as:

$$\begin{aligned} \{\mathbf{V}_m\}_{\{\beta\}} &= \mathbf{T}_{r2\beta} \mathbf{T}_{nr2r} \{\mathbf{V}_m\}_{\{nr\}} \\ &= \mathbf{T}_{r2\beta} \mathbf{T}_{nr2r} \left(\{\mathbf{V}_{hub}\}_{\{nr\}} + \{\vec{\omega}_{hub}\}_{\{nr\}} \times \{\mathbf{r}_e\}_{\{nr\}} \right) \end{aligned} \quad (\text{D.7})$$

where $\{\mathbf{V}_{hub}\}_{\{nr\}}$ is the translational velocity of the rotor hub ($\{\mathbf{V}_T\}_{\{nr\}} = \{[u, v, w]^\top\}_{\{nr\}}$) and $\{\vec{\omega}_{hub}\}_{\{nr\}}$ is the rotational velocity of the rotor ($\{\vec{\omega}_{hub}\}_{\{nr\}} = \{[p, q, r]^\top\}_{\{nr\}}$).

The $\{\mathbf{V}_\Omega\}_{\{\beta\}}$ is caused by the rotation of the blade (Ω), as:

$$\begin{aligned} \{\mathbf{V}_\Omega\}_{\{\beta\}} &= \mathbf{T}_{r2\beta} \{\mathbf{V}_\Omega\}_{\{r\}} \\ &= \mathbf{T}_{r2\beta} \left(\{\vec{\omega}_\Omega\}_{\{r\}} \times \{\mathbf{r}_e\}_{\{r\}} \right) \\ &= \mathbf{T}_{r2\beta} \left(\{[0, 0, \Omega]^\top\}_{\{r\}} \times \{\mathbf{r}_e\}_{\{r\}} \right) \end{aligned} \quad (\text{D.8})$$

D.1 Generic Model Components

191

The $\{\mathbf{V}_{flap}\}_{\{\beta\}}$ is the velocity introduced by the flapping motion of the blade, and the $\{\mathbf{V}_\lambda\}_{\{\beta\}}$ is the induced velocity at the blade element:

$$\begin{aligned}\{\mathbf{V}_{flap}\}_{\{\beta\}} &= \{[0, 0, \dot{\beta}(r_e - R_{ef})]^\top\}_{\{\beta\}} \\ \{\mathbf{V}_\lambda\}_{\{\beta\}} &= \{[0, 0, v_i]^\top\}_{\{\beta\}}\end{aligned}\tag{D.9}$$

where v_i is the induced velocity, and it has the form of:

$$v_i = v_{i0} + v_{is1} \frac{r_e}{R} \sin \psi + v_{ic1} \frac{r_e}{R} \cos \psi\tag{D.10}$$

Combining all parts of the local air flow velocity, the total velocity $\{\mathbf{V}_{air}\}_{\{\beta\}}$ can be derived. The effect of span-wise air flow is neglected in this thesis, and therefore only the components among the y- and the z-axes are used in the following model development. Using the small angle assumption, the velocity can be simplified and result in the perpendicular and tangent velocity as:

D

$$\begin{aligned}v_p &= u\beta \cos \psi - v\beta \sin \psi - w \left(1 - \frac{\beta^2}{2}\right) \\ &\quad - (p \sin \psi - q \cos \psi) r_e + \dot{\beta}(r_e - R_{ef}) \\ &\quad + v_{i0} + v_{is1} \frac{r_e}{R} \sin \psi + v_{ic1} \frac{r_e}{R} \cos \psi\end{aligned}\tag{D.11}$$

$$\begin{aligned}v_t &= u \sin \psi - v \cos \psi \\ &\quad + (p\beta \cos \psi - q\beta \sin \psi) r_e \\ &\quad + (\Omega - r) \left(1 - \frac{\beta^2}{2}\right) r_e\end{aligned}\tag{D.12}$$

With the local velocity derived above, the aerodynamic force generated by the blade element can be calculated using a 2-D static airfoil model. Assuming that the inflow angle is small, it can be calculated as:

$$\begin{aligned}\varphi &= \arctan \left(\frac{v_p}{v_t} \right) \\ &\approx \frac{v_p}{v_t}\end{aligned}\tag{D.13}$$

from which the blade element lift and drag forces can be derived:

$$\alpha = \theta - \varphi \quad (\text{D.14})$$

$$C_l = C_{l_\alpha} \alpha \quad (\text{D.15})$$

$$C_d = C_{d0} + C_{d2} \alpha^2 \quad (\text{D.16})$$

$$\begin{aligned} dL &= \frac{1}{2} \rho (v_p^2 + v_t^2) C_l c dr \\ &\approx \frac{1}{2} \rho v_t^2 C_l c dr \end{aligned} \quad (\text{D.17})$$

$$\begin{aligned} dD &= \frac{1}{2} \rho (v_p^2 + v_t^2) C_d c dr \\ &\approx \frac{1}{2} \rho v_t^2 C_d c dr \end{aligned} \quad (\text{D.18})$$

The pitch angle of the blade element (θ) can be classically expressed as:

D

$$\theta = \theta_0 + \theta_{s1} \sin \psi + \theta_{c1} \cos \psi + \theta_{tw} \frac{r_e}{R} \quad (\text{D.19})$$

where θ_0 , θ_{s1} and θ_{c1} are the collective, longitudinal and lateral cyclic controls respectively, and θ_{tw} is the twist angle of the blade. To analyse the impact of flapping-pitch coupling on the Ornicopter, two coupling terms are added to the model:

$$\theta = \theta_0 + \theta_{s1} \sin \psi + \theta_{c1} \cos \psi + \theta_{tw} \frac{r_e}{R} + k_{\theta 1} \beta + k_{\theta 2} \frac{\dot{\beta}}{\Omega} \quad (\text{D.20})$$

where $k_{\theta 1}$ is the pitch flap angle coupling coefficient and $k_{\theta 2}$ is the pitch flap rate coupling coefficient. The two coupling terms introduce the effects of flapping motion on the blade pitch angle. A positive $k_{\theta 1}$ indicates that the pitch angle of the blade will be increased when the blade is above the shaft plane, i.e. $\beta > 0$. Meanwhile, the $k_{\theta 2}$ is associated with the flapping rate of the blade ($\dot{\beta}$). A positive $k_{\theta 2}$ will increase the blade pitch angle while the blade is flapping upwards ($\dot{\beta} > 0$).

Substituting the velocities (Eqs. D.11 and D.12) and the pitch angle (Eq. D.20) into Eqs. D.17 and D.18 gives the expressions of lift (dL) and drag (dD) forces on the blade element.

The forces and moments in the flapping reference can be derived similarly as Eq. A.5 (see Fig. 2.15):

$$\begin{aligned} dF_x^\beta &= 0 \\ dF_y^\beta &\approx dD + dL \varphi \\ dF_z^\beta &\approx -dL \\ dM_x^\beta &= 0 \\ dM_y^\beta &= -dF_z^\beta r_e \\ dM_z^\beta &= dF_y^\beta r_e \end{aligned} \quad (\text{D.21})$$

D.1 Generic Model Components

193

Transforming these forces and moments into the non-rotating reference and applying the small angle assumption, one can get:

$$\begin{aligned} \{d\mathbf{F}\}_{\{nr\}} &= \mathbf{T}_{nr2r}^{-1} \mathbf{T}_{r2\beta}^{-1} \{d\mathbf{F}\}_{\{\beta\}} \\ &= \left\{ \begin{bmatrix} -dF_z^\beta \beta \cos \psi - dF_y^\beta \sin \psi \\ dF_z^\beta \beta \sin \psi - dF_y^\beta \cos \psi \\ dF_z^\beta (1 - \frac{1}{2}\beta^2) \end{bmatrix} \right\}_{\{nr\}} \end{aligned} \quad (D.22)$$

$$\begin{aligned} \{d\mathbf{M}\}_{\{nr\}} &= \mathbf{T}_{nr2r}^{-1} \mathbf{T}_{r2\beta}^{-1} \{d\mathbf{M}\}_{\{\beta\}} \\ &= r_e \left\{ \begin{bmatrix} dF_z^\beta \sin \psi - dF_y^\beta \beta \cos \psi \\ dF_z^\beta \cos \psi + dF_y^\beta \beta \sin \psi \\ dF_y^\beta (1 - \frac{1}{2}\beta^2) \end{bmatrix} \right\}_{\{nr\}} \end{aligned} \quad (D.23)$$

The total aerodynamic forces and moments generated by one blade can be derived by integrating the above equations through the radius and azimuth angle. During the integration, the blade root cut effect and tip loss are considered through the limits of integration, as:

$$\begin{aligned} \{\mathbf{F}_s\}_{\{nr\}} &= \frac{1}{2\pi} \int_0^{2\pi} d\psi \int_{k_r R}^{k_l R} \{d\mathbf{F}\}_{\{nr\}} \\ \{\mathbf{M}_s\}_{\{nr\}} &= \frac{1}{2\pi} \int_0^{2\pi} d\psi \int_{k_r R}^{k_l R} \{d\mathbf{M}\}_{\{nr\}} \end{aligned} \quad (D.24)$$

where k_r is the root cut ratio, which is determined by the blade design, and k_l is the tip loss factor, for which a constant value (0.97) is used in this thesis.

From the integration, one can obtain three forces and three aerodynamic moments generated by one blade, as:

$$\begin{aligned} \{\mathbf{F}_s\}_{\{nr\}} &= \{[H_s, S_s, -T_s]^\top\}_{\{nr\}} \\ \{\mathbf{M}_s\}_{\{nr\}} &= \{[M_{1s}, M_{2s}, M_{zs}]^\top\}_{\{nr\}} \end{aligned} \quad (D.25)$$

where T_s , H_s and S_s are the blade thrust, horizontal and sideways hub forces respectively, M_{1s} and M_{2s} are the lateral and longitudinal aerodynamic moments generated by the blade (they will be used for the Pitt-Peters dynamic inflow model), and M_{zs} is the shaft torque generated by one blade.

The hub pitch (M_{xs}) and roll (M_{ys}) moments can be calculated based on the flapping motion of the blade. For the k th blade, one can derive:

$$\begin{aligned} M_{xs}^{(k)} &= \frac{1}{2} R_{ef} \left(T_{ss1}^{(k)} - \Omega^2 M_\beta \sin(\beta_{s1}^{(k)}) + 2q\Omega M_{\beta 1} \right) - \frac{1}{2} K_\beta \beta_{s1}^{(k)} \\ M_{ys}^{(k)} &= \frac{1}{2} R_{ef} \left(T_{sc1}^{(k)} - \Omega^2 M_\beta \sin(\beta_{c1}^{(k)}) - 2p\Omega M_{\beta 1} \right) - \frac{1}{2} K_\beta \beta_{c1}^{(k)} \end{aligned} \quad (D.26)$$

where

$$M_{\beta 1} = (M_\beta + R_{ef} M_b) \quad (D.27)$$

D

and $T_{ss1}^{(k)}$ and $T_{sc1}^{(k)}$ are first order harmonic components of the blade thrust. They can be derived as:

$$\begin{aligned} T_s^{(k)}(\psi) &= \int_{k_r R}^{k_l R} dF_z^\beta \left(1 - \frac{1}{2}\beta^2\right) \\ &= T_{s0}^{(k)} + T_{ss1}^{(k)} \sin \psi + T_{sc1}^{(k)} \cos \psi + \text{higher order components} \end{aligned} \quad (\text{D.28})$$

Similarly, all the hub forces and moments generated by one blade as a function of the azimuth angle can be derived, including $T_s^{(k)}(\psi)$, $H_s^{(k)}(\psi)$, $S_s^{(k)}(\psi)$, $M_{xs}^{(k)}(\psi)$, $M_{ys}^{(k)}(\psi)$ and $M_{zs}^{(k)}(\psi)$. They will be used in the vibratory analyses in Section 4.8.

For the forces and moments derived above (Eq. D.24 to D.28), i.e. H_s , S_s , T_s , M_{1s} , M_{2s} , M_{zs} , T_{ss1} and T_{sc1} , their expressions are very long and complex. In this sense, a simplification method based on an ordering scheme is used to simplify the model. The method is described in Appendix C. The simplified final expressions for these forces and moments are presented in Section D.2 (in non-dimensional form).

The forces and moments derived above are derived for a single blade. For the conventional helicopter, all the blades are considered to be working in identical condition. Therefore, the total hub forces and moments can be calculated by multiplying the formulas for a single blade and the number of blades (N_b), i.e.

$$T_{mr} = T_s N_b \quad (\text{D.29})$$

So far, the three hub forces (T_{mr} , H_{mr} , S_{mr}) and three hub moments (M_x , M_y , M_z) are derived in the non-rotating reference. They need to be rotated through the y-axis due to the tilt angle of the rotor shaft (α_{sh} in Fig. 3.1) and transformed to the helicopter c.g. position. Using the small angle assumption gives the total forces and moments generated by the main rotor as:

$$\begin{aligned} X_{mr} &\approx H_{mr} - \alpha_{sh} T_{mr} \\ Y_{mr} &= S_{mr} \\ Z_{mr} &\approx -T_{mr} \end{aligned} \quad (\text{D.30})$$

and

$$\begin{aligned} L_{mr} &\approx M_x + \alpha_{sh} M_z + y_{mr} Z_{mr} - z_{mr} Y_{mr} \\ M_{mr} &= M_y + z_{mr} X_{mr} - x_{mr} Z_{mr} \\ N_{mr} &\approx M_z + x_{mr} Y_{mr} - y_{mr} X_{mr} \end{aligned} \quad (\text{D.31})$$

Flapping Equation

The blade flapping motion is modelled using the Lagrangian equation, which has the general form as:

$$Q_i = \frac{d}{dt} \left(\frac{\partial T_k}{\partial \dot{q}_i} \right) - \frac{\partial T_k}{\partial q_i} \quad (\text{D.32})$$

where Q_i is the generalized force, T_k is the total kinetic energy of the blade, and q_i is the generalized coordinate.

In blade flapping dynamics, the generalized coordinate is the flapping angle (β), and the generalized force is the flapping moment on the blade, which consists of the aerodynamic flapping moment and the moment generated by the flapping spring as shown in Eq. D.1. The aerodynamic moment can be calculated by integrating the lift force on the blade element as:

$$\begin{aligned} M_{aero} &= \int_{k_r R}^{k_l R} dM_{aero} \\ &= \int_{k_r R}^{k_l R} dL (r_e - R_{ef}) \end{aligned} \quad (D.33)$$

The generalized force for a conventional helicopter model is:

$$Q_\beta = M_{aero} + M_k \quad (D.34)$$

Other forces, such as the centrifugal or Coriolis forces, are embedded in the derivatives of the T_k , i.e. the right-hand side of Eq. D.32.

To derive the kinetic energy of the blade, the velocity of a blade element in the non-rotating reference is first derived. Similar to the Eq. D.6, the velocity on the blade element includes the effects of different motions, including the motion of the rotor hub, the rotation of blade and the flapping motion of blade, as:

$$\{\mathbf{V}_e\}_{\{nr\}} = \{\mathbf{V}_m\}_{\{nr\}} + \mathbf{T}_{nr2r}^{-1} \{\mathbf{V}_\Omega\}_{\{r\}} + \mathbf{T}_{nr2r}^{-1} \mathbf{T}_{r2\beta}^{-1} \{\mathbf{V}_{flap}\}_{\{\beta\}} \quad (D.35)$$

Substituting all the velocities and using the transformation matrices (\mathbf{T}_{nr2r} and $\mathbf{T}_{r2\beta}$) results in the velocity on the blade element as:

$$\{\mathbf{V}_e\}_{\{nr\}} = \left\{ \begin{bmatrix} u - \beta q (r_e - R_{ef}) + (\Omega - r) r_e \sin(\psi) \\ v + \beta p (r_e - R_{ef}) - \beta \dot{\beta} (r_e - R_{ef}) \cos(\psi) \\ w - \dot{\beta} (r_e - R_{ef}) + p r_e \sin(\psi) + q r_e \cos(\psi) \end{bmatrix} \right\}_{\{nr\}} \quad (D.36)$$

With the velocity derived above, the total kinetic energy of the blade (T) can be derived:

$$T_k = \int_{R_r}^R \frac{1}{2} \rho_r dr |\{\mathbf{V}_e\}_{\{nr\}}|^2 \quad (D.37)$$

Substituting Eq. D.37 into the right side of Eq. D.32 results in:

$$\begin{aligned} \frac{d}{dt} \left(\frac{\partial T_k}{\partial \dot{\beta}} \right) - \frac{\partial T_k}{\partial \beta} &= I_\beta (\beta^2 + 1) \ddot{\beta} + (uq - vp) M_\beta - (p^2 + q^2 - \dot{\beta}^2) \beta I_\beta \\ &\quad + (I_{\beta 1} (2\Omega - r) q + I_\beta \Omega q \beta^2 - M_\beta \Omega u \beta) \sin(\psi) \\ &\quad - (I_{\beta 1} (2\Omega - r) p + I_\beta \Omega p \beta^2 + M_\beta \Omega v \beta) \cos(\psi) \end{aligned} \quad (D.38)$$

where:

$$\begin{aligned} I_\beta &= \int_{R_{ef}}^R \rho_r dr (r_e - R_{ef})^2 \\ M_\beta &= \int_{R_{ef}}^R \rho_r dr (r_e - R_{ef}) \\ I_{\beta 1} &= I_\beta + M_\beta R_{ef} \end{aligned} \quad (D.39)$$

The flapping rate ($\dot{\beta}$) and flapping acceleration ($\ddot{\beta}$) can be derived from Eq. 3.2, as:

$$\dot{\beta} = \dot{\beta}_0 + \dot{\beta}_{s1} \sin \psi + \dot{\beta}_{c1} \cos \psi + \beta_{s1} \Omega \cos \psi - \beta_{c1} \Omega \sin \psi \quad (D.40)$$

$$\begin{aligned} \ddot{\beta} &= \ddot{\beta}_0 + \ddot{\beta}_{s1} \sin \psi + \ddot{\beta}_{c1} \cos \psi + \dot{\beta}_{s1} \Omega \cos \psi - \dot{\beta}_{c1} \Omega \sin \psi \\ &\quad + \dot{\beta}_{s1} \Omega \cos \psi - \dot{\beta}_{c1} \Omega \sin \psi - \beta_{s1} \Omega^2 \sin \psi - \beta_{c1} \Omega^2 \cos \psi \end{aligned} \quad (D.41)$$

In this thesis, the second order flapping dynamics ($\ddot{\beta}_0$, $\ddot{\beta}_{s1}$ and $\ddot{\beta}_{c1}$) are neglected. Therefore, Eq. D.41 can be simplified as:

$$\ddot{\beta} = 2\dot{\beta}_{s1} \Omega \cos \psi - 2\dot{\beta}_{c1} \Omega \sin \psi - \beta_{s1} \Omega^2 \sin \psi - \beta_{c1} \Omega^2 \cos \psi \quad (D.42)$$

Combining the equations derived above (Eq. D.34, D.38, D.40 and D.42), and collecting coefficients for the constant and harmonic components, the flapping equation of motion can be rewritten in the form of a Fourier series, as:

$$\frac{d}{dt} \left(\frac{\partial T_k}{\partial \dot{q}_i} \right) - \frac{\partial T_k}{\partial q_i} - Q_i = F_{\beta 0}(\vec{\beta}, \dot{\vec{\beta}}) + F_{\beta s1}(\vec{\beta}, \dot{\vec{\beta}}) \sin \psi + F_{\beta c1}(\vec{\beta}, \dot{\vec{\beta}}) \cos \psi + \dots \quad (D.43)$$

where $\vec{\beta} = [\beta_0, \beta_{s1}, \beta_{c1}]^\top$ and $\dot{\vec{\beta}} = [\dot{\beta}_0, \dot{\beta}_{s1}, \dot{\beta}_{c1}]^\top$.

In this thesis, only the first order harmonic components of flapping motion are considered, i.e. $F_{\beta 0}$, $F_{\beta s1}$ and $F_{\beta c1}$, and higher order components are neglected. To conclude, three equations can be formed for the flapping dynamics:

$$\begin{cases} F_{\beta 0}(\vec{\beta}, \dot{\vec{\beta}}) = 0 \\ F_{\beta s1}(\vec{\beta}, \dot{\vec{\beta}}) = 0 \\ F_{\beta c1}(\vec{\beta}, \dot{\vec{\beta}}) = 0 \end{cases} \quad (D.44)$$

Collecting coefficients of the above equations with regard to $\vec{\beta}$ and $\dot{\vec{\beta}}$, they can be rewritten in the matrix form as:

$$\mathbf{M}_\beta \dot{\vec{\beta}} + \mathbf{A}_\beta \vec{\beta} + \mathbf{N}_\beta + \mathbf{b}_\beta = 0 \quad (D.45)$$

where \mathbf{M}_β and \mathbf{A}_β are linear coefficients of $\dot{\vec{\beta}}$ and $\vec{\beta}$, \mathbf{N}_β is the nonlinear combination of $\dot{\vec{\beta}}$ and $\vec{\beta}$, and \mathbf{b}_β is the constant part with regard to $\dot{\vec{\beta}}$ and $\vec{\beta}$. The final expressions of the coefficients (\mathbf{M}_β , \mathbf{A}_β , \mathbf{N}_β and \mathbf{b}_β) can be found in the next section (see D.2).

D.1.2 The Tail Rotor Model

As mentioned before, the tail rotor model is adapted from the main rotor model. The main simplifications applied to the tail rotor are described at the beginning of this section. After simplifications, the non-dimensional thrust and torque coefficients for the tail rotor can be calculated using relatively simple formulas as follows:

$$C_{T_{tr}} = C_{L_{\alpha}}^{tr} \sigma_{tr} \left(\left(\frac{1}{2} \mu^2 k_1 - \bar{\Omega}_e^2 k_3 \right) \theta_0 + \bar{\Omega}_e k_2 \lambda + \frac{1}{2} (\bar{u} \bar{p} + \bar{v} \bar{q}) k_2 \right) \quad (D.46)$$

where:

$$\begin{aligned} \mu &= \bar{u}^2 + \bar{v}^2 \\ \lambda &= \bar{w} - \lambda_i \\ \bar{\Omega}_e &= 1 - \bar{r} \\ k_1 &= k_l - k_{r_{tr}} \\ k_2 &= \frac{1}{2} (k_l^2 - k_{r_{tr}}^2) \\ k_3 &= \frac{1}{3} (k_l^3 - k_{r_{tr}}^3) \end{aligned} \quad (D.47)$$

and

$$\begin{aligned} C_{Q_{tr}} &= \sigma_{tr} C_{L_{\alpha}}^{tr} \left(\bar{C}_{d0}^{tr} k_2 \left(\frac{1}{2} \mu^2 + 2k_1 \bar{\Omega}_e \right) \right. \\ &\quad + \bar{C}_{d2}^{tr} \left(k_2 \theta_0^2 \left(\frac{1}{2} \mu^2 + 2k_1 \bar{\Omega}_e \right) + k_3 \theta_0 (c_1 + 2\lambda \bar{\Omega}_e) + k_2 (c_2 k_1 + \lambda^2) \right) \\ &\quad \left. - \left(k_3 \theta_0 \left(\frac{1}{2} c_1 + \lambda \bar{\Omega}_e \right) + k_2 (c_2 k_1 + \lambda^2) \right) \right) \end{aligned} \quad (D.48)$$

where:

$$\begin{aligned} k_1 &= \frac{1}{4} (k_l^2 + k_{r_{tr}}^2) \\ k_2 &= \frac{1}{4} (k_l^2 - k_{r_{tr}}^2) \\ k_3 &= \frac{1}{6} (k_l^3 - k_{r_{tr}}^3) \\ c_1 &= \bar{u} \bar{p} + \bar{v} \bar{q} \\ c_2 &= \bar{p}^2 + \bar{q}^2 \end{aligned} \quad (D.49)$$

Afterwards, the rotor thrust is transformed into the helicopter body reference as:

$$\begin{aligned} X_{tr} &= 0 \\ Y_{tr} &= -T_{tr} \\ Z_{tr} &= 0 \end{aligned} \quad (D.50)$$

and

$$\begin{aligned} L_{tr} &= -z_{tr}Y_{tr} \\ M_{tr} &\approx 0 \\ N_{tr} &= x_{tr}Y_{tr} \end{aligned} \tag{D.51}$$

The tail rotor torque is neglected in this transformation, since it is relatively small compared with the pitch moment generated by the main rotor. This torque is only used for the power calculations.

D.1.3 Velocity Transformation

It should be noted that in the development of the above model, the velocities used $([u, v, w, p, q, r])$ are velocities of the rotor hub or tail rotor hub. Since the hubs are not located at the c.g. of the helicopter, their velocities as a function of the helicopter body motion should be derived and substituted into the model developed above.

For the main rotor, the hub motion velocity is:

$$\begin{aligned} \{\mathbf{V}_{hub}\}_{\{nr\}} &= \mathbf{T}_{b2nr} \left(\{\mathbf{V}_b\}_{\{b\}} + \{\vec{\omega}_b\}_{\{b\}} \times \{\mathbf{r}_{hub}\}_{\{b\}} \right) \\ \{\vec{\omega}_{hub}\}_{\{nr\}} &= \mathbf{T}_{b2nr} \{\vec{\omega}_b\}_{\{b\}} \end{aligned} \tag{D.52}$$

Expanding the equations above, one can get all the velocities that need to be substituted into the main rotor model:

$$\begin{aligned} u &\equiv \cos(\alpha_{sh})(u + qz_{mr} - ry_{mr}) - \sin(\alpha_{sh})(w + py_{mr} - qx_{mr}) \\ v &\equiv v + rx_{mr} - pz_{mr} \\ w &\equiv \sin(\alpha_{sh})(u + qz_{mr} - ry_{mr}) + \cos(\alpha_{sh})(w + py_{mr} - qx_{mr}) \\ p &\equiv \cos(\alpha_{sh})p - \sin(\alpha_{sh})r \\ q &\equiv q \\ r &\equiv \sin(\alpha_{sh})p + \cos(\alpha_{sh})r \end{aligned} \tag{D.53}$$

For the tail rotor, a similar derivation can be done, resulting in:

$$\begin{aligned} u &\equiv u + qz_{tr} - ry_{tr} \\ v &\equiv w + py_{tr} - qx_{tr} \\ w &\equiv -(v + rx_{tr} - pz_{tr}) \\ p &\equiv p \\ q &\equiv r \\ r &\equiv -q \end{aligned} \tag{D.54}$$

D.1.4 Other Components

Fuselage

The aerodynamic force on the fuselage is calculated through an equivalent drag area F_0 , which is considered to be constant for all flight conditions. The total drag force is:

$$R_{fus} = \frac{1}{2} \rho V^2 F_0 \quad (D.55)$$

where:

$$V^2 = u^2 + v^2 + w^2 \quad (D.56)$$

The projections of the drag force on three axes are:

$$\begin{aligned} X_{fus} &= -\frac{R_{fus}}{V} u \\ Y_{fus} &= -\frac{R_{fus}}{V} v \\ Z_{fus} &= -\frac{R_{fus}}{V} w \end{aligned} \quad (D.57)$$

D

Stabilizer

For the horizontal and the vertical stabilizer, only the lift forces and moments coursed by them are considered, as:

$$\begin{aligned} Z_{hs} &\approx -\frac{1}{2} \rho V_{hs}^2 S_{hs} C_{L\alpha}^{hs} \alpha_{hs} \\ M_{hs} &= -Z_{hs} \cdot x_{hs} \end{aligned} \quad (D.58)$$

$$\begin{aligned} Y_{fin} &\approx -\frac{1}{2} \rho V_{fin}^2 S_{fin} C_{L\alpha}^{fin} \beta_{fin} \\ L_{fin} &= -Y_{fin} \cdot z_{fin} \\ N_{fin} &= -Y_{fin} \cdot x_{fin} \end{aligned} \quad (D.59)$$

with the horizontal stabilizer local angle of attack:

$$\alpha_{hs} = \alpha_{hs0} + \arctan \left(\frac{w - q \cdot x_{hs}}{u} \right) \quad (D.60)$$

and velocity:

$$V_{hs}^2 = u^2 + (w - q \cdot x_{hs})^2 \quad (D.61)$$

The angle of attack of the fin is:

$$\beta_{fin} = \beta_{fin0} + \arctan \left(\frac{v + r \cdot x_{fin} - p \cdot z_{fin}}{u} \right) \quad (D.62)$$

and the local velocity:

$$V_{fin}^2 = u^2 + (v + r \cdot x_{fin} - p \cdot z_{fin})^2 \quad (D.63)$$

Inertia Force

The projections of inertia force in the helicopter body reference can be calculated based on the pitch and roll attitude angle of the helicopter, as:

$$\begin{aligned} X_g &= -M_a g \sin(\Theta) \\ Y_g &= M_a g \cos(\Theta) \sin(\Phi) \\ Z_g &= M_a g \cos(\Theta) \cos(\Phi) \end{aligned} \quad (D.64)$$

and the inertia force will not generate any moments on the c.g..

Inflow Model

For the main rotor, the classical Pitt-Peters dynamic inflow model is used. First order harmonic component of the inflow is considered as:

$$\lambda_i = \lambda_0 + \lambda_{s1} \frac{r_e}{R} \sin \psi + \lambda_{c1} \frac{r_e}{R} \cos \psi \quad (D.65)$$

where λ_0 , λ_{s1} and λ_{c1} are the rotor uniform and first harmonic inflow velocities (normalized by ΩR).

The dynamics of the inflow is represented by following the first-order differential equation [24]:

$$[\mathbf{M}] \begin{bmatrix} \dot{\lambda}_0 \\ \dot{\lambda}_{s1} \\ \dot{\lambda}_{c1} \end{bmatrix} + [\hat{\mathbf{L}}]^{-1} \begin{bmatrix} \lambda_0 \\ \lambda_{s1} \\ \lambda_{c1} \end{bmatrix} = \begin{bmatrix} C_T \\ -C_1 \\ C_2 \end{bmatrix}_{aero} \quad (D.66)$$

where \mathbf{M} is the constant apparent mass matrix, and $\hat{\mathbf{L}}^{-1}$ is the inflow gain matrix corresponding to the flight condition. Their detailed expressions can be found in Ref. [24]. C_T is the thrust coefficient of the main rotor. C_1 and C_2 are non-denominational lateral and longitudinal aerodynamic moments on the rotor, which can be calculated by integrating the lift force on the blade elements throughout the rotor disk plane, as shown in Eq. D.22 to D.24.

For the tail rotor of the conventional helicopter model, a similar first-order differential equation is used. Since the uniform inflow model is used for the tail rotor, the dynamic model contains only one equation as:

$$\tau_i \dot{\lambda}_{tr} = C_{T_b} - C_{T_\lambda} \quad (D.67)$$

where τ_i is the time constant of the inflow dynamics, C_{T_b} is the thrust coefficient calculated using blade element theory and C_{T_λ} is the thrust coefficient from momentum theory.

D.2 Expressions of the Generic Flight Mechanics Model

This section presents the expressions derived for the generic flight mechanics model (in non-dimensional form) before the velocity transformation discussed in Section D.1.3.

This includes: the hub forces (T_s , H_s , S_s), the aerodynamic moments (M_{1s} , M_{2s} , M_{zs}), the first order harmonic components of blade thrust (T_{ss1} , T_{sc1}) and the coefficients of the flapping equation.

D.2.1 Rotor Hub Forces and Moments

Thrust

The thrust coefficient of a single blade is:

$$C_{Ts} = \sigma_s C_{l_\alpha} (t_1 + t_2 \theta_{c1} + t_3 \theta_{s1} + t_4 \theta_0) \quad (\text{D.68})$$

where:

$$\begin{aligned} t_1 &= t_{11} + t_{12} \mu_z + t_{13} \mu_x + t_{14} \mu_y + \left(-\frac{1}{4} K_{\theta 2} \beta_{c1} k_l^2 + \frac{1}{4} K_{\theta 1} k_l^2 \beta_{s1} - \frac{1}{8} k_l^2 \beta_{c1} \right) \mu_x \bar{r} - \frac{1}{8} k_l^2 \mu_y^2 \theta_{tw} \\ &\quad - \frac{1}{8} k_l^2 \bar{q} \mu_y + \frac{1}{4} k_l^2 \bar{r} \mu_z + \left(-\frac{1}{4} k_l^2 \lambda_0 + \frac{1}{3} K_{\theta 1} k_l^3 \beta_0 + \frac{1}{4} \theta_{tw} k_l^4 \right) \bar{r} + t_{15} \mu_x^2 + \frac{1}{2} k_l \beta_0 \beta_{s1} \mu_x \mu_z \\ &\quad - \frac{1}{8} k_l^2 \bar{p} \mu_x \\ t_2 &= \frac{1}{4} k_l^3 \beta_0 \beta_{c1} + \frac{1}{8} k_l^2 \beta_{c1} \beta_{s1} \mu_x + \left(-\frac{1}{4} k_l^2 + \frac{1}{4} r_c^2 + \frac{3}{16} k_l^2 \beta_{c1}^2 \right) \mu_y \\ t_3 &= \frac{1}{4} k_l^3 \beta_0 \beta_{s1} + t_{31} \mu_x + \frac{1}{4} k_l^2 \bar{r} \mu_x + \frac{3}{16} \mu_x^2 k_l \beta_0 \beta_{s1} \\ t_4 &= t_{41} + \frac{1}{2} k_l^2 \beta_0 \beta_{s1} \mu_x + \frac{1}{2} k_l^2 \beta_0 \beta_{c1} \mu_y - \frac{1}{4} k_l \mu_y^2 - \frac{1}{6} k_l^3 \beta_{c1} \bar{p} \\ &\quad + \frac{1}{6} k_l^3 \beta_{s1} \bar{q} + \frac{1}{3} k_l^3 \bar{r} + \left(-\frac{1}{4} k_l + \frac{3}{32} k_l \beta_{s1}^2 + \frac{1}{4} r_c \right) \mu_x^2 \\ t_{11} &= -\frac{1}{4} r_c^2 \lambda_0 + \frac{1}{4} k_l^2 \lambda_0 - \frac{1}{8} \theta_{tw} k_l^4 + \left(-\frac{1}{8} k_l^2 \lambda_0 + \frac{3}{32} \theta_{tw} k_l^4 \right) \beta_{s1}^2 + \left(-\frac{1}{8} k_l^2 \lambda_0 + \frac{3}{32} \theta_{tw} k_l^4 \right) \beta_{c1}^2 \\ &\quad + \frac{3}{16} \theta_{tw} k_l^4 \beta_0^2 - \frac{1}{6} K_{\theta 1} k_l^3 \beta_0 + \frac{3}{8} K_{\theta 1} k_l^3 \beta_0 \beta_{c1}^2 + \frac{3}{8} K_{\theta 1} k_l^3 \beta_0 \beta_{s1}^2 \\ t_{12} &= \frac{3}{16} k_l^2 \beta_{s1}^2 + \frac{3}{16} k_l^2 \beta_{c1}^2 + \frac{3}{8} k_l^2 \beta_0^2 + \frac{1}{4} r_c^2 - \frac{1}{4} k_l^2 \\ t_{13} &= \frac{1}{8} k_l^2 \lambda_{s1} + \frac{3}{16} K_{\theta 1} k_l^2 \beta_{s1}^2 + \left(-\frac{1}{4} K_{\theta 1} k_l^2 + \frac{1}{4} K_{\theta 1} r_c^2 \right) \beta_{s1} \\ &\quad + \left(-\frac{1}{4} K_{\theta 2} r_c^2 + \frac{1}{4} K_{\theta 2} k_l^2 + \frac{1}{4} e_f k_l - \frac{1}{4} e_f r_c \right) \beta_{c1} + \left(-\frac{5}{64} - \frac{1}{16} K_{\theta 2} \right) k_l^2 \beta_{c1}^3 + \frac{3}{4} K_{\theta 1} k_l^2 \beta_0^2 \beta_{s1} \\ &\quad + \left(-\frac{5}{16} - \frac{1}{4} K_{\theta 2} \right) k_l^2 \beta_0^2 \beta_{c1} + \frac{1}{3} \theta_{tw} k_l^3 \beta_0 \beta_{s1} + \frac{3}{16} K_{\theta 1} k_l^2 \beta_{s1} \beta_{c1}^2 + \left(-\frac{5}{64} - \frac{1}{16} K_{\theta 2} \right) k_l^2 \beta_{c1} \beta_{s1}^2 \\ t_{14} &= \frac{1}{8} k_l^2 \lambda_{c1} + \frac{1}{3} \theta_{tw} k_l^3 \beta_0 \beta_{c1} + \left(-\frac{1}{4} e_f k_l + \frac{1}{4} K_{\theta 2} r_c^2 - \frac{1}{4} K_{\theta 2} k_l^2 \right) \beta_{s1} - \frac{1}{4} K_{\theta 1} k_l^2 \beta_{c1} \\ t_{15} &= \left(-\frac{1}{8} k_l^2 + \frac{1}{8} r_c^2 \right) \theta_{tw} - \frac{3}{16} k_l \beta_0 \beta_{s1} \beta_{c1} + \left(-\frac{1}{4} K_{\theta 1} k_l + \frac{1}{4} K_{\theta 1} r_c \right) \beta_0 + \frac{9}{32} K_{\theta 1} k_l \beta_0 \beta_{s1}^2 \end{aligned}$$

Horizontal Force

The horizontal force coefficient of a single blade is:

$$C_{Hs} = \sigma_s C_{l_\alpha} \left(t_1 - \frac{1}{6} \bar{C}_{d2} k_l^3 \theta_0 \theta_{c1} + t_2 \theta_{c1} + t_3 \theta_{s1} + t_4 \theta_0 - \frac{1}{8} \bar{C}_{d2} k_l^2 \mu_x \theta_{s1} \theta_{c1} \right) \quad (\text{D.69})$$

where:

$$\begin{aligned}
 t_1 &= t_{11} + t_{12}\mu_z + t_{13}\mu_x + t_{14}\mu_y - \frac{1}{2}k_l\beta_0\beta_{c1}\mu_z^2 - \frac{1}{12}k_l^3\beta_0\bar{p} + \left(-\frac{1}{4}k_l^2\lambda_0 + \frac{1}{16}\theta_{tw}k_l^4 + \frac{1}{12}K_{\theta 1}k_l^3\beta_0\right)\bar{q} \\
 &\quad + \left(\frac{3}{16}\theta_{tw}k_l^4\beta_{s1} + \frac{5}{12}K_{\theta 1}k_l^3\beta_0\beta_{s1} - \frac{1}{6}K_{\theta 2}\beta_{c1}k_l^3\beta_0\right)\bar{r} + t_{15}\mu_x^2 + t_{16}\mu_y\mu_x + \frac{1}{4}k_l^2\bar{q}\mu_z \\
 &\quad + t_{17}\mu_z\mu_x + \left(\frac{1}{4}K_{\theta 1}k_l\beta_0 + \frac{1}{8}\theta_{tw}k_l^2\right)\mu_z\mu_y - \frac{5}{32}k_l^2\beta_{s1}\bar{p}\mu_x - \frac{7}{32}k_l^2\beta_{c1}\bar{q}\mu_x \\
 t_2 &= t_{21} + t_{22}\mu_z + t_{23}\mu_x + \left(-\frac{3}{8}\beta_{s1}K_{\theta 2}\bar{C}_{d2}k_l^2 - \frac{1}{8}k_l^2\beta_{s1} + \frac{3}{16}e_f k_l\beta_{s1}\right)\mu_y \\
 &\quad + \frac{5}{32}k_l^2\beta_{c1}\bar{r}\mu_x - \frac{1}{4}k_l\beta_0\mu_x\mu_y \\
 t_3 &= \frac{5}{24}k_l^3\beta_0\beta_{s1}^2 - \frac{1}{12}k_l^3\beta_0 + t_{31}\mu_x + \frac{7}{32}k_l^2\beta_{s1}\bar{r}\mu_x + \frac{1}{6}k_l^3\beta_0\bar{r} + \left(-\frac{1}{4}k_l\beta_0 + \frac{1}{4}r_c\beta_0\right)\mu_x^2 \\
 t_4 &= t_{41} - \frac{1}{4}k_l^2\beta_0\beta_{c1}\mu_z + t_{42}\mu_x + \left(-\frac{1}{4}k_l\lambda_0 - \frac{1}{3}\theta_{tw}\bar{C}_{d2}k_l^3\right)\mu_y + \frac{3}{8}k_l^2\beta_0\bar{r}\mu_x + \frac{1}{12}k_l^3\bar{q} \\
 &\quad + \frac{1}{4}k_l^3\beta_{s1}\bar{r} + \left(\frac{1}{4}r_c\beta_{s1} - \frac{1}{4}k_l\beta_{s1}\right)\mu_x^2 + \left(-\frac{1}{4}k_l\beta_{c1} + \frac{1}{4}r_c\beta_{c1}\right)\mu_y\mu_x + \left(\frac{1}{4}k_l - \frac{1}{4}r_c\right)\mu_z\mu_y \\
 t_{11} &= \frac{1}{4}k_l^2\lambda_0\lambda_{c1} - \frac{1}{16}\theta_{tw}k_l^4\lambda_{c1} + \left(\left(-\frac{1}{12} + \frac{1}{12}K_{\theta 2}\right)k_l^3 + \frac{1}{8}e_f k_l^2\right)\beta_{c1}\beta_0 \\
 &\quad + \frac{9}{32}K_{\theta 1}k_l^3\beta_0\beta_{s1}\beta_{c1}^2 + \frac{9}{32}K_{\theta 1}k_l^3\beta_0\beta_{s1}^3 + \frac{7}{128}\theta_{tw}k_l^4\beta_{s1}^3 \\
 &\quad + \left(-\frac{1}{12}K_{\theta 1}\lambda_{c1} + \frac{1}{12}\lambda_{s1}\right)k_l^3\beta_0 + \left(\left(\left(\frac{1}{8}\bar{C}_{d2} - \frac{1}{8} - \frac{1}{8}\bar{C}_{d2}K_{\theta 2}\right)k_l^4 + \frac{1}{12}e_f k_l^3\right)\theta_{tw}\right. \\
 &\quad \left.+ \left(\left(-\frac{1}{8} + \frac{1}{4}\bar{C}_{d2}\right)\lambda_0 K_{\theta 2} + \left(-\frac{1}{4}\bar{C}_{d2} + \frac{3}{8}\right)\lambda_0\right)k_l^2 - \frac{1}{2}e_f k_l\lambda_0 + \frac{1}{2}e_f r_c\lambda_0 - \frac{3}{8}r_c^2\lambda_0\right)\beta_{s1} \\
 &\quad + \left(-\frac{1}{8}K_{\theta 1}k_l^2\lambda_0 - \frac{1}{8}\theta_{tw}\bar{C}_{d2}K_{\theta 1}k_l^4\right)\beta_{c1} + \frac{7}{32}\theta_{tw}k_l^4\beta_0^2\beta_{s1} \\
 &\quad + \left(\left(-\frac{1}{6}\bar{C}_{d2}K_{\theta 2} - \frac{1}{4} + \frac{1}{6}\bar{C}_{d2}\right)K_{\theta 1}k_l^3 + \frac{1}{8}e_f K_{\theta 1}k_l^2\right)\beta_{s1}\beta_0 + \frac{7}{128}\theta_{tw}k_l^4\beta_{c1}^2\beta_{s1} \\
 t_{12} &= -\frac{1}{4}k_l^2\lambda_{c1} - \frac{1}{6}\theta_{tw}k_l^3\beta_0\beta_{c1} + \frac{1}{8}k_l^2\beta_{s1}^3 \\
 &\quad + \left(\left(\left(\frac{1}{8} - \frac{1}{4}\bar{C}_{d2}\right)K_{\theta 2} + \frac{1}{4}\bar{C}_{d2} - \frac{3}{8}\right)k_l^2 + \frac{1}{2}e_f k_l + \left(-\frac{1}{8}K_{\theta 2} + \frac{3}{8}\right)r_c^2 - \frac{1}{2}e_f r_c\right)\beta_{s1} \\
 &\quad + \left(\frac{1}{8} - \frac{1}{4}\bar{C}_{d2}\right)K_{\theta 1}k_l^2\beta_{c1} + \frac{1}{2}k_l^2\beta_0^2\beta_{s1} + \frac{1}{8}k_l^2\beta_{s1}\beta_{c1}^2 \\
 t_{13} &= \left(-\frac{1}{4}K_{\theta 1}k_l^2 + \frac{1}{4}K_{\theta 1}r_c^2\right)\beta_{s1}^2 - \frac{1}{8}K_{\theta 1}k_l^2\beta_{c1}^2 - \frac{3}{8}K_{\theta 1}k_l^2\beta_0^2 \\
 &\quad + \left(\left(-\frac{1}{4} + \frac{1}{6}\bar{C}_{d2}\right)k_l^3\theta_{tw} - \frac{3}{4}r_c\lambda_0 + \frac{3}{4}k_l\lambda_0\right)\beta_0 + \frac{5}{32}k_l^2\beta_{s1}\lambda_{s1} + \frac{7}{32}k_l^2\beta_{c1}\lambda_{c1} \\
 &\quad + \left(\left(\frac{1}{8} - \frac{1}{8}\bar{C}_{d2} + \frac{1}{8}K_{\theta 2}\bar{C}_{d2} + \frac{1}{8}K_{\theta 2}\right)k_l^2 + \left(-\frac{1}{8}e_f - \frac{1}{8}e_f K_{\theta 2}\right)k_l + \left(-\frac{1}{8} - \frac{1}{8}K_{\theta 2}\right)r_c^2\right)\beta_{s1}\beta_{c1} \\
 &\quad + \frac{21}{32}K_{\theta 1}k_l^2\beta_0^2\beta_{s1} + \frac{9}{64}K_{\theta 1}k_l^2\beta_{s1}\beta_{c1}^2 + \frac{5}{32}\theta_{tw}k_l^3\beta_0\beta_{c1}^2 + \frac{7}{32}\theta_{tw}k_l^3\beta_0\beta_{s1}^2 \\
 t_{14} &= -\frac{1}{4}\bar{C}_d k_l^2 - \frac{1}{8}\theta_{tw}k_l^2\lambda_0 + \left(\left(-\frac{1}{8} - \frac{1}{8}K_{\theta 2}\right)k_l^2 + \frac{3}{16}e_f K_{\theta 2}k_l\right)\beta_{s1}^2 - \frac{1}{8}k_l^2\beta_0^2 - \frac{1}{8}K_{\theta 1}k_l^2\beta_{s1}\beta_{c1} \\
 t_{15} &= \left(\left(\frac{1}{4}K_{\theta 2} + \frac{1}{2} - \frac{3}{8}\bar{C}_{d2}\right)k_l + \left(-\frac{1}{2} - \frac{1}{4}K_{\theta 2}\right)r_c\right)\beta_{c1}\beta_0 \\
 &\quad - \frac{1}{8}\theta_{tw}k_l^2\beta_{s1} + \left(\frac{1}{2}K_{\theta 1}r_c - \frac{1}{2}K_{\theta 1}k_l\right)\beta_{s1}\beta_0
 \end{aligned}$$

D

D.2 Expressions of the Generic Flight Mechanics Model

203

$$\begin{aligned}
 t_{16} &= -\frac{1}{2}K_{\theta 1}k_l\beta_0\beta_{c1} - \frac{1}{8}\theta_{tw}k_l^2\beta_{c1} + \left(\left(-\frac{1}{2} - \frac{1}{4}K_{\theta 2}\right)k_l + \frac{1}{2}r_c\right)\beta_{s1}\beta_0 \\
 t_{17} &= \left(\left(-\frac{3}{4} + \frac{1}{2}\bar{C}_{d2}\right)k_l + \frac{3}{4}r_c\right)\beta_0 + \frac{21}{32}k_l\beta_0\beta_{c1}^2 + \frac{15}{32}k_l\beta_0\beta_{s1}^2 \\
 t_{21} &= -\frac{1}{8}\theta_{tw}\bar{C}_{d2}k_l^4 + \left(-\frac{1}{8} + \frac{1}{4}\bar{C}_{d2}\right)\lambda_0k_l^2 + \frac{1}{6}k_l^3\beta_0\beta_{s1}\beta_{c1} - \frac{1}{6}K_{\theta 1}\bar{C}_{d2}k_l^3\beta_0 \\
 t_{22} &= \left(\frac{1}{8} - \frac{1}{4}\bar{C}_{d2}\right)k_l^2 - \frac{1}{8}r_c^2 - \frac{3}{32}k_l^2\beta_{c1}^2 \\
 t_{23} &= \left(\left(\frac{1}{8}\bar{C}_{d2}K_{\theta 2} - \frac{1}{8} + \frac{1}{8}\bar{C}_{d2}\right)k_l^2 - \frac{1}{16}e_fk_l + \frac{1}{8}r_c^2\right)\beta_{c1} + \frac{9}{128}k_l^2\beta_{s1}^2\beta_{c1} \\
 t_{41} &= -\frac{1}{12}k_l^3\lambda_{c1} + \frac{7}{96}k_l^3\beta_{s1}^3 + \left(\left(-\frac{1}{6} + \frac{1}{6}\bar{C}_{d2} - \frac{1}{6}\bar{C}_{d2}K_{\theta 2}\right)k_l^3 + \frac{1}{8}e_fk_l^2 + \frac{1}{6}r_c^3\right)\beta_{s1} \\
 &\quad - \frac{1}{6}K_{\theta 1}\bar{C}_{d2}k_l^3\beta_{c1} + \frac{7}{24}k_l^3\beta_0^2\beta_{s1} + \frac{7}{96}k_l^3\beta_{s1}\beta_{c1}^2 \\
 t_{42} &= \left(\left(\frac{1}{4}\bar{C}_{d2} - \frac{3}{8}\right)k_l^2 + \frac{3}{8}r_c^2\right)\beta_0 + \frac{15}{64}k_l^2\beta_0\beta_{c1}^2 + \frac{21}{64}k_l^2\beta_0\beta_{s1}^2
 \end{aligned}$$

Side Force

The side force coefficient of a single blade is:

D

$$\begin{aligned}
 C_{Ss} = \sigma_s C_{l_\alpha} \left(t_1 - \frac{1}{4}\theta_0^2\bar{C}_{d2}k_l^2\mu_x - \frac{3}{16}\theta_{s1}^2\bar{C}_{d2}k_l^2\mu_x + t_2\theta_{c1} + t_3\theta_{s1} + t_4\theta_0 \right. \\
 \left. + \left(-\frac{3}{8}\bar{C}_{d2}k_l\mu_x^2 - \frac{1}{6}\bar{C}_{d2}k_l^3\right)\theta_0\theta_{s1} \right) \quad (D.70)
 \end{aligned}$$

where:

$$\begin{aligned}
 t_1 &= t_{11} + t_{12}\mu_z + t_{13}\mu_x + t_{14}\mu_y + \frac{1}{2}k_l\mu_y^2\beta_0\beta_{s1} + \frac{5}{32}k_l^2\beta_{c1}\bar{q}\mu_y \\
 &\quad - \frac{1}{2}k_l\beta_0\beta_{s1}\mu_z^2 + \left(-\frac{1}{4}k_l^2\lambda_0 + \frac{1}{16}\theta_{tw}k_l^4 + \frac{1}{12}K_{\theta 1}k_l^3\beta_0\right)\bar{p} \\
 &\quad + \frac{1}{12}k_l^3\beta_0\bar{q} + \left(-\frac{3}{16}\theta_{tw}k_l^4\beta_{c1} - \frac{5}{12}K_{\theta 1}k_l^3\beta_0\beta_{c1} - \frac{1}{6}K_{\theta 2}\beta_{s1}k_l^3\beta_0\right)\bar{r} \\
 &\quad + \frac{3}{16}\bar{C}_{d2}k_l^2\mu_x\theta_{tw}\beta_{c1}K_{\theta 2} + t_{15}\mu_y\mu_x + \frac{1}{4}k_l^2\bar{p}\mu_z + \frac{7}{32}k_l^2\beta_{s1}\bar{p}\mu_y + t_{16}\mu_z\mu_x \\
 &\quad + \left(-\frac{3}{4}r_c\beta_0 + \frac{3}{4}k_l\beta_0\right)\mu_z\mu_y + \left(-\frac{3}{32}K_{\theta 2}\beta_{c1}k_l^2 + \frac{3}{32}K_{\theta 1}k_l^2\beta_{s1}\right)\mu_x\bar{p} \\
 t_2 &= -\frac{5}{24}k_l^3\beta_0\beta_{c1}^2 + \frac{1}{12}k_l^3\beta_0 + \left(-\frac{1}{8}\beta_{s1}K_{\theta 2}\bar{C}_{d2}k_l^2 + \frac{1}{8}\bar{C}_{d2}k_l^2\beta_{s1} + \frac{1}{16}e_fk_l\beta_{s1}\right)\mu_x \\
 &\quad + \frac{1}{4}k_l^2\beta_{c1}\mu_y - \frac{1}{6}k_l^3\beta_0\bar{r} \\
 t_3 &= t_{31} + t_{32}\mu_z + t_{33}\mu_x + \frac{1}{8}k_l^2\beta_{s1}\mu_y - \frac{3}{16}\bar{C}_{d2}k_l^2\mu_x^2\theta_{tw} + \frac{1}{4}k_l\beta_0\mu_x\mu_y + \frac{3}{32}k_l^2\bar{p}\mu_x \\
 t_4 &= t_{41} - \frac{1}{4}k_l^2\beta_0\beta_{s1}\mu_z + t_{42}\mu_x + \frac{3}{8}k_l^2\beta_0\mu_y + \frac{1}{4}\mu_y^2k_l\beta_{c1} + \frac{1}{12}k_l^3\bar{p} \\
 &\quad - \frac{1}{4}k_l^3\beta_{c1}\bar{r} + \left(-\frac{3}{8}\bar{C}_{d2}k_lK_{\theta 1}\beta_{s1} + \frac{3}{8}\bar{C}_{d2}k_lK_{\theta 2}\beta_{c1}\right)\mu_x^2 \\
 &\quad + \left(-\frac{1}{4}r_c\beta_{s1} + \frac{1}{4}k_l\beta_{s1}\right)\mu_y\mu_x + \left(-\frac{1}{4}r_c + \frac{1}{4}k_l - \frac{1}{2}\bar{C}_{d2}k_l\right)\mu_z\mu_x
 \end{aligned}$$

D

$$\begin{aligned}
 t_{11} &= \frac{1}{4}k_l^2\lambda_0\lambda_{s1} - \frac{1}{16}\theta_{tw}k_l^4\lambda_{s1} + \left(\left(\frac{1}{6}\bar{C}_{d2}K_{\theta 2} - \frac{1}{6}\bar{C}_{d2} + \frac{1}{4}\right)K_{\theta 1}k_l^3 - \frac{1}{8}e_fK_{\theta 1}k_l^2\right)\beta_{c1}\beta_0 \\
 &\quad - \frac{9}{32}K_{\theta 1}k_l^3\beta_0\beta_{s1}\beta_{c1} + \left(-\frac{1}{12}K_{\theta 1}\lambda_{s1} - \frac{1}{12}\lambda_{c1}\right)k_l^3\beta_0 \\
 &\quad + \left(-\frac{1}{8}K_{\theta 1}k_l^2\lambda_0 - \frac{1}{8}\theta_{tw}\bar{C}_{d2}K_{\theta 1}k_l^4\right)\beta_{s1} + \left(\left(\left(\frac{1}{8}\bar{C}_{d2}K_{\theta 2} + \frac{1}{8} - \frac{1}{8}\bar{C}_{d2}\right)k_l^4 - \frac{1}{12}e_fk_l^3\right)\theta_{tw}\right. \\
 &\quad \left.+ \left(\left(\frac{1}{8} - \frac{1}{4}\bar{C}_{d2}\right)\lambda_0K_{\theta 2} + \left(\frac{1}{4}\bar{C}_{d2} - \frac{3}{8}\right)\lambda_0\right)k_l^2 + \frac{1}{2}e_fk_l\lambda_0 - \frac{1}{2}e_fr_c\lambda_0 + \frac{3}{8}r_c^2\lambda_0\right)\beta_{c1} \\
 &\quad - \frac{7}{128}\theta_{tw}k_l^4\beta_{c1}^3 - \frac{9}{32}K_{\theta 1}k_l^3\beta_0\beta_{c1}^3 - \frac{7}{32}\theta_{tw}k_l^4\beta_0^2\beta_{c1} \\
 &\quad + \left(\left(-\frac{1}{12} + \frac{1}{12}K_{\theta 2}\right)k_l^3 + \frac{1}{8}e_fk_l^2\right)\beta_{s1}\beta_0 - \frac{7}{128}\theta_{tw}k_l^4\beta_{s1}^2\beta_{c1} \\
 t_{12} &= -\frac{1}{4}k_l^2\lambda_{s1} + \left(\frac{1}{8} - \frac{1}{4}\bar{C}_{d2}\right)K_{\theta 1}k_l^2\beta_{s1} \\
 &\quad + \left(\left(\left(\frac{1}{4}\bar{C}_{d2} - \frac{1}{8}\right)K_{\theta 2} - \frac{1}{4}\bar{C}_{d2} + \frac{3}{8}\right)k_l^2 - \frac{1}{2}e_fk_l + \left(-\frac{3}{8} + \frac{1}{8}K_{\theta 2}\right)r_c^2 + \frac{1}{2}e_fr_c\right)\beta_{c1} \\
 &\quad - \frac{1}{8}k_l^2\beta_{c1}^3 - \frac{1}{2}k_l^2\beta_0^2\beta_{c1} - \frac{1}{6}\theta_{tw}k_l^3\beta_0\beta_{s1} - \frac{1}{8}k_l^2\beta_{s1}^2\beta_{c1} \\
 t_{13} &= -\frac{1}{8}\theta_{tw}^2\bar{C}_{d2}k_l^4 - \frac{1}{4}\bar{C}_{d2}k_l^2 - \frac{1}{8}\theta_{tw}k_l^2\lambda_0 + \left(\left(\frac{1}{8} + \frac{1}{4}\bar{C}_{d2}K_{\theta 2}\right)K_{\theta 1}k_l^2 - \frac{1}{8}e_fK_{\theta 1}k_l\right)\beta_{c1}\beta_{s1} \\
 &\quad + \left(\frac{1}{8}K_{\theta 2}\bar{C}_{d2}k_l^2 + \left(\frac{1}{16}e_fK_{\theta 2} - \frac{1}{16}e_f\right)k_l\right)\beta_{s1}^2 + \left(\left(-\frac{1}{8} - \frac{3}{16}K_{\theta 2}^2\bar{C}_{d2} + \left(\frac{1}{8}\bar{C}_{d2} - \frac{1}{8}\right)K_{\theta 2}\right)k_l^2\right. \\
 &\quad \left.+ \left(\frac{1}{16}e_f + \frac{3}{16}e_fK_{\theta 2}\right)k_l + \left(\frac{1}{8}K_{\theta 2} + \frac{1}{8}\right)r_c^2 - \frac{3}{16}e_fK_{\theta 2}r_c\right)\beta_{c1}^2 + \frac{9}{32}k_l^2\beta_0^2\beta_{c1}^2 \\
 &\quad - \frac{1}{8}k_l^2\beta_0^2 + \left(-\frac{1}{4}K_{\theta 1}k_l\lambda_0 - \frac{1}{3}\theta_{tw}K_{\theta 1}\bar{C}_{d2}k_l^3\right)\beta_0 - \frac{3}{32}K_{\theta 1}k_l^2\beta_{s1}\lambda_{s1} + \frac{3}{32}K_{\theta 2}\beta_{c1}k_l^2\lambda_{s1} \\
 t_{14} &= \left(\frac{1}{8}K_{\theta 2} + \frac{1}{8}\right)k_l^2\beta_{c1}\beta_{s1} + \frac{1}{8}K_{\theta 1}k_l^2\beta_{s1}^2 + \frac{1}{4}K_{\theta 1}k_l^2\beta_{c1}^2 + \frac{3}{8}K_{\theta 1}k_l^2\beta_0^2 \\
 &\quad + \left(\frac{3}{4}r_c\lambda_0 - \frac{3}{4}k_l\lambda_0 + \frac{1}{4}\theta_{tw}k_l^3\right)\beta_0 - \frac{7}{32}k_l^2\beta_{s1}\lambda_{s1} - \frac{5}{32}k_l^2\beta_{c1}\lambda_{c1} \\
 t_{15} &= \left(\left(-\frac{1}{2} - \frac{1}{4}K_{\theta 2}\right)k_l + \frac{1}{2}r_c\right)\beta_{c1}\beta_0 + \frac{1}{8}\theta_{tw}k_l^2\beta_{s1} + \frac{1}{2}K_{\theta 1}k_l\beta_0\beta_{s1} \\
 t_{16} &= \left(\frac{1}{8} - \frac{1}{4}\bar{C}_{d2}\right)k_l^2\theta_{tw} + \left(-\frac{1}{4}K_{\theta 1}r_c + \frac{1}{4}K_{\theta 1}k_l\right)\beta_0 \\
 t_{31} &= -\frac{1}{8}\theta_{tw}\bar{C}_{d2}k_l^4 + \left(\frac{1}{4}\bar{C}_{d2} - \frac{1}{8}\right)\lambda_0k_l^2 - \frac{1}{6}k_l^3\beta_0\beta_{s1}\beta_{c1} - \frac{1}{6}K_{\theta 1}\bar{C}_{d2}k_l^3\beta_0 \\
 t_{32} &= \left(\frac{1}{8} - \frac{1}{4}\bar{C}_{d2}\right)k_l^2 - \frac{1}{8}r_c^2 - \frac{3}{32}k_l^2\beta_{s1}^2 \\
 t_{33} &= -\frac{3}{32}k_l^2\lambda_{s1} - \frac{3}{8}K_{\theta 1}\bar{C}_{d2}k_l^2\beta_{s1} + \left(\left(\frac{1}{8} + \frac{3}{8}\bar{C}_{d2}K_{\theta 2} - \frac{1}{8}\bar{C}_{d2}\right)k_l^2 - \frac{3}{16}e_fk_l + \frac{3}{16}e_fr_c - \frac{1}{8}r_c^2\right)\beta_{c1} \\
 t_{41} &= -\frac{1}{12}k_l^3\lambda_{s1} - \frac{1}{6}K_{\theta 1}\bar{C}_{d2}k_l^3\beta_{s1} + \left(\left(\frac{1}{6} + \frac{1}{6}\bar{C}_{d2}K_{\theta 2} - \frac{1}{6}\bar{C}_{d2}\right)k_l^3 - \frac{1}{8}e_fk_l^2 - \frac{1}{6}r_c^3\right)\beta_{c1} \\
 &\quad - \frac{7}{96}k_l^3\beta_{c1}^3 - \frac{7}{24}k_l^3\beta_0^2\beta_{c1} - \frac{7}{96}k_l^3\beta_{s1}^2\beta_{c1} \\
 t_{42} &= -\frac{1}{3}\theta_{tw}\bar{C}_{d2}k_l^3 + \left(\frac{1}{2}\bar{C}_{d2} - \frac{1}{4}\right)\lambda_0k_l + \frac{1}{4}r_c\lambda_0 - \frac{1}{2}K_{\theta 1}\bar{C}_{d2}k_l^2\beta_0
 \end{aligned}$$

Lateral Aerodynamic Moment

The lateral aerodynamic moment coefficient generated by a single blade is:

$$C_{1s} = \sigma_s C_{l_\alpha} \left(t_1 + \left(\frac{1}{12} k_l^3 \beta_0 \mu_z - \frac{1}{16} k_l^2 \mu_x \mu_y \right) \theta_{c1} + t_2 \theta_{s1} + t_3 \theta_0 \right) \quad (D.71)$$

where:

$$\begin{aligned} t_1 &= t_{11} + t_{12} \mu_z + t_{13} \mu_x - \frac{1}{12} k_l^3 \beta_0 \mu_y + \frac{1}{8} k_l^2 \beta_{c1} \mu_z^2 + \frac{1}{8} \theta_{tw} k_l^4 \bar{r} \mu_x \\ &\quad - \frac{1}{16} k_l^4 \bar{p} + \left(\frac{1}{8} K_{\theta 1} k_l^4 \beta_{s1} - \frac{1}{8} K_{\theta 2} \beta_{c1} k_l^4 + \frac{1}{16} k_l^4 \beta_{c1} \right) \bar{r} + t_{14} \mu_x^2 \\ &\quad + \left(-\frac{1}{16} k_l^2 \beta_{s1} - \frac{1}{16} K_{\theta 1} k_l^2 \beta_{c1} - \frac{1}{16} K_{\theta 2} \beta_{s1} k_l^2 \right) \mu_y \mu_x + \left(\frac{1}{8} r_c^2 - \frac{1}{8} k_l^2 - \frac{11}{64} k_l^2 \beta_{c1}^2 \right) \mu_z \mu_x \\ t_2 &= \frac{1}{32} k_l^4 \beta_{s1}^2 + \frac{1}{32} k_l^4 \beta_{c1}^2 - \frac{1}{16} k_l^4 + \frac{1}{8} k_l^4 \bar{r} + \left(\frac{3}{32} r_c^2 - \frac{3}{32} k_l^2 \right) \mu_x^2 \\ t_3 &= \frac{1}{16} k_l^4 \beta_0 \beta_{s1} - \frac{1}{12} k_l^3 \beta_{c1} \lambda_0 + \frac{1}{12} k_l^3 \beta_{c1} \mu_z + \left(\frac{1}{6} r_c^3 - \frac{1}{6} k_l^3 \right) \mu_x + \frac{1}{6} k_l^3 \bar{r} \mu_x \\ t_{11} &= \frac{1}{16} k_l^4 \lambda_{s1} - \frac{1}{16} K_{\theta 1} k_l^4 \beta_{s1} + \left(\left(\frac{1}{16} K_{\theta 2} - \frac{1}{16} \right) k_l^4 + \frac{1}{12} e_f k_l^3 \right) \beta_{c1} \\ &\quad + \left(\frac{3}{128} - \frac{1}{32} K_{\theta 2} \right) k_l^4 \beta_{c1}^3 + \frac{1}{20} \theta_{tw} k_l^5 \beta_0 \beta_{s1} + \left(\frac{3}{128} - \frac{1}{32} K_{\theta 2} \right) k_l^4 \beta_{c1} \beta_{s1}^2 \\ t_{12} &= \frac{1}{6} K_{\theta 1} k_l^3 \beta_0 \beta_{c1} + \left(\frac{1}{16} \theta_{tw} k_l^4 - \frac{1}{4} k_l^2 \lambda_0 \right) \beta_{c1} + \left(\frac{1}{12} K_{\theta 2} k_l^3 + \frac{5}{8} e_f k_l^2 \right) \beta_{s1} \beta_0 \\ t_{13} &= \frac{1}{8} k_l^2 \lambda_0 - \frac{1}{8} \theta_{tw} k_l^4 + \frac{3}{16} k_l^2 \beta_{c1}^2 \lambda_0 + \left(\left(\frac{5}{48} - \frac{1}{8} K_{\theta 2} \right) k_l^3 - \frac{17}{32} e_f k_l^2 \right) \beta_{c1} \beta_{s1} \beta_0 - \frac{1}{6} K_{\theta 1} k_l^3 \beta_0 \\ t_{14} &= -\frac{3}{32} K_{\theta 1} k_l^2 \beta_{s1} + \left(\left(\frac{1}{32} + \frac{3}{32} K_{\theta 2} \right) k_l^2 - \frac{3}{32} K_{\theta 2} r_c^2 \right) \beta_{c1} + \frac{5}{64} k_l^2 \beta_{c1}^3 + \frac{9}{32} k_l^2 \beta_0 \beta_{c1} \end{aligned}$$

D

Longitudinal Aerodynamic Moment

The longitudinal aerodynamic moment coefficient generated by a single blade is:

$$C_{2s} = \sigma_s C_{l_\alpha} (t_1 + t_2 \theta_{c1} + t_3 \theta_{s1} + t_4 \theta_0) \quad (D.72)$$

where:

$$\begin{aligned} t_1 &= t_{11} + t_{12} \mu_z + t_{13} \mu_x + \left(-\frac{1}{8} \theta_{tw} k_l^4 + \frac{1}{8} k_l^2 \lambda_0 - \frac{1}{6} K_{\theta 1} k_l^3 \beta_0 \right) \mu_y \\ &\quad + \left(-\frac{3}{32} K_{\theta 1} k_l^2 \beta_{c1} - \frac{3}{32} K_{\theta 2} \beta_{s1} k_l^2 \right) \mu_y^2 - \frac{1}{8} k_l^2 \beta_{s1} \mu_z^2 - \frac{1}{12} k_l^3 \beta_0 \bar{r} \mu_x \\ &\quad - \frac{3}{20} k_l^5 \theta_{tw} \beta_0 \bar{p} - \frac{1}{16} k_l^4 \bar{q} + \left(-\frac{1}{16} k_l^4 \beta_{s1} + \frac{1}{8} k_l^4 K_{\theta 2} \beta_{s1} + \frac{1}{8} k_l^4 K_{\theta 1} \beta_{c1} \right) \bar{r} + t_{14} \mu_x^2 \\ &\quad + \left(-\frac{1}{16} K_{\theta 1} k_l^2 \beta_{s1} + \frac{1}{16} K_{\theta 2} \beta_{c1} k_l^2 + \frac{1}{16} k_l^2 \beta_{c1} \right) \mu_y \mu_x + t_{15} \mu_z \mu_x + \left(-\frac{1}{8} k_l^2 - \frac{11}{64} k_l^2 \beta_{s1}^2 \right) \mu_z \mu_y \\ t_2 &= t_{21} + \frac{5}{48} k_l^3 \beta_0 \beta_{s1} \mu_x - \frac{3}{32} k_l^2 \mu_y^2 - \frac{7}{64} k_l^4 \beta_{c1} \bar{p} + \frac{1}{8} k_l^4 \bar{r} - \frac{1}{32} \mu_x^2 k_l^2 \\ t_3 &= -\frac{5}{64} k_l^4 \beta_{s1} \bar{p} + \frac{5}{48} k_l^3 e_f \beta_{s1} \beta_{c1} + \frac{1}{12} k_l^3 \beta_0 \lambda_0 - \frac{1}{16} k_l^2 \mu_x \mu_y \\ &\quad + \frac{3}{32} k_l^2 \beta_{s1} \lambda_0 \mu_x - \frac{3}{32} k_l^2 \beta_{s1} \mu_x \mu_z - \frac{1}{12} k_l^3 \beta_0 \mu_z \end{aligned}$$

D

$$\begin{aligned}
 t_4 &= -\frac{1}{8}k_l^2\beta_0\mu_x\mu_z + \frac{1}{4}k_l^3e_f\beta_0\beta_{c1} - \frac{1}{12}k_l^3\beta_{s1}\mu_z + \frac{1}{16}k_l^4\beta_0\beta_{c1} \\
 &\quad + \frac{1}{6}k_l^3\bar{r}\mu_y - \frac{1}{6}k_l^3\mu_y - \frac{3}{16}k_l^4\beta_0\bar{p} + \frac{1}{12}k_l^3\beta_{s1}\lambda_0 + \frac{1}{24}k_l^3\beta_{s1}\beta_{c1}\mu_x \\
 t_{11} &= \frac{1}{16}k_l^4\lambda_{c1} + \left(\left(\frac{3}{16}k_l^4e_f + \frac{1}{20}k_l^5\right)\theta_{tw} + \left(-\frac{1}{12}K_{\theta 2}\lambda_0 + \frac{1}{12}\lambda_0\right)k_l^3 - \frac{5}{8}k_l^2e_f\lambda_0\right)\beta_{c1}\beta_0 \\
 &\quad + \left(\frac{1}{32}K_{\theta 2} - \frac{3}{128}\right)k_l^4\beta_{c1}^2\beta_{s1} + \left(\frac{1}{16}\theta_{tw}k_l^4\lambda_0 + \left(-\frac{1}{16}K_{\theta 2} + \frac{1}{16} + \frac{1}{16}\bar{C}_d\right)k_l^4 - \frac{1}{12}e_fk_l^3\right)\beta_{s1} \\
 &\quad - \frac{1}{16}k_l^4K_{\theta 1}\beta_{c1} + \frac{1}{32}k_l^4K_{\theta 1}\beta_{c1}^3 + \frac{1}{8}k_l^4K_{\theta 1}\beta_0^2\beta_{c1} + \frac{1}{6}k_l^3K_{\theta 1}\beta_0\beta_{s1}\lambda_0 \\
 &\quad + \frac{1}{32}k_l^4K_{\theta 1}\beta_{s1}^2\beta_{c1} + \left(\frac{1}{32}K_{\theta 2} - \frac{3}{128}\right)k_l^4\beta_{s1}^3 + \frac{1}{16}k_l^4K_{\theta 2}\beta_{s1}\beta_0^2 \\
 t_{12} &= \left(\frac{1}{12}K_{\theta 2}k_l^3 + \frac{5}{8}e_fk_l^2\right)\beta_{c1}\beta_0 + \left(-\frac{1}{16}\theta_{tw}k_l^4 + \frac{1}{4}k_l^2\lambda_0\right)\beta_{s1} - \frac{1}{6}K_{\theta 1}k_l^3\beta_0\beta_{s1} \\
 t_{13} &= \left(-\frac{1}{8}k_l^2\lambda_0 + \frac{1}{32}\theta_{tw}k_l^4\right)\beta_{c1}\beta_{s1} + \left(-\frac{11}{96} + \frac{5}{48}K_{\theta 2}\right)k_l^3\beta_{s1}^2\beta_0 \\
 &\quad + \frac{1}{6}k_l^3K_{\theta 1}\beta_0\beta_{s1}\beta_{c1} + \left(\frac{1}{6}\bar{C}_d + \frac{1}{12}\right)k_l^3\beta_0 - \frac{23}{64}k_l^2e_f\beta_0\beta_{c1}^2 \\
 t_{14} &= -\frac{3}{64}k_l^2\beta_{s1}\beta_{c1}^2 + \left(\frac{1}{32} - \frac{1}{32}K_{\theta 2}\right)k_l^2\beta_{s1} - \frac{1}{32}K_{\theta 1}k_l^2\beta_{c1} \\
 t_{15} &= \left(\frac{5}{32} + \frac{1}{16}K_{\theta 2}\right)k_l^2\beta_{c1}\beta_{s1} - \frac{3}{32}K_{\theta 1}k_l^2\beta_{s1}^2 - \frac{1}{12}\theta_{tw}k_l^3\beta_0
 \end{aligned}$$

Shaft Torque

The shaft torque coefficient generated by a single blade is:

$$\begin{aligned}
 C_{Mzs} &= \sigma_s C_{l_\alpha} \left(t_1 + \frac{1}{16}\theta_{c1}^2\bar{C}_{d2}k_l^4 + \left(\frac{1}{8}\mu_x^2\bar{C}_{d2}k_l^2 + \frac{1}{8}\bar{C}_{d2}k_l^4\right)\theta_0^2 \right. \\
 &\quad \left. + \left(\frac{1}{16}\bar{C}_{d2}k_l^4 + \frac{3}{32}\mu_x^2\bar{C}_{d2}k_l^2\right)\theta_{s1}^2 + \left(-\frac{3}{8}\bar{C}_{d2}k_l^4\beta_0\beta_{c1} + \frac{1}{3}\bar{C}_{d2}k_l^3\mu_y\right)\theta_0\theta_{c1} \right. \\
 &\quad \left. + t_2\theta_{c1} + t_3\theta_{s1} + t_4\theta_0 + \left(\frac{1}{3}\bar{C}_{d2}k_l^3\mu_x - \frac{3}{8}\bar{C}_{d2}k_l^4\beta_0\beta_{s1}\right)\theta_0\theta_{s1} \right)
 \end{aligned} \tag{D.73}$$

where:

$$\begin{aligned}
 t_1 &= t_{11} + t_{12}\mu_z + t_{13}\mu_x + t_{14}\mu_y + \frac{1}{3}k_l^3\beta_0\beta_{s1}\bar{p}\mu_z - \frac{3}{32}k_l^2\beta_{s1}^2\mu_y^2 - \frac{1}{16}\theta_{tw}k_l^4\bar{q}\mu_y \\
 &\quad - \frac{1}{6}k_l^3\beta_0\bar{p}\mu_y - \frac{1}{16}k_l^4\bar{p}^2 + \left(\frac{1}{6}K_{\theta 1}k_l^3\beta_0 + \frac{1}{8}\theta_{tw}k_l^4\right)\bar{r}\mu_z + t_{15}\mu_z^2 \\
 &\quad + \left(-\frac{1}{12}K_{\theta 2}\beta_{s1}k_l^3\beta_0 - \frac{1}{16}\theta_{tw}k_l^4\beta_{c1} - \frac{1}{6}K_{\theta 1}k_l^3\beta_0\beta_{c1}\right)\mu_x\bar{r} - \frac{1}{16}k_l^4\bar{q}^2 \\
 &\quad + t_{16}\bar{p} + t_{17}\bar{q} + t_{18}\bar{r} + t_{19}\mu_x^2 + t_{110}\mu_y\mu_x + \frac{1}{3}k_l^3\beta_0\beta_{c1}\bar{q}\mu_z + t_{111}\mu_z\mu_x \\
 &\quad + t_{112}\mu_z\mu_y + \left(-\frac{1}{12}K_{\theta 1}k_l^3\beta_0 - \frac{1}{16}\theta_{tw}k_l^4\right)\mu_x\bar{p} + \frac{1}{6}k_l^3\beta_0\bar{q}\mu_x
 \end{aligned}$$

D.2 Expressions of the Generic Flight Mechanics Model

207

$$\begin{aligned}
 t_2 &= t_{21} + \frac{1}{4}k_l^3\beta_0\beta_{c1}\mu_z + t_{22}\mu_x + \left(\frac{1}{4}\theta_{tw}\bar{C}_{d2}k_l^4 + \frac{1}{3}K_{\theta1}\bar{C}_{d2}k_l^3\beta_0 + \frac{1}{8}k_l^2\lambda_0\right)\mu_y - \frac{1}{12}k_l^3\beta_0\bar{r}\mu_x \\
 &\quad + \left(\frac{1}{8}\bar{C}_{d2}k_l^4 - \frac{1}{16}k_l^4\right)\bar{q} - \frac{1}{16}k_l^4\beta_{s1}\bar{r} + \left(-\frac{1}{16}\bar{C}_{d2}k_l^2\beta_{s1} + \frac{1}{32}k_l^2\beta_{s1} + \frac{1}{16}\beta_{s1}K_{\theta2}\bar{C}_{d2}k_l^2\right)\mu_x^2 \\
 &\quad + \frac{1}{16}k_l^2\beta_{c1}\mu_x\mu_y + \frac{1}{16}k_l^2\beta_{s1}\beta_{c1}\mu_x\mu_z + \left(\frac{1}{4}\bar{C}_{d2}k_l^2 - \frac{1}{8}k_l^2\right)\mu_z\mu_y \\
 t_3 &= t_{31} + \frac{1}{4}k_l^3\beta_0\beta_{s1}\mu_z + t_{32}\mu_x + \left(\frac{1}{6}\bar{C}_{d2}k_l^3\beta_0 - \frac{1}{12}k_l^3\beta_0 + \frac{1}{6}k_l^3\beta_0\beta_{s1}^2\right)\mu_y \\
 &\quad + \left(\frac{1}{8}\bar{C}_{d2}k_l^4 - \frac{1}{16}k_l^4\right)\bar{p} + \frac{1}{16}k_l^4\beta_{c1}\bar{r} + t_{33}\mu_x^2 - \frac{1}{16}k_l^2\beta_{s1}\mu_x\mu_y + t_{34}\mu_z\mu_x \\
 t_4 &= t_{41} + t_{42}\mu_z + t_{43}\mu_x + t_{44}\mu_y - \frac{1}{12}k_l^3\bar{q}\mu_y + \frac{1}{6}k_l^3\bar{r}\mu_z - \frac{1}{12}k_l^3\beta_{c1}\bar{r}\mu_x + \frac{3}{16}k_l^4\beta_0\beta_{s1}\bar{p} + \frac{3}{16}k_l^4\beta_0\beta_{c1}\bar{q} \\
 &\quad + \left(-\frac{2}{5}\theta_{tw}\bar{C}_{d2}k_l^5 - \frac{1}{6}k_l^3\lambda_0\right)\bar{r} + \left(\frac{1}{4}K_{\theta1}\bar{C}_{d2}k_l^2\beta_0 + \frac{1}{6}\theta_{tw}\bar{C}_{d2}k_l^3 - \frac{3}{32}k_l^2\beta_0\beta_{s1}\beta_{c1}\right)\mu_x^2 \\
 &\quad + \frac{1}{4}k_l^2\beta_0\beta_{s1}\mu_x\mu_z + \left(-\frac{1}{12}k_l^3 + \frac{1}{6}\bar{C}_{d2}k_l^3\right)\mu_x\bar{p} \\
 t_{11} &= \frac{1}{12}\theta_{tw}^2\bar{C}_{d2}k_l^6 + \left(\frac{1}{8} - \frac{1}{4}\bar{C}_{d2}\right)\lambda_0k_l^4\theta_{tw} + \left(-\frac{1}{16}\lambda_{c1}^2 + \frac{1}{8}\bar{C}_d - \frac{1}{16}\lambda_{s1}^2\right)k_l^4 \\
 &\quad + \left(-\frac{1}{4} + \frac{1}{4}\bar{C}_{d2}\right)\lambda_0^2k_l^2 + \frac{1}{4}\lambda_0^2r_c^2 + \left(-\frac{1}{16}\theta_{tw}k_l^4\lambda_0\right. \\
 &\quad \left.+ \left(\frac{1}{16}K_{\theta1}^2\bar{C}_{d2} + \frac{1}{16}K_{\theta2}^2\bar{C}_{d2} + \left(\frac{1}{16} - \frac{1}{8}\bar{C}_{d2}\right)K_{\theta2} - \frac{1}{16} + \frac{1}{16}\bar{C}_{d2} - \frac{3}{32}\bar{C}_d\right)k_l^4\right. \\
 &\quad \left.+ \left(\left(-\frac{1}{12} + \frac{1}{6}\bar{C}_{d2}\right)e_fK_{\theta2} + \left(\frac{1}{6} - \frac{1}{6}\bar{C}_{d2}\right)e_f\right)k_l^3 - \frac{1}{8}e_f^2k_l^2\right)\beta_{s1}^2 + \left(-\frac{1}{16}\theta_{tw}k_l^4\lambda_0\right. \\
 &\quad \left.+ \left(\frac{1}{16}K_{\theta1}^2\bar{C}_{d2} + \frac{1}{16}K_{\theta2}^2\bar{C}_{d2} + \left(\frac{1}{16} - \frac{1}{8}\bar{C}_{d2}\right)K_{\theta2} - \frac{1}{16} + \frac{1}{16}\bar{C}_{d2} - \frac{3}{32}\bar{C}_d\right)k_l^4\right. \\
 &\quad \left.+ \left(\left(-\frac{1}{12} + \frac{1}{6}\bar{C}_{d2}\right)e_fK_{\theta2} + \left(\frac{1}{6} - \frac{1}{6}\bar{C}_{d2}\right)e_f\right)k_l^3 - \frac{1}{8}e_f^2k_l^2\right)\beta_{c1}^2 \\
 &\quad - \frac{1}{4}K_{\theta1}k_l^3\beta_0\beta_{s1}^2\lambda_0 - \frac{1}{16}K_{\theta2}\beta_{c1}^2k_l^4\beta_0^2 - \frac{3}{16}\bar{C}_dk_l^4\beta_0^2 - \frac{1}{16}K_{\theta2}\beta_{s1}^2k_l^4\beta_0^2 \\
 &\quad + \left(\frac{1}{64} - \frac{1}{32}K_{\theta2}\right)k_l^4\beta_{s1}^2\beta_{c1}^2 + \left(\frac{1}{5}\theta_{tw}\bar{C}_{d2}K_{\theta1}k_l^5 + \left(-\frac{1}{3}\bar{C}_{d2} + \frac{1}{6}\right)\lambda_0K_{\theta1}k_l^3\right)\beta_0 \\
 &\quad + \left(\left(\frac{1}{16}K_{\theta1}\lambda_{s1} + \left(\frac{1}{16} - \frac{1}{8}\bar{C}_{d2}\right)\lambda_{c1}K_{\theta2} + \left(\frac{1}{8}\bar{C}_{d2} - \frac{1}{8}\right)\lambda_{c1}\right)k_l^4 + \frac{1}{6}e_fk_l^3\lambda_{c1}\right)\beta_{s1} \\
 &\quad + \left(\left(\frac{1}{16}K_{\theta1}\lambda_{c1} + \left(-\frac{1}{16} + \frac{1}{8}\bar{C}_{d2}\right)\lambda_{s1}K_{\theta2} + \left(\frac{1}{8} - \frac{1}{8}\bar{C}_{d2}\right)\lambda_{s1}\right)k_l^4 - \frac{1}{6}e_fk_l^3\lambda_{s1}\right)\beta_{c1} \\
 &\quad - \frac{1}{64}K_{\theta2}\beta_{c1}^4k_l^4 - \frac{1}{64}K_{\theta2}\beta_{s1}^4k_l^4 - \frac{1}{4}K_{\theta1}k_l^3\beta_0\beta_{c1}^2\lambda_0 \\
 t_{12} &= \left(\frac{1}{4}\bar{C}_{d2} - \frac{1}{8}\right)k_l^4\theta_{tw} + \left(\frac{1}{2} - \frac{1}{2}\bar{C}_{d2}\right)\lambda_0k_l^2 - \frac{1}{2}r_c^2\lambda_0 + \left(-\frac{1}{4}k_l^2\lambda_0 + \frac{3}{32}\theta_{tw}k_l^4\right)\beta_{s1}^2 \\
 &\quad + \left(-\frac{1}{4}k_l^2\lambda_0 + \frac{3}{32}\theta_{tw}k_l^4\right)\beta_{c1}^2 + \frac{3}{8}K_{\theta1}k_l^3\beta_0\beta_{s1}^2 - \frac{1}{3}k_l^3\beta_0\beta_{c1}\lambda_{c1} \\
 &\quad + \left(\frac{3}{16}\theta_{tw}k_l^4 - \frac{1}{2}k_l^2\lambda_0\right)\beta_0^2 + \left(-\frac{1}{6} + \frac{1}{3}\bar{C}_{d2}\right)K_{\theta1}k_l^3\beta_0 - \frac{1}{3}k_l^3\beta_0\beta_{s1}\lambda_{s1} + \frac{3}{8}K_{\theta1}k_l^3\beta_0\beta_{c1}^2
 \end{aligned}$$

D

D

$$\begin{aligned}
 t_{13} = & \frac{1}{16} \theta_{tw} k_l^4 \lambda_{s1} + \left(\left(-\frac{1}{6} \bar{C}_{d2} + \frac{1}{12} - \frac{1}{3} \bar{C}_{d2} K_{\theta 2} \right) K_{\theta 1} k_l^3 + \frac{1}{8} e_f K_{\theta 1} k_l^2 \right) \beta_{c1} \beta_0 - \frac{7}{32} K_{\theta 1} k_l^3 \beta_0 \beta_{s1} \beta_{c1} \\
 & + \left(\frac{1}{12} K_{\theta 1} \lambda_{s1} - \frac{1}{6} \lambda_{c1} \right) k_l^3 \beta_0 - \frac{7}{24} K_{\theta 1} k_l^3 \beta_0^3 \beta_{c1} + \left(\frac{1}{16} - \frac{1}{12} K_{\theta 2} \right) k_l^3 \beta_{c1}^2 \beta_{s1} \beta_0 \\
 & + \left(\frac{1}{16} - \frac{1}{12} K_{\theta 2} \right) k_l^3 \beta_0 \beta_{s1}^3 + \left(\frac{1}{4} \theta_{tw} \bar{C}_{d2} K_{\theta 1} k_l^4 + \left(\frac{1}{8} - \frac{1}{4} \bar{C}_{d2} \right) \lambda_0 K_{\theta 1} k_l^2 \right) \beta_{s1} \\
 & + \left(\left(-\frac{1}{4} K_{\theta 2} \bar{C}_{d2} k_l^4 + \left(-\frac{1}{6} \bar{C}_{d2} + \frac{1}{12} \right) e_f k_l^3 \right) \theta_{tw} \right. \\
 & \quad \left. + \left(\left(\frac{1}{4} \bar{C}_{d2} - \frac{1}{8} \right) \lambda_0 K_{\theta 2} + \left(-\frac{1}{4} + \frac{1}{4} \bar{C}_{d2} \right) \lambda_0 \right) k_l^2 + \left(\frac{1}{8} K_{\theta 2} \lambda_0 + \frac{1}{4} \lambda_0 \right) r_c^2 \right) \beta_{c1} \\
 & + \left(\frac{3}{32} k_l^2 \lambda_0 - \frac{5}{128} \theta_{tw} k_l^4 \right) \beta_{c1}^3 - \frac{7}{32} K_{\theta 1} k_l^3 \beta_0 \beta_{c1}^3 + \left(\frac{3}{8} k_l^2 \lambda_0 - \frac{5}{32} \theta_{tw} k_l^4 \right) \beta_0^2 \beta_{c1} \\
 & + \left(\left(\frac{1}{3} K_{\theta 1}^2 \bar{C}_{d2} + \left(-\frac{1}{6} \bar{C}_{d2} + \frac{1}{12} \right) K_{\theta 2} - \frac{1}{3} \bar{C}_d + \frac{1}{6} \bar{C}_{d2} - \frac{1}{6} \right) k_l^3 + \frac{1}{4} e_f k_l^2 + \frac{1}{6} r_c^3 \right) \beta_{s1} \beta_0 \\
 & + \left(\frac{3}{32} k_l^2 \lambda_0 - \frac{5}{128} \theta_{tw} k_l^4 \right) \beta_{c1} \beta_{s1}^2 \\
 t_{14} = & \frac{1}{16} \theta_{tw} k_l^4 \lambda_{c1} + \left(\left(\left(-\frac{1}{6} \bar{C}_{d2} + \frac{1}{12} \right) K_{\theta 2} + \frac{1}{6} \bar{C}_{d2} - \frac{1}{6} \right) k_l^3 + \frac{1}{4} e_f k_l^2 \right) \beta_{c1} \beta_0 \\
 & + \frac{1}{6} k_l^3 \beta_0 \lambda_{s1} + \left(\left(\frac{1}{4} K_{\theta 2} \bar{C}_{d2} k_l^4 - \frac{1}{12} e_f k_l^3 \right) \theta_{tw} + \left(\frac{1}{8} K_{\theta 2} \lambda_0 + \frac{1}{4} \lambda_0 \right) k_l^2 \right) \beta_{s1} \\
 & + \left(\frac{1}{8} K_{\theta 1} k_l^2 \lambda_0 + \frac{1}{4} \theta_{tw} \bar{C}_{d2} K_{\theta 1} k_l^4 \right) \beta_{c1} + \left(\frac{1}{3} \bar{C}_{d2} K_{\theta 2} - \frac{1}{12} \right) K_{\theta 1} k_l^3 \beta_{s1} \beta_0 \\
 t_{15} = & \left(-\frac{1}{4} + \frac{1}{4} \bar{C}_{d2} \right) k_l^2 + \frac{1}{4} r_c^2 + \frac{3}{16} k_l^2 \beta_{s1}^2 + \frac{3}{16} k_l^2 \beta_{c1}^2 + \frac{3}{8} k_l^2 \beta_0^2 \\
 t_{16} = & \frac{1}{8} k_l^4 \lambda_{s1} - \frac{1}{16} K_{\theta 1} k_l^4 \beta_{s1} \\
 & + \left(\left(\left(\frac{1}{16} - \frac{1}{8} \bar{C}_{d2} \right) K_{\theta 2} + \frac{1}{8} \bar{C}_{d2} - \frac{1}{8} \right) k_l^4 + \frac{1}{6} e_f k_l^3 \right) \beta_{c1} + \frac{3}{20} \theta_{tw} k_l^5 \beta_0 \beta_{s1} \\
 t_{17} = & \frac{1}{8} k_l^4 \lambda_{c1} + \frac{3}{20} k_l^5 \theta_{tw} \beta_0 \beta_{c1} \\
 & + \left(\left(\left(\left(-\frac{1}{16} + \frac{1}{8} \bar{C}_{d2} \right) K_{\theta 2} + \frac{1}{8} - \frac{1}{8} \bar{C}_{d2} \right) k_l^4 - \frac{1}{6} e_f k_l^3 \right) \beta_{s1} - \frac{1}{16} k_l^4 K_{\theta 1} \beta_{c1} \right. \\
 t_{18} = & -\frac{1}{4} \bar{C}_d k_l^4 - \frac{1}{16} K_{\theta 2} \beta_{s1}^2 k_l^4 - \frac{1}{16} K_{\theta 2} \beta_{c1}^2 k_l^4 - \frac{1}{8} \theta_{tw} k_l^4 \lambda_0 \\
 t_{19} = & \frac{1}{8} \bar{C}_d k_l^2 + \frac{1}{16} \theta_{tw}^2 \bar{C}_{d2} k_l^4 + \left(\frac{1}{16} - \frac{1}{8} \bar{C}_{d2} K_{\theta 2} - \frac{1}{8} \bar{C}_{d2} \right) K_{\theta 1} k_l^2 \beta_{c1} \beta_{s1} \\
 & + \left(-\frac{1}{32} + \left(-\frac{1}{16} \bar{C}_{d2} + \frac{1}{32} \right) K_{\theta 2} \right) k_l^2 \beta_{s1}^2 \\
 & + \left(\left(\frac{3}{32} K_{\theta 2}^2 \bar{C}_{d2} + \left(-\frac{1}{32} + \frac{1}{16} \bar{C}_{d2} \right) K_{\theta 2} + \frac{3}{32} \bar{C}_{d2} - \frac{3}{32} \right) k_l^2 + \frac{3}{32} r_c^2 \right) \beta_{c1}^2 \\
 & + \frac{9}{32} k_l^2 \beta_0^2 \beta_{c1}^2 - \frac{1}{8} k_l^2 \beta_0^2 + \frac{3}{64} k_l^2 \beta_{s1}^2 \beta_{c1}^2 + \frac{1}{6} \theta_{tw} K_{\theta 1} \bar{C}_{d2} k_l^3 \beta_0 + \frac{5}{128} k_l^2 \beta_{c1}^4 \\
 t_{110} = & \left(\frac{1}{8} + \left(\frac{1}{8} - \frac{1}{4} \bar{C}_{d2} \right) K_{\theta 2} \right) k_l^2 \beta_{c1} \beta_{s1} - \frac{1}{16} K_{\theta 1} k_l^2 \beta_{s1}^2 + \frac{1}{16} K_{\theta 1} k_l^2 \beta_{c1}^2 \\
 t_{111} = & \frac{3}{32} K_{\theta 1} k_l^2 \beta_{s1} \beta_{c1}^2 + \left(\left(\frac{1}{4} \bar{C}_{d2} - \frac{1}{8} \right) K_{\theta 1} k_l^2 + \frac{1}{8} K_{\theta 1} r_c^2 \right) \beta_{s1} \\
 & + \left(\left(\left(\frac{1}{8} - \frac{1}{4} \bar{C}_{d2} \right) K_{\theta 2} + \frac{1}{4} - \frac{1}{4} \bar{C}_{d2} \right) k_l^2 + \left(-\frac{1}{4} - \frac{1}{8} K_{\theta 2} \right) r_c^2 \right) \beta_{c1} \\
 & - \frac{3}{16} k_l^2 \beta_{c1}^3 - \frac{3}{4} k_l^2 \beta_0^2 \beta_{c1} + \frac{1}{6} \theta_{tw} k_l^3 \beta_0 \beta_{s1} - \frac{3}{16} k_l^2 \beta_{s1}^2 \beta_{c1} + \frac{3}{32} K_{\theta 1} k_l^2 \beta_{s1}^3 + \frac{3}{8} K_{\theta 1} k_l^2 \beta_0^2 \beta_{s1}
 \end{aligned}$$

$$\begin{aligned}
 t_{112} &= \frac{3}{16} k_l^2 \beta_{s1} \beta_{c1}^2 + \left(\left(\left(\frac{1}{4} \bar{C}_{d2} - \frac{1}{8} \right) K_{\theta 2} - \frac{1}{4} + \frac{1}{4} \bar{C}_{d2} \right) k_l^2 + \frac{1}{4} r_c^2 \right) \beta_{s1} \\
 &\quad - \frac{1}{8} K_{\theta 1} k_l^2 \beta_{c1} + \frac{3}{16} k_l^2 \beta_{s1}^3 + \frac{3}{4} k_l^2 \beta_0^2 \beta_{s1} \\
 t_{21} &= \left(\frac{1}{16} - \frac{1}{8} \bar{C}_{d2} \right) \lambda_{c1} k_l^4 + \left(-\frac{1}{6} k_l^3 \lambda_0 - \frac{3}{10} \theta_{tw} \bar{C}_{d2} k_l^5 \right) \beta_{c1} \beta_0 - \frac{1}{64} k_l^4 \beta_{s1} \beta_{c1}^2 \\
 &\quad + \left(\left(-\frac{1}{8} \bar{C}_{d2} + \frac{1}{8} \bar{C}_{d2} K_{\theta 2} + \frac{1}{16} \right) k_l^4 + \left(-\frac{1}{12} + \frac{1}{6} \bar{C}_{d2} \right) e_f k_l^3 \right) \beta_{s1} \\
 &\quad + \frac{1}{8} K_{\theta 1} \bar{C}_{d2} k_l^4 \beta_{c1} - \frac{1}{64} k_l^4 \beta_{s1}^3 - \frac{1}{16} k_l^4 \beta_0^2 \beta_{s1} \\
 t_{22} &= -\frac{1}{12} k_l^3 \beta_0 \beta_{s1}^2 + \left(-\frac{1}{6} \bar{C}_{d2} + \frac{1}{12} \right) k_l^3 \beta_0 - \frac{1}{6} k_l^3 \beta_0 \beta_{c1}^2 \\
 t_{31} &= \left(\frac{1}{16} - \frac{1}{8} \bar{C}_{d2} \right) \lambda_{s1} k_l^4 + \frac{1}{8} K_{\theta 1} \bar{C}_{d2} k_l^4 \beta_{s1} \\
 &\quad + \left(\left(-\frac{1}{8} \bar{C}_{d2} K_{\theta 2} + \frac{1}{8} \bar{C}_{d2} - \frac{1}{16} \right) k_l^4 + \left(-\frac{1}{6} \bar{C}_{d2} + \frac{1}{12} \right) e_f k_l^3 \right) \beta_{c1} \\
 &\quad + \frac{1}{64} k_l^4 \beta_{c1}^3 + \frac{1}{16} k_l^4 \beta_0^2 \beta_{c1} + \left(-\frac{1}{6} k_l^3 \lambda_0 - \frac{3}{10} \theta_{tw} \bar{C}_{d2} k_l^5 \right) \beta_{s1} \beta_0 + \frac{1}{64} k_l^4 \beta_{s1}^2 \beta_{c1} \\
 t_{32} &= \frac{1}{4} \theta_{tw} \bar{C}_{d2} k_l^4 + \left(\frac{1}{8} - \frac{1}{4} \bar{C}_{d2} \right) \lambda_0 k_l^2 - \frac{1}{8} r_c^2 \lambda_0 - \frac{1}{12} k_l^3 \beta_0 \beta_{s1} \beta_{c1} + \frac{1}{3} K_{\theta 1} \bar{C}_{d2} k_l^3 \beta_0 \\
 t_{33} &= \frac{3}{16} K_{\theta 1} \bar{C}_{d2} k_l^2 \beta_{s1} + \left(-\frac{1}{16} \bar{C}_{d2} - \frac{3}{16} \bar{C}_{d2} K_{\theta 2} + \frac{1}{32} \right) k_l^2 \beta_{c1} \\
 t_{34} &= \left(\frac{1}{4} \bar{C}_{d2} - \frac{1}{8} \right) k_l^2 + \frac{1}{8} r_c^2 + \frac{3}{32} k_l^2 \beta_{s1}^2 \\
 t_{41} &= \frac{1}{5} \theta_{tw} \bar{C}_{d2} k_l^5 + \left(-\frac{1}{3} \bar{C}_{d2} + \frac{1}{6} \right) \lambda_0 k_l^3 - \frac{1}{6} r_c^3 \lambda_0 + \left(-\frac{3}{20} \theta_{tw} \bar{C}_{d2} k_l^5 - \frac{1}{12} k_l^3 \lambda_0 \right) \beta_{s1}^2 \\
 &\quad + \left(-\frac{3}{20} \theta_{tw} \bar{C}_{d2} k_l^5 - \frac{1}{12} k_l^3 \lambda_0 \right) \beta_{c1}^2 - \frac{9}{16} K_{\theta 1} \bar{C}_{d2} k_l^4 \beta_0 \beta_{s1}^2 \\
 &\quad - \frac{1}{6} k_l^3 \beta_0^2 \lambda_0 + \frac{1}{4} K_{\theta 1} \bar{C}_{d2} k_l^4 \beta_0 - \frac{9}{16} K_{\theta 1} \bar{C}_{d2} k_l^4 \beta_0 \beta_{c1}^2 \\
 t_{42} &= \left(-\frac{1}{6} + \frac{1}{3} \bar{C}_{d2} \right) k_l^3 + \frac{1}{6} r_c^3 + \frac{1}{8} k_l^3 \beta_{s1}^2 + \frac{1}{8} k_l^3 \beta_{c1}^2 + \frac{1}{4} k_l^3 \beta_0^2 \\
 t_{43} &= \left(-\frac{1}{6} \bar{C}_{d2} + \frac{1}{12} \right) \lambda_{s1} k_l^3 + \frac{1}{3} K_{\theta 1} \bar{C}_{d2} k_l^3 \beta_{s1} \\
 &\quad + \left(-\frac{1}{3} K_{\theta 2} \bar{C}_{d2} k_l^3 + \left(\frac{1}{8} - \frac{1}{4} \bar{C}_{d2} \right) e_f k_l^2 \right) \beta_{c1} - \frac{5}{96} k_l^3 \beta_{c1}^3 - \frac{5}{24} k_l^3 \beta_0^2 \beta_{c1} - \frac{5}{96} k_l^3 \beta_{s1}^2 \beta_{c1} \\
 t_{44} &= \frac{1}{12} k_l^3 \lambda_{c1} + \left(\frac{1}{3} K_{\theta 2} \bar{C}_{d2} k_l^3 - \frac{1}{8} e_f k_l^2 \right) \beta_{s1} + \frac{1}{3} K_{\theta 1} \bar{C}_{d2} k_l^3 \beta_{c1}
 \end{aligned}$$

D

Harmonic Components of Thrust

The first order harmonic thrust components generated by one blade are:

$$C_{Tss} = \sigma_s C_{l_\alpha} (t_1 + t_2 \theta_{c1} + t_3 \theta_{s1} + t_4 \theta_0) \quad (\text{D.74})$$

where:

$$\begin{aligned}
 t_1 &= t_{11} + \frac{3}{4}k_l^2\beta_0\beta_{s1}\mu_z + t_{12}\mu_x + t_{13}\mu_y + \left(\frac{1}{8}K_{\theta 2}\beta_{c1}k_l - \frac{1}{8}k_l\beta_{c1}\right)\mu_y^2 \\
 &\quad + \left(\frac{1}{3}\theta_{tw}k_l^3 + \frac{1}{2}K_{\theta 1}k_l^2\beta_0\right)\mu_x\bar{r} + \left(\frac{1}{6}k_l^3\beta_{s1}^2 - \frac{1}{6}k_l^3\right)\bar{p} + \left(\frac{1}{6}k_l^3\beta_{s1}\beta_{c1} - \frac{1}{6}K_{\theta 2}\beta_{s1}k_l^3\beta_{c1}\right)\bar{q} \\
 &\quad + \left(\frac{1}{6}k_l^3\beta_{c1} + \frac{1}{3}K_{\theta 1}k_l^3\beta_{s1} - \frac{1}{3}K_{\theta 2}\beta_{c1}k_l^3\right)\bar{r} + t_{14}\mu_x^2 + t_{15}\mu_y\mu_x + t_{16}\mu_z\mu_x \\
 t_2 &= \left(\left(-\frac{1}{4}k_l + \frac{1}{4}r_c\right)\mu_y + \frac{1}{4}k_l^2\beta_0\beta_{c1}\right)\mu_x + \frac{1}{8}k_l^3\beta_{s1}\beta_{c1} \\
 t_3 &= t_{31} + \frac{3}{4}k_l^2\beta_0\beta_{s1}\mu_x - \frac{1}{8}\mu_y^2k_l + \frac{1}{4}k_l^3\beta_{s1}\bar{q} + \frac{1}{3}k_l^3\bar{r} + \left(\frac{5}{32}k_l\beta_{s1}^2 - \frac{3}{8}k_l + \frac{3}{8}r_c\right)\mu_x^2 \\
 t_4 &= \frac{1}{2}k_l^3\beta_0\beta_{s1} + t_{41}\mu_x + \frac{1}{4}k_l^2\beta_{s1}\beta_{c1}\mu_y + \frac{1}{2}k_l^2\bar{r}\mu_x + \frac{1}{3}k_l^3\beta_0\bar{q} + \frac{3}{8}\mu_x^2k_l\beta_0\beta_{s1} + \frac{3}{8}k_l^2\beta_{s1}\bar{q}\mu_x \\
 t_{11} &= \frac{1}{6}k_l^3\lambda_{s1} + \frac{3}{16}K_{\theta 1}k_l^3\beta_{s1}\beta_{c1}^2 + \left(\frac{1}{6}K_{\theta 1}r_c^3 - \frac{1}{6}K_{\theta 1}k_l^3\right)\beta_{s1} \\
 &\quad + \left(\left(-\frac{1}{6} + \frac{1}{6}K_{\theta 2}\right)k_l^3 + \frac{1}{4}e_fk_l^2 + \left(\frac{1}{6} - \frac{1}{6}K_{\theta 2}\right)r_c^3 - \frac{1}{4}e_fr_c^2\right)\beta_{c1} \\
 &\quad + \left(-\frac{1}{16}K_{\theta 2} + \frac{1}{24}\right)k_l^3\beta_{c1}^3 + \left(\frac{1}{6} - \frac{1}{4}K_{\theta 2}\right)k_l^3\beta_0^2\beta_{c1} + \left(\frac{3}{8}\theta_{tw}k_l^4 - \frac{1}{2}k_l^2\lambda_0\right)\beta_{s1}\beta_0 \\
 &\quad + \left(-\frac{1}{16}K_{\theta 2} + \frac{1}{24}\right)k_l^3\beta_{c1}\beta_{s1}^2 + \frac{3}{16}K_{\theta 1}k_l^3\beta_{s1}^3 + \frac{3}{4}K_{\theta 1}k_l^3\beta_0^2\beta_{s1} \\
 t_{12} &= \left(\frac{1}{3}r_c^3 - \frac{1}{3}k_l^3\right)\theta_{tw} + \frac{1}{2}k_l\lambda_0 - \frac{1}{2}r_c\lambda_0 + \left(\frac{1}{4}\theta_{tw}k_l^3 - \frac{3}{16}k_l\lambda_0\right)\beta_{s1}^2 + \frac{1}{12}\theta_{tw}k_l^3\beta_{c1}^2 + \frac{9}{8}K_{\theta 1}k_l^2\beta_0\beta_{s1}^2 \\
 &\quad + \frac{1}{3}\theta_{tw}k_l^3\beta_0^2 + \left(-\frac{1}{2}K_{\theta 2} - \frac{1}{4}\right)k_l^2\beta_{c1}\beta_{s1}\beta_0 + \left(\frac{1}{2}K_{\theta 1}r_c^2 - \frac{1}{2}K_{\theta 1}k_l^2\right)\beta_0 + \frac{3}{8}K_{\theta 1}k_l^2\beta_0\beta_{c1}^2 \\
 t_{13} &= \frac{3}{4}K_{\theta 1}k_l^2\beta_0\beta_{s1}\beta_{c1} + \frac{1}{6}\theta_{tw}k_l^3\beta_{s1}\beta_{c1} + \frac{1}{2}k_l^2\beta_0\beta_{s1}^2 - \frac{1}{4}k_l^2\beta_0 \\
 t_{14} &= \left(-\frac{3}{8}K_{\theta 1}k_l + \frac{3}{8}K_{\theta 1}r_c\right)\beta_{s1} + \left(\left(\frac{3}{8}K_{\theta 2} + \frac{1}{8}\right)k_l + \left(-\frac{3}{8}K_{\theta 2} - \frac{1}{8}\right)r_c\right)\beta_{c1} \\
 &\quad + \frac{3}{16}\theta_{tw}k_l^2\beta_0\beta_{s1} + \left(-\frac{3}{32} - \frac{3}{32}K_{\theta 2}\right)k_l\beta_{c1}\beta_{s1}^2 + \frac{5}{32}K_{\theta 1}k_l\beta_{s1}^3 + \frac{9}{16}K_{\theta 1}k_l\beta_0^2\beta_{s1} \\
 t_{15} &= \left(\left(-\frac{1}{4} - \frac{1}{4}K_{\theta 2}\right)k_l + \left(\frac{1}{4} + \frac{1}{4}K_{\theta 2}\right)r_c\right)\beta_{s1} + \left(\frac{1}{4}K_{\theta 1}r_c - \frac{1}{4}K_{\theta 1}k_l\right)\beta_{c1} \\
 t_{16} &= \frac{1}{2}r_c - \frac{1}{2}k_l + \left(-\frac{3}{8}r_c + \frac{3}{8}k_l\right)\beta_{s1}^2 + \frac{1}{8}k_l\beta_{c1}^2 + \frac{1}{2}k_l\beta_0^2
 \end{aligned}$$

$$C_{Tsc} = \sigma_s C_{l_\alpha} (t_1 + t_2\theta_{c1} + t_3\theta_{s1} + t_4\theta_0) \quad (D.75)$$

where:

$$\begin{aligned}
 t_1 &= t_{11} + \frac{3}{4}k_l^2\beta_0\beta_{c1}\mu_z + t_{12}\mu_x + t_{13}\mu_y + t_{14}\mu_y^2 + \frac{1}{3}\theta_{tw}k_l^3\bar{r}\mu_y - \frac{1}{4}k_l^2\beta_0\bar{r}\mu_x \\
 &\quad + \left(\frac{1}{6}k_l^3\beta_{s1}\beta_{c1} - \frac{1}{6}K_{\theta 2}\beta_{s1}k_l^3\beta_{c1}\right)\bar{p} + \left(\frac{1}{6}k_l^3\beta_{c1}^2 - \frac{1}{6}k_l^3\right)\bar{q} \\
 &\quad + \left(-\frac{1}{6}k_l^3\beta_{s1} + \frac{1}{3}K_{\theta 1}k_l^3\beta_{c1} + \frac{1}{3}K_{\theta 2}\beta_{s1}k_l^3\right)\bar{r} + t_{15}\mu_x^2 \\
 &\quad + t_{16}\mu_y\mu_x + \frac{1}{4}k_l\beta_{s1}\beta_{c1}\mu_x\mu_z + \left(-\frac{1}{2}k_l + \frac{3}{8}k_l\beta_{c1}^2 + \frac{1}{2}r_c\right)\mu_z\mu_y \\
 t_2 &= t_{21} + \frac{1}{4}k_l^2\beta_0\beta_{s1}\mu_x + \frac{3}{4}k_l^2\beta_0\beta_{c1}\mu_y + \left(\frac{3}{8}r_c - \frac{3}{8}k_l\right)\mu_y^2 - \frac{1}{4}k_l^3\beta_{c1}\bar{p} + \frac{1}{3}k_l^3\bar{r} + \left(\frac{1}{8}r_c - \frac{1}{8}k_l\right)\mu_x^2
 \end{aligned}$$

$$\begin{aligned}
 t_3 &= \left(\left(-\frac{1}{4}k_l + \frac{1}{4}r_c \right) \mu_y + \frac{1}{4}k_l^2 \beta_0 \beta_{c1} \right) \mu_x + \frac{1}{8}k_l^3 \beta_{s1} \beta_{c1} \\
 t_4 &= \frac{1}{2}k_l^3 \beta_0 \beta_{c1} + \frac{1}{4}k_l^2 \beta_{c1} \beta_{s1} \mu_x + \left(\frac{3}{8}k_l^2 \beta_{c1}^2 - \frac{1}{2}k_l^2 + \frac{1}{2}r_c^2 \right) \mu_y + \frac{1}{2}k_l^2 \bar{r} \mu_y - \frac{1}{3}k_l^3 \beta_0 \bar{p} \\
 t_{11} &= \frac{1}{6}k_l^3 \lambda_{c1} + \left(\frac{3}{8}\theta_{tw}k_l^4 - \frac{1}{2}k_l^2 \lambda_0 \right) \beta_{c1} \beta_0 + \left(\frac{1}{16}K_{\theta 2} - \frac{1}{24} \right) k_l^3 \beta_{c1}^2 \beta_{s1} \\
 &\quad + \left(\left(\frac{1}{6} - \frac{1}{6}K_{\theta 2} \right) k_l^3 - \frac{1}{4}e_f k_l^2 + \left(-\frac{1}{6} + \frac{1}{6}K_{\theta 2} \right) r_c^3 + \frac{1}{4}e_f r_c^2 \right) \beta_{s1} \\
 &\quad + \left(\frac{1}{6}K_{\theta 1} r_c^3 - \frac{1}{6}K_{\theta 1} k_l^3 \right) \beta_{c1} + \frac{3}{16}K_{\theta 1} k_l^3 \beta_{c1}^3 + \frac{3}{4}K_{\theta 1} k_l^3 \beta_0^2 \beta_{c1} \\
 &\quad + \frac{3}{16}K_{\theta 1} k_l^3 \beta_{s1} \beta_{c1} + \left(\frac{1}{16}K_{\theta 2} - \frac{1}{24} \right) k_l^3 \beta_{s1}^3 + \left(-\frac{1}{6} + \frac{1}{4}K_{\theta 2} \right) k_l^3 \beta_0^2 \beta_{s1} \\
 t_{12} &= \frac{1}{6}\theta_{tw}k_l^3 \beta_{s1} \beta_{c1} + \left(-\frac{1}{4} + \frac{1}{4}K_{\theta 2} \right) k_l^2 \beta_{s1}^2 \beta_0 + \frac{3}{4}K_{\theta 1} k_l^2 \beta_0 \beta_{s1} \beta_{c1} \\
 &\quad + \left(\frac{1}{4}k_l^2 - \frac{1}{4}r_c^2 \right) \beta_0 + \left(-\frac{1}{2} - \frac{1}{4}K_{\theta 2} \right) k_l^2 \beta_{c1}^2 \beta_0 \\
 t_{13} &= \frac{1}{2}K_{\theta 2} \beta_{c1} k_l^2 \beta_0 \beta_{s1} - \frac{1}{3}\theta_{tw}k_l^3 + \frac{1}{4}\theta_{tw}k_l^3 \beta_{c1}^2 + \frac{1}{2}k_l \lambda_0 - \frac{1}{2}r_c \lambda_0 + \frac{9}{8}K_{\theta 1} k_l^2 \beta_0 \beta_{c1}^2 - \frac{1}{2}K_{\theta 1} k_l^2 \beta_0 \\
 t_{14} &= \left(\left(-\frac{3}{8}K_{\theta 2} - \frac{1}{8} \right) k_l + \frac{3}{8}K_{\theta 2} r_c \right) \beta_{s1} - \frac{3}{8}K_{\theta 1} k_l \beta_{c1} \\
 t_{15} &= -\frac{3}{32}k_l \beta_{s1} \beta_{c1}^2 + \left(\left(\frac{1}{8} - \frac{1}{8}K_{\theta 2} \right) k_l + \left(\frac{1}{8}K_{\theta 2} - \frac{1}{8} \right) r_c \right) \beta_{s1} + \left(-\frac{1}{8}K_{\theta 1} k_l + \frac{1}{8}K_{\theta 1} r_c \right) \beta_{c1} \\
 t_{16} &= \left(\frac{1}{4}K_{\theta 1} r_c - \frac{1}{4}K_{\theta 1} k_l \right) \beta_{s1} + \left(\left(\frac{1}{4} + \frac{1}{4}K_{\theta 2} \right) k_l + \left(-\frac{1}{4} - \frac{1}{4}K_{\theta 2} \right) r_c \right) \beta_{c1}
 \end{aligned}$$

D

D.2.2 Flapping Equation

The flapping equation of motion can be derived in the matrix form as (see Equ. D.45):

$$\mathbf{M}_\beta \dot{\vec{\beta}} + \mathbf{A}_\beta \vec{\beta} + \mathbf{N}_\beta + \mathbf{b}_\beta = 0 \quad (\text{D.76})$$

Those coefficients matrices/vectors are as following.

$$\mathbf{M}_\beta = \Omega \begin{bmatrix} \frac{1}{4}e_f^2 k_l^2 - \frac{1}{8}k_l^4 \bar{r} & \frac{1}{4}(e_f^2 k_l - e_f k_l^2) & \frac{1}{4}(\frac{1}{3}k_l^3 - e_f k_l^2) \mu_y \\ -\frac{1}{3}e_f k_l^3 + \frac{1}{8}k_l^4 & +\frac{1}{3}k_l^3 & \mu_x \\ \frac{1}{2}(e_f k_l^2 + e_f^2 k_l) & \frac{1}{4}e_f^2 k_l^2 - \frac{1}{8}k_l^4 \bar{r} & -\frac{2}{\gamma} \\ +\frac{1}{3}k_l^3 & -\frac{1}{3}e_f k_l^3 + \frac{1}{8}k_l^4 & \frac{1}{4}e_f^2 k_l^2 - \frac{1}{8}k_l^4 \bar{r} \\ \frac{1}{2}(\frac{1}{3}k_l^3 - e_f k_l^2) \mu_y & \frac{2}{\gamma} & -\frac{1}{3}e_f k_l^3 + \frac{1}{8}k_l^4 \end{bmatrix} \quad (\text{D.77})$$

Elements in matrix \mathbf{A}_β are:

$$\begin{aligned}
 A_{11} &= -\frac{1}{8}K_{\theta 1}k_l^4 + \frac{\bar{K}_\beta}{\gamma} + \frac{1}{6}K_{\theta 1}e_f k_l^3 - \frac{1}{8}\mu_y^2 k_l^2 K_{\theta 1} + \frac{1}{6}\theta_0 k_l^3 \bar{q}\mu_x - \frac{1}{8}\theta_{c1} k_l^4 \bar{p} + \frac{1}{8}\theta_{s1} k_l^4 \bar{q} \\
 &\quad + \left(-\frac{1}{3}K_{\theta 1}e_f k_l^3 + \frac{1}{4}K_{\theta 1}k_l^4\right)\bar{r} + \left(\frac{1}{4}K_{\theta 1}e_f k_l - \frac{1}{4}K_{\theta 1}e_f r_c + \frac{1}{8}K_{\theta 1}r_c^2 - \frac{1}{8}K_{\theta 1}k_l^2\right)\mu_x^2 \\
 A_{12} &= \left(\frac{1}{6}K_{\theta 1}r_c^3 + \frac{1}{4}K_{\theta 1}e_f k_l^2 - \frac{1}{2}\frac{\bar{M}_\beta}{e_f} - \frac{1}{6}K_{\theta 1}k_l^3 - \frac{1}{4}K_{\theta 1}e_f r_c^2\right)\mu_x \\
 &\quad + \left(-\frac{1}{6}K_{\theta 2}k_l^3 + \left(-\frac{1}{8}e_f + \frac{1}{4}K_{\theta 2}e_f\right)k_l^2\right)\mu_y + \frac{1}{6}K_{\theta 1}k_l^3 \bar{r}\mu_x \\
 &\quad + \left(\frac{1}{12} + \frac{1}{6}K_{\theta 2}\right)k_l^3 \mu_y \bar{r} + \frac{1}{12}k_l^3 \bar{q}\mu_z + \frac{1}{8}\theta_{s1} k_l^3 \bar{q}\mu_x + \left(\frac{1}{8}\theta_0 k_l^4 + \frac{1}{10}\theta_{tw} k_l^5\right)\bar{q} \\
 A_{13} &= \left(\frac{1}{6}K_{\theta 2}k_l^3 + \left(-\frac{1}{4}K_{\theta 2}e_f + \frac{1}{8}e_f\right)k_l^2 - \frac{1}{4}e_f^2 k_l + \left(-\frac{1}{12} - \frac{1}{6}K_{\theta 2}\right)r_c^3 + \left(\frac{1}{8}e_f + \frac{1}{4}K_{\theta 2}e_f\right)r_c^2\right)\mu_x \\
 &\quad + \left(-\frac{1}{2}\frac{\bar{M}_\beta}{e_f} + \frac{1}{4}K_{\theta 1}e_f k_l^2 - \frac{1}{6}K_{\theta 1}k_l^3\right)\mu_y + \left(-\frac{1}{12} - \frac{1}{6}K_{\theta 2}\right)k_l^3 \mu_x \bar{r} \\
 &\quad + \frac{1}{6}K_{\theta 1}k_l^3 \bar{r}\mu_y - \frac{1}{12}k_l^3 \bar{p}\mu_z + \left(-\frac{1}{10}\theta_{tw} k_l^5 - \frac{1}{8}\theta_0 k_l^4\right)\bar{p} \\
 A_{21} &= \left(\frac{1}{3}K_{\theta 1}r_c^3 + \frac{1}{2}K_{\theta 1}e_f k_l^2 - \frac{\bar{M}_\beta}{e_f} - \frac{1}{3}K_{\theta 1}k_l^3\right)\mu_x \\
 &\quad + \left(-\frac{1}{6}k_l^3 + \frac{1}{4}e_f k_l^2\right)\mu_y + \frac{1}{3}K_{\theta 1}k_l^3 \bar{r}\mu_x + \left(\frac{1}{4}\theta_0 k_l^4 + \frac{1}{5}\theta_{tw} k_l^5\right)\bar{q} \\
 A_{22} &= -\frac{1}{8}K_{\theta 1}k_l^4 + \frac{1}{6}K_{\theta 1}e_f k_l^3 + \frac{\bar{K}_\beta}{\gamma} - \gamma^{-1} + \left(\frac{1}{4}\theta_0 k_l^3 + \frac{3}{16}\theta_{tw} k_l^4\right)\mu_x \bar{q} \\
 &\quad + \left(\left(-\frac{1}{8}K_{\theta 2} - \frac{1}{8}\right)k_l^2 + \left(\frac{1}{4}K_{\theta 2}e_f + \frac{1}{4}e_f\right)k_l\right)\mu_y \mu_x + \frac{3}{16}\theta_{s1} k_l^4 \bar{q} \\
 &\quad + \left(-\frac{1}{3}K_{\theta 1}e_f k_l^3 + \frac{1}{4}K_{\theta 1}k_l^4\right)\bar{r} + \left(-\frac{3}{16}K_{\theta 1}k_l^2 + \frac{3}{8}K_{\theta 1}e_f k_l + \frac{3}{16}K_{\theta 1}r_c^2 - \frac{3}{8}K_{\theta 1}e_f r_c\right)\mu_x^2 \\
 A_{23} &= \left(\frac{1}{8}K_{\theta 2} - \frac{1}{8}\right)k_l^4 + \left(-\frac{1}{6}K_{\theta 2}e_f + \frac{1}{3}e_f\right)k_l^3 - \frac{1}{4}e_f^2 k_l^2 + \left(-\frac{1}{16} + \frac{1}{16}K_{\theta 2}\right)k_l^2 \mu_y^2 \\
 &\quad + \left(\frac{1}{4}K_{\theta 1}e_f k_l - \frac{1}{8}K_{\theta 1}k_l^2\right)\mu_y \mu_x + \left(\left(\frac{1}{8} - \frac{1}{4}K_{\theta 2}\right)k_l^4 + \frac{1}{3}K_{\theta 2}e_f k_l^3\right)\bar{r} + \left(\left(\frac{3}{16}K_{\theta 2} + \frac{1}{16}\right)k_l^2\right. \\
 &\quad \left.+ \left(-\frac{1}{8}e_f - \frac{3}{8}K_{\theta 2}e_f\right)k_l + \left(-\frac{1}{16} - \frac{3}{16}K_{\theta 2}\right)r_c^2 + \left(\frac{1}{8}e_f + \frac{3}{8}K_{\theta 2}e_f\right)r_c\right)\mu_x^2 \\
 A_{31} &= \left(\frac{1}{6}k_l^3 - \frac{1}{4}e_f k_l^2 - \frac{1}{6}r_c^3\right)\mu_x + \left(-\frac{\bar{M}_\beta}{e_f} - \frac{1}{3}K_{\theta 1}k_l^3 + \frac{1}{2}K_{\theta 1}e_f k_l^2\right)\mu_y \\
 &\quad - \frac{1}{6}k_l^3 \bar{r}\mu_x + \left(-\frac{1}{5}\theta_{tw} k_l^5 - \frac{1}{4}\theta_0 k_l^4\right)\bar{p} \\
 A_{32} &= \left(-\frac{1}{8}K_{\theta 2} + \frac{1}{8}\right)k_l^4 + \left(-\frac{1}{3}e_f + \frac{1}{6}K_{\theta 2}e_f\right)k_l^3 + \frac{1}{4}e_f^2 k_l^2 + \left(-\frac{1}{16} - \frac{3}{16}K_{\theta 2}\right)k_l^2 \mu_y^2 \\
 &\quad + \left(\frac{1}{4}K_{\theta 1}e_f k_l - \frac{1}{8}K_{\theta 1}k_l^2\right)\mu_y \mu_x + \left(\left(-\frac{1}{8} + \frac{1}{4}K_{\theta 2}\right)k_l^4 - \frac{1}{3}K_{\theta 2}e_f k_l^3\right)\bar{r} \\
 &\quad + \left(\left(-\frac{1}{16}K_{\theta 2} + \frac{1}{16}\right)k_l^2 + \left(\frac{1}{8}K_{\theta 2}e_f - \frac{1}{8}e_f\right)k_l + \left(-\frac{1}{16} + \frac{1}{16}K_{\theta 2}\right)r_c^2\right. \\
 &\quad \left.+ \left(-\frac{1}{8}K_{\theta 2}e_f + \frac{1}{8}e_f\right)r_c\right)\mu_x^2
 \end{aligned}$$

D

D.2 Expressions of the Generic Flight Mechanics Model

213

$$\begin{aligned}
 A_{33} = & -\frac{1}{8}K_{\theta 1}k_l^4 + \frac{1}{6}K_{\theta 1}e_f k_l^3 + \frac{\bar{K}_\beta}{\gamma} - \gamma^{-1} - \frac{3}{16}\mu_y^2 k_l^2 K_{\theta 1} \\
 & + \left(\left(\frac{1}{8} + \frac{1}{8}K_{\theta 2} \right) k_l^2 + \left(-\frac{1}{4}e_f - \frac{1}{4}K_{\theta 2}e_f \right) k_l \right) \mu_y \mu_x - \frac{3}{16}\theta_{c1}k_l^4 \bar{p} \\
 & + \left(-\frac{1}{3}K_{\theta 1}e_f k_l^3 + \frac{1}{4}K_{\theta 1}k_l^4 \right) \bar{r} + \left(\frac{1}{8}K_{\theta 1}e_f k_l - \frac{1}{16}K_{\theta 1}k_l^2 \right) \mu_x^2
 \end{aligned}$$

Elements in vector \mathbf{N}_β are:

$$\begin{aligned}
 N_1 = & \frac{1}{4}K_{\theta 1}k_l^3 \beta_0^2 \beta_{s1} \mu_x + \frac{1}{16}K_{\theta 1}k_l^3 \beta_{s1}^3 \mu_x + \frac{1}{2} \frac{\dot{\beta}_{s1}^2 \beta_0}{\gamma \Omega^2} + \frac{\dot{\beta}_0^2 \beta_0}{\gamma \Omega^2} + \frac{1}{8}K_{\theta 1}k_l^4 \beta_0^3 \\
 & + \left(\frac{1}{6} \frac{e_f k_l^3}{\Omega} - \frac{1}{16} \frac{k_l^4}{\Omega} \right) \beta_0 \beta_{s1} \dot{\beta}_{s1} + \left(\frac{1}{6} \frac{e_f k_l^3}{\Omega} - \frac{1}{16} \frac{k_l^4}{\Omega} \right) \beta_0 \beta_{c1} \dot{\beta}_{c1} + \frac{\dot{\beta}_{s1} \dot{\beta}_0 \beta_{s1}}{\gamma \Omega^2} + \frac{\dot{\beta}_{c1} \dot{\beta}_0 \beta_{c1}}{\gamma \Omega^2} \\
 & + \left(-\frac{1}{32} \frac{k_l^4}{\Omega} + \frac{1}{12} \frac{e_f k_l^3}{\Omega} \right) \beta_{c1}^2 \dot{\beta}_0 + \left(-\frac{1}{32} \frac{k_l^4}{\Omega} + \frac{1}{12} \frac{e_f k_l^3}{\Omega} \right) \beta_{s1}^2 \dot{\beta}_0 + \frac{1}{16}K_{\theta 1}k_l^3 \beta_{s1} \beta_{c1}^2 \mu_x \\
 & + \left(\frac{1}{6} \frac{e_f k_l^3}{\Omega} - \frac{1}{16} \frac{k_l^4}{\Omega} \right) \beta_0^2 \dot{\beta}_0 + \left(-\frac{1}{48}K_{\theta 2}k_l^3 \mu_x - \frac{1}{32}k_l^3 \mu_x \right) \beta_{c1}^3 + t_1 \beta_{s1}^2 + t_2 \beta_{c1}^2 \\
 & + t_5 \beta_0^2 + \frac{\dot{\beta}_{s1} \beta_{c1} \beta_0}{\gamma \Omega} - \frac{\dot{\beta}_{c1} \beta_{s1} \beta_0}{\gamma \Omega} + \frac{1}{2} \frac{\dot{\beta}_{c1}^2 \beta_0}{\gamma \Omega^2} + \left(-\frac{1}{12}K_{\theta 2}k_l^3 \mu_x - \frac{1}{8}k_l^3 \mu_x \right) \beta_0^2 \beta_{c1} \\
 & + \left(-\frac{1}{48}K_{\theta 2}k_l^3 \mu_x - \frac{1}{32}k_l^3 \mu_x \right) \beta_{c1} \beta_{s1}^2 + \left(\frac{1}{24}\theta_{c1}k_l^3 \mu_x + \frac{1}{24}\theta_{s1}k_l^3 \mu_y - \frac{1}{12}K_{\theta 2}k_l^3 \bar{q} \mu_x \right) \beta_{s1} \beta_{c1} \\
 & + \left(\frac{3}{16}K_{\theta 1}k_l^4 - \frac{1}{2}\gamma^{-1} - \frac{1}{4}K_{\theta 1}e_f k_l^3 \right) \beta_{c1}^2 \beta_0 \\
 & + \left(\frac{3}{16}K_{\theta 1}k_l^4 - \frac{1}{2}\gamma^{-1} - \frac{1}{4}K_{\theta 1}e_f k_l^3 \right) \beta_{s1}^2 \beta_0 + t_3 \beta_0 \beta_{c1} + t_4 \beta_0 \beta_{s1}
 \end{aligned}$$

D

where:

$$\begin{aligned}
 t_1 = & \left(-\frac{3}{32}\theta_{s1}e_f k_l^2 + \frac{1}{16}\theta_{s1}k_l^3 \right) \mu_x + \left(\frac{1}{12}k_l^3 - \frac{1}{8}e_f k_l^2 \right) \mu_z \\
 & - \frac{1}{12}\theta_0 e_f k_l^3 - \frac{1}{24}k_l^3 \lambda_0 - \frac{1}{16}\theta_{tw}e_f k_l^4 + \frac{1}{20}\theta_{tw}k_l^5 + \frac{1}{16}\theta_0 k_l^4 \\
 t_2 = & \frac{1}{48}\theta_{s1}k_l^3 \mu_x + \frac{1}{16}\theta_{c1}k_l^3 \mu_y + \left(\frac{1}{12}k_l^3 - \frac{1}{8}e_f k_l^2 \right) \mu_z - \frac{1}{12}\theta_0 e_f k_l^3 \\
 & - \frac{1}{24}k_l^3 \lambda_0 - \frac{1}{16}\theta_{tw}e_f k_l^4 + \frac{1}{20}\theta_{tw}k_l^5 + \frac{1}{16}\theta_0 k_l^4 \\
 t_3 = & \left(\frac{1}{6}\theta_0 k_l^3 + \frac{1}{8}\theta_{tw}k_l^4 \right) \mu_y + \left(-\gamma^{-1} - \frac{1}{4}K_{\theta 1}k_l^4 \right) \bar{p} - \frac{1}{6}\theta_{c1}e_f k_l^3 - \frac{1}{8}K_{\theta 2}k_l^4 \bar{q} + \frac{1}{8}k_l^4 \theta_{c1} \\
 t_4 = & \left(\frac{1}{6}\theta_0 k_l^3 + \frac{1}{8}\theta_{tw}k_l^4 - \frac{1}{6}\theta_{tw}e_f k_l^3 + \frac{1}{8}k_l^2 \mu_z - \frac{1}{4}\theta_0 e_f k_l^2 \right) \mu_x \\
 & - \frac{1}{8}K_{\theta 2}k_l^4 \bar{p} + \left(\frac{1}{4}K_{\theta 1}k_l^4 + \gamma^{-1} \right) \bar{q} + \frac{1}{8}\theta_{s1}k_l^4 - \frac{1}{6}\theta_{s1}e_f k_l^3 \\
 t_5 = & -\frac{1}{6}\theta_0 e_f k_l^3 + \frac{1}{8}\theta_0 k_l^4 + \frac{1}{10}\theta_{tw}k_l^5 + \frac{1}{12}\theta_{s1}k_l^3 \mu_x - \frac{1}{12}k_l^3 \lambda_0 + \frac{1}{6}k_l^3 \mu_z
 \end{aligned}$$

D

$$\begin{aligned}
 N_2 = & \left(-\frac{1}{8}k_l^3\mu_x - \frac{1}{6}K_{\theta 2}k_l^3\mu_x \right) \beta_{c1}\beta_{s1}\beta_0 + \left(\frac{1}{3}\frac{e_fk_l^3}{\Omega} - \frac{1}{8}\frac{k_l^4}{\Omega} \right) \beta_{s1}\dot{\beta}_0\beta_0 \\
 & + \left(-\frac{1}{32}\frac{k_l^4}{\Omega} + \frac{1}{12}\frac{e_fk_l^3}{\Omega} \right) \beta_{s1}\beta_{c1}\dot{\beta}_{c1} - 2\frac{\beta_{c1}\dot{\beta}_0\beta_0}{\gamma\Omega} \\
 & + \left(-\frac{9}{16}K_{\theta 1}e_fk_l^2\mu_x + \frac{3}{16}k_l^3\mu_y + \frac{3}{8}K_{\theta 1}k_l^3\mu_x \right) \beta_{s1}^2\beta_0 + \left(-\frac{1}{2}\gamma^{-1} + \frac{3}{32}K_{\theta 1}k_l^4 \right) \beta_{s1}\beta_{c1}^2 \\
 & + \left(\frac{3}{8}K_{\theta 1}k_l^4 - \gamma^{-1} \right) \beta_0^2\beta_{s1} + \left(-\frac{1}{8}K_{\theta 2}k_l^4 + \frac{1}{16}k_l^4 \right) \beta_0^2\beta_{c1} + t_2\beta_0\beta_{s1} + t_3\beta_{s1}\beta_{c1} \\
 & + \left(\frac{1}{24}\theta_0k_l^3\mu_x + \frac{1}{32}\theta_{s1}k_l^4 + \frac{1}{32}\theta_{tw}k_l^4\mu_x \right) \beta_{c1}^2 + \left(\frac{1}{8}\theta_{tw}k_l^4\mu_x + \frac{1}{6}\theta_0k_l^3\mu_x + \frac{1}{8}\theta_{s1}k_l^4 \right) \beta_0^2 \\
 & + \left(-\frac{1}{32}K_{\theta 2}k_l^4 + \frac{1}{64}k_l^4 \right) \beta_{c1}^3 + \left(-\frac{1}{2}\gamma^{-1} + \frac{3}{32}K_{\theta 1}k_l^4 \right) \beta_{s1}^3 + t_1\beta_{s1}^2 + 2\frac{\dot{\beta}_{s1}\dot{\beta}_0\beta_0}{\gamma\Omega^2} \\
 & + \frac{1}{2}\frac{\dot{\beta}_{c1}\dot{\beta}_{s1}\beta_{c1}}{\gamma\Omega^2} + \left(\frac{1}{6}\frac{e_fk_l^3}{\Omega} - \frac{1}{16}\frac{k_l^4}{\Omega} \right) \dot{\beta}_{s1}\beta_0^2 + \left(\frac{1}{8}\frac{e_fk_l^3}{\Omega} - \frac{3}{64}\frac{k_l^4}{\Omega} \right) \dot{\beta}_{s1}\beta_{s1}^2 \\
 & + \left(-\frac{1}{64}\frac{k_l^4}{\Omega} + \frac{1}{24}\frac{e_fk_l^3}{\Omega} \right) \dot{\beta}_{s1}\beta_{c1}^2 + \left(-\frac{1}{32}K_{\theta 2}k_l^4 + \frac{1}{64}k_l^4 \right) \beta_{c1}\beta_{s1}^2 - \frac{\dot{\beta}_{c1}\beta_{s1}^2}{\gamma\Omega} + \frac{3}{4}\frac{\dot{\beta}_{s1}^2\beta_{s1}}{\gamma\Omega^2} \\
 & + \frac{1}{4}\frac{\dot{\beta}_{c1}^2\beta_{s1}}{\gamma\Omega^2} + \frac{\dot{\beta}_0^2\beta_{s1}}{\gamma\Omega^2} - \frac{\dot{\beta}_{c1}\beta_{c1}^2}{\gamma\Omega} - 2\frac{\dot{\beta}_{c1}\beta_0^2}{\gamma\Omega} + \frac{1}{8}K_{\theta 1}k_l^3\beta_0\beta_{c1}^2\mu_x + \frac{1}{12}\theta_{c1}k_l^3\beta_0\beta_{c1}\mu_x
 \end{aligned}$$

where:

$$\begin{aligned}
 t_1 = & \left(\frac{3}{32}\theta_{tw}k_l^4 + \frac{1}{8}\theta_0k_l^3 - \frac{3}{16}\theta_0e_fk_l^2 + \frac{3}{32}k_l^2\mu_z \right) \mu_x + \left(\frac{3}{4}\gamma^{-1} + \frac{3}{16}K_{\theta 1}k_l^4 \right) \bar{q} - \frac{1}{8}\theta_{s1}e_fk_l^3 + \frac{3}{32}\theta_{s1}k_l^4 \\
 t_2 = & \left(-\frac{3}{8}\theta_{s1}e_fk_l^2 + \frac{1}{4}\theta_{s1}k_l^3 \right) \mu_x + \left(\frac{1}{3}k_l^3 - \frac{1}{2}e_fk_l^2 \right) \mu_z \\
 & + \frac{1}{4}\theta_0k_l^4 + \frac{1}{5}\theta_{tw}k_l^5 - \frac{1}{4}\theta_{tw}e_fk_l^4 - \frac{1}{3}\theta_0e_fk_l^3 - \frac{1}{6}k_l^3\lambda_0 \\
 t_3 = & -\frac{1}{12}\theta_{c1}e_fk_l^3 + \frac{1}{16}k_l^4\theta_{c1} - \frac{1}{8}K_{\theta 2}k_l^4\bar{q} + \frac{1}{12}k_l^3\theta_0\mu_y
 \end{aligned}$$

$$\begin{aligned}
 N_3 = & \left(\frac{1}{8}\frac{e_fk_l^3}{\Omega} - \frac{3}{64}\frac{k_l^4}{\Omega} \right) \dot{\beta}_{c1}\beta_{c1}^2 + \left(\frac{1}{6}\frac{e_fk_l^3}{\Omega} - \frac{1}{16}\frac{k_l^4}{\Omega} \right) \dot{\beta}_{c1}\beta_0^2 + \left(-\frac{1}{64}\frac{k_l^4}{\Omega} + \frac{1}{24}\frac{e_fk_l^3}{\Omega} \right) \dot{\beta}_{c1}\beta_{s1}^2 \\
 & + 2\frac{\dot{\beta}_{s1}\beta_0^2}{\gamma\Omega} + \frac{\dot{\beta}_{s1}\beta_{c1}^2}{\gamma\Omega} + \frac{\dot{\beta}_{s1}\beta_{s1}^2}{\gamma\Omega} + \frac{3}{4}\frac{\dot{\beta}_{c1}\beta_{c1}}{\gamma\Omega^2} + \frac{\dot{\beta}_0^2\beta_{c1}}{\gamma\Omega^2} + \frac{1}{4}\frac{\dot{\beta}_{s1}^2\beta_{c1}}{\gamma\Omega^2} + t_2\beta_0\beta_{c1} \\
 & + t_4\beta_{c1}^2\beta_0 + \left(-\frac{1}{32}\frac{k_l^4}{\Omega} + \frac{1}{12}\frac{e_fk_l^3}{\Omega} \right) \beta_{s1}\beta_{c1}\dot{\beta}_{s1} + \left(\frac{1}{3}\frac{e_fk_l^3}{\Omega} - \frac{1}{8}\frac{k_l^4}{\Omega} \right) \beta_{c1}\dot{\beta}_0\beta_0 \\
 & + 2\frac{\beta_{s1}\dot{\beta}_0\beta_0}{\gamma\Omega} + t_3\beta_{s1}\beta_{c1} + t_1\beta_{c1}^2 + \left(-\frac{1}{2}\gamma^{-1} + \frac{3}{32}K_{\theta 1}k_l^4 \right) \beta_{c1}^3 \\
 & + \left(-\frac{1}{64}k_l^4 + \frac{1}{32}K_{\theta 2}k_l^4 \right) \beta_{s1}^3 + \left(\frac{1}{6}K_{\theta 2}k_l^3\mu_y + \frac{1}{4}K_{\theta 1}k_l^3\mu_x \right) \beta_{c1}\beta_{s1}\beta_0 \\
 & + 2\frac{\dot{\beta}_{c1}\dot{\beta}_0\beta_0}{\gamma\Omega^2} + \frac{1}{2}\frac{\dot{\beta}_{c1}\dot{\beta}_{s1}\beta_{s1}}{\gamma\Omega^2} + \left(-\frac{1}{16}k_l^3\mu_x + \frac{1}{12}K_{\theta 2}k_l^3\mu_x \right) \beta_{s1}^2\beta_0 \\
 & + \left(-\frac{1}{64}k_l^4 + \frac{1}{32}K_{\theta 2}k_l^4 \right) \beta_{s1}\beta_{c1}^2 + \left(\frac{1}{8}K_{\theta 2}k_l^4 - \frac{1}{16}k_l^4 \right) \beta_0^2\beta_{s1} + \left(\frac{3}{8}K_{\theta 1}k_l^4 - \gamma^{-1} \right) \beta_0^2\beta_{c1} \\
 & + \left(-\frac{1}{2}\gamma^{-1} + \frac{3}{32}K_{\theta 1}k_l^4 \right) \beta_{c1}\beta_{s1}^2 + \frac{1}{12}k_l^3\theta_{c1}\beta_0\beta_{s1}\mu_x + \frac{1}{32}k_l^4\theta_{c1}\beta_{s1}^2 + \frac{1}{8}k_l^4\theta_{c1}\beta_0^2
 \end{aligned}$$

D.2 Expressions of the Generic Flight Mechanics Model

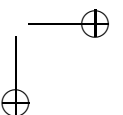
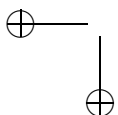
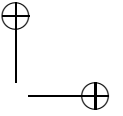
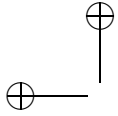
215

where:

$$\begin{aligned}
 t_1 &= \left(\frac{1}{8} \theta_0 k_l^3 + \frac{3}{32} \theta_{tw} k_l^4 \right) \mu_y + \left(-\frac{3}{16} K_{\theta 1} k_l^4 - \frac{3}{4} \gamma^{-1} \right) \bar{p} - \frac{1}{8} \theta_{c1} e_f k_l^3 + \frac{3}{32} k_l^4 \theta_{c1} \\
 t_2 &= \frac{1}{12} \theta_{s1} k_l^3 \mu_x + \frac{1}{4} \theta_{c1} k_l^3 \mu_y + \left(\frac{1}{3} k_l^3 - \frac{1}{2} e_f k_l^2 \right) \mu_z + \frac{1}{4} \theta_0 k_l^4 \\
 &\quad + \frac{1}{5} \theta_{tw} k_l^5 - \frac{1}{4} \theta_{tw} e_f k_l^4 - \frac{1}{3} \theta_0 e_f k_l^3 - \frac{1}{6} k_l^3 \lambda_0 \\
 t_3 &= \left(\frac{1}{12} \theta_0 k_l^3 + \frac{1}{16} \theta_{tw} k_l^4 + \frac{1}{16} k_l^2 \mu_z \right) \mu_x - \frac{1}{8} K_{\theta 2} k_l^4 \bar{p} + \frac{1}{16} \theta_{s1} k_l^4 - \frac{1}{12} \theta_{s1} e_f k_l^3 \\
 t_4 &= \left(-\frac{1}{12} K_{\theta 2} k_l^3 - \frac{3}{16} k_l^3 + \frac{9}{32} e_f k_l^2 \right) \mu_x + \frac{3}{8} K_{\theta 1} k_l^3 \mu_y
 \end{aligned}$$

Elements in vector \mathbf{b}_β are:

$$\begin{aligned}
 b_1 &= \left(\frac{1}{8} \theta_{tw} e_f k_l^2 - \frac{1}{12} \theta_{tw} k_l^3 \right) \mu_x^2 + \left(\left(\frac{1}{8} e_f k_l^2 - \frac{1}{12} k_l^3 \right) \bar{p} + \frac{1}{12} k_l^3 \lambda_{s1} + \frac{\bar{M}_\beta \bar{q}}{e_f} - \frac{1}{8} e_f k_l^2 \lambda_{s1} \right) \mu_x \\
 &\quad - \frac{1}{12} \mu_y^2 k_l^3 \theta_{tw} + \left(\frac{1}{12} k_l^3 \lambda_{c1} - \frac{1}{12} k_l^3 \bar{q} - \frac{\bar{M}_\beta \bar{p}}{e_f} \right) \mu_y + \left(\frac{1}{6} r_c^3 - \frac{1}{6} k_l^3 + \frac{1}{4} e_f k_l^2 + \frac{1}{6} k_l^3 \bar{r} \right) \mu_z \\
 &\quad + \left(\frac{1}{5} \theta_{tw} k_l^5 - \frac{1}{6} k_l^3 \lambda_0 \right) \bar{r} - \frac{1}{10} \theta_{tw} k_l^5 + \frac{1}{8} \theta_{tw} e_f k_l^4 + \frac{1}{6} k_l^3 \lambda_0 - \frac{1}{4} e_f k_l^2 \lambda_0 \\
 &\quad + \left(\frac{1}{4} e_f k_l^2 + \frac{1}{6} k_l^3 \bar{r} - \frac{1}{6} k_l^3 \right) \mu_y \theta_{c1} + \left(-\frac{1}{4} e_f r_c^2 + \frac{1}{4} e_f k_l^2 - \frac{1}{6} k_l^3 + \frac{1}{6} r_c^3 + \frac{1}{6} k_l^3 \bar{r} \right) \mu_x \theta_{s1} \\
 &\quad + \left(\left(-\frac{1}{8} k_l^2 + \frac{1}{8} r_c^2 - \frac{1}{4} e_f r_c + \frac{1}{4} k_l e_f \right) \mu_x^2 - \frac{1}{8} \mu_y^2 k_l^2 + \left(\frac{1}{4} k_l^4 - \frac{1}{3} e_f k_l^3 \right) \bar{r} - \frac{1}{8} k_l^4 + \frac{1}{6} e_f k_l^3 \right) \theta_0 \\
 b_2 &= \left(\left(\frac{1}{4} r_c^2 + \frac{1}{2} k_l e_f - \frac{1}{4} k_l^2 - \frac{1}{2} e_f r_c \right) \mu_z + \frac{1}{4} k_l^2 \lambda_0 - \frac{1}{4} \theta_{tw} k_l^4 - \frac{1}{4} r_c^2 \lambda_0 + \frac{1}{4} \theta_{tw} k_l^4 \bar{r} + \frac{1}{2} e_f r_c \lambda_0 \right. \\
 &\quad \left. + \frac{1}{3} \theta_{tw} e_f k_l^3 - \frac{1}{2} e_f k_l \lambda_0 \right) \mu_x + \left(-\frac{1}{8} k_l^4 + \frac{1}{6} e_f k_l^3 \right) \bar{p} \\
 &\quad + (2\bar{M}_\beta + 2\gamma^{-1}) \bar{q} + \frac{1}{8} k_l^4 \lambda_{s1} - \frac{1}{6} e_f k_l^3 \lambda_{s1} + \left(-\frac{1}{8} k_l^2 + \frac{1}{4} k_l e_f \right) \mu_y \mu_x \theta_{c1} \\
 &\quad + \left(\left(-\frac{3}{8} e_f r_c - \frac{3}{16} k_l^2 + \frac{3}{16} r_c^2 + \frac{3}{8} k_l e_f \right) \mu_x^2 - \frac{1}{16} \mu_y^2 k_l^2 + \left(\frac{1}{4} k_l^4 - \frac{1}{3} e_f k_l^3 \right) \bar{r} - \frac{1}{8} k_l^4 + \frac{1}{6} e_f k_l^3 \right) \theta_{s1} \\
 &\quad + \left(\frac{1}{3} k_l^3 \bar{r} + \frac{1}{3} r_c^3 - \frac{1}{2} e_f r_c^2 + \frac{1}{2} e_f k_l^2 - \frac{1}{3} k_l^3 \right) \mu_x \theta_0 \\
 b_3 &= \left(\left(\frac{1}{2} k_l e_f - \frac{1}{4} k_l^2 \right) \mu_z + \frac{1}{4} k_l^2 \lambda_0 + \frac{1}{3} \theta_{tw} e_f k_l^3 - \frac{1}{2} e_f k_l \lambda_0 - \frac{1}{4} \theta_{tw} k_l^4 \right) \mu_y \\
 &\quad + (-2\bar{M}_\beta - 2\gamma^{-1}) \bar{p} + \left(-\frac{1}{8} k_l^4 + \frac{1}{6} e_f k_l^3 \right) \bar{q} - \frac{1}{6} e_f k_l^3 \lambda_{c1} + \frac{1}{8} k_l^4 \lambda_{c1} \\
 &\quad + \left(\left(\frac{1}{16} r_c^2 - \frac{1}{8} e_f r_c + \frac{1}{8} k_l e_f - \frac{1}{16} k_l^2 \right) \mu_x^2 - \frac{3}{16} \mu_y^2 k_l^2 + \left(\frac{1}{4} k_l^4 - \frac{1}{3} e_f k_l^3 \right) \bar{r} - \frac{1}{8} k_l^4 + \frac{1}{6} e_f k_l^3 \right) \theta_{c1} \\
 &\quad + \left(-\frac{1}{8} k_l^2 + \frac{1}{4} k_l e_f \right) \mu_y \mu_x \theta_{s1} + \left(\frac{1}{2} e_f k_l^2 + \frac{1}{3} k_l^3 \bar{r} - \frac{1}{3} k_l^3 \right) \mu_y \theta_0
 \end{aligned}$$

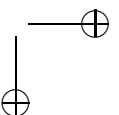
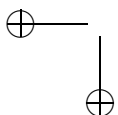
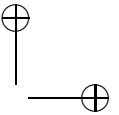
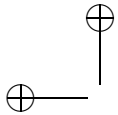


Bibliography

- [1] Anonymous (2012a). Silence evo. <http://www.vario-helicopter.net/products/pod-and-boom/electric-pod-boom/silence-evo.html>.
- [2] Anonymous (2012b). Vlad Savov’s Home Page. <http://www.aviation.ru/contrib/vsavov/>.
- [3] Anonymous (2012c). X-treme. <http://www.vario-helicopter.net/products/pod-and-boom/methanol-pod-boom/x-treme/x-treme.html>.
- [4] AVSCOM (2000). Aeronautical design standard (ads-33e-prf)-handling qualities requirements for military rotorcraft. *US Army Aviation and Missile Command, Aviation Engineering Directorate*.
- [5] Betz, A. (1912). Ein beitrag zur erkläerung des segelfluges. *Zeitschrift für Flugtechnik und Motorluftschiffahrt*, 3:269–272.
- [6] Byrd, R. H., Gilbert, J. C., and Nocedal, J. (2000). A trust region method based on interior point techniques for nonlinear programming. *Mathematical Programming*, 89(1):149–185.
- [7] Byrd, R. H., Hribar, M. E., and Nocedal, J. (1999). An interior point algorithm for large-scale nonlinear programming. *SIAM Journal on Optimization*, 9(4):877–900.
- [8] DeLaurier, J. (1999). Development and testing of a full-scale piloted ornithopter. *Canadian Aeronautics and Space Journal*, 45(2):72–82.
- [9] Filippone, A. (2006). *Flight performance of fixed and rotary wing aircraft*. Elsevier Aerospace Engineering Series. Butterworth-Heinemann.
- [10] Gareth D. Padfield, C. (2008). *Helicopter Flight Dynamics*. AIAA education series. Wiley.
- [11] Geißler, W. and van der Wall, B. G. (2010). Rotor without reaction torque, a historical review of H.G. Küssner’s rotorcraft research. In *66th American Helicopter Society Annual Forum*.
- [12] Geißler, W. and van der Wall, B. G. (2012). The flapping propulsion rotor, single rotor without tail rotor. In *1st Asian-Australia Rotorcraft Forum*.

- [13] Glaz, B., Friedmann, P. P., and Liu, L. (2009). Helicopter vibration reduction throughout the entire flight envelope using surrogate-based optimization. *Journal of the American Helicopter Society*, 54(1).
- [14] Harris, F. D., Kasper, E. F., and Iseler, L. E. (2000). U.S. civil rotorcraft accidents, 1963 through 1997. NASA Technical Memorandum 209597, NASA.
- [15] Heiligers, M., Kuiper, R., van Holten, T., and van den Bulcke, S. (2005a). Development of a radio-controlled ornicopter: A single rotor helicopter without reaction torque. In *The 2005 International Powered Lift Conference*.
- [16] Heiligers, M., van Den Bulcke, S., van Holten, T., and Kuiper, R. (2005b). A radio-controlled ornicopter model. In *31st European Rotorcraft Forum*.
- [17] Heiligers, M., van Holten, T., and van Den Bulcke, S. (2006). Test results of a radio-controlled ornicopter: A single rotor helicopter without reaction torque. In *Collection of Technical Papers - 44th AIAA Aerospace Sciences Meeting*, volume 13, pages 9832–9854.
- [18] Katzmayr, R. (1922). Effect of periodic changes of angle of attack on behavior of airfoils. NACA Technical Memorandum 147, NACA.
- [19] Knoller, R. (1909). Die gesetze des luftwiderstandes. *Flug-und Motortechnik (Vieena)*, 3(21):1–7.
- [20] Küssner, H. G. (1937). Helicopter problems. NACA Technical Memorandum 827, NACA.
- [21] Leishman, J. (2006). *Principles of Helicopter Aerodynamics*. Cambridge Aerospace Series. Cambridge University Press.
- [22] Milluzzo, J. and Leishman, J. G. (2010). Assessment of rotorcraft brownout severity in terms of rotor design parameters. *Journal of the American Helicopter Society*, 55(3):0320091–0320099.
- [23] Mouille, R. (1970). The fenestron shrouded tail rotor of the sa. 341 gazelle. *Journal of the American Helicopter Society*, 15(4):31–37.
- [24] Peters, D. A. and Ninh, H. (1988). Dynamic inflow for practical applications. *Journal of the American Helicopter Society*, 33(4):64–68.
- [25] Platzer, M. F., Jones, K. D., Young, J., and Lai, J. C. S. (2008a). Flapping-wing aerodynamics: Progress and challenges. *AIAA Journal*, 46(9):2136–2149.
- [26] Platzer, M. F., Jones, K. D., Young, J., and S. Lai, J. (2008b). Flapping wing aerodynamics: progress and challenges. *AIAA journal*, 46(9):2136–2149.
- [27] Prouty, R. (2009). *Helicopter Aerodynamics Volume II*. Helicopter Aerodynamics. Eagle Eye Solutions, LLC.

- [28] Taylor, J. (1988). *Jane’s All the World’s Aircraft, 1988-1989*. IHS Jane’s All the World’s Aircraft. Jane’s Information Group, Incorporated.
- [29] Tischler, M. B. (1990). System identification requirements for high-bandwidth rotorcraft flight control system design. *Journal of Guidance, Control, and Dynamics*, 13(5):835–841.
- [30] Torenbeek, E. and Deconinck, H. (2005). *Innovative configurations and advanced concepts for future civil aircraft: June 6-10, 2005*. Lecture series. Von Karman Institute for Fluid Dynamics.
- [31] van Gerwen, D. J. and van Holten, T. (2007). Ornicopter yaw control: Testing a single rotor helicopter without reaction torque. In *45th AIAA Aerospace Sciences Meeting*.
- [32] van Holten, T. (2002). A single rotor without reaction torque: a violation of Newton’s Laws or feasible? In *28th European Rotorcraft Forum*.
- [33] van Holten, T. (2004). Helicopter. Patent Application. WO 2004/002825 A1.
- [34] van Holten, T. and Heiligers, M. (2004a). Configuration analysis of a torqueless helicopter concept. In *24th International Congress of the Aeronautical Sciences*.
- [35] van Holten, T. and Heiligers, M. (2004b). The influence of flexible blades on the characteristics of the ornicopter. In *30th European Rotorcraft Forum*.
- [36] van Holten, T., Heiligers, M., Kuiper, R., Vardy, S., van de Waal, G. J., and Krijnen, J. (2004a). Forced flapping mechanisms for the ornicopter: A single rotor helicopter without reaction torque. In *30th European Rotorcraft Forum*.
- [37] van Holten, T., Heiligers, M., and van de Waal, G. J. (2004b). The ornicopter: A single rotor without reaction torque, basic principles. In *24th International Congress of the Aeronautical Sciences*.



Samenvatting

De staartrotor van conventionele helikopters wordt altijd al als een noodzakelijk kwaad beschouwd. De rotor is noodzakelijk om het reactiekoppel van de motor tegen te gaan en om de helikopter te controleren in de gierbeweging. Echter, hij verbruikt een substantieel vermogen, heeft enkel een marginaal controlevermogen in ongunstige windcondities, en hij is lawaaierig, kwetsbaar en gevaarlijk. Een oplossing voor deze problemen zou een helikopterconcept zijn dat de nood voor een staartrotor elimineert. De zogenoemde ‘Ornicopter’, een helikopter met flapperende rotorbladen is zo’n concept.

Het mechanisme van de Ornicopter is geïnspireerd door de manier waarop vogels vliegen. Vogels creëren met het flappen van hun vleugels zowel een opstijgende als een voortstuwende kracht in één beweging. In het geval van een conventionele helikopter, worden de rotorbladen aangedreven in een roterende wijze, en wordt er lift gegenereerd door de roterende rotorbladen. Echter, de Ornicopter drijft de rotorbladen enkel aan op een flappende wijze, zoals een vogel, en genereert op deze manier zowel lift als een voortstuwende kracht. In dit geval roteren de rotorbladen van zichzelf door de flappende beweging en niet meer doordat er een koppel direct doorgegeven wordt aan de rotorbladen. Daarom zal de Ornicopter’s rotor geen reactiekoppel genereren op de romp zodat een staartrotor overbodig wordt.

Het doel van dit proefschrift is het ontwikkelen van een grondig inzicht in het Ornicopter concept en de haalbaarheid van het concept voor een realistisch bereik in het vluchtregime. Het proefschrift bestaat uit twee delen. Het eerste deel beschrijft de analyse van de voornaamste karakteristieken van de Ornicopter met betrekking tot vluchtprestaties, stabiliteit, controleerbaarheid, bestuurbaarheid, alsook een onderzoekende trillingsanalyse. In het tweede deel wordt een voorlopig ontwerp beschreven gebaseerd op de conclusies van het eerste deel.

De basis voor de studie over de Ornicopter is een model van de vliegdynamica dat analytisch is afgeleid. Het model is gebaseerd op de bladelement theorie (BET) en gebruikt zes bewegingsvrijheden voor starre lichamen, drie voor de dynamica van de flappende rotorbladen en drie voor de Pitt-Peters instroming dynamica. Vorige mathematische modellen die ontwikkeld waren voor het analyseren van het Ornicopter concept waren vooral gericht op stil hangende vlucht. Het model dat in dit proefschrift is ontwikkeld kan de vliegdynamica van de Ornicopter over het gehele operationele vluchtregime beschrijven. Als referentiepunt voor de specificaties van de Ornicopter is de Bölkow Bo-105 gebruikt. De Bo-105 helikopter is een lichte, tweemotorige, mul-

tifunctionele helikopter die ontwikkeld is in Duitsland in de jaren 1970. De initiële parameters voor het ontwerp van de Ornicopter (zoals de rotorblad diameter, de rotorbladbelasting, de snelheid van de rotorbladuiteinden, de grootte van het verticale staarvlak) zijn gebaseerd op het ontwerp van de Bo-105. Er is gekozen voor een 2×2 antisymmetrische flappende rotorblad configuratie (d.w.z. tegenovergestelde rotorbladen flappen in dezelfde richting) voor de Ornicopter zodat de noodzaak voor een staartrotor wordt geëlimineerd. Gebruik makende van deze ontwerpparameters wordt aangetoond dat de rotor van de Ornicopter genoeg koppel kan genereren om de rotorbladen te doen roteren met bescheiden flapamplitudes (met een maximum van minder dan 9°). Dit proefschrift toont ook de nadelen van het Ornicopter concept in vergelijking met de Bo-105 helikopter aan. Deze nadelen zijn een hoger benodigd vermogen, een kleiner bereik in het vluchtregime (vooral door een groter gebied in het vluchtregime waarin liftverlies bij de rotorbladen kan optreden) en een lagere gierstabiliteit. Deze nadelen kunnen worden toegeschreven aan de grote invalshoek variatie van de rotorbladen die ontstaat door de geforceerde flappende beweging en de afwezigheid van een staartrotor.

In het tweede deel van dit proefschrift wordt het concept van de Ornicopter geoptimaliseerd in termen van vluchtprestaties. In dit geval geldt als ontwerpdoel de vluchtprestaties van de Bo-105 en worden de ontwerpparameters (rotorbladdiameter, rotorbladbelasting, enz.) aangepast aan het Ornicopter concept. De ontwerpoptimalisatie is gebaseerd op het minimaliseren van het benodigd vermogen, terwijl er voldaan wordt aan de liftverliesgebied eis. Dit proefschrift bewijst dat het optimaal ontwerp voor de Ornicopter gekarakteriseerd is door een lagere rotorbladbelasting, een hogere rotorbladtipsnelheid en een groter verticaal staarvlak in vergelijking met de Bo-105. Dit optimaal ontwerp resulteert in een vergroot bereik in het vluchtregime door een kleiner gebied waarin liftverlies bij de rotorbladen optreedt en een verbeterde gierstabiliteit in voorwaartse vlucht. Echter, niettegenstaande deze verbeteringen in het vluchtregime van de Ornicopter, is er een hoger benodigd vermogen in vergelijking met de Bo-105 specificatie (ongeveer 5% bij 150 knopen). Ter compensatie voor het hoger benodigd vermogen van het optimale ontwerp van de Ornicopter, is een grotere rotordiameter nodig zodat het geïnduceerde vermogen kan verminderd worden zodanig dat het totale benodigde vermogen tot een minimum kan behouden blijven.

Dit proefschrift kan als een eerste stap in het rationaliseren van de verwachtingen van de Ornicopter's staartloze helikopter ontwerp beschouwd worden. Er wordt aangetoond dat dit nieuw concept licht verminderde prestaties heeft in vergelijking met conventionele helikopters op vlak van vermogensverbruik in voorwaartse vlucht en dienstplafond. Dit is teleurstellend aangezien één van de aannames was dat het elimineren van de staartrotor ook het vermogensverbruik van de staartrotor zou elimineren. Verdere analyse van de prestaties van het Ornicopter concept (zoals vliegbereik, laadvermogen, klimprestaties, duurzaamheid met betrekking tot veiligheid en geluidproductie), de kosten en het onderhoud zijn nodig voor een volledig begrip van de voor- en nadelen van dit helikopter concept.

Acknowledgements

My PhD research was carried out in the faculty of Aerospace Engineering at the Delft University of Technology. I started my research in the SEAD (Systems Engineering and Aircraft Design) department, and stayed there for the first year. Afterwards, I moved to the C&S (Control and Simulation) department for the rest of my PhD study. I am really glad that I had the opportunity to work in the two departments, so I can meet more great researchers in different fields, from whom I really learned a lot. I am very grateful to all these people, and I would like to mention some of them in particular.

First I would like to thank my promotor Prof. Michel van Tooren. Without him, I wouldn't have had the opportunity to come to this nice place (assuming the weather is not considered) for my PhD study. He gave me the freedom to decide the direction to go for my research, and provided very productive suggestions.

I would also like to thank my co-promoter, Dr. Marilena Pavel. Without her patience and most valuable help, I would not have been able to finish my PhD successfully. I could always show up in her office without an appointment, and her critical and detailed comments at all stages of my research really made my PhD much easier.

Likewise, I would like to give my thanks to Prof. Max Mulder for his kind help and support, which made my transition between the two departments quick and smooth. I really enjoyed my time in C&S. My thanks also goes to Prof. Theo van Holten. His invention, the Ornicopter concept, is the foundation of my research and his suggestions are very helpful.

As the consequence of working in two departments, the number of colleagues I had is too large to mention individually. I appreciate the nice time we shared, and I would like to mention some of them specifically. Olaf, thank you for your help on the SIMUNA test. It was great fun. Dennis, Ligu, Reinier, Fred and Xiajiao, though I am not smart enough to understand everything, I enjoyed all those technical discussions we had. I have had the pleasure to share rooms with several colleagues who made my office time much more enjoyable (sorted alphabetically): Dennis, Fred, Haiqiang, Jaime, Jan, Laurens, Ligu, Reinier, Rolf, Sophie, Wouter and Yazdi.

Without the entertainment after office hours, one would not be able to keep his efficiency in the office. I enjoyed a lot of activities in Delft, and I would like to thank my tennis buddies, all members of the Nerd basketball team and my teammates in the DCF (Delft Chinese Football team).

Also, thanks are due to all the supporting staffs in both departments and the CICAT of TU Delft, specially: Andries, Bertine, Bettie, Cees, Franca, Harold, Lin, Michiel and

Nana. All their help made my life in Delft easy and cozy.

Last but not least, my deepest gratitude goes to my parents, as well as my girlfriend Weiwei. Their unconditional love and support are the most powerful ‘thrust force’ which keeps me moving forward. The force can be more powerful when I am thousands of miles away from home.

Curriculum Vitae

On October 21, 1983, Jia Wan was born in Leshan, Sichuan province, China. From 1999 to 2002, he attended the Leshan 1st high school, where he decided to take the long and difficult path to become an aerospace engineer.

For this reason, in 2002 he enrolled as an aerospace engineering student at the Beihang University (formerly called Beijing University of Aeronautics and Astronautics), Beijing, China. He majored in aircraft design and graduated in 2006. Afterwards, he continued for his master program in the field of rotorcraft aerodynamics. His thesis works investigated the application of the free wake model on co-axil helicopters and developed a Fortran program for the free wake model.

Besides the academic research, he was trained as a UAV/model aircraft pilot. He has been entitled the national champion for six times in China National Aeromodelling Tournament, and he is keeping one national record. Meanwhile, he also extensively participated the development of a small co-axil unmanned helicopter as a system engineer and test pilot.

After receiving his M.Sc. degree in 2009, he started his Ph.D. research at the SEAD (Systems Engineering and Aircraft Design) department of the Faculty of Aerospace Engineering at Delft University of Technology. After one year, due to the reorganization of the faculty, he joined the C&S (Control and Simulation) department. His Ph.D. research focused on the concept analyses, comparisons and design optimization for the Ornicopter, which is a new single rotor tailless helicopter configuration.